ALTERATION AND FLUID FLOW ASSOCIATED WITH SEDIMENT-HOSTED STRATIFORM COPPER MINERALISATION IN THE 1.1 GA MIDCONTINENT RIFT SYSTEM, USA

Simon Mark Jones

A Thesis Submitted for the Degree of PhD
at the
University of St Andrews

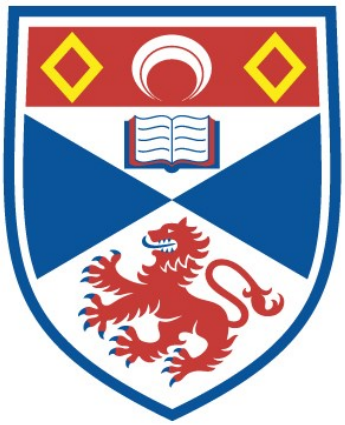

2020

Full metadata for this item is available in
St Andrews Research Repository
at:
http://research-repository.st-andrews.ac.uk/

Identifiers to use to cite or link to this thesis:

DOI: https://doi.org/10.17630/sta/137
http://hdl.handle.net/10023/23982

This item is protected by original copyright

Alteration and fluid flow associated with sediment-hosted stratiform copper mineralisation in the 1.1 Ga Midcontinent Rift System, USA

Simon Mark Jones

University of
St Andrews

This thesis is submitted in partial fulfilment for the degree of

Doctor of Philosophy (PhD)

at the University of St Andrews

February 2020

Candidate's declaration

I, Simon Mark Jones, do hereby certify that this thesis, submitted for the degree of PhD, which is approximately 38,300 words in length, has been written by me, and that it is the record of work carried out by me, or principally by myself in collaboration with others as acknowledged, and that it has not been submitted in any previous application for any degree.

I was admitted as a research student at the University of St Andrews in September 2016.

I received funding from an organisation or institution and have acknowledged the funder(s) in the full text of my thesis.

Date *4th October 2020* Signature of candidate

Supervisor's declaration

I hereby certify that the candidate has fulfilled the conditions of the Resolution and Regulations appropriate for the degree of PhD in the University of St Andrews and that the candidate is qualified to submit this thesis in application for that degree.

Date *4th October 2020* Signature of supervisor

Permission for publication

In submitting this thesis to the University of St Andrews we understand that we are giving permission for it to be made available for use in accordance with the regulations of the University Library for the time being in force, subject to any copyright vested in the work not being affected thereby. We also understand, unless exempt by an award of an embargo as requested below, that the title and the abstract will be published, and that a copy of the work may be made and supplied to any bona fide library or research worker, that this thesis will be electronically accessible for personal or research use and that the library has the right to migrate this thesis into new electronic forms as required to ensure continued access to the thesis.

I, Simon Mark Jones, confirm that my thesis does not contain any third-party material that requires copyright clearance.

The following is an agreed request by candidate and supervisor regarding the publication of this thesis:

Printed copy

No embargo on print copy.

Electronic copy

Embargo on all of electronic copy for a period of 1 year on the following ground(s):

- Publication would preclude future publication

Supporting statement for electronic embargo request

We intend to submit chapters 3 and 4 for publication in the journals Economic Geology and Geosphere respectively. Since the other chapters refer to and cite parts of chapters 3 and 4, we have requested the entire thesis be embargoed.

Title and Abstract

- I agree to the title and abstract being published.

Date *4th October 2020* Signature of candidate

Date *4th October 2020* Signature of supervisor

Underpinning Research Data or Digital Outputs

Candidate's declaration

I, Simon Mark Jones, hereby certify that no requirements to deposit original research data or digital outputs apply to this thesis and that, where appropriate, secondary data used have been referenced in the full text of my thesis.

Date *4th October 2020* Signature of candidate

Funding sources

First Quantum Minerals Ltd.
Financial support that was the foundation for this project.

Natural Environment Research Council
Grant for stable isotope geochemistry at the East Kilbride facility (SUERC).
Grant for high precision U-Pb zircon dating at Nottingham facility (NIGL).

Highland Copper Company Inc.
Permitted access to drill core and samples.
Provided field and logistical support.

Michigan Department of Natural Resources
Enabled access to drill core and samples in the Marquette core archive.

Table of Contents

Table of contents i
List of figures and tables iv
Acknowledgements vii
Abstract viii

Chapter 1: Introduction, background and project rationale 1
1.1. Sediment-hosted Cu deposits 2
1.1.1. Characteristics 2
1.1.2. Genetic model 3
1.2. Research approach and limitations of previous research 6
1.3. Selected examples of sediment-hosted copper systems 8
1.3.1. Central African Copperbelt (Katangan basin) 8
1.3.2. Kupferschiefer (Zechstein basin) 12
1.3.3. Dzhezkazgan (Chu-Sarysu basin) 15
1.4. Project justification and aims 18
1.4.1. Why study the Midcontinent Rift System and White Pine? 18
1.4.2. Uncertainties in the understanding of White Pine and the MRS 18
1.4.3. Key questions 20
1.4.4. Research aims 22
1.4.5. Research methods and techniques 23
1.5. Background 25
1.5.1. Midcontinent Rift System 25
1.5.2. Keweenaw Supergroup 26
1.5.3. The White Pine deposit and other copper mineralisation 28
1.6. References 30

Chapter 2: A marine origin for the late Mesoproterozoic Copper Harbor and Nonesuch formations of the Midcontinent Rift of Laurentia 39
2.1. Introduction 40
2.2. Geological background 42
2.2.1. Non-marine palaeoenvironments 42
2.3. Sedimentological observations 48
2.3.1. Upper Copper Harbor Formation stromatolite interval 48
2.3.2. Uppermost Copper Harbor Formation 52
2.3.3. Nonesuch Formation 52
2.4. Discussion: marine-influenced sedimentation 56
2.4.1. Features indicative of oscillatory or combined flows 56
2.4.2. Features indicative of periodically reversing or flashy flows 61
2.4.3. Periodically repetitive sedimentary structures 62

2.4.4. Evaporite minerals and oolites 63
2.4.5. Absence of depositional cyclicity 64
2.5. Depositional setting 64
2.6. Conclusions 65
2.7. References 67

Chapter 3: Fluid flow, alteration and Cu-Ag mineralisation associated with the White Pine deposit 73
3.1. Introduction 74
3.2. Regional geology 76
3.2.1. Portage Lake volcanics Group 78
3.2.2. Copper Harbor Formation 78
3.2.3. Nonesuch Formation 80
3.3. White Pine deposit 80
3.4. Paragenesis 84
3.4.1. Pre-mineralisation stage 85
3.4.2. Mineralisation stage 89
3.4.3. Post-mineralisation stage 96
3.4.4. Late faults 98
3.5. Geochemical data 99
3.6. Analytical results 101
3.6.1. Illite crystallinity 101
3.6.2. Carbon and oxygen isotopes 101
3.6.3. Sulphur isotopes 102
3.6.4. Re-Os geochronology 103
3.7. Discussion 104
3.7.1. Pre-mineralisation basin architecture and faulting 104
3.7.2. Timing of mineralisation 105
3.7.3. Diagenetic evolution 106
3.7.4. Mineralisation stage 107
3.7.5. Stable isotope constraints on mineralising processes 108
3.7.6. Genetic model 110
3.8. Conclusions 112
3.9. References 113

Chapter 4: Is the Midcontinent Rift actually a Midcontinent Sag? 121
Note to readers 123
4.1. Introduction 124
4.2. Background 125
4.3. Keweenaw Supergroup 127
4.4. New geochronology 129

4.4.1. Porcupine Mountains volcanics 132
4.4.2. Copper Harbor Formation 133
4.5. Backstripping analysis 135
4.6. Keweenawan stratigraphic cross-section 136
4.7. Reflection seismic profiles 140
4.8. Discussion 145
4.9. Conclusions 150
4.10. References 151

Chapter 5: Conclusions 157
5.1. Overview 158
5.2. Chapter 2 – Sedimentology 158
5.3. Chapter 3 – The White Pine deposit 161
5.4. Chapter 4 – Basin dynamics 162
5.5. Future research 164
5.6. References 165

Chapter 6: Lessons applicable to the sediment-hosted stratiform Cu deposit model 167
6.1. Introduction 168
6.2. Paleo-environment 168
6.3 Basin architecture 170
6.4. Fluid flow 172
6.5. Ore deposition 173
6.6. References 175

Appendices 179
A3 Supplementary data for White Pine 179

List of figures and tables

Fig. 1.1	Map of selected global sediment-hosted Cu deposit	3
Fig. 1.2.	Relationship between formation of major sediment-hosted Cu deposits, halite, glaciation events and ocean chemistry	4
Fig. 1.3.	Schematic diagram of a sediment-hosted Cu basin	6
Fig. 1.4.	Central African Copperbelt geological map	8
Fig. 1.5.	Comparative stratigraphy of the Zambian and Congolese Parts of the Central African Copperbelt	10
Fig. 1.6.	Facies map of the late Permian Z2 carbonate in the Zechstein basin	13
Fig. 1.7.	Simplified Rotliegend-Zechstein (ore bearing) stratigraphic column	14
Fig. 1.8.	Map of elevation of the base of the Pennsylvanian red bed Unit in the Chu Sarysu basin	16
Fig. 1.9.	Stratigraphy of the Chu Sarysu basin	17
Fig. 1.10.	(A) Location map of the Midcontinent Rift System in North America and (B) Simplified geological map of the Midcontinent Rift System	25
Fig. 1.11.	Keweenaw Supergroup stratigraphic column	27
Fig. 1.12.	Geological map of the Keweenaw Peninsula	29
Fig. 1.13.	Geological map of the White Pine district	29
Fig. 2.1.	Simplified geological maps of the Lake Superior area and the Keweenaw Peninsula	40
Fig. 2.2.	Generalised stratigraphy of the Keweenaw Peninsula	41
Fig. 2.3.	Photographs of braided fluvial features in the Copper Harbor Formation	43
Fig. 2.4.	Photographs of diagenetic fluid-flow features in the Nonesuch Formation	44
Fig. 2.5.	Photographs of diagenetic fluid-flow features in the Nonesuch Formation	46
Fig. 2.6.	Subaqueous (syneresis) cracks in siltstones and very fine sandstones of the Nonesuch Formation	47
Fig. 2.7.	Stratigraphic cross-section of the Nonesuch Formation	49
Fig. 2.8.	Logged section of Horseshoe Harbor stromatolite-bearing interval in the upper Copper Harbor Formation	50
Fig. 2.9.	Photographs of Horseshoe Harbor stromatolites	50
Fig. 2.10.	Photographs of tide-influenced sedimentary structures in Horseshoe Harbor siliclastic rocks	51
Fig. 2.11.	Photographs of evaporite fabrics and features in the uppermost Harbor Formation	53

Fig. 2.12.	Photographs of desiccation cracks in the Nonesuch Formation	55
Fig. 2.13.	Photographs of microbial laminae and structures in the Nonesuch Formation	56
Fig. 2.14.	Photographs of tide-influenced sedimentary structures in the Nonesuch Formation	57
Fig. 2.15.	Photographs of shelf-shoreline sedimentary structures in the Nonesuch Formation	58
Fig. 2.16.	Photographs of fabrics and textures of former Ca-sulphate evaporites in the Nonesuch Formation	60
Table 2.1.	The main sedimentary features identified in the Copper Harbor and Nonesuch formations classified by genesis and relative abundance in lacustrine and marine settings	66
Fig. 3.1.	(A) Map of the location of the Midcontinent Rift System in North America, (B) Simplified geological map of the Midcontinent Rift System, and (C) Geological map of the Keweenaw Peninsula	75
Fig. 3.2.	(A) Stratigraphic column of the Keweenaw Supergroup and (B) Stratigraphic column of the Oronto Group	77
Fig. 3.3.	Photographs of rock units in the footwall of White Pine	79
Fig. 3.4.	Stratigraphic column of the White Pine “mine sequence”	81
Fig. 3.5.	Photograph of drill core from the White Pine “mine sequence”, drill hole WP233	82
Fig. 3.6.	Geological map of the Porcupine district	83
Fig. 3.7.	Paragenetic sequence chart for White Pine	84
Fig. 3.8.	Photographs of alteration textures in the Copper Harbor Formation sandstone units	86
Fig. 3.9.	Photographs, photomicrographs and SEM images of diagenetic and alteration textures in the Copper Harbor Formation	88
Fig. 3.10.	Photographs of mineralised rocks in White Pine	90
Fig. 3.11.	Photomicrographs and SEM images of Cu-mineralised rocks in White Pine	92
Fig. 3.12.	Maps of the White Pine deposit showing: (A) thickness of chlorite and pyrobitumen zones, and (B) stratigraphic height of the “fringe zone”	94
Fig. 3.13.	Geological cross sections through White Pine. (A) present-day geometry, (B) alteration and pyrobitumen distribution and (C) mineralisation zones	95
Fig. 3.14.	Photographs of late structures – post-mineralisation veins and faults	98
Fig. 3.15.	X-Y plot of carbon and oxygen isotopes	102

Fig. 3.16.	Histograms of sulphur isotopes: (A) by mineralogy, and (B) by host lithology	103
Fig. 4.1.	Geological terrane map of eastern North America	124
Fig. 4.2.	Simplified geological map of the Lake Superior portion of the Midcontinent Rift System with reflection seismic lines	126
Fig. 4.3.	Stratigraphic column of the Keweenaw Supergroup in the southwest Lake Superior area	128
Fig. 4.4.	U-Pb Concordia plots from zircon geochronology	130
Table 4.1.	Summary of the U-Pb ages and their uncertainties	131
Fig. 4.5.	Photographs of geochronology samples	131
Fig. 4.6.	Geological map of the Porcupine Mountains district with geochronology sample locations	132
Fig. 4.7.	Geological map of surrounding area and stratigraphic log of drill hole JBY-002	133
Fig. 4.8.	(A) Burial history plot of the Keweenaw Supergroup, and (B) subsidence curves for the Midcontinent Rift System	134
Table 4.2.	Parameters used in subsidence analysis and backstripping	135
Fig. 4.9.	Geological map of the Keweenaw Peninsula with location of drill holes and field transects used in cross section	137
Fig. 4.10.	Geological cross section through the Oronto Group on the Keweenaw Peninsula	138
Fig. 4.11.	Photograph of the unconformity between the Portage Lake volcanics Group and the Copper Harbor Formation in outcrop	139
Fig. 4.12.	Reflection seismic line GLIMPCE A and interpretation	141
Fig. 4.13.	Reflection seismic lines GLIMPCE C and Petty-Ray 1 and interpretations	142
Fig. 4.14.	Reflection seismic lines LS-08 and interpretation	143
Fig. 4.15.	Schematic diagram of the key geometries and relationships observed in the geological cross section and reflection seismic profiles	146
Fig. 4.16.	Cartoon timeline of key events in the evolution of the Midcontinent Rift System	149
Table 5.1.	Summary of key research questions and findings	159-160
Fig. 6.1.	Paleo-reconstruction of Rodinia at 1080 Ma	170
Fig. 6.2.	Geodynamic setting of the Midcontinent Rift System at the time of mineralisation	173
Fig. 6.3.	Schematic representation of the paleo-fluid flow regime at White Pine	175
Table A3.1.	Carbon and oxygen isotope data from White Pine	179-182
Table A3.2.	Sulphur isotope data from White Pine	183-185
Table A3.3.	Re-Os geochronology data from White Pine	186

Acknowledgements

I wish to express my gratitude to my supervisors: Tony Prave, Tim Raub and Jonathan Cloutier. You made me think about rocks differently and to challenge everything *I think I know*.

I am grateful to Mike Christie and First Quantum Minerals for funding this research and for allowing me to take four years off. Lots of companies talk about investing in their people, but very few do it in a way that is as meaningful as FQM.

David Wood and many others provided the inspiration and encouragement to undertake this PhD. Thank you.

Finally, thanks also to Aishling Fagan. You put up with a lot.

"It's easy to get marinaded in an idea if you've been thinking about it for a long time"

Abstract

The White Pine Cu-Ag deposit is one of the World's largest examples of a sediment-hosted copper (SHC) mineral system, with a pre-mining resource of >10 Mt of Cu metal. The deposit is located on the southern shore of Lake Superior, in Michigan's Upper Peninsula. Mineralisation is hosted in the late-Mesoproterozoic Keweenawan Supergroup of the Midcontinent Rift System (MRS). This succession comprises 20 km of flood basalts overlain by 10 km of clastic sedimentary rocks. The age, extraordinary volume of basalt and paucity of evaporite minerals distinguishes the MRS from other major sediment-hosted Cu basins. Basin formation commenced at c. 1111 Ma, possibly in response to a mantle plume impacting the base of the lithosphere. The mass of basalts loaded onto the crust initially drove rapid basin subsidence, forming sag-geometry basalt flows in the absence of syn-volcanic faults. Volcanism ceased abruptly at c. 1090 Ma and the Oronto Group sediments were deposited at a lower rate of subsidence. The Copper Harbor and Nonesuch Formations were deposited in a braided fluvial-marine embayment-sabkha environment. Seawater formed the basis for the ore-forming fluids. Metals were sourced from the breakdown of basaltic detrital grains in the Copper Harbor Formation. A Re-Os age of chalcocite mineralisation of 1039 ± 4 Ma corresponds to the early Ottawan phase of the Grenvillian orogenesis, which caused incipient basin inversion and deposition of the Freda Formation molasse. This simultaneous burial and mild compression expelled fluids from the Copper Harbor Formation aquifer. Ore precipitated via reduction of fluids by both *in situ* organic matter and liquid petroleum, and thermochemical sulphate reduction, at temperatures of c. 125˚C. Early Cu-Fe-sulphides nucleated on detrital and authigenic chlorite. The advancement of the peneconcordant ore zones resulted in their eventual replacement by chalcocite and native Cu, reflecting the relatively oxidised conditions and the low sulphur content of late-Mesoproterozoic seawater.

Chapter 1

Introduction, background and project rationale

1.1. Sediment-hosted copper deposits

1.1.1. Characteristics

Globally, sediment-hosted copper (SHC) deposits constitute an important source of copper, accounting for 15% of resources (https://pubs.usgs.gov/fs/2014/3004 /pdf/fs2014-3004.pdf, USGS, 2013) and 23% of production (Taylor et al., 2013). This style of deposit is characterised by relatively high grade ores, low concentrations of deleterious elements and minerals, and may form large to giant deposits. SHC deposits are known on every continent except for Antarctica (Fig. 1.1) and formed at multiple periods in Earth's history (Hitzman et al., 2010). Sediment-hosted copper deposits are currently a favourable exploration target for mining companies and explorers.

Sedimentary units exert a strong control on the distribution of ore and deposits display high aspect ratios with thickness of 1s to 10s of meters and aerial extents of up to 10s to 100s of km^2. Structural controls are often important at both the deposit and basin-scales. Host lithologies include sandstones, carbonates, shales and siltstones that contain either in situ reductants or previously contained mobile reductants such as gas or liquid petroleum, and overlie redbeds (Hitzman et al., 2005). Copper mineralisation is commonly vertically and laterally zoned, reflecting the paleo-redox architecture that prevailed during precipitation of ore minerals from pore fluids (e.g. White Pine, Brown, 1971; Kupferschiefer, Oszczepalski, 1999).

Sediment hosted copper deposits contain a variety of primary and secondary copper-bearing minerals of disseminated, replacement and vein styles (Taylor et al., 2013). They also host significant quantities of accessory metals: commonly Ag, Co, Pb and Zn and occasionally U and Mo (e.g. Kansanshi, Zambia, Torrealday et al., 2000); Au and Platinum Group Elements (e.g. Kupferschiefer, Poland, Wodzicki and Piestrzyński, 1994); Ni (e.g. Enterprise, Zambia, Capistrant et al., 2015) and Ge (e.g. Kipushi, Democratic Republic of Congo, Schneider et al., 2007).

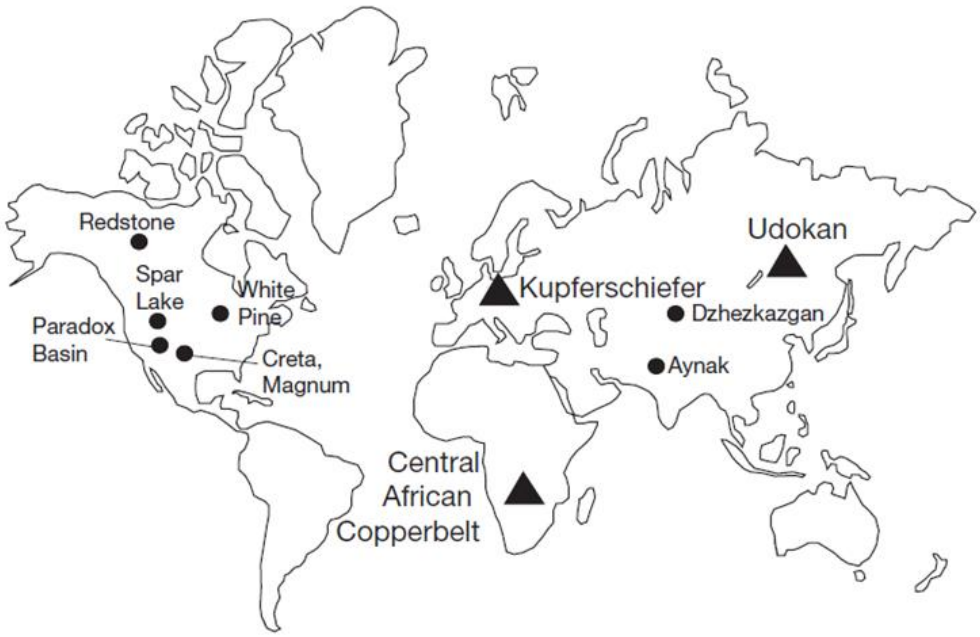

Fig. 1.1. Map of selected, major global SHC deposits (Hitzman et al., 2010).

1.1.2. Genetic model

The formation of SHC deposits is contingent on the availability of redbeds, as an aquifer and a source of Cu, and organic matter capable of reducing oxidised fluids (Kirkham, 1989; Hitzman et al., 2005). The formation of both of these is temporally restricted to after the Great Oxygenation Event (GOE) at 2.4 to 2.1 Ga (Lyons et al., 2014). Paleo-environment exerted a first-order control on the formation of SHC systems. The lower portions of the stratigraphy of basins hosting major SHC systems typically contains a package of rocks formed at paleolatitudes of < 30˚, where evaporation exceeded precipitation, resulting in the formation of evaporites and oxidised, immature redbeds (Kirkham, 1989; Hitzman et al., 2010; Brown, 2014). The expansive interiors of supercontinents, such as Rodinia (1100 to 750 Ma) and Pangea (335 – 175 Ma) further promoted arid conditions (Hitzman et al., 2010).

The two largest SHC systems coincide with periods of widespread glaciation: the Sturtian (c. 730 Ma) and Marinoan (c. 635 Ma) with the Central African Copperbelt (CACB) and the Permo-Carboniferous with the Zechstein or Kupferschiefer (c. 300 Ma) (Hitzman et al., 2010). Although the interrelationships between periods of glaciation, evaporite accumulation and Mg-rich ocean chemistry are poorly understood, they appear to exert a secular control on SHC mineralisation (Hitzman et al., 2010) (Fig. 1.2).

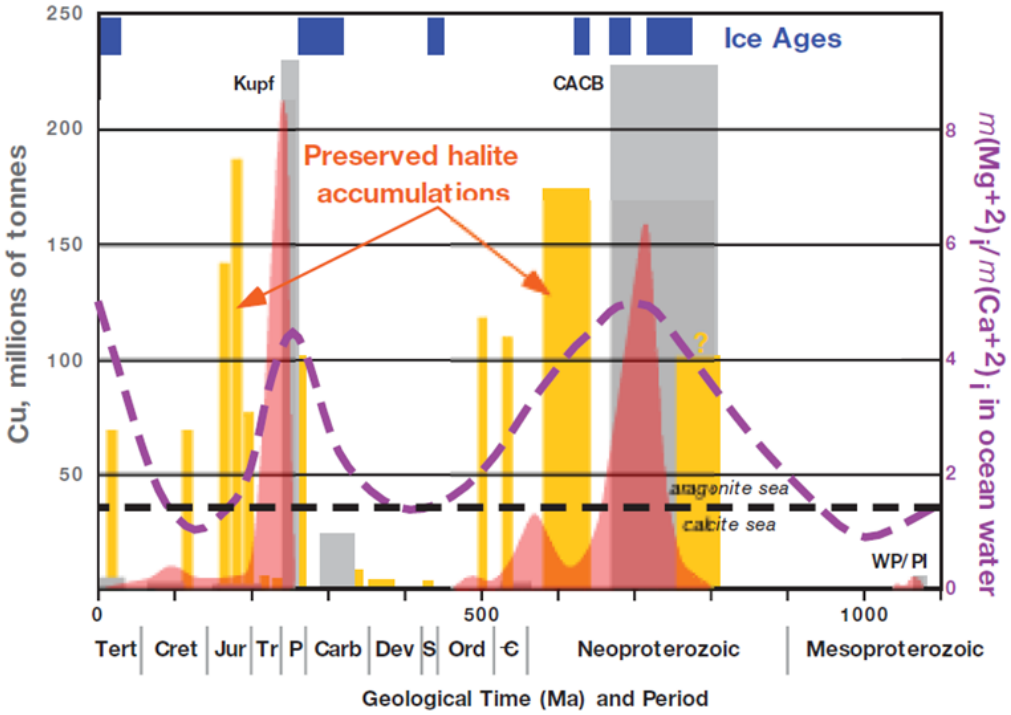

Fig. 1.2. Relationship between the formation of major SHC deposits and the accumulation of halite, global glaciation events and ocean chemistry (Hitzman et al., 2010).

Disassembly of supercontinents resulted in heterogeneous extension of the crust and generation of basins that would ultimately become failed rifts or aulacogens (Brown, 1997). Many of these basins are characterised by a relatively thin fill (2 to 3 km) that may be a function of small degrees of extension of stable and buoyant crust (Hitzman et al., 2005). Unlike passive margins, intracratonic basins were often hydrologically isolated from the oceans for significant periods, permitting the concentration of metals in ground waters (Hitzman et al., 2005). Restricted circulation of surface waters resulted in thick evaporite accumulations and preservation of organic matter in shale that would develop into hydrocarbon source rocks.

Saline fluids responsible for the transport of metals in SHC systems are either residual brines or the product of evaporite dissolution, are oxidised and in equilibrium with redbed aquifers (Hitzman et al., 2005). Evaporites contribute to both the sulphur budget (from gypsum and anhydrite) and Cl- (from halite and residual seawater) which complexes with Cu during metal transport (Rose, 1976). Estimated fluid temperatures during metal precipitation vary from c. 100 to 400˚C (Hitzman et al., 2005). Analysis of fluid inclusions from SHC systems reveal temperatures of ≈120˚C and salinities of 23.3 wt% NaCl eq. in the Kupferschiefer (Tonn et al., 1987); and 72 to 103˚C and 5 to 20 wt% NaCl eq. in the Paradox basin (Morrison & Parry, 1986). Fluid inclusion data from

the Zambian Copperbelt is sparse and data suggest a range of temperatures (110 to 400˚C) and salinities (11 to 39 wt% NaCl eq.) (Selley et al., 2005). Pore fluids transport metals at concentration of c. 10s to 100s of ppm (Hitzman et al., 2005; Brown, 2014), although concentrations of up to 7000 ppm have been reported in the CACB (Davey et al., 2019).Pore fluids often contain a variety of cations including Na, Ca, K and Mg, derived from evaporites, residual brines and leaching of host rocks. These fluids caused widespread alteration in some SHC systems, including calcium, magnesium, potassic and sodic (Selley et al., 2005).

The most commonly ascribed source of metals in SHC systems is the redbeds (e.g. Kirkham, 1989; Hitzman, 2000; Brown, 2005). The breakdown of labile minerals during diagenesis releases K, Fe, Mg, Al and Si as well as heavy metals into pore waters (Walker, 1986). Metals are initially adsorbed onto amorphous iron minerals but as diagenesis progresses, become incompatible with the new products (e.g. hematite) and enter solution in pore waters (Zielinski et al., 1983). In certain basins, mass balance calculations suggest the volume of redbeds is insufficient to account for the known copper resources, and a substantial proportion of the metal must therefore have been derived from other sources such as volcanic rocks and/or basement (e.g. Kupferschiefer, Blundell et al., 2003; CACB, Hitzman, 2000).

The drivers of the large volumes of low metal concentration fluids vary between basins, and basins often record multiple mineralising events (Hitzman et al., 2010). Many SHC deposits formed early in the basin histories during diagenesis and are located on fluid-escape routes, with fluids driven out of the basin towards trap sites by compaction during overburden loading (e.g. Swenson et al., 2004). Tectonism may induce fluid flow through orogenesis or salt tectonics (halokinesis) (Cathles and Adams, 2005). Density driven contrasts may cause brine movement, with thermal gradients caused by lithospheric stretching or magmatic activity (e.g. Blundell et al., 2003), or density contrasts caused by salt dissolution (Koziy et al., 2009). Hydrological gradients may also drive fluid movement in basins (e.g. Brown, 2006; 2008).

Ore deposits commonly nucleate on sites of focused fluid-flow which may include paleo-topographic highs, syn-sedimentary faults, margins of salt diapirs and stratigraphic pinch-outs (Hitzman et al., 2005) (Fig. 1.3). Reduction of oxidised, sulphate-bearing fluids is the dominant mechanism of ore precipitation in SHC systems. Oxidising fluids are progressively reduced across a redox front between

oxidised redbeds and either in situ organic matter (e.g. organic shale) or mobile hydrocarbons (oil or gas) (Kirkham, 1989). Sulphate is reduced to sulphide either prior to mineralisation, as diagenetic pyrite in the upper few meters of the sediment column at <80˚C via bacterial sulphate reduction (BSR), or at temperature > 100˚C via thermochemical sulphate reduction (TSR) (Machel, 1995).

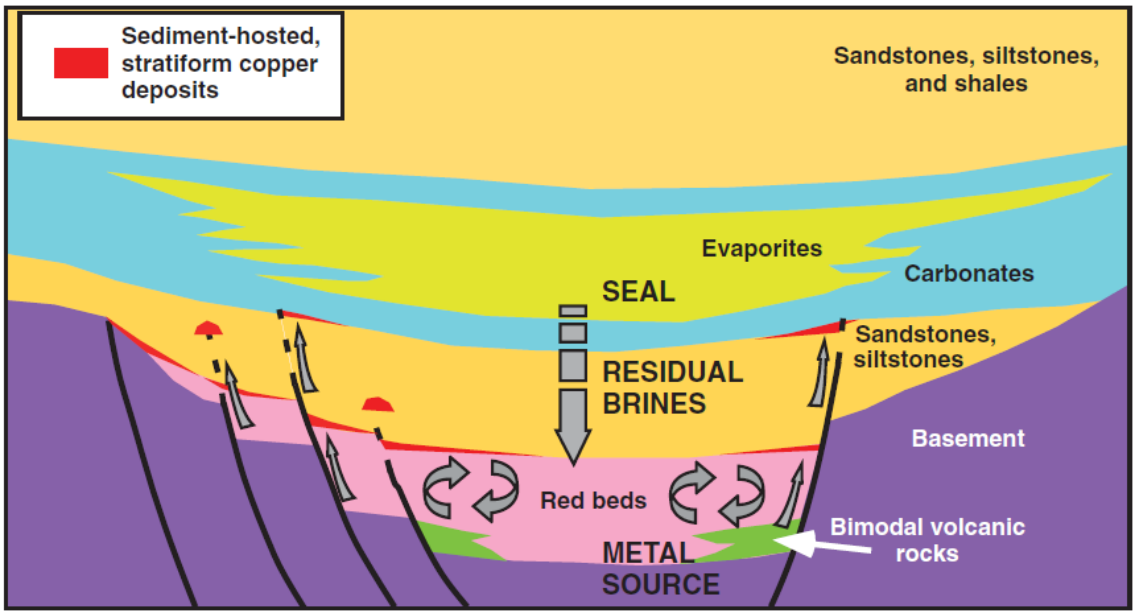

Fig. 1.3. Schematic diagram of a SHC basin (Hitzman et al., 2010).

1.2. Research approach and limitations of previous research

Numerous deposit-scale studies of SHC systems have provided important insights into the mechanisms of ore deposition and certain aspects of SHC systems (e.g. Hitzman et al., 2005 and references therein). These studies elucidate processes at the site of ore deposition and provide an understanding of why the deposits form where they do. Absolute age dating of deposits provides a broad context for the mineralisation but often overlooks the nuances of what else is happening in the basin in the lead-up to, and during mineralisation, in terms of porosity, burial, temperatures, deformation and other factors. Whilst these studies make an important contribution to understanding SHC systems at the deposit-scale, they leave unanswered questions about why certain basins are so well endowed with copper.

Alternative approaches to understanding SHC systems at a basin scale include computational and theoretical models. Computational models simulate fluid

movement in the subsurface in response to an array of different inputs such as porosity, heat flux and aquifer geometry. The results are unbiased and permit modelling in the absence of firm data, but are often stymied by inaccurate inputs and an oversimplification of the subsurface environment. Examples include brine circulation driven by salt dissolution (Koziy et al., 2009) and fluid flow driven by burial compaction (Swenson et al., 2004).

Conceptual models rely on soft observations such as the geometry of basins and the location of major faults controlling sub-surface fluid flow systems. These models are largely unconstrained by hard data and their application is therefore greatest in areas of low data density. Conceptual models of SHC systems include meteoric recharge where a hydrological gradient results in continuous displacement of pore fluids (Brown, 2006; 2008), thermal anomalism inducing convective fluid flow in sub-basins (Jowett, 1986) and latent heat from a caldera driving fluid flow (Brown, 2014; 2017). Conceptual models often inherit our biases around fluid drive mechanisms and do not account for temporal changes in basin geometry, permeability and temperature. However, the models do provide important hypotheses to guide both research and exploration programs.

Many studies combine several of the aforementioned approaches to studying sub-surface fluid flow. Typically, direct dating of mineralisation or coeval alteration minerals provides an age bracket that often corresponds with a significant change in the circumstances of the basin such as deformation, burial or heating. In these scenarios a link between mineralisation and a causal or trigger event can be established. At the Redstone Cu-Ag deposit, Canada, Milton et al. (2017) dated mineralisation at c. 100 m.y. after deposition of the host rocks, determining its formation to be the result of free convection of fluids in a redbed aquifer during a thermal sag phase of basin development. Perelló et al. (2019) dated Cu-Ag mineralisation at Janice Lake, Canada, at 1775 Ma – coincident with the Trans-Hudson orogeny. These approaches provide an important step forward in understanding the formation of SHC systems in the context of regional events but still rely on assumptions around the origin of fluids and fluid pathways, and may overlook important and subtle paragenetic relationships.

The ideal approach, if possible, is to measure parameters directly. This involves obtaining large, coherent datasets from both mineralised and barren portions

of a basin over large geographical areas. Detailed studies at a range of scales are also required to investigate the broader geology of the basins in respect of sedimentology, diagenetic and alteration histories and structure. This project aims to take a truly holistic approach to understanding the White Pine mineral system, and to test some of the platitudes of the sediment-hosted stratiform copper deposit model.

1.3. Selected examples of sediment-hosted copper systems

1.3.1. Central African Copperbelt (Katangan basin)

The Central African Copperbelt (CACB) straddles the border between Zambia and the Democratic Republic of Congo (DRC) and is the world's largest SHC system. Numerous deposits, including eight containing > 10 Mt of Cu metal, are distributed along a 500 km arc (Fig. 1.4) (Hitzman et al., 2012). The pre-mining copper metal endowment of the basin is estimated at approximately 166 Mt and the basin is the world's largest resource of Co (Taylor et al., 2013).

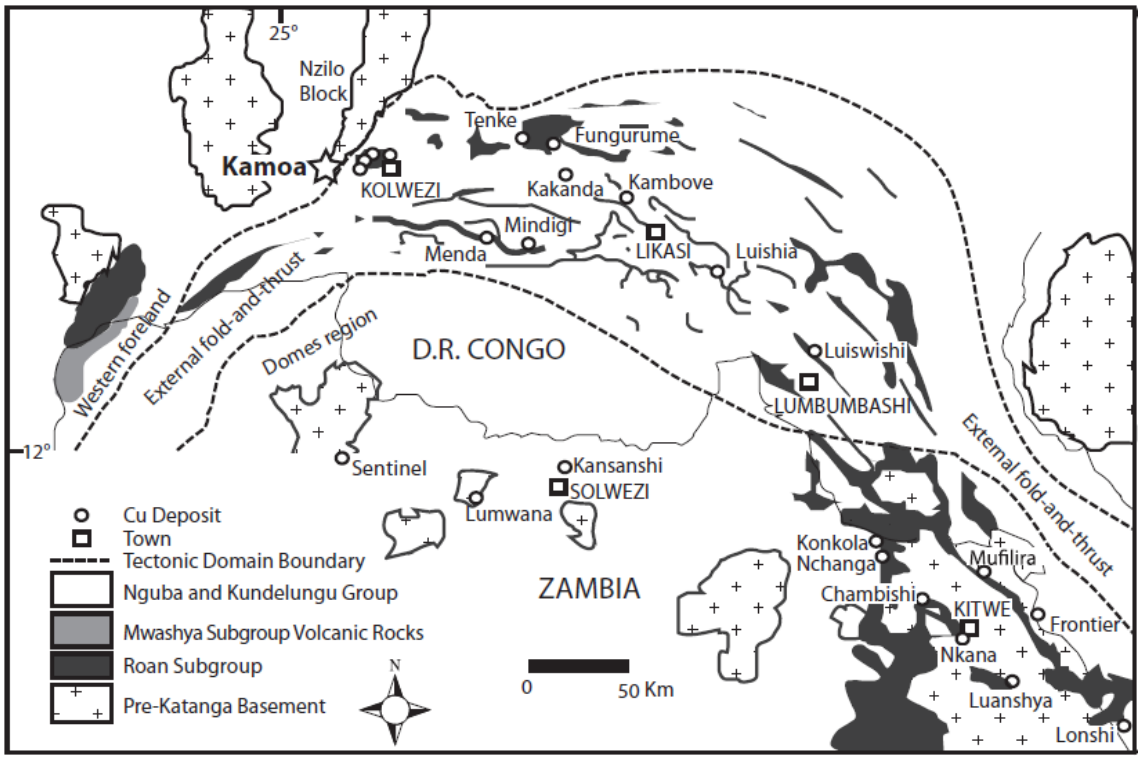

Fig. 1.4. CACB geological map (Cailteux et al., 1994, modified after Schmandt et al., 2013).

The host Katangan basin is one of a series of Neoproterozoic basins between the Kalahari and Congo cratons (Kampunzu and Cailteux, 1999). The stratigraphy of the CACB comprises the Katangan Supergroup (Fig. 1.5) which lies unconformably on

Archaean to early-Neoproterozoic basement (Binda, 1994; Cailteux, 1994). The maximum age of the Katangan Supergroup is constrained by the 883 ± 10 Ma Nchanga granite in Zambia (Armstrong et al., 2005). The Katangan Supergroup is divided into three Groups which can be correlated across the basin, including the stratigraphically lowest Roan Group, the Nguba Group and the Kundelungu Group (Selley et al., 2018).

In Zambia, the Roan Subgroup comprises up to 2,000 m (average 300 m) of sub-arkosic and conglomeritic syn-rift strata in semi-isolated sub-basins. West of the Kafue anticline clastics are locally overlain by the c. 25 m thick, transgressive shale referred to as the Copperbelt Orebody Member. The shale is overlain by coarse siliclastics which are in turn overlain by evaporites and intertidal carbonates of the Upper Roan Subgroup. Stratabound and discordant breccia bodies in this unit are interpreted as the residual material remaining after evaporite dissolution or evacuation (Bull et al., 2011).

Correlation of the Katangan Supergroup between the Zambian and Congolese portions of the CACB is complicated by the absence of exposures of basal stratigraphy in the DRC. The lowest residual breccias in the DRC are overlain by red, argillaceous arenites and siltstones of the Mines Subgroup.

Notable attempts of stratigraphic correlation include the Upper Roan Subgroup of Zambia with the Mines Subgroup of the DRC on a lithostratigraphic basis (Mendelsohn, 1961; Fleischer et al., 1976; Cailteux et al., 1994); Lower Roan Subgroup of Zambia with the Mines Subgroup of the DRC using sequence- and chemostratigraphy (Bull et al., 2011); and Upper Roan Subgroup of Zambia with the Mines Subgroup of the DRC using sequence stratigraphy (Woodhead, 2013). There is broad agreement that the Congolese Dipeta Subgroup correlates with Upper Roan Subgroup stratigraphy in Zambia and records the end of the initial rift phase (Selley et al., 2018).

A second rift phase resulted in a transition from carbonate deposition on a platform to deeper-water locally reduced siltstone facies of the Mwashya Subgroup (Selley et al., 2018). Mafic volcanic rocks dated at c. 765 Ma (Kampunzu et al., 2000) were emplaced into the Upper Roan evaporites during this extensional phase.

The overlying Nguba Group contains the Grand Conglomerate, a glacial diamictite of Cryogenian age (c. 740 Ma, Batumike et al., 2007). The Nguba Group records a progressive widening of the basin with deposition directly onto basement:

e.g. Kamoa (Schmandt et al., 2013) and Fishtie (Hendrickson et al., 2015). A second glacial diamictite, the Petit Conglomerate, was deposited during the Sturtian glaciation (c. 635 Ma, Batumike et al., 2007), marks the base of the Kundelungu Group. The upper portion of the Kundelungu comprises shallow water carbonate and siliclastic rocks.

The basin underwent metamorphism at c. 600 to 560 Ma in response to the Lufilian orogeny and synorogenic intrusive activity (Selley et al., 2018). Metamorphic grade averaged greenschist facies but generally increases towards the Kafue anticline and the Domes region of Zambia (Bernau et al., 2013).

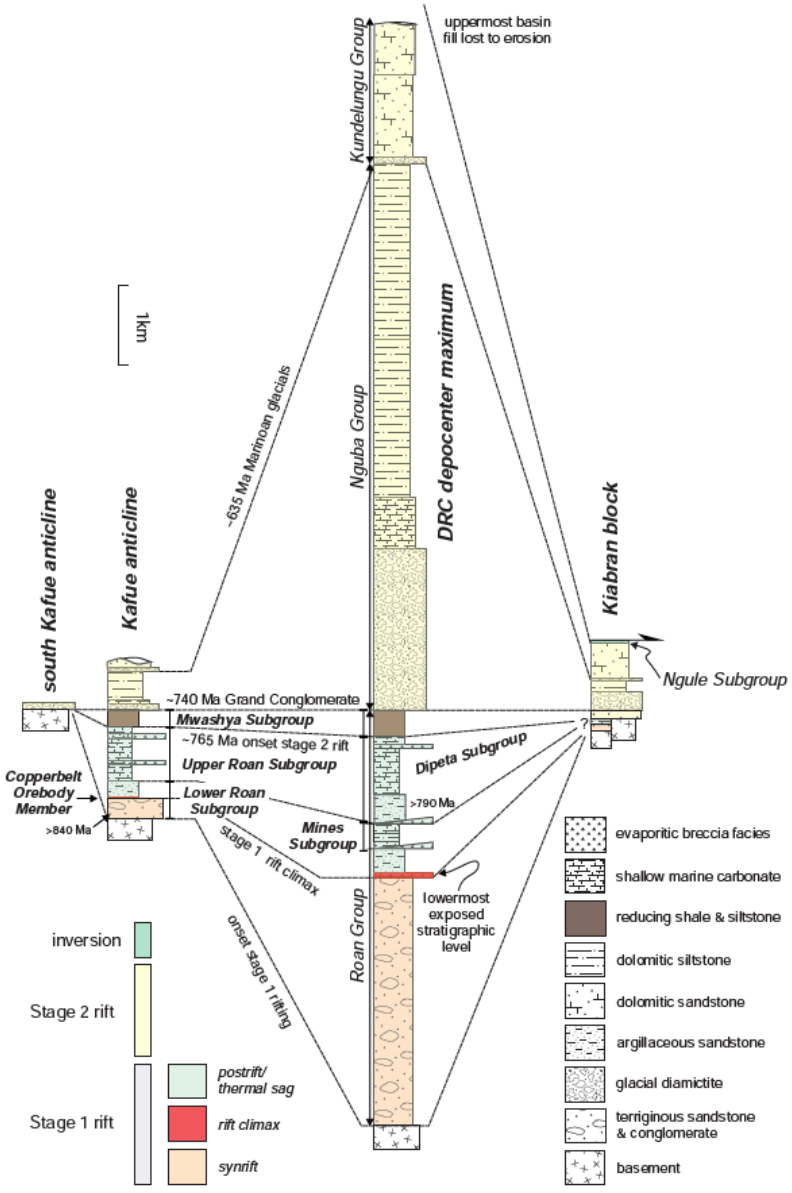

Fig. 1.5. Comparative stratigraphy of the ZCB (Kafue anticline) and CCB (DRC depocenter) (Selley et al., 2018).

Ore deposits in the CACB exhibit a varied array of styles, metal associations, ages and host lithologies. Deposits occur at multiple stratigraphic levels from the basement (e.g. Lumwana, Bernau et al., 2013), to the Grand Conglomerate at the base of the Nguba Group (e.g. Kamoa, Schmandt et al., 2013), and in isolated cases, in the Kundelungu Group (e.g. Dikulushi, Dewaele et al., 2006).

Once considered syn-sedimentary in origin (e.g. Bateman, 1930), there is now broad agreement that the deposits of the CACB are epigenetic and formed at multiple times during the basin history (Hitzman et al., 2012). Recent Re-Os dating by Sillitoe et al. (2017) suggested all mineralisation formed at 540 to 490 Ma but this is widely disputed on the basis that it discounts a considerable amount of rock observations that suggest otherwise (e.g. Hitzman and Broughton, 2017; Muchez et al., 2017). Mineralisation was accompanied by widespread alteration, both stratiform and around faults and veins, which reflected an evolving hydrological system (Hitzman et al., 2012).

Early, syn-diagenetic ores typically contain disseminated mineralisation in interstices and post-date diagenetic gangue minerals (Hitzman et al., 2012). The earliest example of syn-diagenetic mineralisation is Konkola, dated at 816 Ma by the Re-Os isochron method (Barra et al., 2004). Arenite-hosted deposits may also show precipitation of ore minerals with interstitial hydrocarbons (e.g. Mufulira, Muchez et al., 2019). Early stratiform ore fluids display residual brine signatures, rich in Mg and K, causing dolomitisation and silicification of carbonate units and potassium feldspar alteration of clastic rocks below the Mwashya Subgroup (Selley et al., 2018). Magnesian alteration in the form of chlorite, tourmaline and magnesite is particularly well developed around evaporite horizons in the DRC. Congolese-style écailles or rafts are interpreted to have been mineralised prior to disaggregation of the host beds during halokinesis (Hitzman et al., 2012).

Post-orogenic ores are commonly located at higher stratigraphic levels than early ores and are typically quartz-calcite veins accompanied by albite alteration, such as Kansanshi, dated at 512 to 503 Ma by Re-Os (Torrealday et al., 2000). Later deposits are often associated with Cu, U, Mo and Au (Hitzman et al., 2012). Fluid inclusions from late ore deposits typically display halite dissolution signatures, accounting for the widespread Na-alteration (Selley et al., 2018). One of the youngest deposits in the

CACB is Kipushi, comprising breccia-pipe hosted Cu, Pb, Zn and Ge ores dated at 451 Ma by Re-Os (Schneider et al., 2007).

Despite their diverse nature, deposits in the CACB share several common denominators (Hitzman et al., 2012). Ore minerals were precipitated across a redox gradient, from oxidised rocks to reduced rocks containing in situ organic matter or mobile hydrocarbons. Ore is also zoned at a range of scales, from the scale of individual minerals to across reduction zones. Deposits nucleate on the margins of domes where thinned stratigraphy focused fluids into overlying reduced strata, and adjacent to syn-sedimentary faults which focused fluid flow and provided cross-stratal fluid conduits. Salt beds served as long-lived aquicludes, channelling fluids to the peripheries of the basin or discrete rupture points.

Supergene weathering of ore deposits in the CACB has resulted in significant increases in ore grades, and a change from sulphide to oxide-dominated mineralogy in many CACB deposits.

1.3.2. Kupferschiefer (Zechstein basin)

The unmetamorphosed Permian age Zechstein basin (Fig. 1.6) contains the supergiant "Kupferschiefer" deposits of western Poland (Jowett et al., 1986; Vaughan et al., 1989; Wodzicki and Piestrzyński, 1994). Historic production and remaining reserves at the largest of the deposits, Lubin-Sieroszowice, is estimated at c. 68 Mt of copper metal (Hitzman et al., 2005) although the basin may contain up to 350 Mt of Cu metal (Cathles et al., 1993). The deposits are also an important source of Ag, Pb, Zn, Au and Platinum Group Elements (PGE) (Oszczepalski, 1999).

Three principal basement terranes are identified beneath the Zechstein basin: the Eastern European craton to the NE, the central Epi-Caledonian platform and the Epi-Variscan Platform to the SW (Bechtel et al., 1996). The Epi-Variscan terrane which underlies the major Cu deposits was deformed during the late Carboniferous Variscan orogeny and contains coals that are the source of methane accumulations in the Zechstein stratigraphy (Hitzman, 2005).

Basal rocks of the Zechstein basin (Fig. 1.7) are the 300 to 290 Ma Rotliegendes continental redbeds, deposited in sub-basins either side of Wolsztyn Highlands with a thickness > 1000 m (Vaughan et al., 1989). The lower Rotliegendes contains Autunian bimodal volcanics. Upper Rotliegendes include fluvial conglomerate

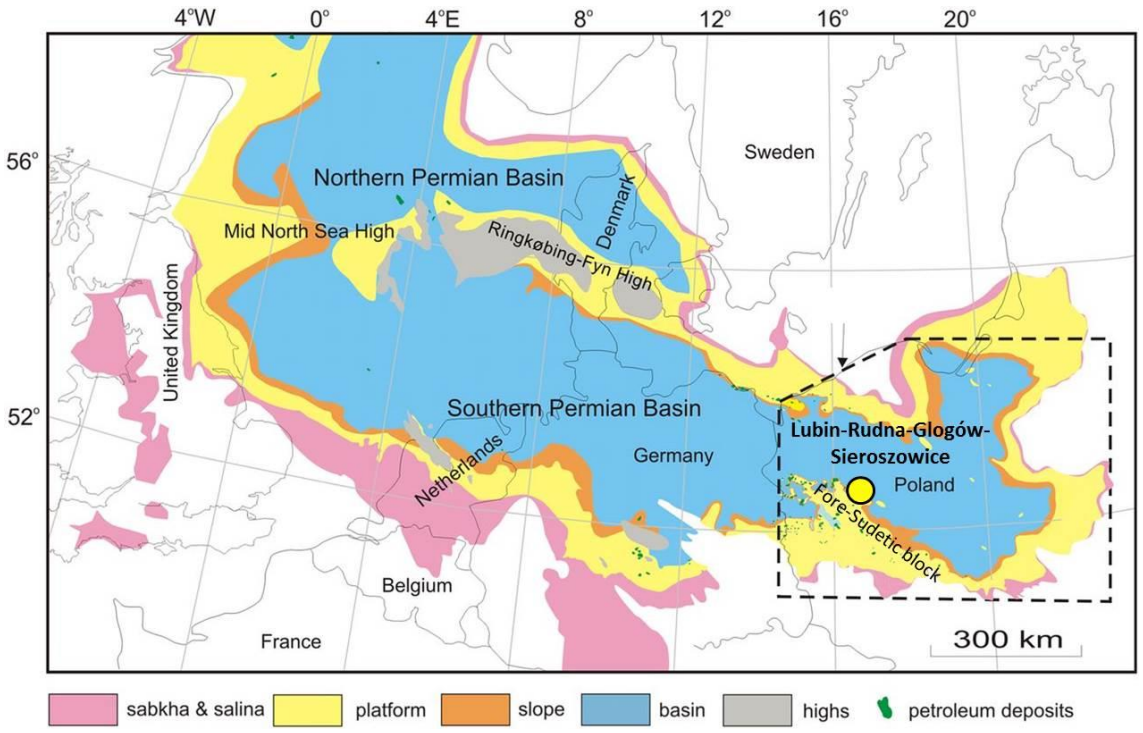

Fig. 1.6. Facies map of the late Permian Z2 carbonate in the Zechstein basin (Słowakiewicz and Mikołajewski, 2011).

and sandstone, aeolian sandstone and sabkha deposits. The Rotliegendes is overlain by white Weissliegendes sandstones. The Kupferschiefer shale abruptly overlies the continental sandstones and is dated by the Re-Os isochron technique at 257 ± 1.6 Ma (Brauns et al., 2003) to 247 ± 20 Ma (Pašava et al., 2010). The Kupferschiefer shale is up to 30 cm thick (Wodzicki and Piestrzyński, 1994) and represents a marine transgression into the basin from the NW and marks the first of four shale-carbonate-anhydrite-halite cycles termed Z1 to Z4. Triassic extension resulted in further clastic sedimentation above, and the deposition of 600 to 800m of continental Buntsandstein sandstone and mudstone. Alpine compression during Mesozoic to Cenozoic resulted in weak basin inversion and closure.

Cu mineralisation is restricted to the southern limit of the Zechstein basin. Mineralisation occurs in upper Rotliegends sandstone to lower Zechstein limestone, rising to higher stratigraphic levels around the Fore-Sudetic block (Jowett, 1986; Speczik, 1995). A significant proportion of ore is located in the Weissliegende sandstone underlying the Kupferschiefer and in the overlying Zechstein dolomite (Hitzman et al., 2005; Symons et al., 2011). Mineralisation exhibits lateral and vertical zoning, from hematite (termed the Rote Fäule) through chalcocite, bornite and

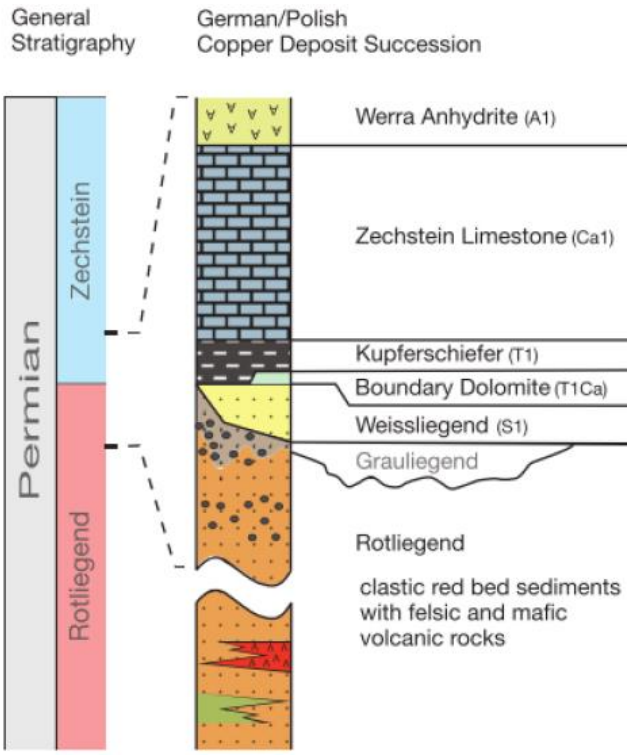

Fig. 1.7. Simplified Rotliegend – Zechstein (ore bearing) stratigraphy (Borg et al., 2012).

chalcopyrite to Pb Zn (Jowett, 1986; Vaughan et al., 1989; Wodzicki and Piestrzyński, 1994).

Disseminated ores display replacement of framboidal pyrite and inherit the sulphur isotope signature of bacterial sulphate reduction with $\delta^{34}S$ values of -30 to -35 ‰ (Sawlowicz, 1989; Jowett et al., 1991). Ores associated with massive anhydrite bodies at structural highs (e.g. paleo-dunes) display $\delta^{34}S$ values of -10 to -20 ‰, indicating down-welling of fluids derived from Zechstein marine evaporites (Wodzicki and Piestrzyński, 1994). Fluid inclusions contain average salinities of >23.3 wt% NaCl eq. (Tonn et al., 1987). There is no evidence that fluids reached stratigraphic levels higher than the basal Zechstein evaporites.

Zonation of the Rote Fäule and copper mineralisation suggest the dominant fluid direction of fluid migration was towards ENE, controlled by faulting or lithology (Hitzman et al., 2005). Permo-Triassic heat flow and helium isotope anomalies around the Wolsztyn Ridge suggest deep-circulation of brines into the basement, which drove the fluid system and leached metals from the Rotliegendes and basement rocks (Blundell et al., 2001; 2003).

The timing of ore formation is debated and different geochronology techniques date different components of the ore system at between 255 to 53 Ma (see

Alderton et al., 2016 and references therein). Paleomagnetism ages of the Rote Fäule hematite zone vary from 250 to 255 Ma (Jowett et al., 1987; Nawrocki, 1997; Torsvik et al., 2001). K-Ar ages of authigenic illite in mineralised Kupferschiefer shale range from 190 to 216 Ma and record a waning of the hydrothermal system (Bechtel et al., 1999). Ore mineral veinlets directly dated by the Re-Os techniques are 212 Ma (Mikulski and Stein, 2012).

1.3.3. Dzhezkazgan (Chu-Sarysu basin)

The Dzhezkazgan, Zhaman-Aibat and the Zhilandy cluster of sandstone-hosted SHC deposits are located in the Chu-Sarysu basin of Central Kazakhstan. The largest of the deposits, Dzhezkazgan, contains an estimated 2 billion tonnes of ore at an average grade of 1.1 % Cu, (22 Mt of Cu metal) (Box et al., 2012). The principal ore minerals, in order of abundance, are chalcocite, bornite and minor chalcopyrite. Significant accessory metals include Pb, Zn, Ag and Re (Box et al., 2012). The group of deposits are located at the northern end of the present-day limit of the Chu-Sarysu basin (Fig. 1.8). The basin is elongate north-south along a suture between Proterozoic continental blocks. Basement is Proterozoic to Paleozoic strata intruded by early Devonian granites.

Basin fill is divided into four units (Fig. 1.9) (Syusyura et al., 2010). The first and stratigraphically lowest unit is a 1 to 2 km thick sequence of early to mid-Devonian intermediate volcanics which transition upwards into mid- to upper-Devonian continental red beds. The second is a 1 to 2 km thick sequence of upper Devonian to Mississippian limestones and dolomites with lagoonal evaporites, which formed part of southward-facing passive margin, and is capped by shale. The third sequence is a c. 1 km thick package of Pennsylvanian continental red beds of alluvial facies, which hosts Cu mineralisation. The forth unit is a 1 to 2 km thick sequence of fine-grained red clastics and salt deposited in a lacustrine environment, which grades up into non-marine fine-grained clastics and limestones.

The structural history of the Chu Sarysu basin is unclear. Alexeiev et al. (2009) proposed a foreland basin model related to northeast-directed thrusting but this contradicts isopach maps which demonstrate a symmetrical basin-fill geometry(Bykadorov et al., 2003). The timing of major faults including the Kokshetau and Karatau faults is uncertain (Box et al., 2012). Evidence of paleo-topography within

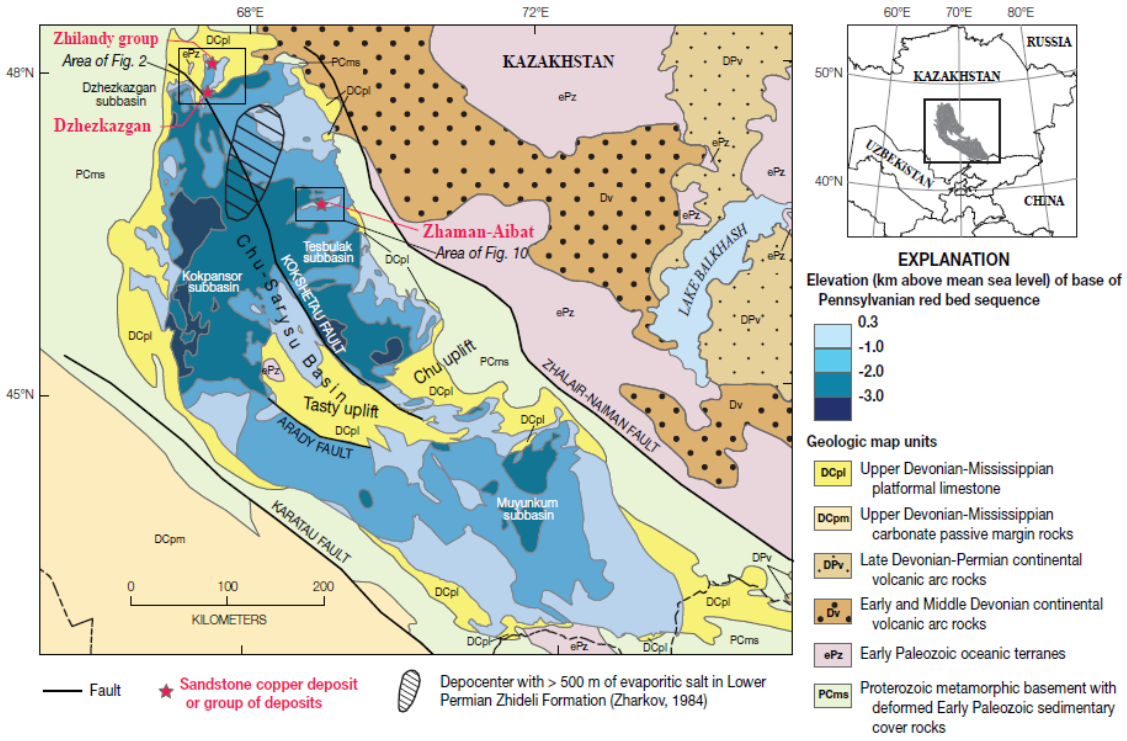

Fig. 1.8. Map of elevation of the base of the Pennsylvanian red bed unit in the Chu Sarysu basin with deposit locations marked (Box et al., 2012).

the basin is provided by distinct Permian salt (Zhidelisai Formation) sub-basins and thinning of the Pennsylvanian redbeds (Dzhezkazgan Formation) over the Kingir anticline (Gablina, 1981). Rocks were deformed by two near-orthogonal phases of upright folding: an early east-trending set (F1) and a later north-trending set (F2) (Allen et al., 2001). Map patterns and the long (10s of km-scale) length of folds are strongly suggestive of salt tectonics.

Re-Os ages of chalcopyrite and bornite mineralisation from the Dzhezkazgan deposit range from 309 to 299 Ma (Box et al., 2012). This overlaps with the age of the youngest parts of the Dzhezkazgan Formation and is in agreement with the pore-filling (early diagenetic) nature of copper mineralisation. Surface water at the time of ore formation was likely meteoric, suggesting ore-forming brines obtained salinity via dissolution of underlying marine evaporites or overlying lacustrine evaporites. The Pb-isotope composition of galena ore suggests derivation of Pb, and likely other metals, from Pennsylvanian red beds (Box et al., 2012). The absence of contemporaneous igneous activity and the presence of djurleite suggest maximum temperatures of 93˚C (Rose, 1976) with brine circulation driven by density contrasts related to salt dissolution. Low temperatures and negative sulphur isotopes suggest sulphide

precipitation via bacterial sulphate reduction (BSR), although the origin and composition of the sulphate source is uncertain (Box et al., 2012). Early hydrocarbons, likely dominated by gas, filled F1 anticlines and resulted in widespread bleaching or hematite destruction of the ore horizon. Unfolding and reconstructing early stratal geometries demonstrates ore was deposited in structural lows where F1 anticlines are crossed by F2 synclines; pathways for dense brines evacuating or circulating along the base of the aquifer. Mineral zoning within ore bodies elucidates the directions of fluid flow in individual deposits (Box et al., 2012).

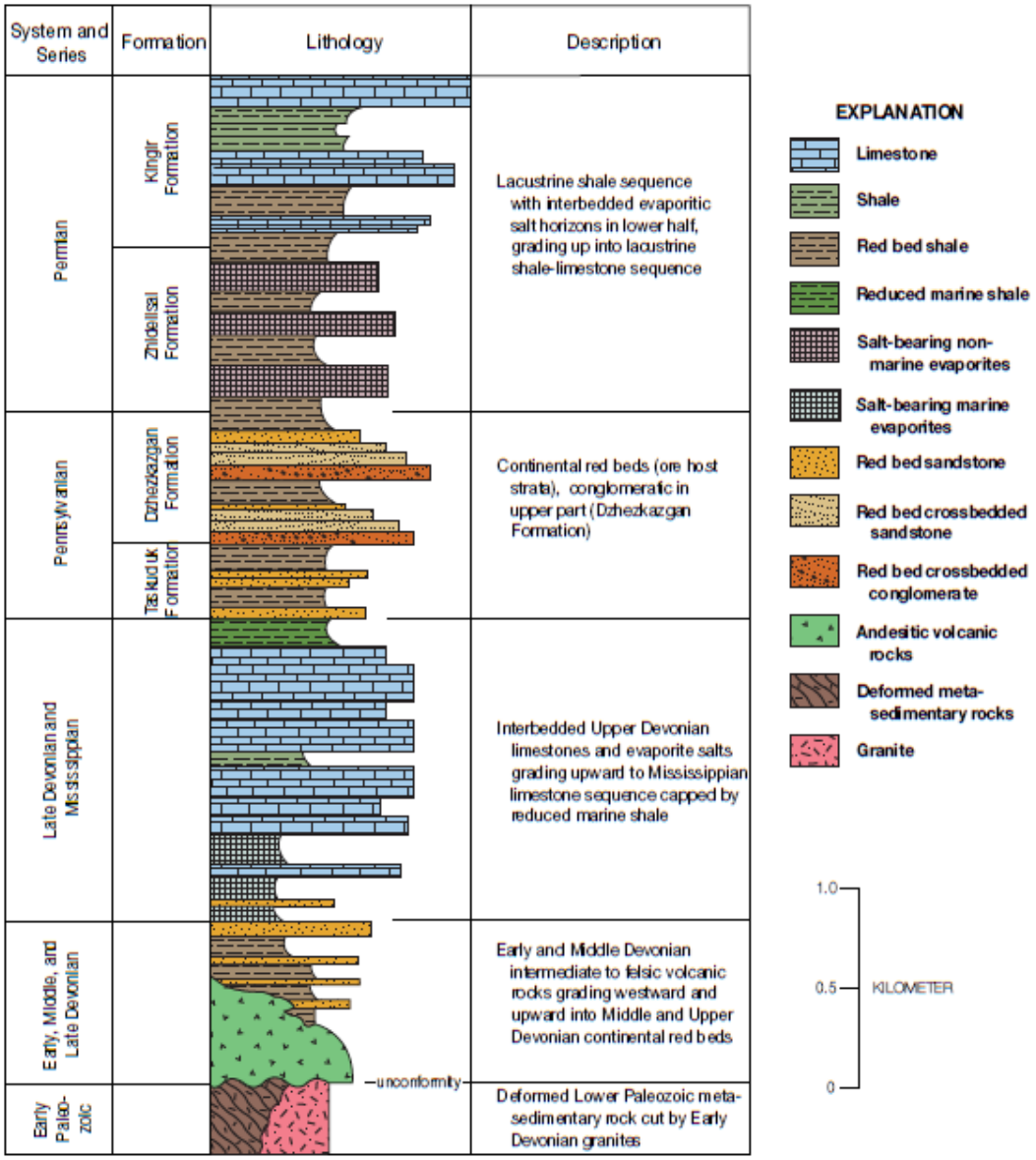

Fig. 1.9. Stratigraphy of the Chu Sarysu basin (Box et al., 2012).

1.4. Project justification and aims

1.4.1. Why study the Midcontinent Rift and White Pine?

Of the approximately 20 basins known to host significant quantities of sediment-hosted copper mineralisation, the vast majority of resources are located in six of these basins. The Central African Copperbelt (CACB), Kupferschiefer and Udokan (Russia) systems host supergiant deposits defined as containing >24 Mt of copper metal. Three other basins host deposits containing >2 Mt of copper metal: Dzhezkazgan, Aynak (Afghanistan) and White Pine. Research into the formation of the largest sediment-hosted copper deposits must therefore include one of these districts (Hitzman et al., 2005).

Logistics in the United States of America are more straightforward than in alternative countries. The Midcontinent Rift System (MRS) affords an abundant archive of the rocks in the form of readily accessible drill cores and surface exposures over a large (>250km-long) portion of a basin; a dataset not available in other basins. In addition, significant amounts of mineral exploration, oil and gas exploration and government-funded research provides a rich understanding of the broader geology of the basin, and a framework within which to interpret the mineralising system. These data includes high-precision geochronology, geophysical surveys, geochemistry and well-established stratigraphic correlations. The rocks were subject to almost no post-mineralisation alteration overprint, weathering or structural re-organisation and provide a rare opportunity to study near-pristine Proterozoic rocks. The simplicity of the Cu-bearing stratigraphy of the Midcontinent Rift System – a single redbed aquifer overlain by a single reducing horizon – removes a degree of complexity.

1.4.2. Uncertainties in the understanding of White Pine and the MRS

The late-Mesoproterozoic (c. 1.1 Ga) age of the Midcontinent Rift System distinguishes it from other major SHC districts as it marked a period of supercontinent assembly (Cawood and Pisarevsky, 2017). In contrast, other deposits formed during periods of continent break-up (Jowett, 1989; Brown, 1997; Hitzman et al., 2010). The disassembly of Rodinia at c. 750 Ma coincided with the formation of the CACB, Aynak and Redstone deposits and the break-up of Pangea at c. 260 Ma coincided with the formation of the Kupferschiefer, Permian basin (USA) and Dzhezkazgan (Hitzman et al., 2005).

Many SHC systems are characterised by the presence of bimodal volcanic rocks, particularly in the lower, syn-rift stratigraphy. Whilst the MRS contains both mafic and felsic rocks, the enormous volume of the flood basalts comprising the lowermost 20 km of the Keweenawan Supergroup are particularly striking (Ojakangas et al., 2001). Basaltic rocks may constitute a rich source of Cu and other metals in many SHC basins and allude to significant heat flux in the lower crust which may have driven fluid flow.

The MRS is also unique amongst major SHC districts in that the Oronto Group was purportedly deposited in an entirely lacustrine environment (Elmore, 1989; Suszek, 1997; Stewart and Mauk, 2017). Many basins that host SHC systems record a degree of restriction and periods of isolation from oceans (e.g. Hitzman et al., 2010), they are characterised by the presence of marine bedforms and, or, ichnofacies. In addition, only isolated examples of evaporite minerals have been reported in the Copper Harbor Formation (Elmore, 1984). The absence of significantly saline surface water in the basin history is problematic for the transport of metals in solution, although Brown (2006; 2008) suggested meteoric water could have been responsible for the formation of SHC deposits in the basin.

Although the MRS is one of the most studied rift system in the world, the interplay between fluid flow, diagenesis, alteration and mineralisation is seldom described or discussed with respect to its SHC deposits. Moreover, previous studies have made little reference to the timing, style and significance of gangue mineralogy which played a key role in the evolution of fluid-pathways, particularly in the Copper Harbor Formation aquifer.

Sediment- and volcanic rock-hosted copper deposits of the Keweenaw Peninsula are notable for the dominance of native copper and chalcocite over Cu-Fe-sulphides such as bornite and chalcopyrite; the typical ore minerals of SHC deposits. This association suggests precipitation of ore minerals under unique conditions.

At least two phases of mineralisation are reported at White Pine. Early disseminated-style mineralisation dominated by chalcocite forms a peneconcordant zone in dark siltstones in the basal Nonesuch Formation (White and Wright, 1954; Ensign et al., 1968; Brown, 1971). A second stage of native copper-dominated mineralisation overprints the disseminated ore and is spatially associated with reverse faults in the southwest portion of the deposit (Mauk et al., 1992). A third style of

mineralisation, possibly coeval with one of the other two styles, is native copper in pyrobitumen-bearing sandstones of the upper Copper Harbor Formation (Brady, 1960; Hamilton, 1967). The relationship between these mineralising events, and other geological events that affected the basin, remains unclear.

1.4.3. Key questions

What was the paleo-environment?

Depositional environment plays a primary role in the nature of sedimentary deposits and initial pore fluid compositions. Sediment grain size and composition, the nature of sedimentary bedforms, the lateral continuity of units and early diagenetic cements determine the initial rock properties. Evaporitic and sabhka environments may promote the formation of salt and saline brines amenable to transporting metals. Water bodies with restricted circulation may also promote deposition of evaporite minerals and the preservation of organic matter that develops into reductants.

What was the rate of sediment accumulation and what controlled it?

Burial compaction is postulated to have been a key driver of fluids in the MRS. Precise geochronological dating of the Upper Keweenawan Supergroup will constrain rates of overburden accumulation and the thickness of overburden at the time of mineralisation. Airy “backstripping” of sedimentary and volcanic units, to remove the effects of sediment loading, will isolate the amount of subsidence attributable to tectonic stretching. This will inform an understanding of the amount and timing of crustal thinning which may have provided thermal energy into the mineralising system.

What was the timing, nature and extent of faults?

Faulting can have a variety of effects on fluid flow in sedimentary basins. Faults are commonly regarded as vertical fluid conduits, but faults lined with impermeable gouge may inhibit lateral fluid flow yet permit vertical passage of fluids, acting as barriers that compartmentalise an aquifer. Faults with large vertical offsets may juxtapose different lithologies and either seal aquifers or rupture aquitards. Syn-rift clastic sequences that fill graben and half graben structures may display good aquifer properties but faulting may dismember the units into small, hydrologically isolated “sub-basins”. Syn-sedimentary or growth faulting can produce facies and thickness variations which have

significant effects on fluid flow pathways, with strong asymmetry between the permeability of the foot wall and hanging wall.

What were the principal fluid pathways and how did they evolve over time?

We will define the principal flow routes of formation waters and liquid hydrocarbons. Fluid migration pathways include primary porosity (pore throats), secondary porosity (voids created by mineral dissolution) and fractures (faults and veins). Migration pathways will change over time in response to reactions between fluids and wall rocks. Establishing key paragenetic relationships and the spatial distribution of diagenetic and alteration minerals will facilitate the mapping of these processes. The "plumbing system" is also a function of the distribution of aquifers and aquitards, so mapping the extent of lithogical or diagenetic facies is also important.

What was the timing of fluid flow?

Fluids in sedimentary basins move in response to external forces such as burial, tilting, deformation and heating. Fluid flow events may be protracted or short-lived and may produce mineralisation, or diagenetic and alteration mineral assemblages. Understanding the timing and duration of these fluid flow events, and placing them in the context of the broader basin evolution, is imperative for understanding driving mechanisms, pathways and prevailing conditions.

What was the origin and composition of the mineralising fluid?

The composition of formation waters is a function of the initial surface water and its interaction with, or buffering by, host rocks. The fluid composition in the majority of SHC systems is considered to have been oxidised, metal-bearing (including Cu and S) and saline. It is not intuitive how, in a lacustrine setting, the requisite concentrations of Cl^- and SO_4^{2-} would be attained.

Why is there an abundance of chalcocite and native copper?

The MRS is unique for the abundance of native copper and chalcocite which suggest a paucity of sulphur in mineralising fluids. However, the presence of pyrite in barren shales and a purported change from temporally early, disseminated chalcocite ore to

later, structurally-controlled native copper suggests sulphate availability in the basin fluctuated with time.

What was the temperature of ore formation?

Documenting peak temperatures is fundamental to understanding the mechanisms of ore formation. Several key processes are sensitive to temperature, including sulphate reduction, metal solubility, mineral stability fields and petroleum maturation. Peak temperature estimates can also be cross-referenced against known overburden thicknesses to constrain geothermal gradients.

Can alteration be distinguished from diagenesis?

The distinction between diagenetic processes, which are common to all basins, and alteration related to mineralising processes, is crucial knowledge for appraising a basin's prospectivity.

1.4.4. Research aims

Cross section along the southern margin of the MRS

A large-scale cross section spanning approximately 200 km parallel to the axis of the MRS, along the southern shoreline of Lake Superior, will be constructed and include the Copperwood and White Pine deposits as well as copper prospects and barren parts of the basin. It will show the mineralisation in the context of the large-scale lithological units. The geological cross section can be integrated with reflection seismic data to enhance the understanding of the subsurface structure.

Subsidence model

Integration of sedimentary and volcanic unit thicknesses from interpretations of reflection seismic sections with high-precision U-Pb geochronology will permit accurate determinations of depositional rates. Backstripping of units to remove the effects of sediment loading, compaction and the weight of the water column will enable the analysis of the timing, cause and amount of extension (Allen and Allen, 2005).

Mineral paragenesis

The relative timing of the precipitation and dissolution of minerals, formation of veins and movement of faults will be established in a paragenesis for the MRS. This paragenesis will be augmented by dating of specific phases to provide absolute age constraints.

Genetic model of mineralisation in the MRS

Data from all sources – geological, stable isotope, hyperspectral, clay mineralogy and geochronology – will be synthesised into a holistic model of copper mineralisation in the MRS. The model will include the development of the basin from sedimentation through diagenesis, fluid chemistry and flow evolution, and alteration and mineralisation events.

1.4.5. Research methods and techniques

Drill core logging and outcrop mapping

Logging of exploration drill cores and mapping of surface exposures will provide information on lithology, structure and visible alteration. Interpretation of sedimentary facies will provide insights into both the depositional environmental and the subsurface nature of units including their likely porosities and geographical extents. Mapping or logging of alteration, mineralisation and structures will demonstrate key relationships and the extend of these processes.

Paragenesis

Petrographic examination of key lithological and alteration units will be completed early in the project. This will establish a detailed paragenetic sequence for diagenetic minerals and textures against which later alteration and mineralisation overprints can be referenced. It will also distinguish between detrital and authigenic phases and the relationships between cross-cutting, replacement and dissolution features.

XRD

A significant proportion of the low-temperature diagenetic minerals in the Oronto Group are clays. The composition of the clay fraction (<2µm) of sediments can be determined by powder X-ray diffraction (XRD) analysis. Information on the polytypes

(detrital versus authigenic) and crystallinity can also be obtained. The crystallinity of illite, which can be calculated from the 1nm diffraction peak, is a proxy for peak temperature.

Stable isotopes

Geological processes may cause fractionation of stable isotopes, leaving unique "fingerprints" that permit identification of causal processes. Differences between the isotopic composition of elements in fluids from those in rocks enable identification of paleo-fluid pathways and calculations of fluid:rock ratios. We intend to use carbon and oxygen isotopes to map processes including thermochemical and bacterial sulphate reduction, oxidation of organic matter by formation water and to estimate fluid:rock ratios. Sulphur isotope analysis will inform an understanding of the origins of sulphur and the mechanisms of sulphide ore formation.

Geochronology

Direct dating of copper sulphides by the Re-Os technique will provide the first ages of mineralisation at White Pine. High precisions U-Pb dating of zircons by chemical abrasion isotope dilution thermal ionization mass spectrometry (CA-ID-TIMS) will be employed to define the ages of igneous rocks (tuffs, flows and intusive rocks). Samples will be selected on the basis of improving the accuracy of age constraints on key geological units, particularly the Oronto Group, and key events such as basin inversion.

Seismic interpretation

Two-dimensional reflection seismic sections available from the United States Geological Survey (USGS) and state Geological Surveys will be re-interpreted to provide a robust understanding of stratal geometries. The 2D data will be interpreted in Leapfrog software to produce a 3D geological model of the basin and the White Pine deposit.

Subsidence analysis

Modelling of subsidence rates with "Backstrip" software (http://www.ux.uis.no/~nestor/work/programs.html) will permit analysis of basin subsidence from observed stratigraphic columns to understand the causes of basin formation.

1.5. Background

1.5.1. The Midcontinent Rift System

The Mesoproterozoic (~1.1 Ga) Midcontinent Rift System (MRS) is a c. 2000 km-long arcuate feature located in central North America (Fig. 1.10) (Hinze et al., 1997). The MRS is characterised by a suite of dense and magnetic rocks that dissect the Archaean Superior craton and Proterozoic terranes accreted to its southeast margin (Whitmeyer and Karlstrom, 2007). The width of the MRS varies from 75 to 150 km and is filled with a lower sequence of c. 20 km of basaltic volcanic rocks and an upper sequence of c. 10km of sedimentary rocks that constitute the Keweenaw Supergroup (Ojakangas et al. 2001). The MRS is noteworthy amongst rifts for its great length and the volume of mafic igneous rocks that is comparable with Large Igneous Provinces (LIPs) (Stein et al., 2015). Multiple felsic and ultramafic bodies are present within the Keweenaw Supergroup that are contemporaneous with the majority of flood basalts (Vervoort et al. 2007).

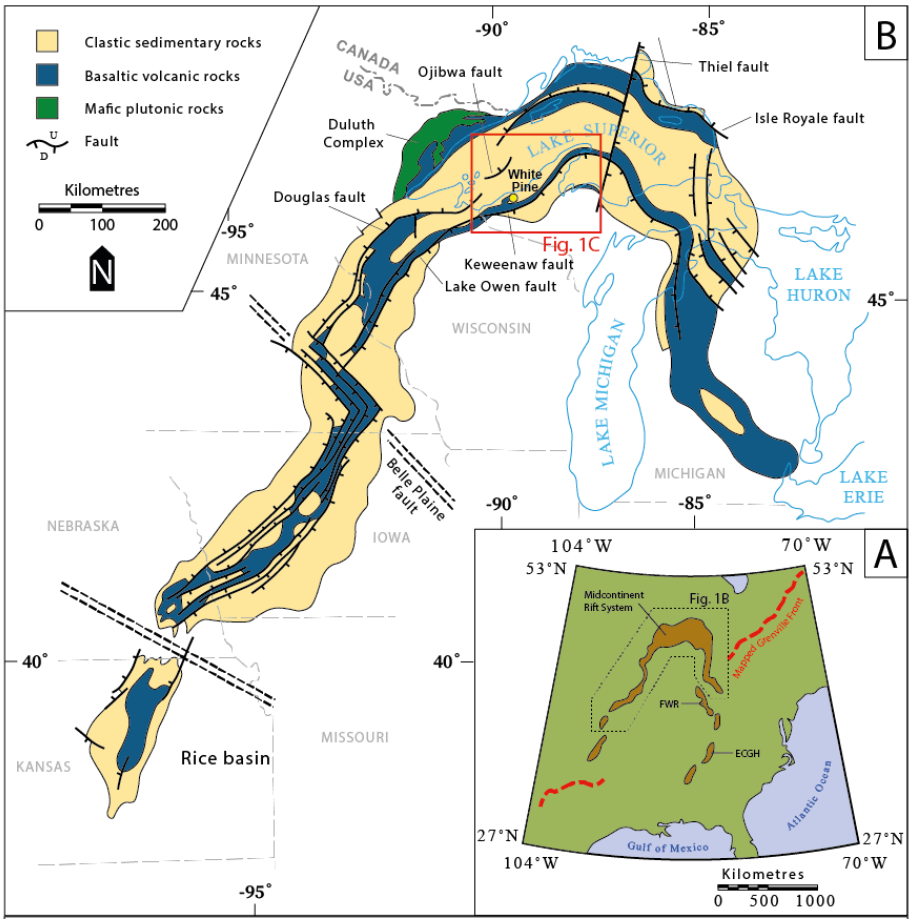

Fig. 1.10. (A) Geological map of MRS in North America (modified after Dickas, 1986). **(B)** Simplified map of the location of the MRS in North America (Stein et al., 2018).

Extension in the MRS is interpreted to have commenced at the switch from strike-slip to extensional plate motion between Amazonia and Laurentia at c. 1120 Ma (Tohver et al., 2006), that is recorded in Laurentia's apparent polar wander path as the 1100 Ma Logan Loop (Stein et al., 2014). Estimates of maximum crustal extension beneath the MRS vary from 32 km (Stein et al., 2015) to ~75km (Chandler 1983). The focus of extension on master faults, such as the Keweenaw fault, resulted in the unusually thick accumulations of lower Keweenawan volcanic rocks (Dickas and Mudrey 1997). Flood basalt volcanism ceased at c. 1090 Ma and the subsequent accommodation space was generated by thermal sag and filled with sediments (Stein et al., 2015). Rb-Sr ages of reverse faults suggest inversion occurred at 1060 ± 20 Ma (Cannon et al., 1993). The cause of rift cessation, and the failure of the MRS to develop into a seafloor spreading centre, is debated. Cannon (1994) invokes Grenville orogenesis, where the deformation front migrated westward across Laurentia before eventually impinging on the eastern wide of the MRS. Stein et al. (2018) argue the Grenville Front is located further east, towards the Appalachian Mountains, and that a re-arrangement of microplates on the eastern margin of Laurentia resulted in extension shifting away from the MRS.

1.5.2. The Keweenaw Supergroup

The Keweenaw Supergroup (Fig. 1.11) in Michigan's Upper Peninsula is approximately 30 km thick and lies unconformably on Archaean and Paleoproterozoic basement (Ojakangas et al., 2001). The basal Bessemer Quartzite is a c. 100 m thick, texturally and compositionally mature quartzarenite that contains bimodal paleocurrent indicators indicative of tidal currents (Ojakangas and Morey, 1982). The unit is correlated with the c. 1108 Ma Nipigon Sills (Ojakangas et al., 2001). The Bessemer Quartzite is conformably overlain by the c. 6 km thick Powder Mill Group. The lower portion of this group comprises c. 2 km of the undated Siemens Creek Formation basalt flows and pillows. The upper 4.5 km of the group comprises the Kallender Creek Formation and Mellen Intrusive Complex. The Kallender Creek Formation is subdivided into a lower basalt-dominated part and an upper andesite-dominated part (Nicholson et al., 1997), dated at 1107.3 ± 1.6 Ma (Davis and Green, 1997) and 1098.24 ± 0.45 Ma (Swanson-Hysell et al., 2019) respectively. The c. 5 km thick Portage Lake Volcanic (PLV) Group flood basalts contain interflow conglomerate

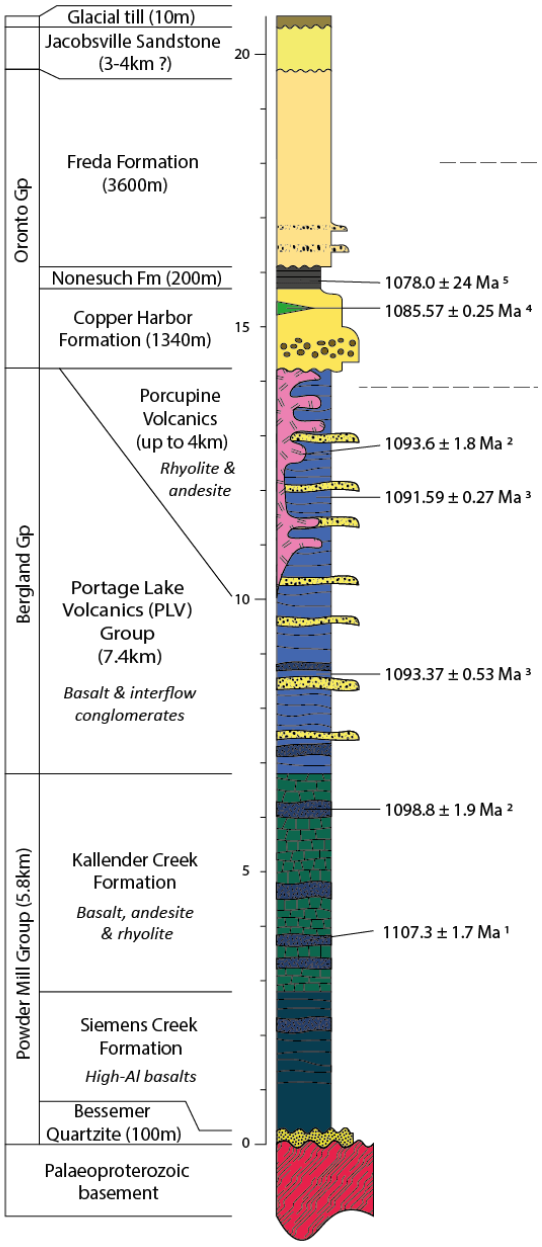

Fig. 1.11. Keweenaw Supergroup stratigraphic column with thickness scale in meters (modified after Nicholson, 1997).

beds and rhyolite domes. Flood basalts were extruded between c. 1094 and 1091 Ma (Swanson-Hysell et al., 2019). The Oronto Group lies unconformably on the PLV Group, and from base includes the Copper Harbor, Nonesuch and Freda Formations. The Copper Harbor Formation is up to 1340 m thick and comprises sandstones and conglomerates rich in basaltic detritus (White and Wright, 1960). The Lake Shore Traps andesite flow in the middle of the formation is dated at 1085.57 ± 0.25 Ma (Fairchild et al., 2017). The Nonesuch Formation comprises siltstones and shales including organic-rich and micritic beds and is interpreted to be of a lacustrine origin (Elmore, 1989;

Imbus et al., 1990; Suszek, 1997) although organic geochemistry studies have highlighted evidence of marine influences (Hieshima & Pratt, 1991; Pratt et al., 1991; Imbus et al., 1992). The basal part of the formation is dated by Re-Os on pyrite at 1078 ± 24 Ma (Cumming et al., 2013). The Freda Formation is a brown-coloured alluvial sandstone of greater textural and compositional maturity than the Copper Harbor (Daniels, 1982). In the western Lake Superior basin the Oronto Group is unconformably overlain by the sub-arkosic composition Jacobsville Sandstone (Kalliokoski, 1982; Ojakangas & Dickas, 2002). The Jacobsville Sandstone contains detrital zircons as young as 959 ± 19 Ma, suggesting the unit may be considerably younger than the underlying Oronto Group (Malone et al., 2016).

1.5.3. The White Pine deposit and other copper mineralisation

The White Pine deposit is located on the southern side of the Lake Superior basin (Fig. 1.12). Upper PLV and Oronto Group rocks dip at approximately 20˚ towards the north, into the basin. Here, the lower part of the Keweenawan Supergroup is truncated by the Keweenaw fault; a reverse fault which juxtaposes PLV Group rocks on its northern (hanging wall) side against Jacobsville Sandstone on its southern side (footwall) (Hubbard, 1975). The upper PLV Group contains the Porcupine rhyolite, a volcanic caldera c. 30 km long and several kms thick, that forms the topography of the Porcupine Mountains (Woodruff et al., 2013). The overlying Oronto Group is deflected around the Porcupine caldera causing a pronounced perturbation in the regional strike (Fig. 1.13).

White Pine is located on the eastern flank of the Porcupine Mountains. Mineralisation is hosted in the upper 10 m of the Copper Harbor Formation (Hamilton, 1967) and the lower 10 m of the Nonesuch Formation and straddles the northwest-southeast trending White Pine fault (White and Wright, 1954; Ensign et al., 1968; Brown, 1971). In the southwest part of the mine a second phase of mineralisation is associated with reverse faulting (Mauk et al., 1992).

Additional resources of stratiform copper mineralisation in the basal Nonesuch Formation occur at the Copperwood deposit in the Western Syncline (Bornhorst and Williams, 2013), west of the Porcupine Mountains, and at the JBY and Bald Mountain prospects. Significant native copper and chalcocite deposits are hosted in basalt flows and interflow conglomerates on the Keweenaw Peninsula, northeast of

White Pine (Brown, 1974; Bornhorst et al., 1988; Brown, 2006). The estimated mined and pre-mining copper reserves are 13.6 million metric tonnes of metal (Bornhorst & Barron, 2011).

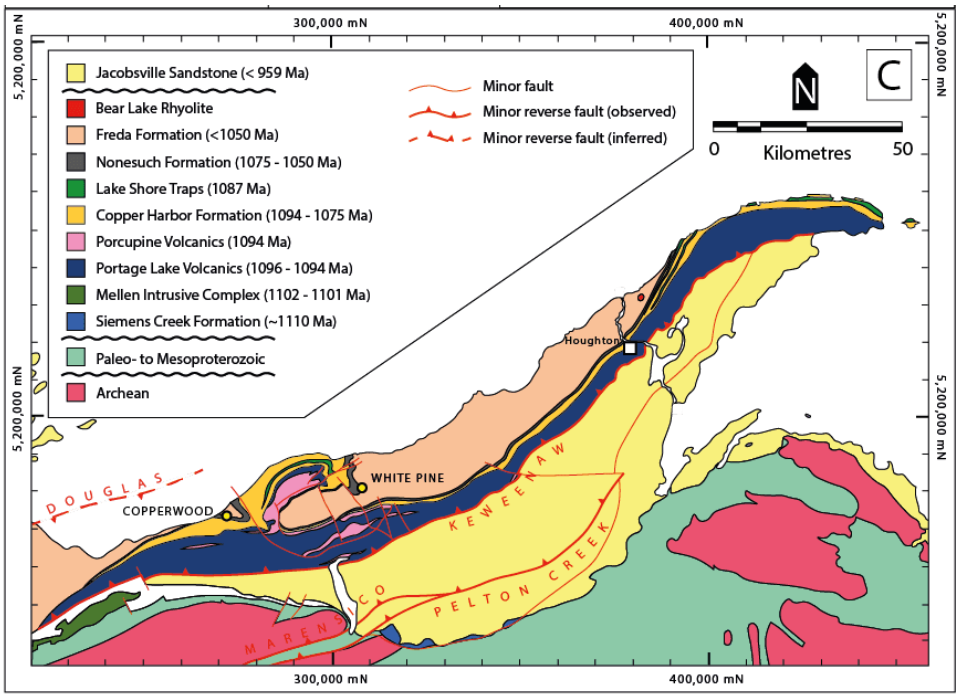

Fig. 1.12. Geological map of the Keweenaw Peninsula (Cannon et al. 1995).

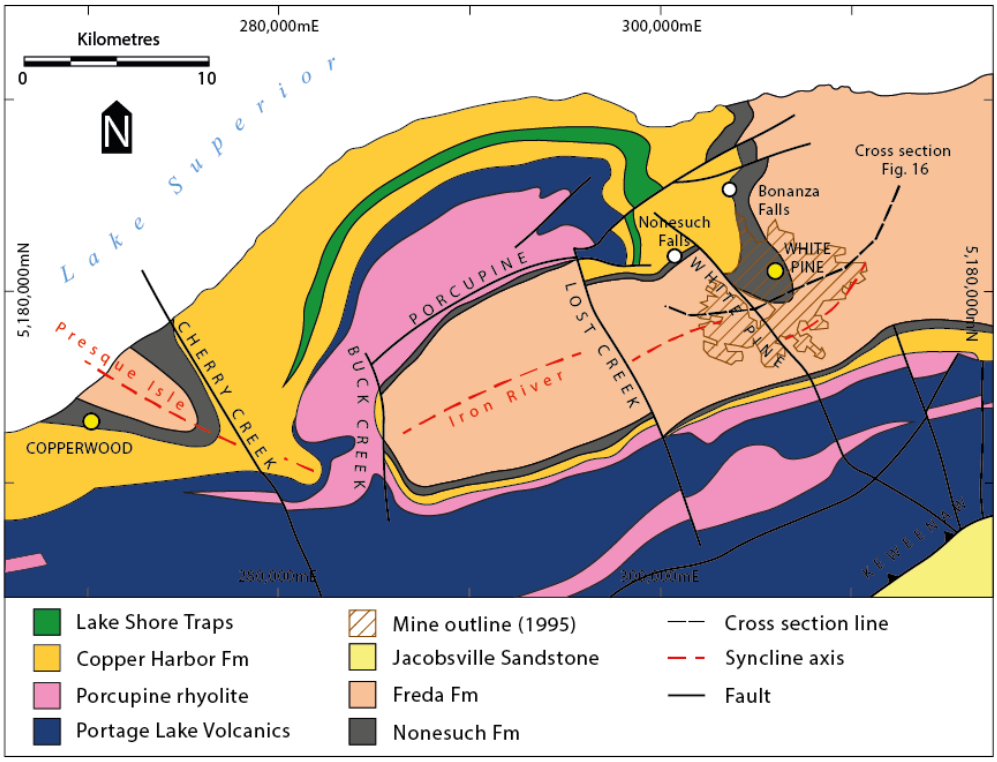

Fig. 1.13. Geological map of the White Pine district (Hubbard, 1975).

1.6. References

Alderton, D.H., Selby, D., Kucha, H. and Blundell, D.J., 2016. A multistage origin for Kupferschiefer mineralization. Ore Geology Reviews, 79, pp.535-543.

Alexeiev, D.V., Cook, H.E., Buvtyshkin, V.M. and Golub, L.Y., 2009. Structural evolution of the Ural–Tian Shan junction: A view from Karatau ridge, South Kazakhstan. Comptes Rendus Geoscience, 341(2-3), pp.287-297.

Allen, M.B., Alsop, G.I. and Zhemchuzhnikov, V.G., 2001. Dome and basin refolding and transpressive inversion along the Karatau Fault System, southern Kazakstan. Journal of the Geological Society, 158(1), pp.83-95.

Allen, P.A. and Allen, J.R., 2005. Basin analysis: Principles and applications.

Armstrong, R.A., Master, S. and Robb, L.J., 2005. Geochronology of the Nchanga Granite, and constraints on the maximum age of the Katanga Supergroup, Zambian Copperbelt. Journal of African Earth Sciences, 42(1-5), pp.32-40.

Barra, F., Broughton, D., Ruiz, J. and Hitzman, M., 2004, November. Multi-stage mineralisation in the Zambian Copperbelt based on Re-Os isotope constraints. In The Geological Society of America, 2004 Denver Annual Meeting.

Bateman, A.M., 1930. Ores of the Northern Rhodesian Copperbelt: Economic Geology. v. 25.

Batumike, M.J., Cailteux, J.L.H. and Kampunzu, A.B., 2007. Lithostratigraphy, basin development, base metal deposits, and regional correlations of the Neoproterozoic Nguba and Kundelungu rock successions, central African Copperbelt. Gondwana Research, 11(3), pp.432-447.

Bechtel, A., Elliott, W.C. and Oszczepalski, S., 1996. Indirect age determination of Kuperfschiefer-type mineralization in the Polish Basin by K/Ar dating of illite; preliminary results. Economic Geology, 91(7), pp.1310-1319.

Bechtel, A., Elliott, W.C., Wampler, J.M. and Oszczepalski, S., 1999. Clay mineralogy, crystallinity, and K-Ar ages of illites within the Polish Zechstein Basin; implications for the age of Kupferschiefer mineralization. Economic Geology, 94(2), pp.261-272.

Bernau, R., Roberts, S., Richards, M., Nisbet, B., Boyce, A. and Nowecki, J., 2013. The geology and geochemistry of the Lumwana Cu (±Co±U) deposits, NW Zambia. Mineralium Deposita, 48(2), pp.137-153.

Bernau, R., Roberts, S., Richards, M., Nisbet, B., Boyce, A. and Nowecki, J., 2013. The geology and geochemistry of the Lumwana Cu (±Co±U) deposits, NW Zambia. Mineralium Deposita, 48(2), pp.137-153.

Binda, P.L., 1994. Stratigraphy of Zambian Copperbelt orebodies. Journal of African Earth Sciences, 19(4), pp.251-264.

Blundell, D.J., Aldereton, D.H.M., Karnkowski, P.H., Oszczepalski, S., Stroetmann-Heinen, V. and Kucha, H., 2001. A new genetic model for the copper mineralisation of the Polish Kupferschiefer. Mineral deposits at the beginning of the 21th century, pp.215-218.

Blundell, D.J., Karnkowski, P.H., Alderton, D.H.M., Oszczepalski, S. and Kucha, H., 2003. Copper mineralization of the Polish Kupferschiefer: a proposed basement fault-fracture system of fluid flow. Economic Geology, 98(7), pp.1487-1495.

Borg, G., Piestrzynski, A., Bachmann, G.H., Püttmann, W., Walther, S. and Fiedler, M., 2012. An overview of the European Kupferschiefer deposits. Economic Geology Special Publication, 16, pp.455-486.

Bornhorst, T.J. and Barron, R.J., 2011. Copper deposits of the western Upper Peninsula of Michigan. Geological Society of America Field Guide, 24, pp.83-99.

Bornhorst, T.J. and Williams, W.C., 2013. The Mesoproterozoic Copperwood sedimentary rock-hosted stratiform copper deposit, Upper Peninsula, Michigan. Economic Geology, 108(6), pp.1325-1346.

Bornhorst, T.J., Paces, J.B., Grant, N.K., Obradovich, J.D. and Huber, N.K., 1988. Age of native copper mineralization, Keweenaw Peninsula, Michigan. Economic Geology, 83(3), pp.619-625.

Box, S.E., Syusyura, B., Hayes, T.S., Taylor, C.D., Zientek, M.L., Hitzman, M.W., Seltmann, R., Chechetkin, V., Dolgopolova, A., Cossette, P.M., and Wallis, J.C., 2012, Sandstone copper assessment of the Chu-Sarysu basin, central Kazakhstan: Chap. E of Zientek, M.L., Hammarstrom, J.M., and Johnson, K.M., eds., Global mineral resource assessment: U.S. Geological Survey Scientific Investigations Report 2010-5090B, 63 p. and GIS data (available at http://pubs.usgs.gov/sir/2010/5090/e/).

Box, S.E., Syusyura, B., Seltmann, R., Creaser, R.A., Dolgopolova, A. and Zientek, M.L., 2012. Dzhezkazgan and associated sandstone copper deposits of the Chu-Sarysu basin, Central Kazakhstan. Society of Economic Geologists, pp.303-328.

Brady, J.M., 1960. Ore and sedimentation of the lower sandstone at the White Pine mine. Michigan [MS thesis]: Houghton, Michigan Technological University, 72.

Brauns, C.M., Pätzold, T. and Haack, U., 2003. A Re-Os study bearing on the age of the Kupferschiefer black shale at Sangerhausen (Germany). In Abstracts XVth International Congress on Carboniferous and Permian Stratigraphy, Utrecht, Netherlands (p. 66).

Brown, A.C., 1971. Zoning in the White Pine copper deposit, Ontonagon County, Michigan. Economic Geology, 66(4), pp.543-573.

Brown, A.C., 1997. World-class sediment-hosted stratiform copper deposits: Characteristics, genetic concepts and metallotects. Australian Journal of Earth Sciences, 44(3), pp.317-328.

Brown, A.C., 2005. Refinements for footwall red-bed diagenesis in the sediment-hosted stratiform copper deposits model. Economic Geology, 100(4), pp.765-771.

Brown, A.C., 2006. Genesis of native copper lodes in the Keweenaw district, northern Michigan: a hybrid evolved meteoric and metamophogenic model. Economic Geology, 101(7), pp.1437-1444.

Brown, A.C., 2008. District-scale concentration of native copper lodes from a tectonically induced thermal plume of ore fluids on the Keweenaw Peninsula, northern Michigan. Economic Geology, 103(8), pp.1691-1694.

Brown, A.C., 2014. Latent thermal effects from Porcupine Volcanics calderas underlying the White Pine-Presque Isle stratiform copper mineralization, northern Michigan. Economic Geology, 109(7), pp.2035-2050.

Brown, A.C., 2018. Latent volcanic heat and further unique aspects of early diagenetic stratiform copper mineralization in the White Pine-Presque Isle District, northern Michigan. Mineralium Deposita, 53(5), pp.721-728.

Bull, S., Selley, D., Broughton, D., Hitzman, M., Cailteux, J., Large, R. and McGoldrick, P., 2011. Sequence and carbon isotopic stratigraphy of the Neoproterozoic Roan Group strata of the Zambian copperbelt. Precambrian Research, 190(1-4), pp.70-89.

Bykadorov, V.A., Bush, V.A., Fedorenko, O.A., Filippova, I.B., Miletenko, N.V., Puchkov, V.N., Smirnov, A.V., Uzhkenov, B.S. and Volozh, Y.A., 2003. ORDOVICIAN—PERMIAN PALAEOGEOGRAPHY OF CENTRAL EURASIA: DEVELOPMENT OF PALAEOZOIC PETROLEUM-BEARING BASINS. Journal of Petroleum Geology, 26(3), pp.325-350.

Cailteux, J., 1994. Lithostratigraphy of the Neoproterozoic Shaba-type (Zaire) Roan Supergroup and metallogenesis of associated stratiform mineralization. Journal of African Earth Sciences, 19(4), pp.279-301.

Cailteux, J., Binda, P.L., Katekesha, W.M., Kampunzu, A.B., Intiomale, M.M., Kapenda, D., Kaunda, C., Ngongo, K., Tshiauka, T. and Wendorff, M., 1994. Lithostratigraphical correlation of the Neoproterozoic Roan Supergroup from Shaba (Zaire) and Zambia, in the central African copper-cobalt metallogenic province. Journal of African Earth Sciences, 19(4), pp.265-278.

Cannon, W.F., 1994. Closing of the Midcontinent rift-A far—field effect of Grenvillian compression. Geology, 22(2), pp.155-158.

Cannon, W.F., Peterman, Z.E. and Sims, P.K., 1993. Crustal-scale thrusting and origin of the Montreal River monocline-A 35-km-thick cross section of the midcontinent rift in northern Michigan and Wisconsin. Tectonics, 12(3), pp.728-744.

Capistrant, P.L., Hitzman, M.W., Wood, D., Kelly, N.M., Williams, G., Zimba, M., Kuiper, Y., Jack, D. and Stein, H., 2015. Geology of the enterprise hydrothermal nickel deposit, North-Western Province, Zambia. Economic Geology, 110(1), pp.9-38.

Cathles, L.M. and Adams, J.J., 2005. Fluid flow and petroleum and mineral resources in the upper (< 20 km) continental crust. Economic Geology 100th Anniversary Volume, pp.77-110.

Cathles, L.M., Oszczepalski, S. and Jowett, E.C., 1993. Mass balance evaluation of the late diagenetic hypothesis for Kupferschiefer Cu mineralization in the Lubin basin of southwestern Poland. Economic Geology, 88(4), pp.948-956.

Cawood, P.A. and Pisarevsky, S.A., 2017. Laurentia-Baltica-Amazonia relations during Rodinia assembly. Precambrian Research, 292, pp.386-397.

Chandler, V.W., 1983. Correlation of magnetic anomalies in east-central Minnesota and northwestern Wisconsin: Constraints on magnitude and direction of Keweenawan rifting. Geology, 11(3), pp.174-176.

Cumming, V.M., Poulton, S.W., Rooney, A.D. and Selby, D., 2013. Anoxia in the terrestrial environment during the late Mesoproterozoic. Geology, 41(5), pp.583-586.

Daniels Jr, P.A., 1982. Upper Precambrian sedimentary rocks: Oronto Group, Michigan-Wisconsin. Geology and tectonics of the Lake Superior basin: Geological Society of America Memoir, 156, pp.107-133.

Davey, J., 2019. Anomalous metal enrichment of Basin Brines in the Zambian Copperbelt: a comparison of fluid chemistry in contrasting sediment-hosted copper systems (Doctoral dissertation, University of Southampton).

Davis, D.W. and Green, J.C., 1997. Geochronology of the North American Midcontinent rift in western Lake Superior and implications for its geodynamic evolution. Canadian Journal of Earth Sciences, 34(4), pp.476-488.

Dewaele, S., Muchez, P., Vets, J., Fernandez-Alonzo, M. and Tack, L., 2006. Multiphase origin of the Cu–Co ore deposits in the western part of the Lufilian fold-and-thrust belt, Katanga (Democratic Republic of Congo). Journal of African Earth Sciences, 46(5), pp.455-469.

Dickas, A.B., 1986. Comparative Precambrian stratigraphy and structure along the mid-continent rift. AAPG Bulletin, 70(3), pp.225-238.

Dickas, A.B., Mudrey, M.G., Ojakangas, R.W. and Green, J.C., 1997. Segmented structure of the middle Proterozoic Midcontinent rift system, North America. SPECIAL PAPERS-GEOLOGICAL SOCIETY OF AMERICA, pp.37-46.

Elmore, R.D., 1984. The Copper Harbor Conglomerate: A late Precambrian fining-upward alluvial fan sequence in northern Michigan. Geological Society of America Bulletin, 95(5), pp.610-617.

Elmore, R.D., Milavec, G.J., Imbus, S.W. and Engel, M.H., 1989. The Precambrian Nonesuch Formation of the North American mid-continent rift, sedimentology and organic geochemical aspects of lacustrine deposition. Precambrian Research, 43(3), pp.191-213.

Ensign, C.O., Jr., and eight others, 1968, Copper deposits in the Nonesuch Shale, White Pine, Michigan, in Ridge, J.D., ed., Ore deposits of the United States 1933-1967, Volume 1: New York, American Institute of Mining, Metallurgical and Petroleum Engineers, p. 459-488.

Fairchild, L.M., Swanson-Hysell, N.L., Ramezani, J., Sprain, C.J. and Bowring, S.A., 2017. The end of Midcontinent Rift magmatism and the paleogeography of Laurentia. Lithosphere, 9(1), pp.117-133.

Fleischer, V.D., 1984. Discovery, geology and genesis of copper—cobalt mineralisation at Chambishi Southeast prospect, Zambia. Precambrian Research, 25(1-3), pp.119-133.

Gablina, I.F., 1981. New data on formation conditions of the Dzhezkazkan copper deposit. International Geology Review, 23(11), pp.1303-1311.

Geological Survey (US), Cannon, W.F. and Nicholson, S.W., 2001. Geologic map of the Keweenaw Peninsula and adjacent area, Michigan (pp. 1-7). The Survey.

Hamilton, S.K., 1967. Copper mineralization in the upper part of the Copper Harbor Conglomerate at White Pine, Michigan. Economic Geology, 62(7), pp.885-904.

Hendrickson, M.D., Hitzman, M.W., Wood, D., Humphrey, J.D. and Wendlandt, R.F., 2015. Geology of the Fishtie deposit, Central Province, Zambia: iron oxide and copper mineralization in Nguba Group metasedimentary rocks. Mineralium Deposita, 50(6), pp.717-737.

Hieshima, G.B. and Pratt, L.M., 1991. Sulfur/carbon ratios and extractable organic matter of the Middle Proterozoic Nonesuch Formation, North American Midcontinent rift. Precambrian research, 54(1), pp.65-79.

Hinze, W.J., Allen, D.J., Braile, L.W. and Mariano, J., 1997. The Midcontinent rift system: A major Proterozoic continental rift. Geological Society of America Special Papers, 312, pp.7-35.

Hitzman, M., Kirkham, R., Broughton, D., Thorson, J. and Selley, D., 2005. The sediment-hosted stratiform copper ore system. Economic geology, 100.

Hitzman, M.W. and Broughton, D.W., 2017. Discussion:“Age of the Zambian Copperbelt” by Sillitoe et al.(2017) Mineralium Deposita. Mineralium Deposita, 52(8), pp.1273-1275.

Hitzman, M.W., 2000. Source basins for sediment-hosted stratiform Cu deposits: implications for the structure of the Zambian Copperbelt. Journal of African Earth Sciences, 30(4), pp.855-863.

Hitzman, M.W., Broughton, D., Selley, D., Woodhead, J., Wood, D. and Bull, S., 2012. The Central African Copperbelt: diverse stratigraphic, structural, and temporal settings in the world's largest sedimentary copper district. Society of Economic Geologists Special Publication 16, (Paper 19), pp.487-514.

Hitzman, M.W., Selley, D. and Bull, S., 2010. Formation of sedimentary rock-hosted stratiform copper deposits through Earth history. Economic Geology, 105(3), pp.627-639.

Hubbard, H.A., 1975. Geology of Porcupine Mountains in Carp River and White Pine quadrangles, Michigan. US Geological Survey Journal Research, 3, pp.519-528.

Imbus, S.W., Engel, M.H. and Elmore, R.D., 1990. Organic Geochemistry and Sedimentology of Middle Proterozoic Nonesuch Formation--Hydrocarbon Source Rock Assessment of a Lacustrine Rift Deposit: Chapter 12.

Imbus, S.W., Macko, S.A., Elmore, R.D. and Engel, M.H., 1992. Stable isotope (C, S, N) and molecular studies on the Precambrian Nonesuch Shale (Wisconsin-Michigan, USA): Evidence for differential preservation rates, depositional environment and hydrothermal influence. Chemical Geology: Isotope Geoscience Section, 101(3-4), pp.255-281.

Jowett, E.C., 1986. Genesis of Kupferschiefer Cu-Ag deposits by convective flow of Rotliegendes brines during Triassic rifting. Economic Geology, 81(8), pp.1823-1837.

Jowett, E.C., 1989. Effects of continental rifting on the location and genesis of stratiform copper-silver deposits. In Geological Association of Canada (pp. 53-66).

Jowett, E.C., Roth, T., Rydzewski, A. and Oszczepalski, S., 1991. "Background" δ 34 S values of Kupferschiefer sulphides in Poland: pyrite-marcasite nodules. Mineralium Deposita, 26(2), pp.89-98.

Jowett, E.C., Rydzewsk, A. and Jowett, R.J., 1987. The Kupferschiefer Cu–Ag ore deposits in Poland: a re-appraisal of the evidence of their origin and presentation of a new genetic model. Canadian Journal of Earth Sciences, 24(10), pp.2016-2037.

Kalliokoski, J., 1982. Jacobsville sandstone. Geology and Tectonics of the Lake Superior Basin: Geological Society of America Memoir, 156, pp.147-156.

Kampunzu, A.B. and Cailteux, J., 1999. Tectonic evolution of the Lufilian Arc (Central Africa Copper Belt) during Neoproterozoic Pan African orogenesis. Gondwana Research, 2(3), pp.401-421.

Kampunzu, A.B., Tembo, F., Matheis, G., Kapenda, D. and Huntsman-Mapila, P., 2000. Geochemistry and tectonic setting of mafic igneous units in the Neoproterozoic Katangan Basin, Central Africa: implications for Rodinia break-up. Gondwana Research, 3(2), pp.125-153.

Kirkham, R.V., 1989. Distribution, settings, and genesis of sediment-hosted stratiform copper deposits. Geological Association of Canada Special Paper, 36, pp.3-38.

Koziy, L., Bull, S., Large, R. and Selley, D., 2009. Salt as a fluid driver, and basement as a metal source, for stratiform sediment-hosted copper deposits. Geology, 37(12), pp.1107-1110.

Lyons, T.W., Reinhard, C.T. and Planavsky, N.J., 2014. The rise of oxygen in Earth's early ocean and atmosphere. Nature, 506(7488), p.307.

Machel, H.G., Krouse, H.R. and Sassen, R., 1995. Products and distinguishing criteria of bacterial and thermochemical sulfate reduction. Applied geochemistry, 10(4), pp.373-389.

Malone, D.H., Stein, C.A., Craddock, J.P., Kley, J., Stein, S. and Malone, J.E., 2016. Maximum depositional age of the Neoproterozoic Jacobsville Sandstone, Michigan: Implications for the evolution of the Midcontinent Rift. Geosphere, 12(4), pp.1271-1282.

Mauk, J.L., Kelly, W.C., Van Der Pluijm, B.A. and Seasor, R.W., 1992. Relations between deformation and sediment-hosted copper mineralization: Evidence from the White Pine part of the Midcontinent rift system. Geology, 20(5), pp.427-430.

Mendelsohn, F. ed., 1961. The geology of the northern Rhodesian copperbelt. Macdonald.

Mikulski, S.Z. and Stein, H.J., 2012. Re-Os age of late bornite-chalcopyrite vein ores, Kupferschiefer, SW Poland. In Abstract, Goldschmidt Conference, Montreal.

Milton, J.E., Hickey, K.A., Gleeson, S.A., Falck, H. and Allaz, J., 2017. In situ monazite dating of sediment-hosted stratiform copper mineralization in the Redstone Copper belt, Northwest Territories, Canada: Cupriferous fluid flow late in the evolution of a Neoproterozoic sedimentary basin. Economic Geology, 112(7), pp.1773-1806.

Morey, G.B. and Ojakangas, R.W., 1982. Keweenawan sedimentary rocks of eastern Minnesota and northwestern Wisconsin. Geology and tectonics of the Lake Superior basin: Geological Society of America Memoir, 156, pp.135-146.

Morrison, S.J. and Parry, W.T., 1986. Formation of carbonate-sulfate veins associated with copper ore deposits from saline basin brines, Lisbon Valley, Utah; fluid inclusion and isotopic evidence. Economic Geology, 81(8), pp.1853-1866.

Muchez, P., André-Mayer, A.S., Dewaele, S. and Large, R., 2017. Discussion: age of the Zambian Copperbelt. Mineralium Deposita, 52(8), pp.1269-1271.

Muchez, P., Minnen, M., Dewaele, S. and Hulsbosch, N., 2019. The Geology of the Mufulira Deposit: Implications for the Metallogenesis of Arenite-Hosted Ore Deposits in the Central African Copperbelt. Ore Deposits: Origin, Exploration, and Exploitation, pp.57-74.

Nawrocki, J., 2000. Clay mineralogy, crystallinity, and K-Ar ages of illites within the Polish Zechstein basin: Implications for the age of Kupferschiefer mineralization—a discussion. Economic Geology, 95(1), pp.241-242.

Nicholson, S.W., Schulz, K.J., Shirey, S.B. and Green, J.C., 1997. Rift-wide correlation of 1.1 Ga Midcontinent rift system basalts: implications for multiple mantle sources during rift development. Canadian Journal of Earth Sciences, 34(4), pp.504-520.

Ojakangas, R.W. and Dickas, A.B., 2002. The 1.1-Ga Midcontinent Rift System, central North America: sedimentology of two deep boreholes, Lake Superior region. Sedimentary Geology, 147(1-2), pp.13-36.

Ojakangas, R.W., Morey, G.B. and Green, J.C., 2001. The Mesoproterozoic midcontinent rift system, Lake Superior region, USA. Sedimentary Geology, 141, pp.421-442.

Oszczepalski, S., 1999. Origin of the Kupferschiefer polymetallic mineralization in Poland. Mineralium Deposita, 34(5-6), pp.599-613.

Pašava, J., Oszczepalski, S. and Du, A., 2010. Re–Os age of non-mineralized black shale from the Kupferschiefer, Poland, and implications for metal enrichment. Mineralium Deposita, 45(2), pp.189-199.

Perelló, J., Valencia, V.A., Cornejo, P., Clifford, J., Wilson, A.J. and Collins, G., 2019. Timing of sediment-hosted Cu-Ag mineralization in the Trans-Hudson orogen at Janice Lake, Wollaston Domain, Saskatchewan, Canada. Mineralium Deposita, 54(1), pp.81-100.

Polito, P.A., Kyser, T.K., Southgate, P.N. and Jackson, M.J., 2006. Sandstone diagenesis in the Mount Isa basin: An isotopic and fluid inclusion perspective in relationship to district-wide Zn, Pb, and Cu mineralization. Economic Geology, 101(6), pp.1159-1188.

Pratt, L.M., Summons, R.E. and Hieshima, G.B., 1991. Sterane and triterpane biomarkers in the Precambrian Nonesuch formation, North American midcontinent rift. Geochimica et Cosmochimica Acta, 55(3), pp.911-916.

Rose, A.W., 1976. The effect of cuprous chloride complexes in the origin of red-bed copper and related deposits. Economic Geology, 71(6), pp.1036-1048.

Sawlowicz, Z., 1989. On the origin of copper mineralization in the Kupferschiefer: a sulphur isotope study. Terra Nova, 1(4), pp.339-343.

Schmandt, D., Broughton, D., Hitzman, M.W., Plink-Bjorklund, P., Edwards, D. and Humphrey, J., 2013. The Kamoa copper deposit, Democratic Republic of Congo: stratigraphy, diagenetic and hydrothermal alteration, and mineralization. Economic Geology, 108(6), pp.1301-1324.

Schneider, J., Melcher, F. and Brauns, M., 2007. Concordant ages for the giant Kipushi base metal deposit (DR Congo) from direct Rb–Sr and Re–Os dating of sulfides. Mineralium Deposita, 42(7), pp.791-797.

Selley, D., Broughton, D., Scott, R.J., Hitzman, M., Bull, S.W., Large, R.R., McGoldrick, P.J., Croaker, M. and Pollington, N., 2005. A new look at the geology of the Zambian Copperbelt. Society of Economic Geologists, Inc., 100.

Selley, D., Scott, R., Emsbo, P., Koziy, L., Hitzman, M.W., Bull, S.W., Duffett, M., Sabagenzi, S., Halpin, J. and Broughton, D.W., 2018. Structural configuration of the Central African Copperbelt: roles of evaporites in structural evolution, basin hydrology, and ore location. Economic Geology and The Bulletin of The Society of Economic Geologists, 21, pp.115-156.

Sillitoe, R.H., Perelló, J., Creaser, R.A., Wilton, J., Wilson, A.J. and Dawborn, T., 2017. Age of the Zambian Copperbelt. Mineralium Deposita, 52(8), pp.1245-1268.

Słowakiewicz, M. and Mikołajewski, Z., 2011. Upper Permian Main Dolomite microbial carbonates as potential source rocks for hydrocarbons (W Poland). Marine and Petroleum Geology, 28(8), pp.1572-1591.

Speczik, S., 1995. The Kupferschiefer mineralization of Central Europe: New aspects and major areas of future research. Ore Geology Reviews, 9(5), pp.411-426.

Stein, C.A., Kley, J., Stein, S., Hindle, D. and Keller, G.R., 2015. North America's Midcontinent Rift: when rift met LIP. Geosphere, 11(5), pp.1607-1616.

Stein, C.A., Stein, S., Elling, R., Keller, G.R. and Kley, J., 2018. Is the "Grenville Front" in the central United States really the Midcontinent Rift?. GSA Today, 28(5), pp.4-10.

Stein, C.A., Stein, S., Merino, M., Randy Keller, G., Flesch, L.M. and Jurdy, D.M., 2014. Was the Midcontinent Rift part of a successful seafloor-spreading episode?. Geophysical Research Letters, 41(5), pp.1465-1470.

Stewart, E.K. and Mauk, J.L., 2017. Sedimentology, sequence-stratigraphy, and geochemical variations in the Mesoproterozoic Nonesuch formation, Northern Wisconsin, USA. Precambrian Research, 294, pp.111-132.

Suszek, T., 1997. Petrography and sedimentation of the middle Proterozoic (Keweenawan) Nonesuch Formation, western Lake Superior region, Midcontinent Rift System. Geological Society of America Special Papers 312, pp. 195–210.

Swanson-Hysell, N.L., Ramezani, J., Fairchild, L.M. and Rose, I.R., 2019. Failed rifting and fast drifting: Midcontinent rift development, Laurentia's rapid motion and the driver of Grenvillian orogenesis. Bulletin, 131(5-6), pp.913-940.

Swenson, J.B., Person, M., Raffensperger, J.P., Cannon, W.F., Woodruff, L.G. and Berndt, M.E., 2004. A hydrogeologic model of stratiform copper mineralization in the Midcontinent rift system, northern Michigan, USA. Geofluids, 4(1), pp.1-22.

Symons, D.T., Kawasaki, K., Walther, S. and Borg, G., 2011. Paleomagnetism of the Cu–Zn–Pb-bearing Kupferschiefer black shale (Upper Permian) at Sangerhausen, Germany. Mineralium Deposita, 46(2), pp.137-152.

Syusyura, B., Box, S.E. and Wallis, J.C., 2010. Spatial databases of geological, geophysical, and mineral resource data relevant to sandstone-hosted copper deposits in central Kazakhstan (No. 2010-1124). US Geological Survey.

Taylor, C.D., Causey, J.D., Denning, P., Hammarstrom, J.M., Hayes, T.S., Horton, J.D., Kirschbaum, M.J., Parks, H.L., Wilson, A.B., Wintzer, N.E. and Zientek, M.L., 2013. Descriptive models, grade-tonnage relations, and databases for the assessment of sediment-hosted copper deposits: with emphasis on deposits in the Central Africa Copperbelt, Democratic Republic of the Congo and Zambia: Chapter J in Global mineral resource assessment (No. 2010-5090-J, pp. i-154). US Geological Survey.

Tohver, E., Teixeira, W., van der Pluijm, B., Geraldes, M.C., Bettencourt, J.S. and Rizzotto, G., 2006. Restored transect across the exhumed Grenville orogen of Laurentia and Amazonia, with implications for crustal architecture. Geology, 34(8), pp.669-672.

Tonn, H., Schmidt, F.-P., Porada, H., and Horn, E.-E., 1987, Untersuchungen von Flüssigkeitseinschläüssen im Zechstein als Beitrag zur Genese des Kupferschiefers: Fortschrift für Mineralogie [abs.], v. 65, Supplement 1, p.184.

Torrealday, H.I., Hitzman, M.W., Stein, H.J., Markley, R.J., Armstrong, R. and Broughton, D., 2000. Re-Os and U-Pb dating of the vein-hosted mineralization at the Kansanshi copper deposit, northern Zambia. Economic Geology, 95(5), pp.1165-1170.

Torsvik, T.H., Van der Voo, R., Meert, J.G., Mosar, J., Walderhaug, H.J., 2001. Reconstructions of the continents around the North Atlantic at about the 60th parallel. Earth Planet. Sci. Lett. 187, 55–69.

Vaughan, D.J., Sweeney, M.A., Friedrich, G., Diedel, R. and Haranczyk, C., 1989. The Kupferschiefer; an overview with an appraisal of the different types of mineralization. Economic Geology, 84(5), pp.1003-1027.

Vervoort, J.D., Wirth, K., Kennedy, B., Sandland, T. and Harpp, K.S., 2007. The magmatic evolution of the Midcontinent rift: New geochronologic and geochemical evidence from felsic magmatism. Precambrian Research, 157(1-4), pp.235-268.

Walker, T.R., 1986, March. Diagenetic alterations in red beds and their application to the origin of copper and other heavy-metals in stratiform ore-deposits. In Canadian Mineralogist (Vol. 24, pp. 210-211). Cityview 78087, Nepean on K2G 5W2, Canada: Mineralogical Association Canada.

White, W.S. and Wright, J.C., 1954. The White Pine copper deposit, Ontonagon County, Michigan. Economic Geology, 49(7), pp.675-716.

White, W.S. and Wright, J.C., 1960. Lithofacies of the Copper Harbor Conglomerate, northern Michigan. US Geol. Surv. Prof. Pap.

Whitmeyer, S.J. and Karlstrom, K.E., 2007. Tectonic model for the Proterozoic growth of North America. Geosphere, 3(4), pp.220-259.

Wodzicki, A. and Piestrzyński, A., 1994. An ore genetic model for the Lubin—Sieroszowice mining district, Poland. Mineralium Deposita, 29(1), pp.30-43.

Woodhead, J., 2013. The Neoproterozoic Roan Group in the Zambian Copperbelt: sequence stratigraphy, alteration, and mineralization. Unpub (Doctoral dissertation, Ph. D. dissertation, Colorado School of Mines, Golden, CO).

Woodruff, L.G., Cannon, W.F., Nicholson, S.W., Schulz, K.J. and Wild, R., 2013. Geology of the Keweenawan Supergroup, Porcupine Mountains, Ontonagon and Gogebic counties, Michigan. Institute on Lake Superior Geology, Proceedings, 59(2), pp.69-96.

Zielinski, R.A., Bloch, S. and Walker, T.R., 1983. The mobility and distribution of heavy metals during the formation of first cycle red beds. Economic Geology, 78(8), pp.1574-1589.

Blank page

Chapter 2

A marine origin for the late Mesoproterozoic Copper Harbor and Nonesuch formations of the Midcontinent Rift of Laurentia

Based on: Jones, S.M., Prave, A.R., Raub, T.D., Cloutier, J., Stüeken, E.E., Rose, C.V., Linnekogel, S. and Nazarov, K., 2020. A marine origin for the late Mesoproterozoic Copper Harbor and Nonesuch Formations of the Midcontinent Rift of Laurentia. Precambrian Research, 336, p.105510.

2.1. Introduction

Between the early Palaeoproterozoic Great Oxidation Event and the Cryogenian Snowball Earth episodes, Earth's marine sedimentary record archives a protracted transformation from the anoxic, bacterial world of the Archaean to the oxygenated, metazoan world of the Phanerozoic. This transformation has invited hypotheses about the potential role of freshwater habitats in the origin and early diversification of complex life because these environments may have become hospitable early on in Earth history (e.g. Sánchez-Baracaldo et al. 2017; Parnell et al. 2015). However, few examples of lacustrine sedimentary rocks are preserved thus

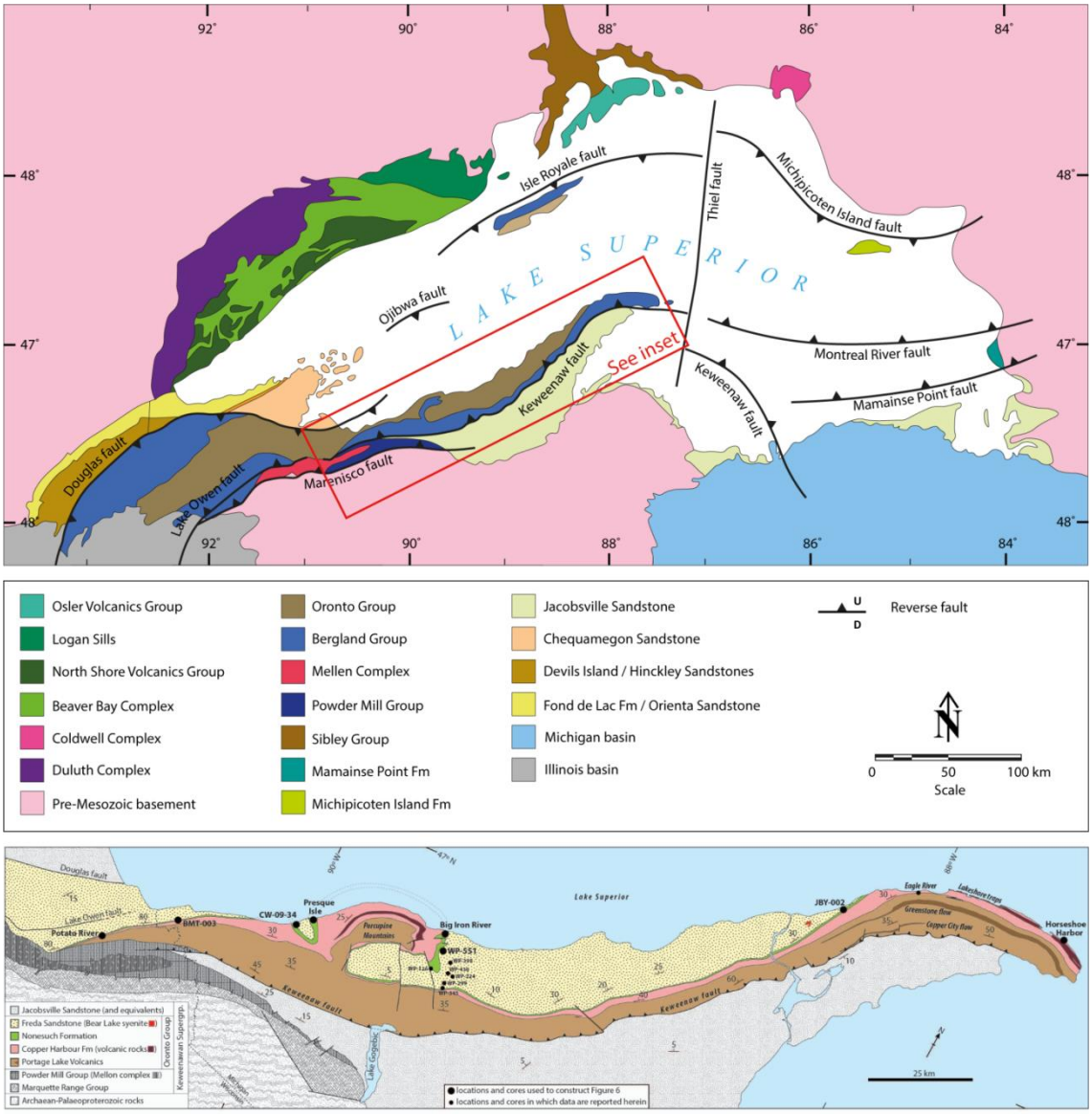

Fig. 2.1. Simplified geological maps of the Lake Superior area, top, and Keweenaw Peninsula, bottom (after Cannon and Nicholson 2001; Cannon et al. 1995, 1996).

determining the environmental conditions in non-marine settings during this time has remained relatively elusive.

The Keweenawan Supergroup, a c. 1.1 Ga volcanic-sedimentary succession exposed along the Canadian-USA shorelines of Lake Superior (Figs. 2.1, 2.2), has been identified as one of the rare windows into lacustrine conditions, based in part on geochemical characteristics (e.g. Cumming et al. 2013). These strata have played a pivotal role in assessing the oxygenation of Earth's atmosphere (Cumming et al. 2013; Slotznick et al. 2018; Mitchell and Sheldon 2016) and the complexity of the non-marine biosphere (Wellman and Strother 2015; Fedorchuk et al. 2016). This succession also hosts a world class sediment-hosted Cu system (Bornhorst and Williams 2013; Ho and Mauk 1996; Mauk and Heisham 1992) the emplacement of which involved extensive post-depositional hydrothermal fluid circulation. Although some primary biogeochemical signatures may not have been modified by those fluids, the validity of palaeoenvironmental interpretations based on those signatures requires independent geological support. Here we report new sedimentological observations that show that parts of the upper Copper Harbor Formation and all of the Nonesuch Formation were deposited in marine-influenced settings, which necessitate reinterpretation of the biogeochemical and micropaleontological data from these rocks.

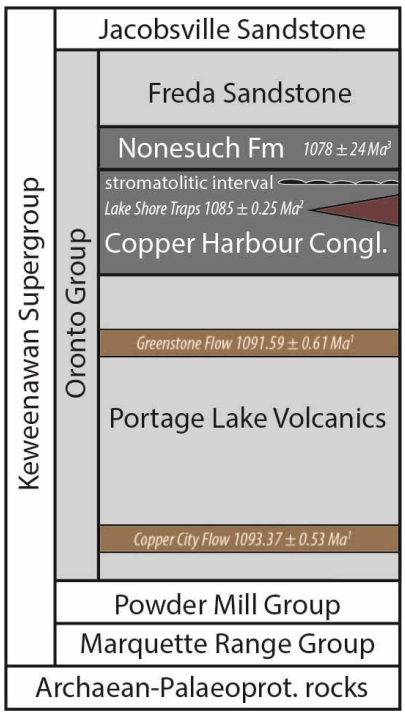

Fig. 2.2. Generalised stratigraphic framework of the geology of the Keweenaw Peninsula and adjacent areas. Age constraints from [1]Fairchild et al. (2017), [2]Swanson-Hysall et al. (2019) and [3]Cumming et al. (2014).

2.2. Geological background

The Keweenawan Supergroup, which represents the exposed northern portion of the 2000-km-long subsurface geophysical feature known as the Mid-continent Rift (Hinze et al. 1997; Ojakangas et al. 2001; Stein et al. 2018), is estimated from geophysical data to be as much as 30 km thick (Behrendt et al. 1988). Volcanic rocks comprise the initial 18-20 km of the Supergroup and the remainder is a mostly sedimentary succession, which is the focus of our work, in particular the Copper Harbor and Nonesuch formations (Fig. 2.2). The former is interpreted as a mostly conglomeratic braided-fluvial deposit (White and Wright 1960; Wolff and Huber 1973; Elmore 1984) and the latter is mostly dark shale and fine sandstone interpreted to be lacustrine (Elmore 1989; Suszek 1997). U-Pb zircon dates for the eruptive ages of the volcanic rocks in the Copper Harbor Formation and on the underlying Portage Lake Volcanics constrain deposition of the two units to between c. 1093 – 1085 Ma (Swanson-Hysell et al. 2019 and references therein). A Re-Os isochron age of 1078 ±24 Ma on shales from the lower part of the Nonesuch Formation (Cumming et al. 2013) in context with a U-Pb zircon date of 1085.57 ± 0.25 Ma (Fairchild et al. 2017) on the underlying Lake Shore Traps in the upper part of the Copper Harbor Formation place the timing of deposition of the Nonesuch Formation to c. 1080 – 1060 Ma, immediately after the expansion of eukaryotic diversity (e.g. Beghin et al. 2017).

2.2.1. Non-marine palaeoenvironments

Most workers interpret the Copper Harbor-Nonesuch succession as a fluvial-to-lacustrine couplet (White and Wright 1960; Wolff and Huber 1973; Elmore 1983, 1984; Elmore et al. 1989; Suszek 1997; Ojakangas et al. 2001; Cumming et al. 2013). The 100 to 2000 m thick, overall fining-upward succession of red, cross-bedded to massive, clast- and matrix-supported cobble conglomerate, pebbly sandstone and sandstone of the Copper Harbor Formation is clearly braided fluvial (Fig. 2.3). The Nonesuch Formation is a 50-200 m thick mostly grey, variably organic-rich, fine-grained siliciclastic unit that, combined with thin stromatolitic intervals in the upper part of the Copper Harbor Formation, is inferred to record lacustrine settings.

The original workers who performed the detailed facies analysis on the upper Copper Harbor and Nonesuch rocks noted explicitly that many of the sedimentological features in those formations were inconclusive in pinpointing either a lacustrine or a

Fig. 2.3. Braided-fluvial features of the Copper Harbor Formation. **A.** Metres-thick massive cobble-boulder conglomerate at Horseshoe Harbor. **B.** Clast-supported cobble-boulder conglomerate and pebbly sandstone interbeds at Eagle River Falls; note clast imbrication (20cm-long notebook is aligned with imbrication). **C.** Small-scale, trough cross-bedded, coarse to pebbly sandstone interbedded with fining-upward cobble conglomerate lenses at Potato River Falls (9cm-long scale bar). **D.** Cobble conglomerate with imbricated clasts at Potato River Falls; majority of clasts are felsic volcanic rocks with minor quartzite, granitoid gneiss and mafic igneous clasts (12cm-long pen for scale is circled). **E.** Sharp-based sandy and carbonate-cemented matrix-supported conglomerate interbedded with flat- to low-angle laminated sandstone at 255-251 m depth in core WP-345 (68-64 m below base Nonesuch Formation). **F.** Interbedded red-brown mudstone and cross-bedded feldspathic litharenite at 204 m depth in core WP-345 (17 m below base Nonesuch Formation). **G.** Feldspathic litharenite with brown mudstone partings at 215 m depth in core WP-345 (28 m below base Nonesuch Formation); white arrows point to desiccation cracks and many mudstone partings recovered in this core display crinkled-wrinkled laminae and roll-up structures typical of microbial lamination; white bar is c. 10 mm for scale.

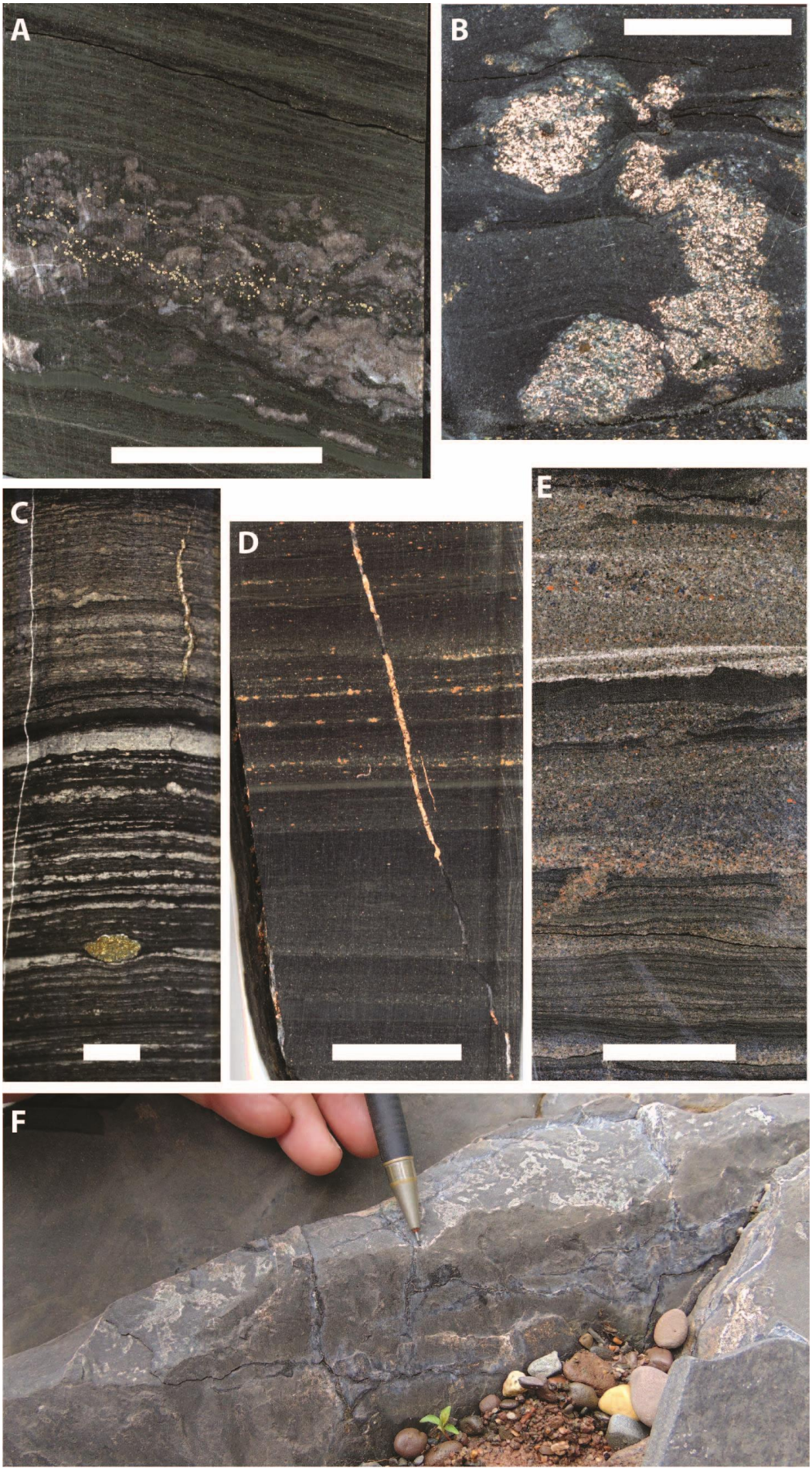
A
B
C
D
E
F

← Fig. 2.4. Diagenetic fluid-flow features in the Nonesuch Formation. **A.** Late pyrite crystals growing across calcite-pseudomorphed evaporite nodules (core JBY-002 depth 121.6 m; 5.8 m above base of Formation). **B.** Native Cu in calcite-pseudomorphed evaporite nodules, pellets and syneresis crack (core WP-436 depth 250.3 m; 0.95 m above base of Formation). **C.** Pre-compactional early pyrite crystal replacing cauliflower-shaped calcite pseudomorphed evaporite nodule; cross-cutting veins are calcite (core WP-224 depth 28.6 m; 13.8 m above base of Formation). **D.** Native Cu vein cutting chalcocite-rich laminae (core WP-126 depth 644.3 m; 0.41 m above base of Formation). **E.** Early chalcocite formed *in situ* and reworked as infill in desiccation cracks (core WP-398 depth 727.9; 0.18 m above base of Formation). **F.** Remobilised hydrocarbons forming pyrobitumen vein network (20 m above base of Big Iron River section). White bars in images are c. 10 mm for scale.

marine environment (Elmore 1983, 1984, 1989; Suszek 1997). Consequently, the geological evidence for a lacustrine depositional setting became reliant on two lines-of-reasoning: the first was that the Nonesuch strata and stromatolitic intervals in the upper Copper Harbor Formation must be non-marine because they are sandwiched between thick non-marine red beds (the overlying Freda and underlying Copper Harbor formations) and the second was that the position of those rocks several hundreds of kilometres into the interior of the Laurentian craton made it doubtful that they were part of a marine embayment (e.g. Ojakangas et al. 2001). Regarding the first line-of-reasoning, there are ample examples of braided rivers and alluvial fans that interfinger with marine bodies of water and encase marine sediment, exemplars include the fringing shorelines of the Gulf of California, Red Sea and Persian Gulf. Schumm (1968) highlighted that, prior to the evolution of bank-stabilising land plants, many pre-Phanerozoic fluvial systems were braided in character; such settings would have occurred across all latitudes and climatic regimes and were capable of delivering coarse detritus directly to coastal and nearshore marine zones worldwide. Hence, the presence of braided fluvial rocks above and below the Nonesuch Formation and Copper Harbor stromatolites does not imply a lacustrine setting for the rocks in between. Regarding the second line-of-reasoning, it is important to note that many modern intra-cratonic marine-influenced water bodies are located hundreds of kilometres from their associated open-marine shorelines: St Petersburg (Russia), the 700-km-long Gulf of Bothnia, western margin of Hudson Bay and 400-km-long James Bay in Hudson Bay are 1400 km, 500 km, 800 km and 1300 km, respectively, from their

Fig. 2.5. Diagenetic fluid-flow features in the Nonesuch Formation. **A.** Early calcite concretion cut by desiccation cracks (24.5 m above base of Big Iron River section). **B.** Pre-compaction/lithification network of calcite concretions (23 m above base of Big Iron River section). **C.** Abundant early formed calcite concretions in bedding-plane view (24 m above base of Big Iron River section). **D.** Late calcite concretion cutting across laminae (17 m above base of Big Iron River section). **E.** Chloritised concretion cutting dark-grey shale with abundant blebs of calcite-pseudomorphed evaporites; ghost laminae present in middle part of concretion (core JBY-002 core depth 113.6 m; 41.6 m above base of Nonesuch Formation); white bar is c. 10 mm for scale.

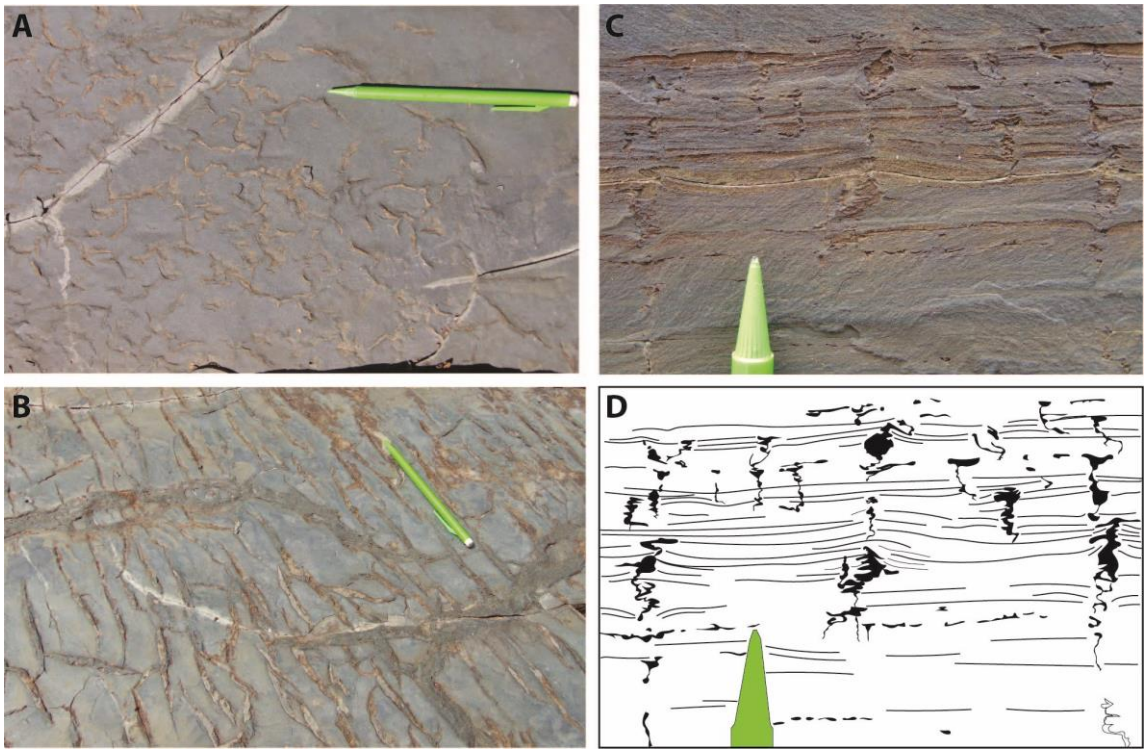

Fig. 2.6. Subaqueous (syneresis) cracks in siltstones and very fine sandstones of the Nonesuch Formation, note that most are bound with calcite cement. **A-B.** Irregularly shaped and spaced (bifurcating and bird-foot shapes) versus more regularly spaced and aligned to branching cracks; note that in B the calcite-cement filled cracks are cut by mud-filled desiccation cracks attesting to the former's syn-depositional formation. **C.** Ptygmatically folded subaqueous cracks in cross-section view; note upward and downward tapering of the cracks, as well as bowing of laminae at many crack tips. **D.** Line drawing of C. Examples A-D, and many others like them, occur from c. 2 to 30 m above the base of the Big Iron River section.

nearest open-marine shorelines. Inferred paleogeography of the basin therefore cannot be used to disprove a marine setting.

Regarding biogeochemical data, S:C ratios, sulphur isotopes and molecular biomarkers in the Nonesuch Formation would be consistent with deposition under marine conditions (Pratt et al. 1991; Hieshima and Pratt 1991; Imbus et al. 1992). However, Os isotope data from the Formation have been considered incompatible with the postulated Os composition of 1-billion-year-old seawater (Cumming et al. 2013). Given the volume of early- and late-stage diagenetic fluids that have moved through those rocks, as evident by several generations of pyrite, differing oxidation states of Fe- and Cu-bearing minerals, remobilised hydrocarbons, subaqueous (syneresis) cracks and abundant concretions (Figs. 2.4-2.6), it is conceivable that some geochemical records may be compromised. We present new sedimentological observations from the upper Copper Harbor and Nonesuch formations with the aim to

provide independent evidence for assessing the depositional setting and geochemistry of this crucial palaeoenvironmental archive.

2.3. Sedimentological observations

More than 150 years of copper mining in the Keweenaw Peninsula region has resulted in several hundred drill cores through the Copper Harbor-Nonesuch formations; we studied 80 that contain the most complete sections of the Nonesuch Formation and the upper part of the Copper Harbor Formation. To complement the core data, we logged sections of the formations in exposures at Potato River, Presque Isle, Big Iron River, Nonesuch Mine, Eagle River and Horseshoe Bay (Fig. 2.1) and used those combined datasets to construct the stratigraphic framework shown on Figure 2.7. The datum for that framework is a surface that marks a facies change in the upper part of the Nonesuch Formation. This change is expressed Peninsula-wide and is pinpointed in core and outcrop as a contact separating an underlying succession of dm-thick beds of grey to reddish-grey, flat-laminated and shallow trough cross-bedded sandstone, shale and mudstone, in places arranged into many-metres-thick, thickening- and coarsening-upward cycles, from an overlying succession of rippled dark grey shale and thin-bedded grey sandstone. To aid correlations in the north-eastern part of the outcrop belt we also used the 'Marker Bed', a fine-grained marl-mudstone unit containing abundant mm- to cm-scale blebs of calcite, which constitutes one of the informal members mining company geologists have defined to subdivide the Cu-bearing part of the lower Nonesuch Formation (Fig. 2.7).

2.3.1. Upper Copper Harbor Formation stromatolite interval (Horseshoe Harbor)

The upper part of the Copper Harbor Formation contains two stromatolitic-oncolitic-oolitic limestone-bearing intervals (Elmore 1983) that have received considerable attention because of their potential as indicators for Mesoproterozoic non-marine life (e.g. Fedorchuk et al. 2016). We examined one of those, Horseshoe Harbor (Fig. 2.1; the other occurrence is Dan's Point, c. 15 km further west), and there the limestones occur as lenses to laterally continuous beds that are many centimetres to several decimetres thick (Figs. 2.8-2.10). Bases and tops of the limestone layers are sharp: bases commonly drape across underlying surface irregularities and cobbles that

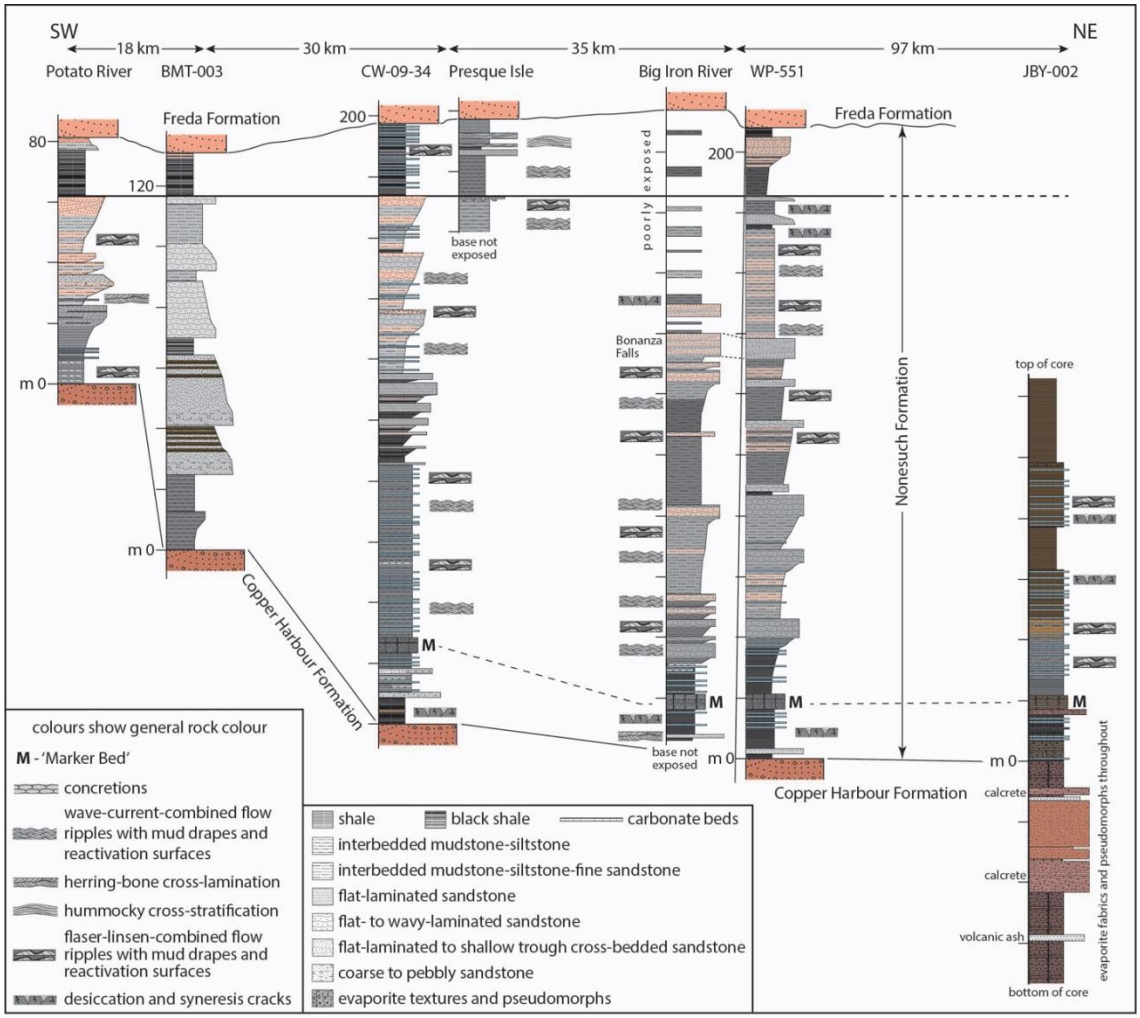

Fig. 2.7. Stratigraphic cross-section of the Nonesuch Formation illustrating key outcrop sections and cores. See Figure 2.1 for locations and text for discussion.

were standing proud prior to calcium carbonate deposition, whereas tops are onlapped and buried by the overlying siliciclastic rocks. Stromatolites are laterally-linked, multi-digitate domal and hemispheric forms marked internally by sub-mm-thick crinkled-wrinkled laminae commonly separated by thin mud drapes and partings (Fig. 2.9A). In many places the stromatolites are broken, folded and brecciated (Fig. 2.9B). Detailed petrography by Fedorchuk et al. (2016) identified laminae formed by both biogenic and abiogenic (e.g. isopachus cements) calcium carbonate precipitation. The limestone layers are interbedded with patchily exposed reddish siltstone, sandstone and pebbly sandstone with calcium carbonate-filled desiccation cracks that penetrate downward for several to many centimetres (Fig. 2.9C-D). All previous workers have noted the observations described above for the limestones. Here we highlight

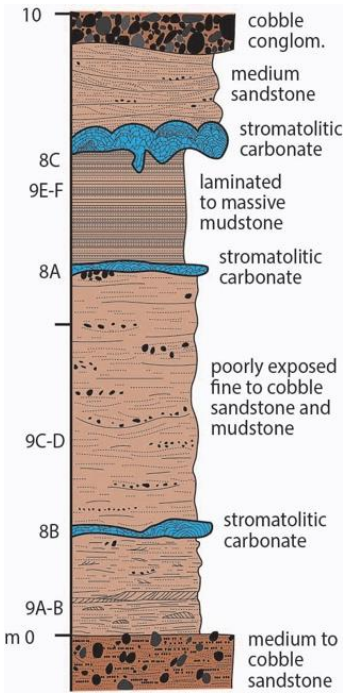

← Fig. 2.8. Logged section of Horseshoe Harbor stromatolite-bearing interval in the upper Copper Harbor Formation. Numbers to left of column are keyed to photographs in Figures 2.9 and 2.10. See Figure 2.1 for location and text for discussion.

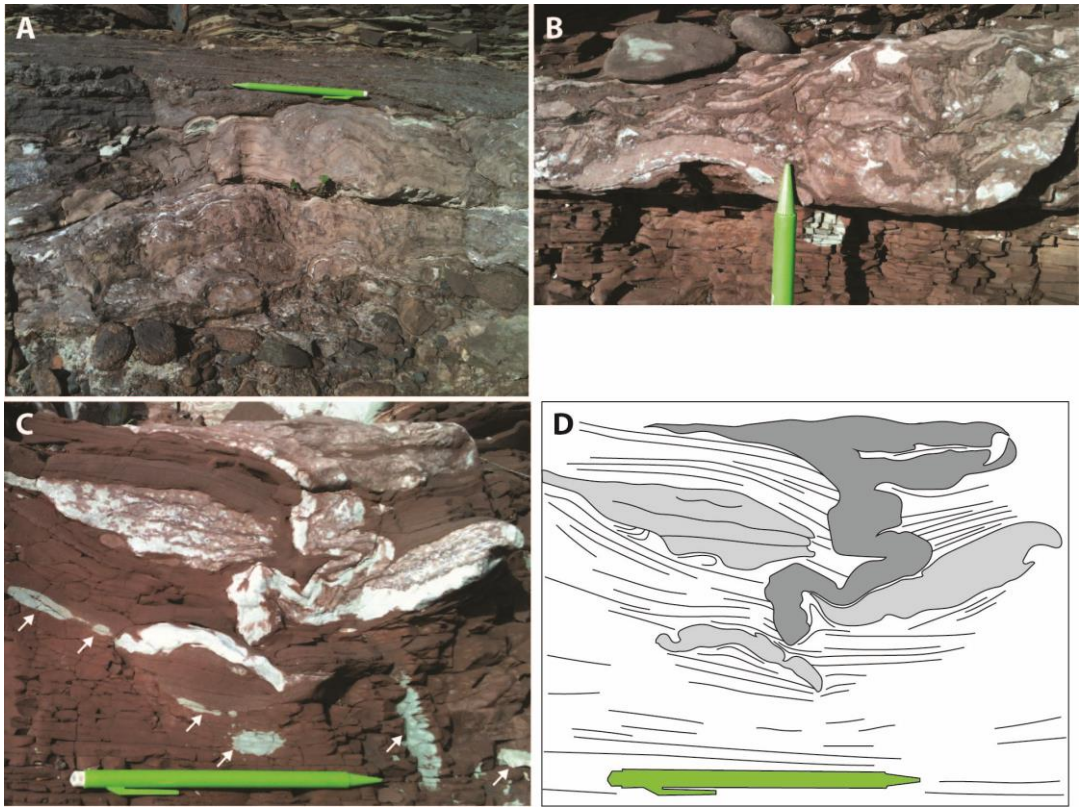

Fig. 2.9. Horseshoe Harbor stromatolitic limestones. **A.** Stromatolite mound growing upward off a cobble conglomerate bed; note numerous mud partings between laminae. **B.** Broken and brecciated stromatolite layer; note tepee-like and thrusted geometries for some of the fragments. **C.** Tightly folded calcite-filled desiccation crack; white arrows point to pale green coloured reduction spots and fracture surfaces. **D.** Line drawing of C. The calcite-filled desiccation crack is shaded a darker grey. Calcium carbonate layers that lack stromatolitic/ microbial textures or laminae and instead display clotted to massive textures are shown in lighter grey; their growth has caused disruption and folding of lamination in the adjacent siliciclastic layers. See text for discussion and Fig. 2.8 for stratigraphic location of features.

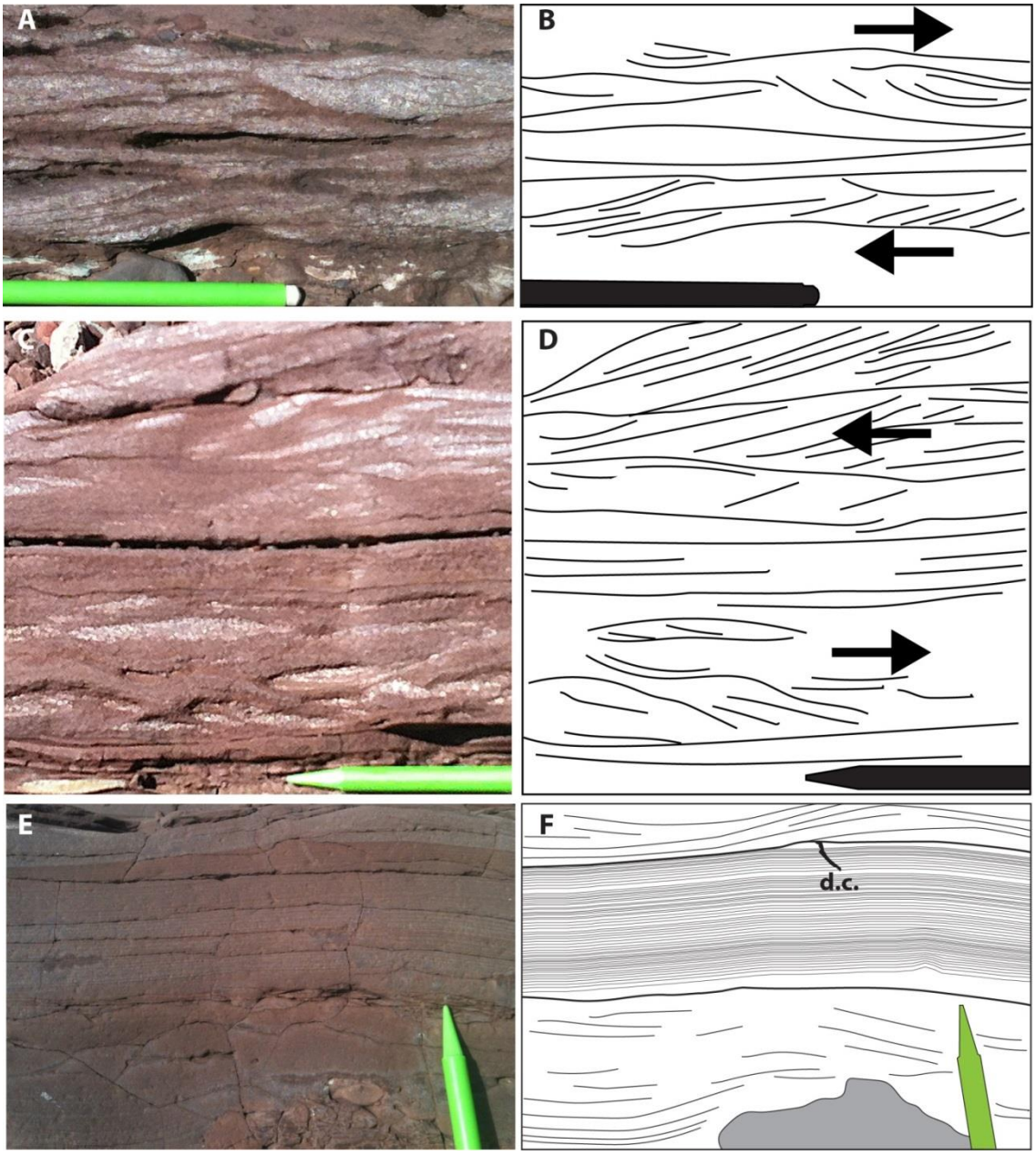

Fig. 2.10. Tide-influenced sedimentary structures in Horseshoe Harbor siliciclastic rocks. **A-D.** Photographs and associated line drawings of linsen and flaser bedded sandstone exhibiting superposed bimodal (herring-bone) sediment transport directions and abundant reactivation surfaces and laminae with mud drapes; planar cross-bedded sand-waves with reactivation surfaces cap the succession in A. **E-F.** Bundles of repetitively varying thick-thin laminae couplets (d.c. – desiccation crack); grey region at base of photo outlines micrite nodules and clots, likely calcite pseudomorphs of precursor evaporites. See text for discussion and Figure 2.8 for locations of features within the stratigraphy.

sedimentological features in the siliciclastic intervals that have received less attention but bear strongly on interpretations when placed within the context of the upper Copper Harbor-Nonesuch succession. The key features are superposed ripple sets that display bimodal (herring-bone) sediment transport directions and are marked by mud-drapes and reactivation surfaces (Fig. 2.10A-D). There are also dm-thick intervals of red

mudstone that display well-preserved laminae arranged in cm-thick stacked bundles of repetitively alternating thicker and thinner couplets implying a cyclical periodicity (Fig. 2.10E-F). Further, in instances where calcium carbonate layers lack microbial lamination and instead are characterised by massive or clotted textures, both the siliciclastic strata along the contact with those layers and the limestone layers themselves display isoclinal folding and warping (Fig. 2.9C-D).

2.3.2. Uppermost Copper Harbor Formation

In cores, as much as 200 m of the upper Copper Harbor Formation consists of interbedded red conglomerate and sandstone and reddish-brown mudstone that contain abundant evaporitic fabrics and pseudomorphs (Fig. 2.11). Many conglomerate and sandstone intervals are calcrete marked by cobbles coated with cm-thick rinds of calcite cement embedded within a calcite-impregnated matrix of poorly sorted silt to pebble grain sizes (Fig. 2.11A-B). The sandstones and mudstones are replete with cm- to dm-thick zones of chicken-wire fabric, closely spaced clots, nodules and stringers of calcite-pseudomorphed evaporite fabrics and caliche containing tepee structures, desiccation cracks and, in places, light grey cm-thick micritic limestone and gypsum layers (Figs. 2.11C-H).

2.3.3. Nonesuch Formation

The Nonesuch Formation has been described in detail by a number of workers (Elmore 1989; Suszek 1997; Stewart and Mauk 2017). In brief, it is a succession of grey

→ **Fig. 2.11.** Evaporite fabrics and features in the uppermost Copper Harbor Formation. **A-B.** Calcrete and caliche conglomerate (A – core JBY-002 depth 164-162 m, 37-35 m below base of Nonesuch Formation; B – core WP-345 depth 276 m, 89 m below base of Nonesuch Formation). **C.** Zones of caliche, calcite-pseudomorphed evaporite nodules and chicken-wire fabrics in fine to medium sandstone (core WP-345 depth 346-345 m; 160-159 m below base of Nonesuch Formation). **D.** Red-brown mudstone with abundant calcite-pseudomorphed evaporite nodules and thin limestone layers (core JBY-002 depth 199-198 m; 71-70 m below base of Nonesuch Formation). **E.** Tepee and caliche fabrics in fine sandstone (core WP-345 depth 363 m; 176 m below base of Nonesuch Formation). **F.** Close up of chicken-wire fabric in C. **G.** Caliche in fine sandstone (core WP-345 depth 326 m; 139 m below base of Nonesuch Formation). **H.** Gypsum layers in red-brown fine sandstone (core CW-09-95 depth c. 131 m or 433'; lower layer is 18 cm below base of Nonesuch Formation). White bars are c. 10 mm for scale.

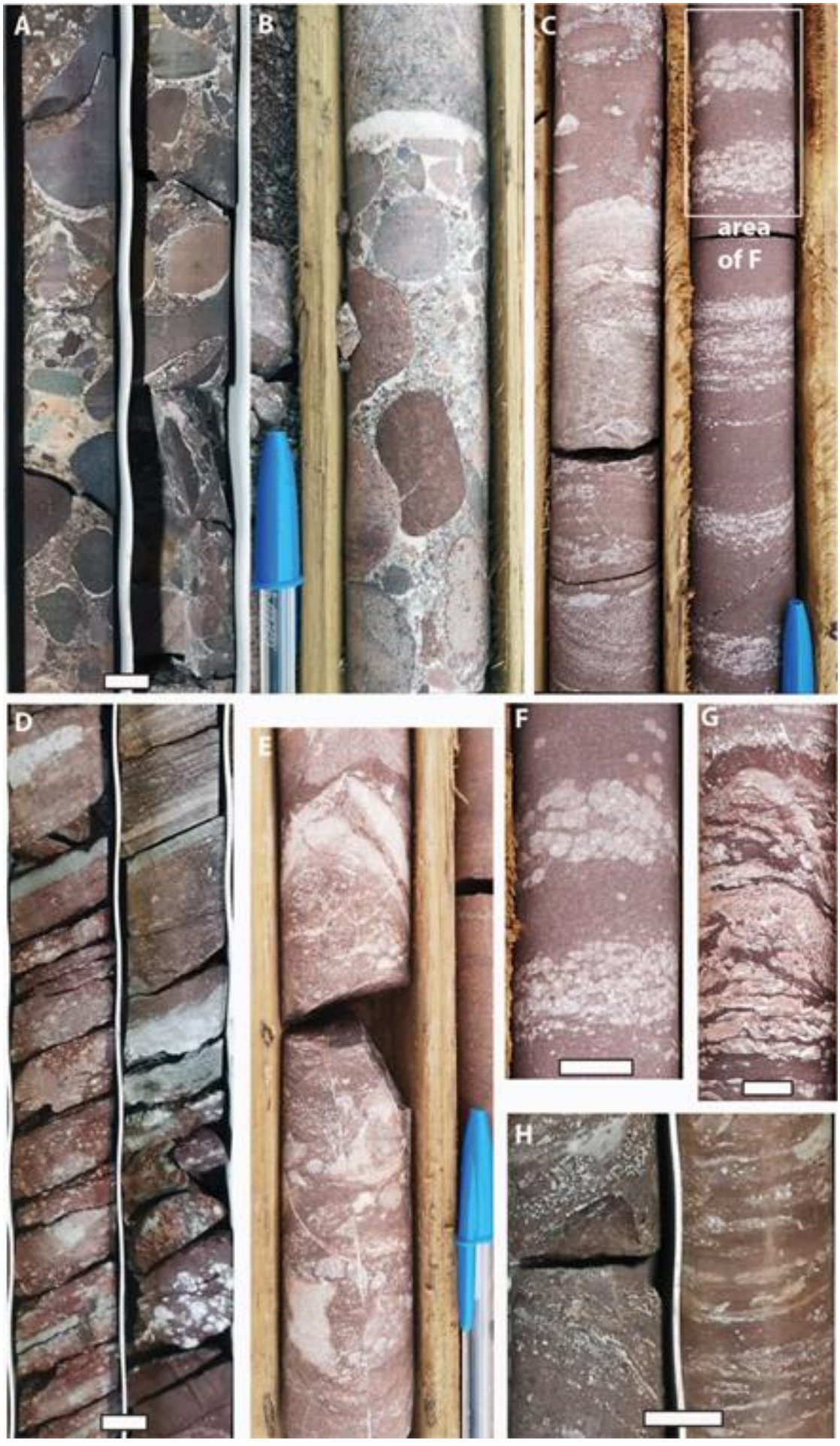
A
B
C
area
of F
D
E
F
G
H

to black mudstone, shale and fine sandstone in beds from a few centimetres to many decimetres in thickness. Thin calcium carbonate beds punctuate the Formation, particularly in its lower part. Sedimentary features that have been documented previously include desiccation cracks, cm-scale wave and other ripple forms and microbially induced sedimentary structures (Figs. 2.12, 2.13).

What is striking about the Nonesuch rocks is the ubiquity of flaser, wavy, linsen and pinstripe bedding, combined-flow ripples, flat-topped symmetric ripples, climbing ripples, mud drapes and reactivation surfaces associated with all ripple forms, local presence of repetitively stacked sets and co-sets of bimodal (herring-bone) ripple cross lamination, metre- to decametre-scale thickening- and coarsening-upward depositional cycles and in places metre-scale hummocky cross-stratification (Figs. 2.14, 15). The flaser-linsen-wavy-pinstripe ripples exhibit heights ranging from a few millimetres to as much as 5 cm and in almost all instances crests, troughs and individual foresets are outlined by mud drapes or encased in mudstone partings. Wavelengths for current and combined-flow ripple forms, as measured on bedding planes, range from 3 cm to as much as 10 cm whereas those for symmetric and flat-topped symmetric ripples are smaller, typically between 3 cm and 5 cm. Further, ripple sets and co-sets in many places display repetitive patterns of thicker and thinner foresets in which the thicknesses of mudstone partings and drapes are inverse to the thickness of the sand-silt foresets and these are associated, laterally and vertically, with dm-scale repetitions of pinstripe, linsen, wavy and flaser-bedded ripples.

Although there is only one other report of the presence of syn-sedimentary evaporites in the Nonesuch Formation (gypsum laths in mudstone; see Fig. 2.4d in Elmore et al. 1989) there are an abundance of evaporite pseudomorphed minerals and fabrics present (Fig. 2.16). In the Nonesuch drill cores that we examined, these features were present at different stratigraphic levels and through the entirety of the Formation in the easternmost studied occurrences. They take the form of needles, laths, clots, nodules, blebs, clusters of nodules and as irregular blebs/clots arranged in discontinuous laminae. Sizes of all these forms vary from sub-mm to as much as several centimetres in diameter or length (Fig. 2.16).

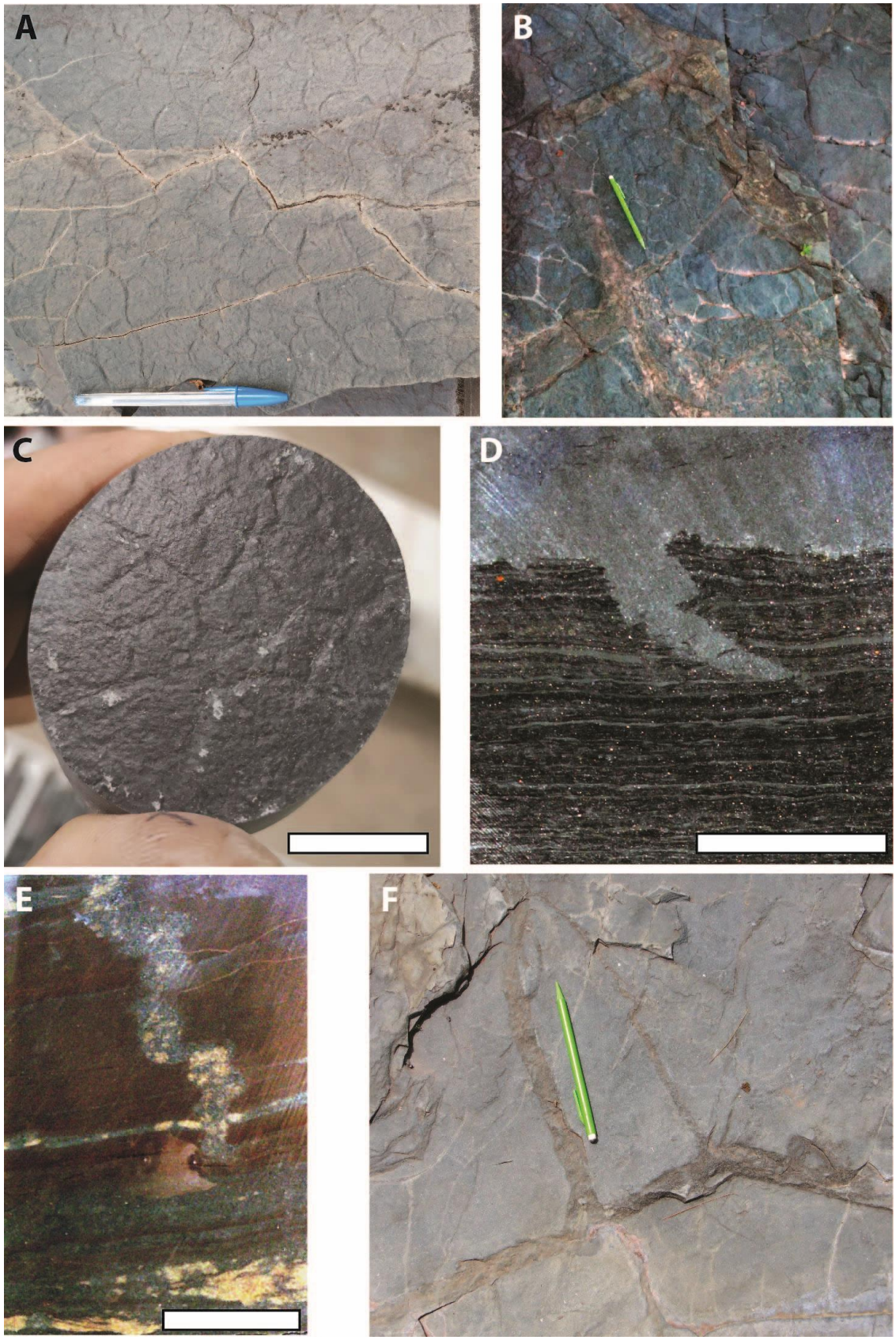

Fig. 2.12. Desiccation cracks in the Nonesuch Formation. **A.** 1 m above base of Big Iron River section. **B.** 161 m above base of Big Iron River section. **C.** 45 m above base of Formation in core JBY-002 (core depth 81.5 m). **D.** 0.5 m above base of Formation in core WP-299 (core depth 250.7 m). **E.** 39 m above base of Formation in core JBY-022 (core depth 88.2 m). **F.** 20 m above base of Big Iron River section.

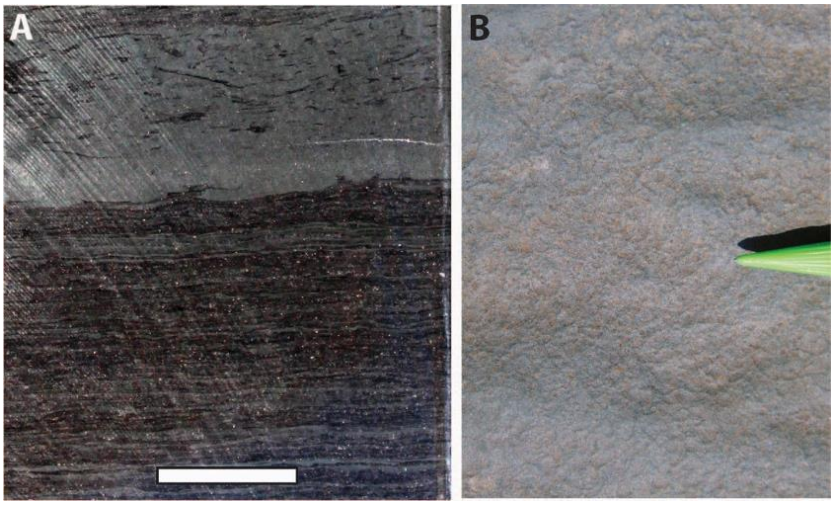

Fig. 2.13. Microbial laminae and structures in the Nonesuch Formation. **A.** Black crinkle-wrinkle laminae 3 m above base of Formation in core WP-299 (core depth of 250.7 m); note rip-up flakes of microbial laminae in the overlying lighter grey mudstone. White bar c. 10 mm for scale. **B.** Elephant-skin textured bedding surface 17 m above base of Big Iron River section.

2.4. Discussion: marine-influenced sedimentation

We combine our new sedimentological observations with previously reported ones to compare and contrast the abundance of sedimentary features known from lacustrine shoreline-littoral-sublittoral zones to those from tide- and wave-influenced marine shoreline-shoreface-shelf settings (see Table 2.1). Although these environments share many of the same sedimentological features, we use the presence/absence of key features, combined with their commonality/paucity, to inform and guide our interpretation of the upper Copper Harbor and Nonesuch rocks. We conclude that the weight of evidence indicates a marine influence on the sedimentation of those strata.

2.4.1. Features indicative of oscillatory or combined flows

Wave periods of many seconds and associated horizontal orbital velocities of many $dm*s^{-1}$ to as much as $1m*s^{-1}$ or more are common in marine settings and known to be generated by storm events in large lakes. Their associated flows can mobilise and mould a spectrum of sedimentary structures across a wide range of grain sizes (e.g. bedform stability diagrams of Middleton and Southard 1984). These structures include symmetric and combined-flow ripples (ripples with symmetric form but marked internally by foresets migrating in one direction) and hummocky cross-stratification.

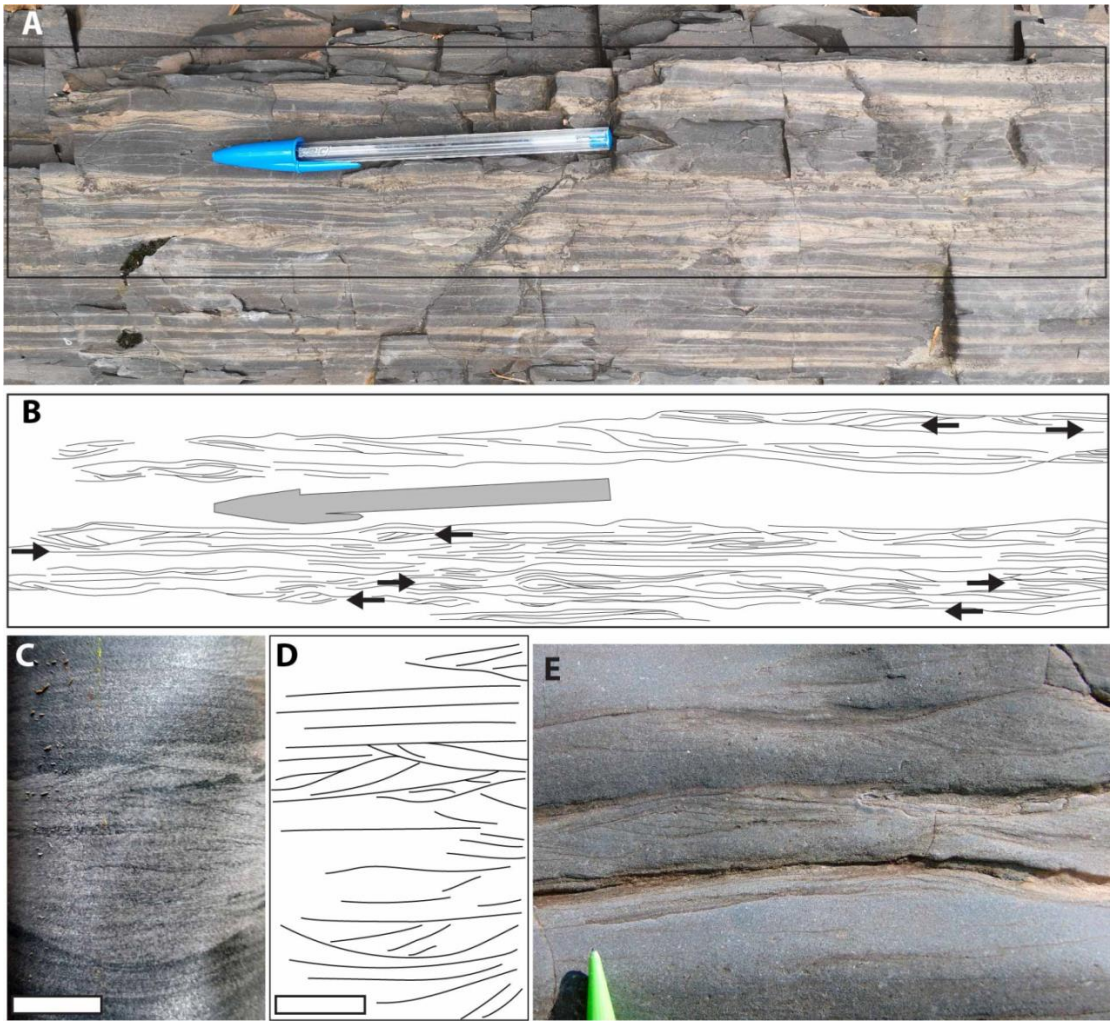

Fig. 2.14. Tide-influenced sedimentary structures in the Nonesuch Formation. **A.** Repetitive sets of flaser, linsen and pin-stripe bedding 27 m above base of Formation in Potato River section. **B.** Line drawing of boxed area in A showing the bimodal sediment transport directions (black arrows) in ripple cross-lamination and reactivation surfaces. **C.** Flaser bedding with bimodal (herring-bone) ripple cross lamination 164 m above base of Formation in core WP-551 (core depth 430 m); white bar is c. 10 mm for scale. **D.** Line drawing of C. **E.** Combined-flow ripples with mud drapes and reactivation surfaces 57.5 m above base of Big Iron River section.

The former two occur in both marine and lacustrine settings, although combined-flow ripples are more prevalent in marine settings hence their abundance in the Nonesuch Formation is noteworthy, however the presence of large-scale hummocky cross-stratification in the Nonesuch Formation (Fig. 2.15A) is of particular significance.

Hummocky cross stratification (HCS) forms mostly in silt- and fine-sand-sized sediment under strong oscillatory flows (many tens of cms^{-1}), with or without a weaker superimposed unidirectional component (e.g. Arnott and Southard 1990; Southard et al. 1990; Myrow and Southard 1996; Dumas et al. 2005). This process-product is

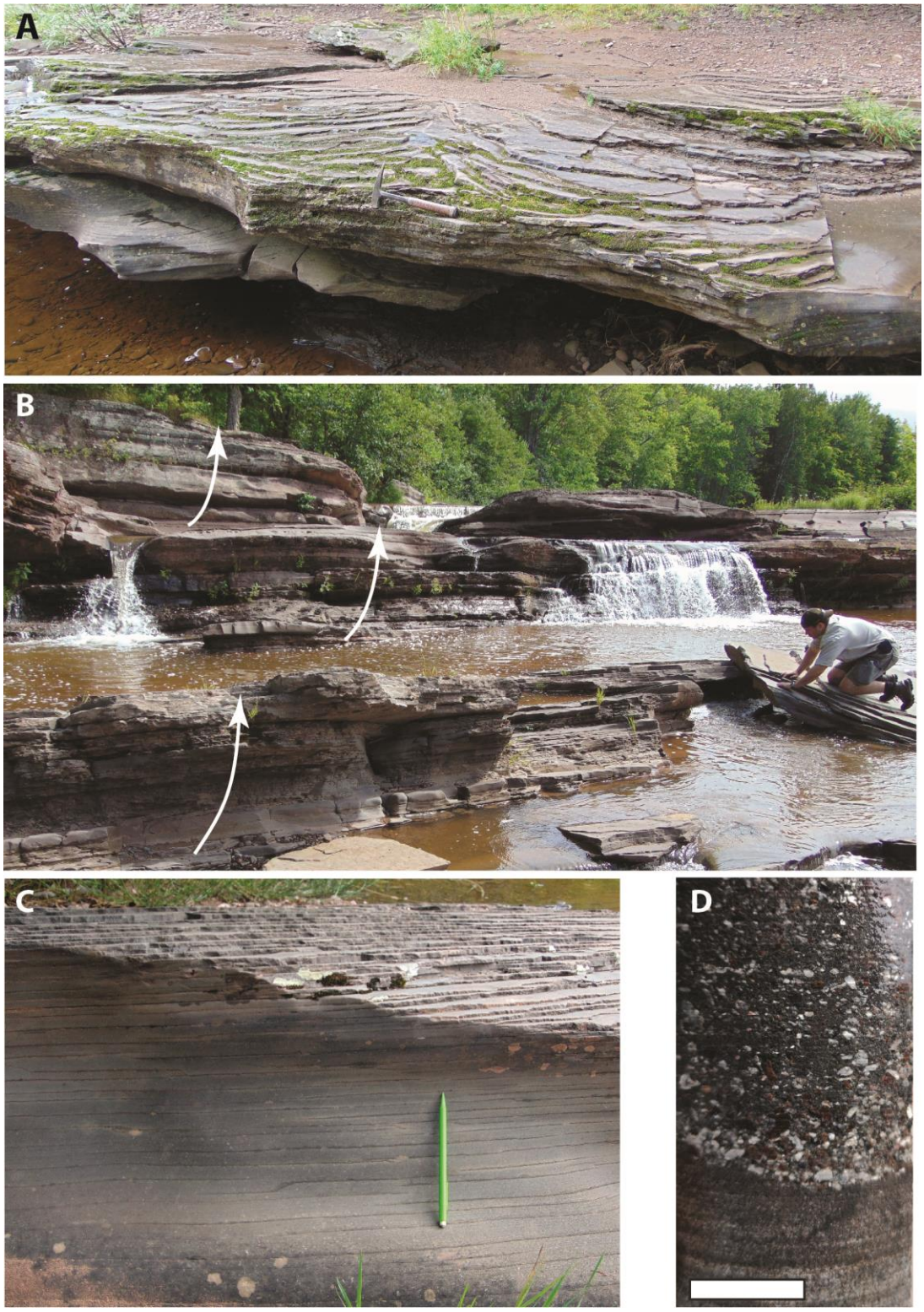

Fig. 2.15. Shelf-shoreline sedimentary structures in the Nonesuch Formation. **A.** Metre-scale hummocky cross-stratification (hammer at crestline for scale); Presque Isle section 4 m below base of Freda Formation. **B.** Many-metres-thick thickening- and coarsening-upward cycles composed of interbedded mudstone and flaser-linsen-combined-flow rippled siltstones and fine sandstones upward into flat-laminated medium sandstone (Bonanza Falls 138 m above base of Big Iron River section). **C.** Flat to low-angle laminated sandstone that mark the top of thickening and coarsening-upward cycles (this is the uppermost sandstone bed shown in B). **D.** Sharp-based oolitic-lithic grainstone-packstone (core JBY-002 depth 120 m; 7 m above base Nonesuch Formation).

attributed to sedimentation under storm waves acting on geostrophically driven storm-surge ebb flows that transport sediment from the shoreface across the shelf (Dott and Bourgeois 1982; Duke 1990; Duke et al. 1991). Central to that interpretation is that the spacings of hummocks scale to the horizontal diameters of wave-orbitals that penetrate downward through the water column to the seabed beneath the irregular (non-periodic, non-uniform) surface-gravity waves that typify a storm-generated sea state. This embodies the concept of the tempestite facies model (Ager 1974; Aigner 1982; Myrow and Southard 1996) whereby HCS is seen as part of a spectrum of storm-related features; *sensu stricto*, it is a bed of dm-scale thickness with a sharp, nearly flat base overlain by low-angle ($<15^{o}$) intersecting sets of convex- and concave-up laminae arranged into domes (hummocks) and basins (swales) with spacings on the scale of metres and capped by wave ripples; laminae dip-directions are quaquaversal, reflecting the overall sculpting of the seabed into an irregular hummock/dome and swale/basin topography (Dott and Bourgeois 1982; Duke et al. 1990; Myrow 2005); although anisotropic aggradation can occur with a strong enough unidirectional flow component (e.g. Arnott and Southard 1990).

Hummock spacings of c. 1 m and larger are considered a key criterion for assigning a genesis to storm waves on a marine shelf (e.g. Duke et al. 1990; Myrow 2005). In contrast, low-angle convex-upward bundles of laminae having spacings on dm-scales in siltstones and sandstones can form under a wide variety of combined oscillatory and unidirectional flow conditions, internal waves, scour-and-drape processes and short-term spatial-temporal contractions and expansions in flow thicknesses (e.g. Prave and Duke 1990; Prave 1990; Morsilli and Pomar 2012). The latter flow variations in particular can create hydraulic jumps between the lower-flow-regime subcritical states under which ripples form, and the upper-flow-regime critical states under which planar wavy laminae form and result in stacked sets of hummocky-wavy laminae intercalated with cross-lamination and ripple forms. Prave and Duke (1990) termed these features small-scale HCS, which are not diagnostic to any particular setting as evident by their recognition in facies ranging from abyssal turbidites (Prave and Duke 1990) to intertidal and shoreline sand bodies (e.g. Greenwood and Sherman 1986; Yang et al. 2006). Almost all HCS identified in lacustrine strata is small-scale HCS, i.e. wavy-parallel laminae with crest-to-crest

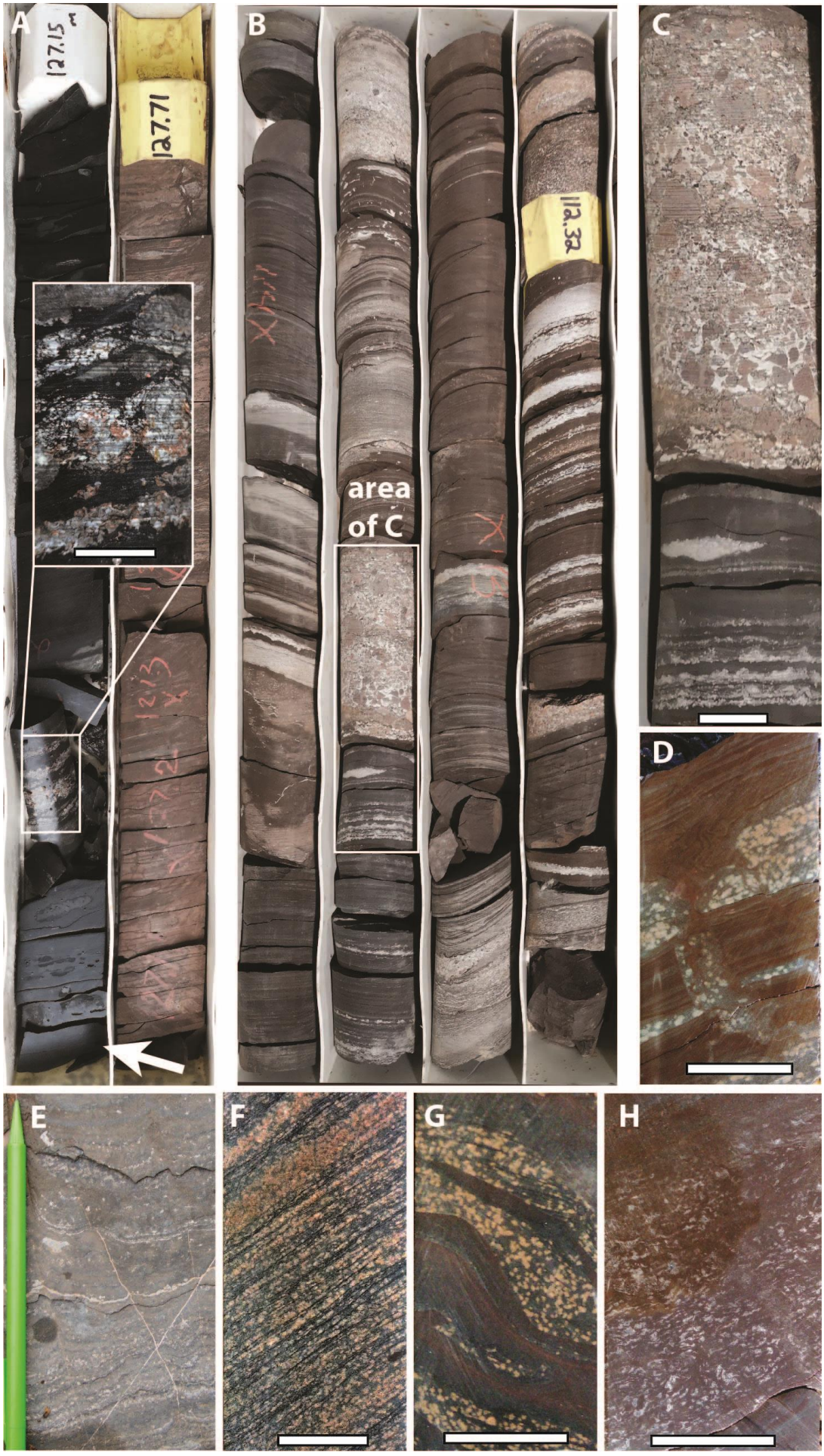
A
B
C
D
E
F
G
H
area of C

← Fig. 2.16. Fabrics and textures of former Ca-sulphate evaporites in the Nonesuch Formation. **A.** Sharp contact (marked by arrow) of basal black shale of Nonesuch Formation on red-brown mudstone of Copper Harbor Formation; calcite-pseudomorphed evaporite nodules and pellets are present within both formations with inset photo highlighting those in the basal Nonesuch Formation (core JBY-002 depth 127 m; base Nonesuch Formation). **B.** Interbedded polylithic caliche with red-brown, grey and black mudstone/shale containing calcite-pseudomorphed evaporite nodules (core JBY-002 depth 118-16 m; 9-11 m above base Nonesuch Formation). **C.** Close-up of polylithic caliche and underlying black shale with calcite-replaced evaporite layers in B. **D.** Calcite pseudomorphed evaporite nodules in red-grey mudstone and in desiccation crack (core JBY-002 depth 113 m; 14 m above base Nonesuch Formation). **E.** Marker Bed showing laminated grey shale with stringers of calcite-pseudomorphed evaporite blebs (17.5 m above base Nonesuch Formation Big Iron River section). **F.** Stringers of calcite-pseudo-morphed evaporite blebs in black shale (core JBY-002 depth 72 m; 55 m above base Nonesuch Formation). **G.** Interbedded red-brown and dark grey mudstone with the latter containing abundant calcite-pseudomorphed evaporite blebs (core JBY-002 depth 97 m; 30 m above base Nonesuch Formation. **H.** Calcite-pseudomorphed former evaporite laths in red-brown mudstone (core JBY-002 depth 109 m; 18 m above base Nonesuch Formation). White bar in photos is c. 10 mm for scale.

spacings <1 m and associated with intervals of wave or combined-flow ripples or scour-and-drape features (e.g. Andrews and Hartley 2015; Dam and Surlyk 1993; Eyles and Clark 1986; Greenwood and Sherman 1986; Ilgar and Nemec 2005; Jiang et al. 2018). In contrast, the HCS observed in outcrop of the Nonesuch Formation is identical to large-scale HCS recognised elsewhere that is unequivocally attributable to storm waves in inner-mid marine shelf settings, i.e. dm-thick fine sandstone beds with flat bases and characterised internally by hummocky cross-stratification with crest-to-crest spacings of 1-4 m.

2.4.2. Features indicative of periodically reversing or flashy (frequently accelerating-decelerating) flows

Flaser, linsen, wavy and pinstripe bedding, reactivation surfaces and mud drapes, flat-topped wave ripples, bimodal (herring-bone) cross lamination and combined-flow ripples are hallmark features of sedimentation in shallow-marine settings. They reflect the frequent alternations in flow directions, flow accelerations and decelerations and associated changes in bed-generated shear stresses that mark tides and currents in marine shoreface-inner shelf settings. However, these sedimentary structures have also been reported from numerous ancient lacustrine settings where they can form by flashy fluvial discharge along shorelines and into the

littoral zones of lakes as fluvial flow competency decreases via dissipation and flow expansion and via interactions with waves (e.g. Greenwood and Sherman, 1986; Ilgar and Nemec, 2005; Smith et al., 2015; Andrews and Hartley, 2015; O'Connell et al., 2017; Bright et al., 2018; Dorsey et al., 2018; Shchepetkina et al., 2019). In contrast to the discrete intervals in which such rippled facies are reported in lacustrine strata (*op. cit*.), what is striking about the Nonesuch Formation is the ubiquity of these ripple forms throughout its stratigraphy. This implies that the process by which they formed was similarly pervasive, which is a characteristic more readily attributable to marine than lacustrine settings.

2.4.3. Periodically repetitive sedimentary structures

Both the upper Copper Harbor and Nonesuch formations contain intervals in which sedimentary structures are present that display well-developed, periodically repetitive patterns or bundles of thinning and thickening of individual laminae or dm-thick rippled intervals. Foreset thicknesses and mudstone-to-sandstone ratios are inversely related, including instances showing systematic vertical change from pinstripe-linsen-wavy-flaser beds and *vice versa*. These features regularly occur interbedded with one another, indicating that they formed in settings with flows that fluctuated from being strong enough to generate shear stresses capable of transporting sand-sized sediment to stagnant periods in which clays and muds settled out of the water column. Those fluctuations were short-lived, occurring on the temporal scale of laminae/ripple deposition and, further, many of these intervals also contain desiccation cracks. This eliminates varves as an interpretation of these repetitive features because varves form in the open, low-energy, deeper profundal portions of water bodies (e.g. Zolitschka et al. 2015). Consequently, the most straightforward interpretation of all of these rhythmic to periodically repetitive sedimentation patterns is as tidal bundles. Given that tidal currents are negligible even in the largest lakes (e.g. Lake Superior's tidal range is typically 5 cm or less; NOAA Great Lakes website) the environment of deposition of these strata is reasonably viewed as a tidally influenced marine shoreline-nearshore setting.

We have not determined periodicities of the Nonesuch tidal bundles to see if they match tidal spectra for 1 Ga but such spectra require additional evidence to be

conclusive. For example, Fourier transformations on laminae and foreset couplets preserved in the Neogene Bouse Formation, California, USA, yielded power spectra interpreted by some workers as daily-monthly tidal rhythmites (O'Connel et al. 2017) and by others as decadal-scale climatic lacustrine cycles (Bright et al. 2018). A tidal interpretation was confirmed by the presence of herring-bone cross strata (Dorsey et al. 2019). Sedimentological observations also underpin our interpretation of the periodically rhythmic features in the upper Copper Harbor and Nonesuch rocks as tidal bundles: they are interbedded with facies having desiccation cracks, herring-bone cross-lamination, abundant flaser bedding and wave- and combined-flow ripples.

2.4.4. Evaporite minerals and oolites

Oolites are not uncommon in lakes, hence their presence is inconclusive in differentiating between lacustrine and marine settings. In situations where freshwater has dissolved Ca^{+2} + Mg^{+2} > HCO_3^-, and notwithstanding its generally low concentration of S species, gypsum precipitation (rather than Na-rich evaporates) can occur as lakes evaporate (Eugster and Hardie 1975; Smoot and Lowenstein 2000; Schreiber and El Tabakh 2000; Jagniecki and Lowenstein 2015); examples include the Miocene lake beds in the Ebro Basin, Spain (e.g. Orti et al. 2003), and the Triassic Passaic Formation in eastern USA (El-Tabkh et al. 1997). The presence of gypsum evaporites and pseudomorphs in the upper Copper Harbor and Nonesuch formations indicate clearly that their water bodies were more saline than freshwater. Combined with the sedimentological features with which they occur, the precipitation of these evaporite minerals and oolite formation from marine waters is the most likely scenario.

The upper Copper Harbor stromatolite intervals can also be inferred to have formed in saline water. The origin of intense folding exhibited by the limestone layers has puzzled previous workers (e.g. see discussions in Elmore 1983; Fedorchuk et al. 2016). We propose that the ptygmatically folded and broken limestones and similarly deformed laminae in the siliciclastic layers that encompass those limestones are, at least in part, enterolithic-style deformation due to the expansive growth and dissolution of former marine evaporite minerals. Storm waves are also a likely contributing factor to breaking and disrupting those beds. The caliche, calcrete and evaporite-mineral fabrics documented elsewhere in the upper Copper Harbor

Formation are further evidence in support of widespread evaporative processes occurring at that time.

2.4.5. Absence of depositional cyclicity

In certain instances, the lack of key sedimentary features is worthy of note. In the case of the Nonesuch Formation, one of the striking aspects is the lack of widespread, laterally correlative and uniform metre-scale depositional cycles. Many ancient lacustrine settings are typified by such cycles, which record repetitive shallowing (marked by evaporite-bearing sediments) and deepening (marked by well-laminated fine-grained siliciclastic sediments) patterns attributed to Milankovitch-driven climatic forcing mechanisms (Eugster and Hardie 1975; van Houten 1962; Olsen 1986 [who termed these van Houten cycles]; Aswasereelert et al. 2013; Smith et al. 2015). Although the Nonesuch Formation has numerous stratigraphic intervals that indicate shallowing and deepening, the hallmark cyclicity of lakes is lacking. In our interpretation, these sedimentation patterns are readily explained by tides and other short-term changes in relative sea level (e.g. lateral migration of fluvial influx centres).

2.5. Depositional setting

The weight of evidence based on sedimentological observations (Table 2.1) leads us to conclude that the most direct and objective interpretation of the uppermost parts of the Copper Harbor Formation, including the stromatolitic intervals, is that they represent braidplains along an evaporitic shoreline under an arid climate and that the entirety of the Nonesuch Formation was a mostly shallow-marine, saline body of water that experienced both tide- and storm-influenced sedimentation. This implies a marine embayment large enough to reach well into the Laurentian craton and fringed with sabkha-like shorelines and caliche- and calcrete-bearing braidplains. Our interpretation is compatible with inferences that an arid climate prevailed during deposition of the Copper Harbor Formation (e.g. Wright 1960; Elmore 1983) and, given the evidence for abundant evaporite and desiccated mudstone facies in the Nonesuch Formation, it is likely that this climatic regime persisted through Nonesuch time. The lack of continuous outcrops of late Mesoproterozoic rocks beyond those fringing Lake

Superior hinders efforts to determine the exact palaeogeography of this evaporitic shoreline-shallow marine embayment.

The widespread distribution of former evaporite fabrics and minerals, combined with the abundance of sedimentary structures that are attributable to tidal and shallow-marine settings, challenge ideas and hypotheses about non-marine habitats in the Proterozoic that rely on the Nonesuch Formation and Copper Harbor stromatolites having formed in a lacustrine environment. Our sedimentological findings show that the Nonesuch water body was saline, not fresh, and was shallow throughout much of its existence (abundance of desiccation cracks and strong-current-formed features) and these findings therefore require a reinterpretation of some existing geochemical datasets (e.g. Cumming et al. 2013). Our data also raise questions about the origin of the microfossils in the Nonesuch Formation (e.g. Wellman and Strother 2015; Strother and Wellman 2016); if the reported microfossils do indeed represent non-marine flora, they may have been transported from land environments via river systems and/or aeolian processes into the Nonesuch marine embayment. If so, such re-sedimentation processes will need to be considered and evaluated in palaeobiological studies focussing on assessing life in marine versus non-marine settings in Precambrian successions elsewhere.

2.6. Conclusions

The long-held inference that the late Mesoproterozoic sedimentary strata exposed along the Canadian and USA shorelines of Lake Superior were totally non-marine is not supported by sedimentological data. Numerous features in the upper Copper Harbor Formation and throughout the Nonesuch Formation, ranging from herring-bone (bimodal) ripples to ubiquitous flaser-linsen-wavy-pinstripe bedded intervals replete with reactivation surfaces, tidal bundles and desiccation cracks, to metre-scale hummocky cross stratification, to abundant evaporite fabrics and pseudmorphs after sulphate minerals, are most directly explained by a marine influence on sedimentation. Water composition throughout the deposition of these units was saline and the presence of networks of desiccation cracks at numerous stratigraphic levels in the Nonesuch Formation indicate that water depths were generally shallow for much of its sedimentation history. Instead of a fluvial-lacustrine couplet, the Copper Harbor-Nonesuch succession was a braided fluvial-evaporitic

shoreline-marine embayment triplet. Consequently, ideas regarding biospheric evolution and Earth's surface redox and oxygenation state based on the premise that those sedimentary rocks were deposited within lacustrine settings require reassessment.

Process	Sedimentary feature	Common		May be present		Rare to not present	
		Lake	Marine	Lake	Marine	Lake	Marine
Unidirect-ional flows	dm-scale trough x-bdg	X	X				
	dm-scale planar x-bdg	X	X				
	Asymmetric ripples	X	X				
	Climbing ripples			X	X		
Oscillatory or combined flows	Combined-flow ripples		X	X			
	Symmetric ripples	X	X				
	Small-scale HCS		X	X			
	Large-scale HCS		X			X	
Periodically reversing or flashy (frequently accelerating and decelerating) flows	Pinstripe-linsen-wavy-flaser bedding		X	X			
	Ripple and foreset mud drapes and partings		X	X			
	Rhythmically repetitive variations in laminae thicknesses			X	X		
	Repetitive bundles showing systematic variation in proportion of sand and mud in ripple sets and co-sets		X	X			
	Bimodal (herring-bone) sediment transport				X	X	
Chemically precipitated minerals in evaporitic settings	Limestones			X	X		
	Oolites			X	X		
	Ca-SO_4 evaporites (laths, nodules, clots, chicken-wire)			X	X		
Other features	Planar to wavy laminated sand/silt	X	X				
	m- to decameter-scale thicken- and coarsen-upward cycles		X	X			
	Desiccation cracks			X	X		
	Subaqueous (syneresis) cracks			X	X		
	Calcite concretions			X	X		

Table 2.1. The main sedimentary features identified in the upper Copper Harbor and Nonesuch formations classified by genesis and relative abundance in lacustrine shoreline-littoral-sublittoral zones ('lacustrine' column) and storm- and tide-influenced marine shoreline-shoreface-shelf settings ('marine' column). The features marked by a black-box 'X' are those we use to conclude that deposition occurred in a marine setting. Abundance criteria summarised from references cited in text and authors' own experience. See text for discussion.

2.7. References

Ager, D.V. 1974. Storm deposits in the Jurassic of the Moroccan High Atlas. Palaeogeography, Palaeoclimatology, Palaeoecology 15, 83-93.

Aigner T. 1982. Calcareous tempestites: storm-dominated stratification in Upper Muschelkalk limestones (middle Trias, SW-Germany). In: G. Einsele and A. Seilacher (eds.) Cyclic and Event Stratification. Springer, Berlin, Heidelberg, 180-198.

Andrews, S.D. and Hartley, A.J. 2015. The response of lake margin sedimentary systems to climatically driven lake level fluctuations: middle Devonian Orcadian Basin, Scotland. Sedimentology 62, 1693-1716.

Arnott, R.W. and Southard, J.B. 1990. Exploratory flow-duct experiments on combined-flow bed configurations and some implications for interpreting storm event stratification: Journal of Sedimentary Petrology 60, 211–219.

Aswasereelert, W., Meyers, S.R., Carroll, A.R., Peters, S.E., Smith, M.E. and Feigl, K.L. 2013. Basin-scale cyclostratigraphy of the Green River Formation, Wyoming. Geological Society of America Bulletin 125, 216-228.

Beghin, J., Storme, J.Y., Blanpied, C., Gueneli, N., Brocks, J.J., Poulton, S.W. and Javaux, E.J. 2017. Microfossils from the late Mesoproterozoic–early Neoproterozoic Atar/El Mreïti Group, Taoudeni Basin, Mauritania, northwest Africa. Precambrian Research 291, 63-82.

Behrendt, J.C., Green, A.C., Cannon, W.F., Hutchinson, D.R., Lee, W.M., Milkereit, B., Agena, W.F. and Spencer, C. 1988. Crustal structure and deep rift basin of the Mid-continent Rift system---results from GLIMPCE deep seismic reflection profile. Geology 16, 81-85.

Bornhorst, T.J. and Williams, W.C. 2013. The Mesoproterozoic Copperwood sedimentary rock-hosted stratiform copper deposit, Upper Peninsula, Michigan. Economic Geology 108, 1325-1346.

Bright, J., Cohen, A.S. and Starratt, S.W. 2018. Distinguishing brackish lacustrine from brackish marine deposits in the stratigraphic record: A case study from the late Miocene and early Pliocene Bouse Formation, Arizona and California, USA. Earth Science Reviews 185, 974-1003.

Cannon, W.F. and Nicholson, S.W. 2001. Geologic map of the Keweenaw Peninsula and adjacent area, Michigan. Misc. Investigation Series Map 1-2696. US Geological Survey.

Cannon, W.F., Nicholson, S.W., Woodruff, L.G., Hedgman, C.A. and Schulz, K.J. 1995. Geologic map of the Ontonagon part of the Wakefield 30’ x 60’ Quadrangle, Michigan. Misc. Investigation Series Map 1-2499. US Geological Survey.

Cannon, W.F., Woodruff, L.G., Nicholson, S.W. and Hedgman, C.A. 1996. Geologic map of the Ashland and the northern part of the Ironwood 30’ x 60’ Quadrangles, Michigan. Misc. Investigation Series Map 1-2566. US Geological Survey.

Cumming, V.M., Poulton, S.W., Rooney, A.D. and Selby, D. 2013. Anoxia in the terrestrial environment during the late Mesoproterozoic. Geology 41, 583-586.

Dam, G. and Surlyk, F. 1993. Cyclic sedimentation in a large wave and storm-dominated anoxic lake; Kap Stewart Formation (Rhaetian-Sinemurian), Jameson Land, East Greenland. Special Publication of the International Association of Sedimentology 18, 419-448.

Dorsey, R.J., O’Connell, B., McDougall, K., Homan, M.B. 2018. Punctuated sediment discharge during early Pliocene birth of the Colorado River: evidence from regional stratigraphy, sedimentology, and paleontology. Sedimentary Geology 363, 1–33.

Dott, R.H., Jr. and Bourgeois J. 1982. Hummocky stratification: significance of its variable bedding sequences. Bulletin Geological Society of America 93, 663-680.

Duke, W.L. 1990. Geostrophic circulation or shelf turbidity currents: the dilemma of paleoflow patterns in storm-influenced prograding shoreline systems. Journal of Sedimentary Petrology 60, 870-883.

Duke, W.L., Arnott, R.W.C. and Cheel, R.J. 1991. Shelf sandstones and hummocky cross-stratification: new insights on a stormy debate: Geology 19, 625–628.

Dumas, S., Arnott, R.W.C. and Southard, J.B. 2005. Experiments on oscillatory and combined-flow bed forms: implications for interpreting parts of the shallow marine sedimentary record. Journal of Sedimentary Research 75, 501–513.

El-Tabakh, M., Riccioni, R. and Schreiber, B.C. 1997. Evolution of late Triassic rift basin evaporites (Passaic Formation): Newark Basin, eastern North America. Sedimentology 44, 767-790.

Elmore, R.D. 1983. Precambrian non-marine stromatolites in alluvial fan deposits, the Copper Harbor Conglomerate, Upper Michigan. Sedimentology 30, 829-842.

Elmore, R.D. 1984. The Copper Harbor Conglomerate: a late Precambrian fining-upward alluvial fan sequence in northern Michigan. Geol. Soc. Amer. Bull. 95, 610-617.

Elmore, R.D., Milavec, G.J., Imbus, S.W. and Engel, M.H. 1989. The Precambrian Nonesuch Formation of the North American Mid-Continent Rift, sedimentology and organic geochemical aspects of lacustrine deposition. Precambrian Research 43, 191-213.

Eugster, H.P. and Hardie, L.A. 1975. Sedimentation in an ancient playa-lake complex: the Wilkins Creek Member of the Green River Formation, Wyoming. Geological Society of America Bulletin 86, 319-334.

Eyles, N. and Clark, B.M. 1986. Significance of hummocky and swaley cross-stratification in late Pleistocene lacustrine sediments of the Ontario basin, Canada. Geology 14, 679-682.

Fairchild, L.M., Swanson-Hysell, N.L., Ramezani, J., Sprain, C.J. and Bowring, S.A. 2017. The end of Midcontinent Rift magmatism and the paleogeography of Laurentia. Lithosphere 9, 117-133.

Fedorchuk, N.D., Dornbus, S.Q., Corsetti, F.A., Isbell, J.L., Petryshyn, V.A., Bowles, J.A. and Wilmeth, D.T. 2016. Early non-marine life: evaluating the biogenicity of Mesoproterozoic fluvial-lacustrine stromatolites. Precambrian Research 275, 105-118.

Greenwood, B. and Sherman, D. 1986. Hummocky cross stratification in the surf zone: flow parameters and bedding genesis. Sedimentology 33, 33-46.

Hieshima, G.B. and Pratt, L.M. 1991. Sulfur/carbon ratios and extractable organic matter of the middle Proterozoic Nonesuch Formation, North American Midcontinent Rift. Precambrian Research 54, 65-79.

Hinze, W.J., Allen, D.J., Braile, L.W. and Mariano, J. 1997. The Midcontinent Rift system: a major Proterozoic continental rift, In: Ojakangas, R.W., Dickas, A.B. and Green, J.C. (eds.) *Middle Proterozoic to Cambrian Rifting, Central North America*. Geological Society of America Special Paper 312, 7-35.

Ho, E.S. and Mauk, J.L. 1996. Relationship between organic matter and copper mineralization in the Proterozoic Nonesuch Formation, northern Michigan. Ore Geology Review 11, 71-88.

Ilgar, A. and Nemec, W. 2005. Early Miocene lacustrine deposits and sequence stratigraphy of the Ermenek Basin, central Taurides, Turkey. Sedimentary Geology 173, 233-275.

Imbus, S.W., Macko, S.A., Elmore, D.R. and Engel, M.H. 1992. Stable isotope (C,S,N) and molecular studies on the Precambrian Nonesuch Shale (Wisconsin-Michigan, USA): evidence for differential preservation rates, depositional environment and hydrothermal influence. Chemical Geology 101, 255-281.

Jagniecki, E.A. and Lowenstein, T.K. 2015. Evaporites of the Green River Formation, Bridger and Piceance Creek Basins: deposition, diagenesis, paleobrine chemistry and Eocene atmospheric CO_2. In: M.E. Smith, A.R. Carroll (eds.) *Stratigraphy and Paleolimnology of Green River Formation, Western USA*, Syntheses in Limnogeology 1, Springer, Dordecht, 277-312.

Jiang, Z., Wang, J., Fulthrope, C.S., Liu, L., Zhang, Y. and Liu, H. 2018. A quantitative model of paleowind reconstruction using subsurface lacustrine longshore bar deposits – an attempt. Sedimentary Geology 371, 1-15.

Martin-Bello, L., Arenas, C. and Jones, B. 2019. Lacustrine stromatolites: useful structures for environmental interpretation – an example from the Miocene Ebro Basin. Sedimentology, 1-36 doi: 10.1111/sed.12577

Mauk, J.L. and Heishima, G.B. 1992. Organic matter and copper mineralization at White Pine, Michigan, USA. Chemical Geology 99, 189-211.

Middleton, G.V. and Southard, J.B. 1984. Mechanics of sediment movement: SEPM Short Course 3, 2nd Ed., 401 p.

Mitchell, R.L. and Sheldon, N.D. 2016. Sedimentary provenance and weathering processes in the 1.1 Ga Midcontinent Rift of Keweenaw Peninsula, Michigan, USA. Precambrian Research 275, 225-240.

Morsilli, M. and Pomar, L. 2012. Internal waves vs. surface storm waves: a review on the origin of hummocky cross-stratification. Terra Nova 24, 273-282.

Myrow, P. 2005. Storms and storm deposits. Encyclopedia of Geology, 580-587.

Myrow, P. and Southard, J.B. 1996. Tempestite deposition. Journal of Sedimentary Research 66, 875-887.

O'Connell, B., Dorsey, R.J., Humphreys, E.D. 2017. Tidal rhythmites in the southern Bouse Formation as evidence for post-Miocene uplift of the lower Colorado River corridor. Geology 45, 99–102.

Ojakangas, R.W., Morey, G.B. and Green, J.C. 2001. The Mesoproterozoic Midcontinent Rift System, Lake Superior region, USA. Sedimentary Geology 141-142, 421-442.

Olsen, P.E. 1986. A 40-million-year lake record of early Mesozoic orbital climatic forcing. Science 234, 842-848.

Ortí, F., Rosell, L. and Anadón, P. 2003. Deep to shallow lacustrine evaporites in the Libros Gypsum (southern Tereuk Basin, Miocene, Spain): an occurrence of pelletal gypsum rhythmites. Sedimentology 50, 361-386.

Parnell, J., Spinks, S., Andrews, S., Thayalan, W. and Bowden, S. 2015. High Molybdenum availability for evolution in a Mesoproterozoic lacustrine environment. Nature communications 6, 6996, 1-6 DOI: 10.1038/ncomms7996

Pratt, L.M., Summons, R.E. and Hieshima, G.B. 1991. Sterane and triterpane biomarkers in the

Precambrian Nonesuch Formation, North American Midcontinent Rift: Geochimica et Cosmochimica Acta 55, 911–916.

Prave, A.R. 1990. Clarification of some misconceptions about antidune geometry and flow character. Sedimentology 37, 1049-1052.

Prave, A.R. and Duke, W.L. 1990. Small-scale hummocky cross-stratification in turbidites: a form of antidune stratification? Sedimentology 37, 531-539.

Sánchez-Baracaldo, P., Raven, J.A., Pisani, D. and Knoll, A.H. 2017. Early photosynthetic eukaryotes inhabited low-salinity habitats. Proceedings National Academy of Sciences 114, E7737-E7745.

Schreiber, B.C. and El Tabakh, M. 2000. Deposition and early alteration of evaporites. Sedimentology 47, 215-238.

Schumm, S.A. 1968. Speculations concerning paleohydrologic controls on terrestrial vegetation. Geol. Soc. Of Amer. Bull. 79, 1573-1588.

Shchepetkina, A., Gingras, M.K., Mángano, M.G. and Buatois, L.A. 2019. Fluvio-tidal transition zone: terminology, sedimentological and ichnological characteristics and significance. Earth Science Reviews 192, 214-235.

Slotznick, S.P., Swanson-Hysell, N.L. and Sperling, E.A. 2018. Oxygenated Mesoproterozoic lake revealed through magnetic mineralogy. Proceed. Nat. Acad. Sciences USA 115, 12938-12943.

Smith, M.E., Carroll, A.R. and Scott, J.J. 2015. Stratigraphic expression of climate, tectonism and geomorphic forcing in an underfilled lake basin: Wilkins Creek Member of the green River formation. In: M.E. Smith, A.R. Carroll (eds.) *Stratigraphy and Paleolimnology of Green River Formation, Western USA*, Syntheses in Limnogeology 1, Springer, Dordecht, 61-102.

Smoot, J.P. and Lowenstein, T.K. 1991. Depositional environments of non-marine evaporites. In: Evaporites, Petroleum and Mineral Resources (J.L. Melvin, ed.), Developments in Sedimentology 50, 189–347

Southard, J.B., Lambie, J.M., Fedemco, D.C., Pine, H.T. and Weidman, C.R. 1990. Experiments on bed configurations in fine sands under bidirectional purely oscillatory flow, and the origin of hummocky cross-stratification: Journal Sedimentary Petrology 60, 1-17.

Stein, S., Stein, C.A., Elling, R., Kley, J., Keller, G.R., Wysession, M., Rooney, T., Frederiksen, A. and Moucha, R. 2018. Insights from North America's failed Midcontinent Rift into the evolution of continental rifts and passive continental margins. Tectonophysics 744, 403-421.

Stewart, E.K. and Mauk, J.L. 2017. Sedimentology, sequence-stratigraphy, and geochemical variations in the Mesoproterozoic Nonesuch Formation, northern Wisconsin, USA. Precambrian Research 294, 111-132.

Strother, P.K. and Wellman, C.H. 2016. Palaeoecology of a billion-year-old non-marine cyanobacterium from the Torridon Group and Nonesuch Formation. Palaeontology 59, 89-108.

Suszek, T. 1997. Petrography and sedimentation of the Middle Proterozoic (Keweenwan) Nonesuch Formation, western Lake Superior region, Midcontinent Rift System. In: Ojakangas, R.W., Dickas, A.B. and Green J.C. (eds.) Middle Proterozoic to Cambrian Rifting, Central North America. Geol. Soc. Amer. Spec. Paper 312, 195-210.

Swanson-Hysell, N.L., Ramezani, J., Fairchild, L.M. and Rose, I.R. 2019. Failed rifting and fast drifting: Midcontinent Rift development, Laurentia's rapid motion and the driver of Grenvillian orogenesis. Geological Society of America Bulletin 131, 913-940.

Van Houten, F.B. 1962. Cyclic sedimentation and the origin of analcime-rich upper Triassic Lockatong Formation, west-central New Jersey and adjacent Pennsylvania. American Journal of Science 260, 561-576.

Wellman, C.H. and Strother, P.K. 2015. The terrestrial biota prior to the origin of land plants (embrophytes): a review of the evidence. Palaeontology 58, 601-627.

White, W.S. and Wright, J.C. 1960. Lithofacies of the Copper Harbor conglomerate, northern Michigan. U.S. Geological Survey Prof. Paper 400-B, 5-7.

Wolff, R.G. and Huber, N.K. 1973. The Copper Harbor Conglomerate (Middle Keweenawan) on Isle Royale, Michigan, and its regional implications. US Geological Survey Prof. Paper 754-B, 15 p.

Yang, B., Dalrymple, R.W. and Chun, S., 2006. The significance of hummocky cross-stratification (HCS) wavelengths: evidence from an open-coast tidal flat, South Korea. Journal of Sedimentary Research, 76(1), pp.2-8.

Zolitschka, B., Francus, P., Ojala, A.E.K. and Schimmelmann, A. 2015. Varves in lake sediments – a review. Quaternary Science Reviews 117, 1-41.

Blank page

Chapter 3

Fluid flow, alteration and Cu-Ag mineralisation associated with the White Pine deposit

3.1. Introduction

The 1.1 Ga Midcontinent Rift System (MRS) contains the world-class White Pine copper-silver deposit, often viewed as an outstanding example of a low-temperature sediment-hosted stratiform copper (SHSC) system. The lack of significant post-mineralisation structural re-organisation (folding or faulting), a shallow weathering profile, a relatively simple stratigraphy and apparently weak alteration makes the White Pine deposit an excellent candidate for studying SHSC ores. The deposit is contained within the lowermost dark shales of the c. 1.08 Ga Nonesuch Formation, part of the late Mesoproterozoic Keweenaw Supergroup exposed along the eponymous peninsula of Lake Superior, Michigan, USA. Mineralised rock at White Pine covers an area of at least 250 km^2 and has a total vertical extent of up to 30 meters. The principal copper minerals are native copper and chalcocite, accounting for approximately 13% and 87% respectively of historic mine production (Brown, 2006). Copper sulphides grade vertically from native copper at the base through chalcocite, djurleite, purple bornite, pink bornite and chalcopyrite. Galena, sphalerite, wurtzite (ZnS) and greenockite (CdS) mark the transition to pyrite at the top of the ore zone (Wight & Wright, 1966; Ensign et al., 1968; Brown, 1971). The predominance of native copper and chalcocite contrasts with other SHSC deposits, such as those in the Central African Copperbelt (Hitzman et al., 2012), Dzhezkazgan (Box et al., 2012) and Kupferschiefer (Vaughan et al., 1989), that contain much higher proportions of chalcopyrite and bornite. This makes White Pine a new and exciting model to use in assessing the Cu-bearing potential of other sedimentary successions.

In spite of intensive research focused on the Keweenaw Cu-bearing district, no previous study has attempted to integrate completely the paragenesis and chemistry of different ore minerals, alteration minerals, textures, veins and structures across the deposit and between key lithologies. Here we propose a paragenesis model and offer a more comprehensive understanding of the main fluid pathways, mineralisation process and how the chemistry of the fluids changed spatially and temporally. We also place the genesis of the deposit and its footprint into the context of the broader geological evolution of the basin – both important contributions to future mineral exploration programs for analogous deposits within the MRS and in other basins. Identification of factors critical for the formation of this major SHSC deposit has implications for basin selection in early-stage generative exploration programs.

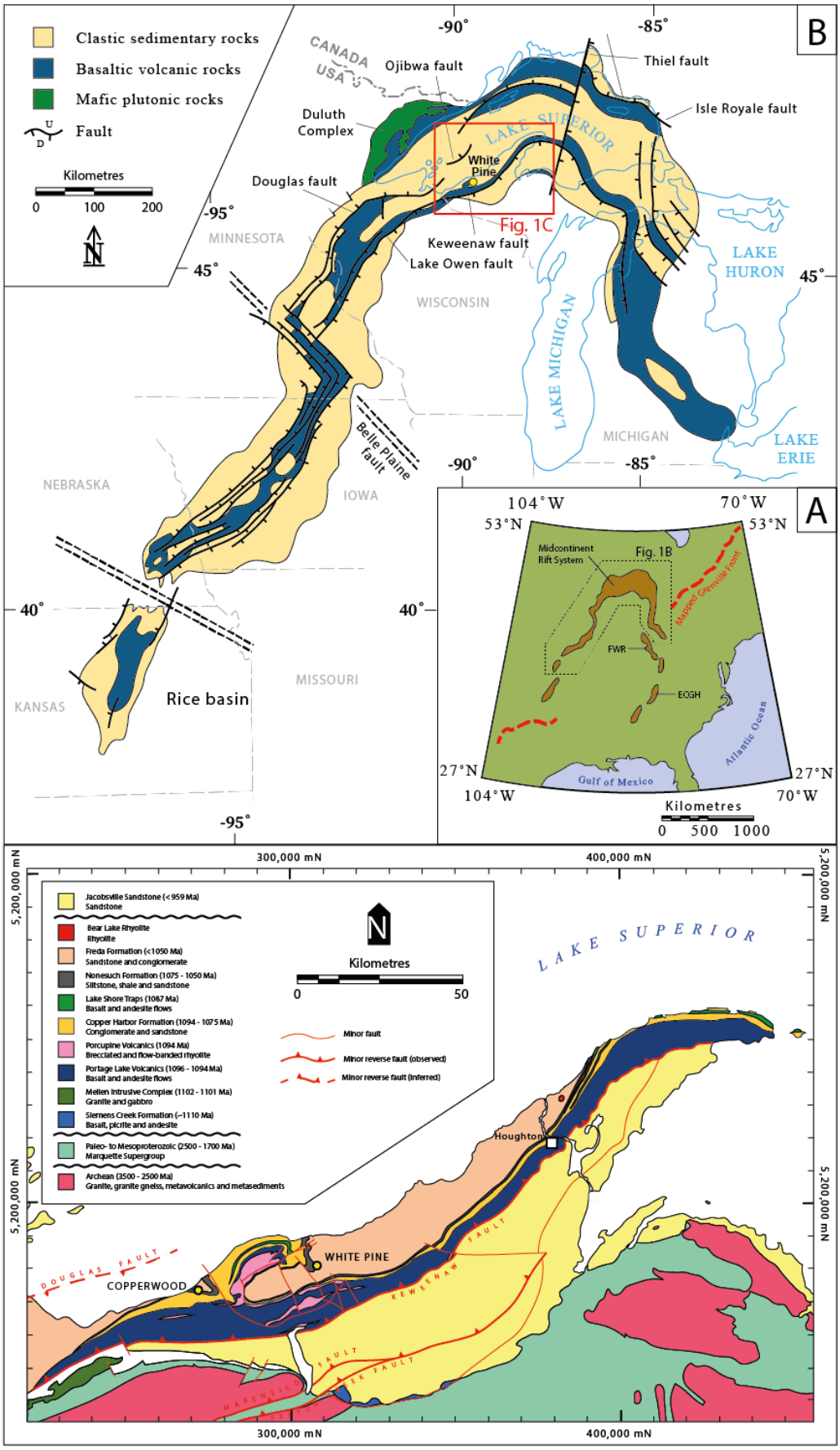

Figure 3.1. (A) Map of the location of the MRS within North America with the mapped Grenville Front (modified after Stein et al., 2015). **(B)** Simplified geological map of the MRS (Dickas, 1986). **(C)** Geological map of the Keweenaw Peninsula.

3.2. Regional geology

The MRS is a 2000 km-long arcuate-shaped geophysical anomaly identified in the subsurface of the eastern North American craton (Hinze et al., 1997; Figs. 3.1A-C). Its genesis is attributed widely to extensional tectonism between ~1120 and ~1096 Ma (e.g. Stein et al., 2014, 2015). Contrasting theories to explain the cessation of rifting include northwest-directed compression during the Ottawan phase of the Grenvillian Orogeny (Cannon, 1994, Soofi and King, 2002) and a shift in accommodation of extension across microplate boundaries (Stein et al., 2014). The segmented character of the MRS is interpreted as a series of sub-basins (alternately verging half grabens) separated by accommodation zones (e.g. Dickas and Mudrey, 1997). The only surface expression of the MRS is along the shoreline and adjacent areas of Lake Superior. There the rocks define the Keweenaw Supergroup (Fig. 3.2A,B), consisting of 20 km of mafic volcanic rocks of the Powder Mill and Portage Lake Volcanics groups and 10 km of sedimentary rocks of the Oronto Group and Jacobsville Sandstone (and equivalents; Ojakangas et al., 2001).

The three key units for our purposes are the Portage Lake Volcanics (PLV), the overlying braided fluvial to alluvial fan conglomerate and sandstone of the Copper Harbor Formation (Baumann et al., 2018; Daniels, 1982; Elmore, 1984) and shale (containing up to 3.0% organic carbon) and subordinate sandstone of the Nonesuch Formation (Imbus et al., 1990). The Nonesuch Formation is often considered lacustrine in origin (Elmore et al., 1989; Ojakangas et al., 2001) but a marine influence was indicated from S/C ratios (Hieshima & Pratt, 1991), sterane and triterpene biomarkers (Pratt et al., 1991) and C, N and S isotopes (Imbus et al., 1992). Our recent work (Jones et al., 2020) indicates that it is best interpreted as a tidally influenced shoreline and shallow-marine embayment experiencing evaporative conditions.

Age constraints on the Keweenawan Supergroup include 1091.59 ± 0.27 Ma and 1093.37 ± 0.53 Ma (U-Pb zircon by CA-ID-TIMS, Swanson-Hysell et al., 2019) for two lava flows in the PLV, 1085.57 ± 0.25 Ma (U-Pb zircon by CA-ID-TIMS; Fairchild et al., 2017) on Lakeshore Traps andesite interbedded in the Copper Harbor Formation and 1093.6 ± 1.8 Ma (U-Pb zircon by LA-ICP-MS; Zartman et al., 1997) on rhyolite and andesite units of the Porcupine Mountains Volcanic Structure (see Fig. 3.1C). A Re-Os isochron age of 1078.0 ± 23 Ma has been obtained on pyrite in the Nonesuch Formation (Cummings et al., 2013) and the “Junior” calcite bed at the base of the

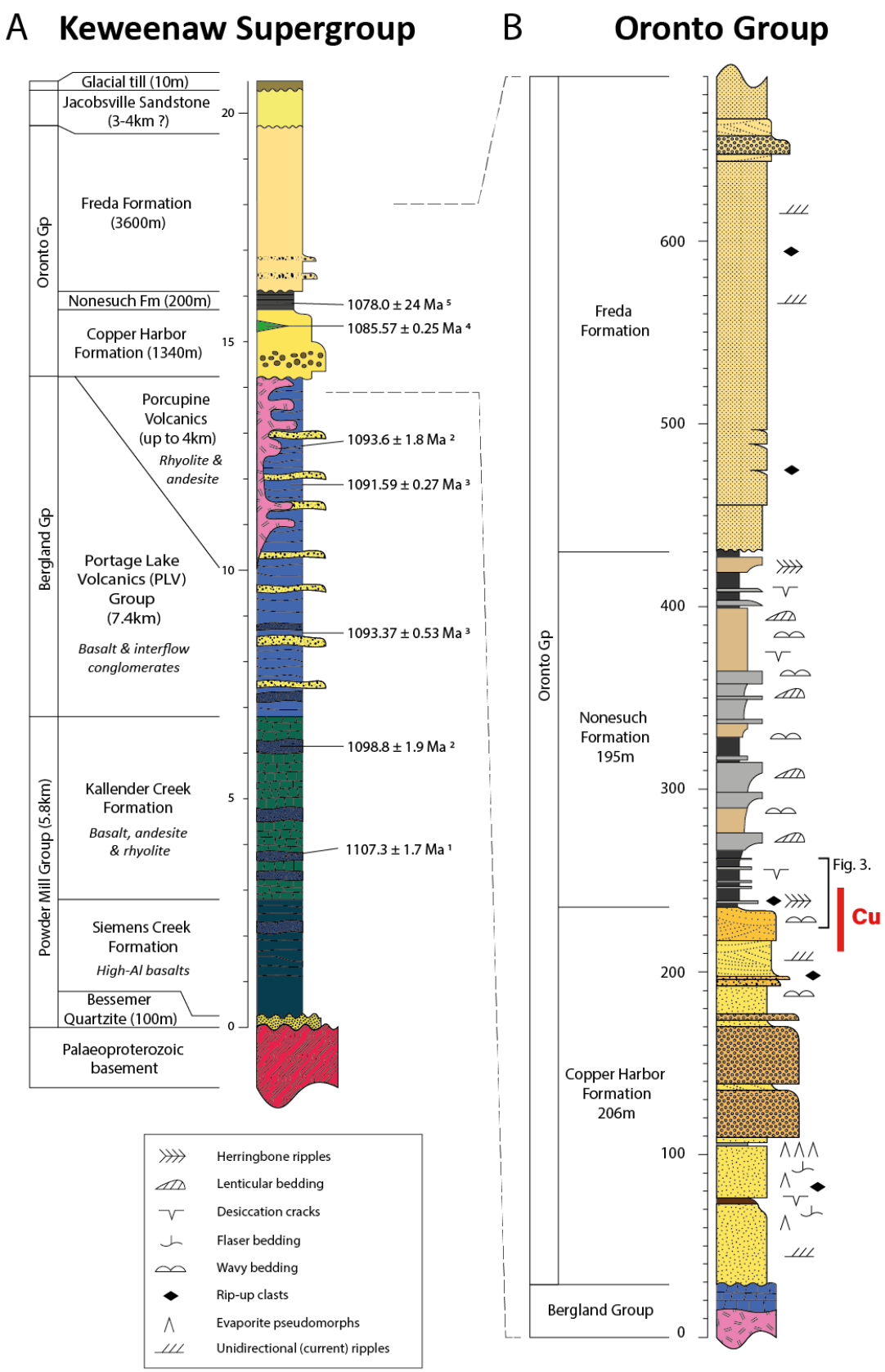

Fig. 3.2. (A) Stratigraphic column of the Keweenaw Supergroup (modified after Nicholson et al., 1997). Age determinations: 1. Davis and Green (1997), 2. Zartman et al. (1997), 3. Swanson-Hysell et al. (2019), 4. Fairchild et al. (2017), and 5. Cumming et al. (2013). **(B)** Stratigraphic column of the Oronto Group in the White Pine area (this study).

formation yielded a Pb-Pb age of 1081 ± 9 Ma (Ohr, 1993). A remnant magnetism age was determined for Copper Harbor Formation red beds of 1063 ± 8 Ma (Symons et al. 2013; later revised to 1074 ± 7 Ma in Brown, 2014), and is thought to be synchronous with the main Cu mineralisation event. Calcite veins that post-date stratiform Cu mineralisation yield a Rb-Sr isochron age of 1047 ± 35 Ma (Ruiz et al., 1984) and many workers consider these veins to have formed syn-thrust faulting (e.g. Kelly and Nishioka,1985; Mauk et al., 1992; Bornhorst et al., 1988) related to basin inversion during Grenville orogenesis (Cannon, 1994). In the Lake Superior region, this inversion occurred along the Keweenaw and Isle Royale faults and is dated at 1060 ± 20 Ma (Rb-Sr biotite; Cannon et al., 1993).

3.2.1. Portage Lake Volcanics Group

The Portage Lake Volcanics is a 2-5 km thick succession of basaltic lavas (Fig. 3.3A) and minor intermediate to felsic volcanic rocks (Fig. 3.3B) and, in places, interbedded conglomerate and sandstone (White, 1968; Paces, 1988). The flows are mostly olivine tholeiites, vary from 1 m to as much as 450 m in thickness and are variably vesicular to amygdaloidal. Amygdaloids are commonly filled with secondary calcite and native copper and many flow tops are marked by brecciation. The Keweenaw Fault truncates the base of the Formation and the top is marked by a sharp contact with the Copper Harbour Formation.

3.2.2. Copper Harbor Formation

The Copper Harbor Formation is c. 100 to 2100 m thick and consists of interbedded sandstone and clast-supported pebble conglomerate (clasts up to ~15 cm in diameter) with a matrix of finer sediment, chlorite, illite and calcite (Fig. 3.3C-F). Detrital grains are dominated by basaltic and felsic material derived from underlying Portage Lake Volcanics and Porcupine Volcanics, respectively. The majority of drill holes at the White Pine deposit terminate in the upper ~10 m of the Copper Harbor Formation and lithofacies display significant lateral variability, from interbedded silty sandstone and pebble conglomerate to repetitively stacked upward-fining cycles of pebble conglomerate to cross- and flaser-bedded sandstone to mudstone.

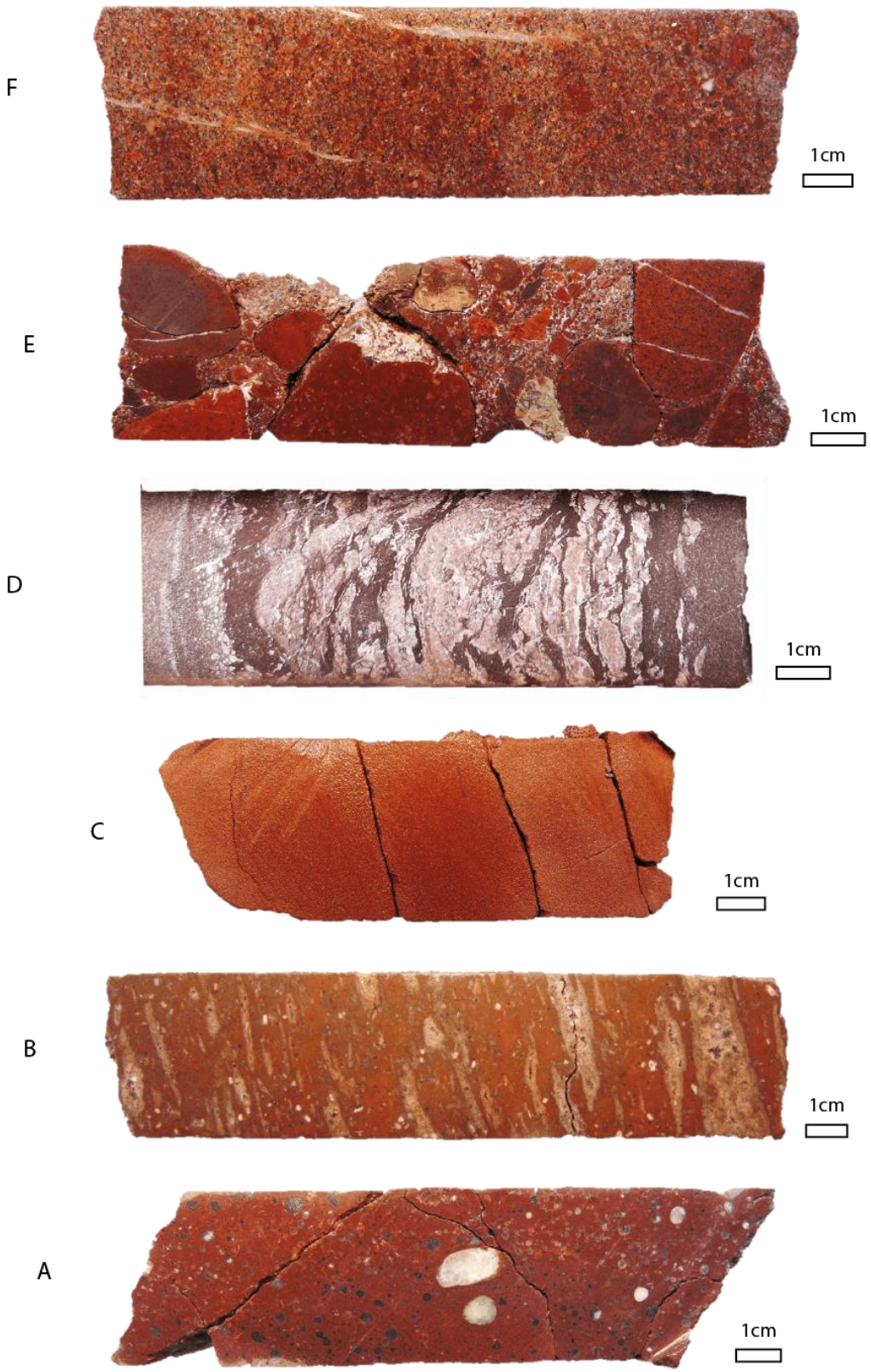

Fig. 3.3. Footwall units arranged in stratigraphic order. **(A)** Hematised amygdaloidal basalt flow, PLV Group. WP345 398.10m. **(B)** hematised rhyolite, Porcupine volcanic unit. WPB-1 328.47m. **(C)** strongly hematised quartz arenite, Copper Harbor Formation. WP345 392.30m. **(D)** Chicken-wire texture of calcite pseudomorphs after evaporite minerals. WP345 345.50m. **(E)** Pebble conglomerate, Copper Harbor Formation. WP345 305.40m. **(F)** Weakly hematized lithic arenite, Copper Harbor Formation. WP345 191.60m.

3.2.3. Nonesuch Formation

The Nonesuch Formation is 40 to 200 m thick. Its lower part is the ore-bearing interval and has received the most attention, including a detailed "mine stratigraphy" developed by Copper Range Company geologists (Fig. 3.4; Ensign et al., 1968). The contact with the Copper Harbor Formation is transitional over c. 0.5 m and is placed at the base of the first black shale. The contact with the overlying Freda Formation is a regional angular unconformity marked by a sharp erosional surface.

The "mine stratigraphy" consists upward of the Parting Shale, Upper Sandstone and Upper Shale and these are divided into 14 'sub-units' or 'beds' (Fig. 3.5). The interval of mineralised rock occurs between the Lower Transition Zone and Stripey beds and generally thickens northward from 12 to 17 m but syn-depositional movement on the White Pine fault disrupts this trend (see below). The Parting and Upper Shale are characterized by micrite-filled desiccation and syneresis cracks, ball-and-pillow structures, slump folds, rare calcite-pseudomorphed evaporite fabrics and in places contain cm-scale calcite nodules/concretions. This stratigraphy encompasses three overall fining-upward trends: sharp-based coarse-grained sandstone (Transition Zone, Upper Sandstone, Tiebel Sandstone) into black shale, then red siltstone with nodular limestone, dark-grey massive siltstone and laminated grey siltstone. Sandstone units contain rip-up clasts, current ripples, flaser bedding, and isopachous chlorite rims, pore-filling calcite cements and locally quartz overgrowths surrounding grains. Siltstone and shales beds contain much detrital chlorite and well-developed isopachous chlorite rims on grains.

3.3. White Pine Deposit

Open folds and gentle to moderate dips mark the area of the White Pine deposit. It occurs along the east flank of the Porcupine Volcanics (Fig. 3.6), a ~30 km long caldera (Hubbard, 1975; Woodruff, 2013) that formed an ancestral high over which the Copper Harbor Formation thins (White, 1971). The discovery of sediment-hosted copper in the White Pine area was made in 1865 at Nonesuch Falls, 4 km west of the modern White Pine mine site (Ensign et al., 1968). The White Pine Copper Company extracted high-grade native copper from the White Pine fault between 1915 and 1921 (Mauk et al., 1992) and in 1929 the property was sold to the Copper Range Company who started exploratory drilling in 1937, sinking the first shaft in 1945 with

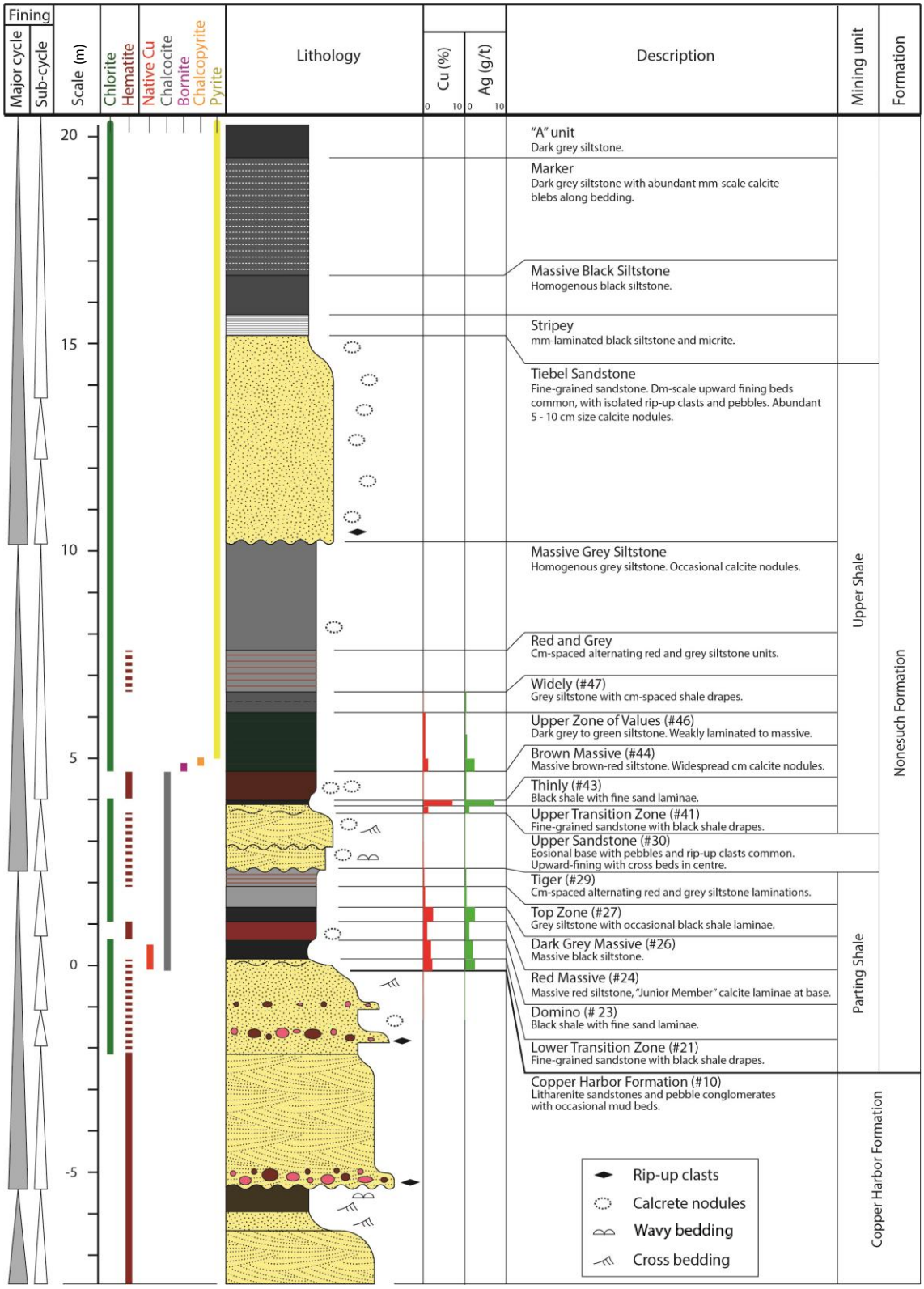

Fig. 3.4. Stratigraphic column of the White Pine "mine sequence" based on drill hole WP198 (terminology after Ensign et al., 1968).

first production in 1953 (Ensign et al., 1968). Peak annual copper production of 82,956 tonnes was reached in 1975 and by 1995 the mine had produced 179,686,975 tonnes of ore (given average grades of 1.14% Cu and 7.81 g/t Ag, this equates to c. 2M tonnes of Cu and c. 50M ounces of Ag; Johnson et al., 1995, 2014). Native copper and chalcocite accounted for approximately 13% and 87%, respectively, of historic mine production (Brown, 2006). Recent work by Highland Copper Company Inc. has identified Indicated Resources of 133.4 Mt at 1.07% Cu and 14.9 g/t Ag, and Inferred Resources of 97.2 Mt at 1.03% Cu and 8.7 g/t Ag with total contained copper of 2.45 Mt (www.highlandcopper.com/19-09-23-news). Highland Copper also owns the Copperwood deposit, 35 km west of White Pine (see Figs. 3.1 and 3.6), and expects to commence construction of a new mine within the next few years (www.highlandcopper.com/Copperwood-project).

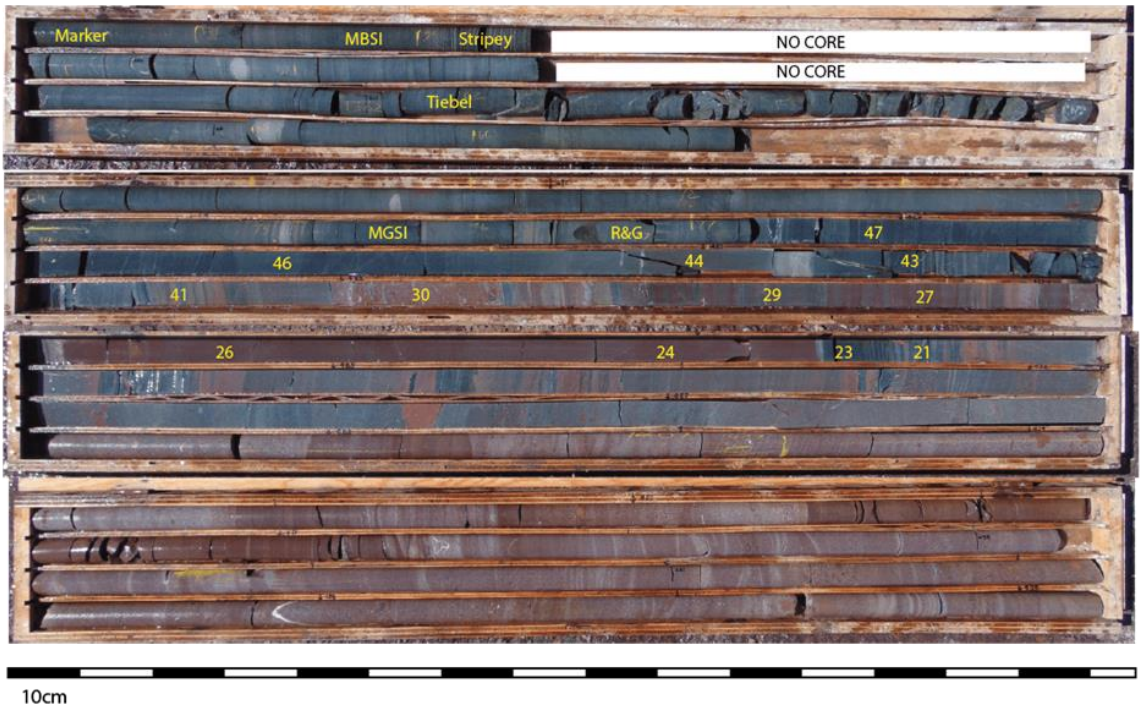

Fig. 3.5. Photograph of drill core from the White Pine mine sequence, WP233 (B23), 411.18 to 435.25m. Bed numbers correspond to those in figure 3.4. MBSI – massive black siltstone, MGSI – massive grey siltstone, and R&G – red and grey siltstone.

Previous studies (White & Wright, 1954; Carpenter, 1963; White & Wright, 1966; Ensign et al., 1968; Brown, 1971; Wiese, 1973; Mauk et al., 1992; Bornhorst and Williams, 2013) identified widespread stratiform Cu minerals in basal Nonesuch Formation shales, cross-cutting Cu-bearing veins and Cu-mineralised thrust faults.

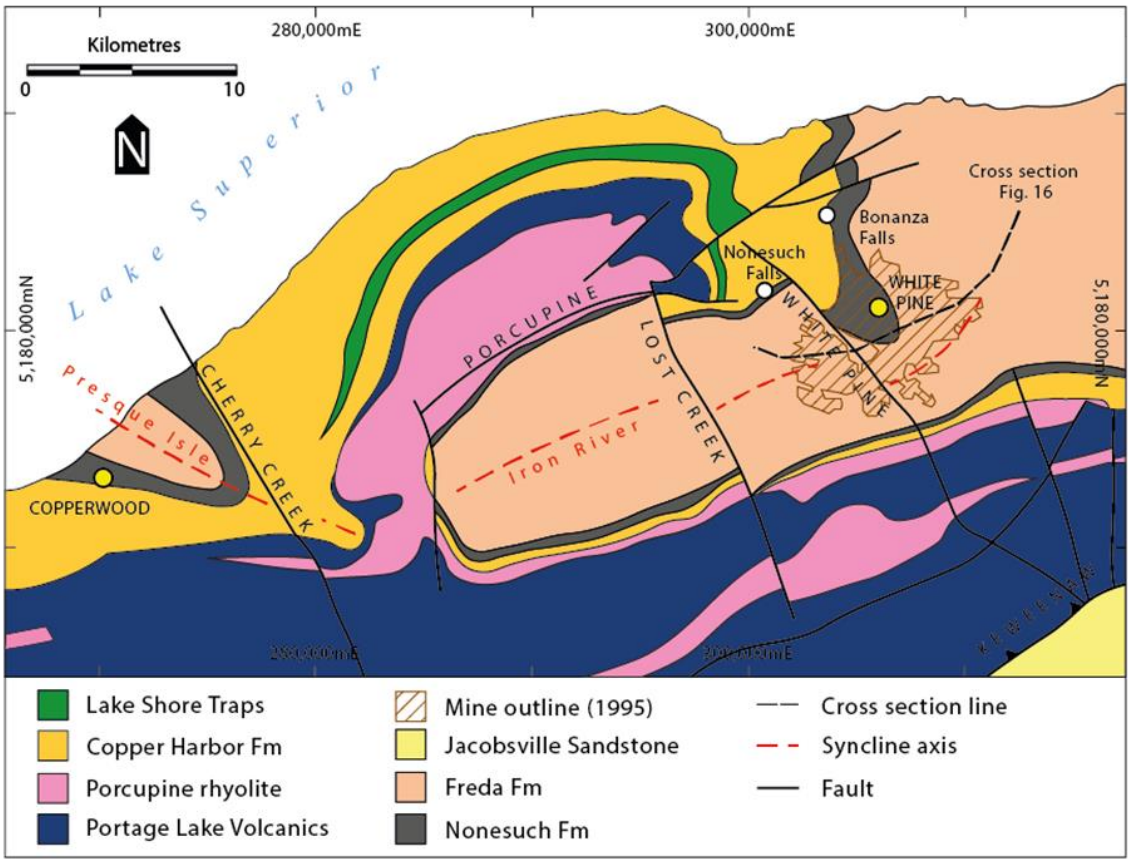

Fig. 3.6. Geological map of the Porcupine district (Hubbard, 1975; Cannon et al, 1995).

Burnie et al. (1972) and Mauk (1993) concluded replacement of diagenetic pyrite by copper-sulphides was the dominant mechanism of sulphide formation. Brady (1960) and Hamilton (1967) investigated the occurance of native Cu in the underlying Copper Harbor Formation and showed that early chlorite rims were succeeded by oil emplacement and disseminated native copper with pyrobitumen within the upper few meters of the Formation (Brady, 1960; Hamilton, 1967) and that native silver occurred in the uppermost few centimetres (Ensign, 1968; Brown, 1971). Livnat (1983) analysed fluid inclusions in calcite, quartz, chalcocite, ankerite and barite on Portage Lake basalts to determine salinities of 2.7 to 19.8 % and $\delta^{18}O$ and δD data on chlorite, epidote and pumpellyite from the same basalts were consistent with seawater as a dominant component of mineralising fluids. A clear relationship between organic matter (in situ and liquid petroleum), structure and Cu minerals has been documented (e.g. Kelly and Nishioka, 1985; Mauk and Hieshima, 1992; Mauk et al., 1992) and several workers have highlighted a relationship between Cu grade and Fe content of chlorite (Wiese et al., 1973; Li et al., 1995).

3.4. Paragenesis

Stratigraphy exerted a strong control on mineralisation via porosity, redox potential (e.g. organic C and chlorite content) and rheology, and two styles of copper ore are recognized at White Pine: (i) an early disseminated style characterised by pore filling, replacement and sheet textures that account for >95% of ore; and (ii) a later phase of veins and small-scale faults restricted to Nonesuch Formation shales that account for <5% of ore. Copper mineralisation was demonstrably epigenetic, occurring along sedimentary laminations, infilling sedimentary structures such as desiccation cracks, syneresis cracks, slump folds, pseudomorphed evaporite fabrics and in

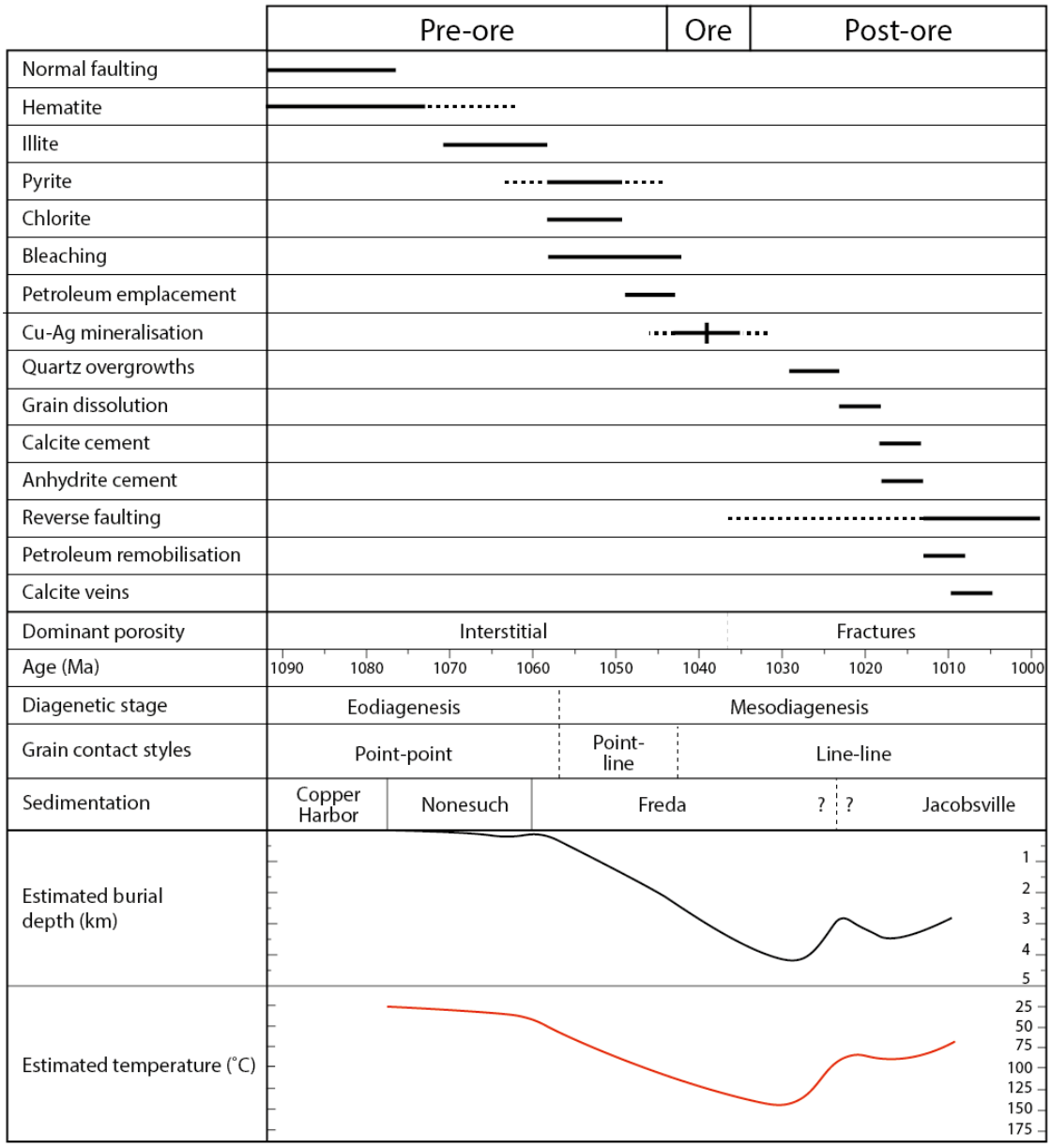

Fig. 3.7. Paragenetic sequence chart showing timing, of key mineral phases and structures.

interstitial pores in sandstone beds. Reduction of metalliferous fluids occurred principally via interaction with pyrobitumen and in situ organic matter. Fe^{2+} in detrital and authigenic chlorite may also have played a role. Further, authigenic minerals can be grouped as either due to regional diagenesis or related to localised, spatially limited mineralisation events (e.g. Cu-Ag ores). Consequently, based on a suite of observations of faults, veins and authigenic minerals across the White Pine deposit a pre-, early- and post-mineralisation paragenesis can be reconstructed (summarised in Fig. 3.7).

3.4.1. Pre-mineralisation stage

Hematite. Amorphous, red-coloured hematite rims are the earliest authigenic phase surrounding detrital grains (Fig. 3.8A) and are ubiquitous in the Freda Formation and lower and middle Copper Harbor Formation, including on mafic volcanic rock fragments where it nucleates on ferromagnesian minerals. Hematite is generally absent from the Nonesuch Formation, with the exception of isolated red-coloured shales, including the Red Massive, Tiger, Brown Massive and Red and Grey Beds. Early hematite was likely preserved in these beds due to their fine-grainsize and low permeabilities. Hematite rims are only poorly preserved in upper Copper Harbor Formation rocks due to varying hematite destruction or 'bleaching' resulting in lighter red-brown, beige (Figs. 3.8B, 3.9A), light grey (Figs. 3.8C, 3.9B) or light brown (Fig. 3.8D) colours. Partial bleaching to light-brown colours occurs along bedding planes in the upper 100 m of the Copper Harbor Formation as far as ~15 km from the centre of the White Pine deposit. Beige-coloured bleaching occurs in coarser sandstone laminae in the uppermost ~5 m of Copper Harbor Formation at the peripheries of the White Pine deposit. Grey-coloured rocks are restricted to the upper ~20 m of Copper Harbor Formation and around faults and reflect the complete removal of hematite rims, typically associated with pyrobitumen-bearing rocks devoid of chlorite rims. Hematite destruction likely commenced shortly after formation and spanned mineralisation and post-mineralisation processes based upon variable preservation beneath later cement.

Illite. Illite rims up to ~10 μm wide surround detrital grains in much of the Copper Harbor Formation (Figs. 3.9C,E). Illite blades are generally oriented tangentially to grain surfaces and locally fill pores. They are commonly inter-grown with amorphous hematite rims in red sandstones and mostly at line-line grain contacts but not line-

point grain contacts suggesting neoformation (direct precipitation from fluids) during eodiagenesis. Illite is also observed partially replacing felsic lithic fragments but, interestingly, not feldspar grains. The widespread occurrence of illite in Copper Harbor Formation rocks implies a regional diagenetic origin.

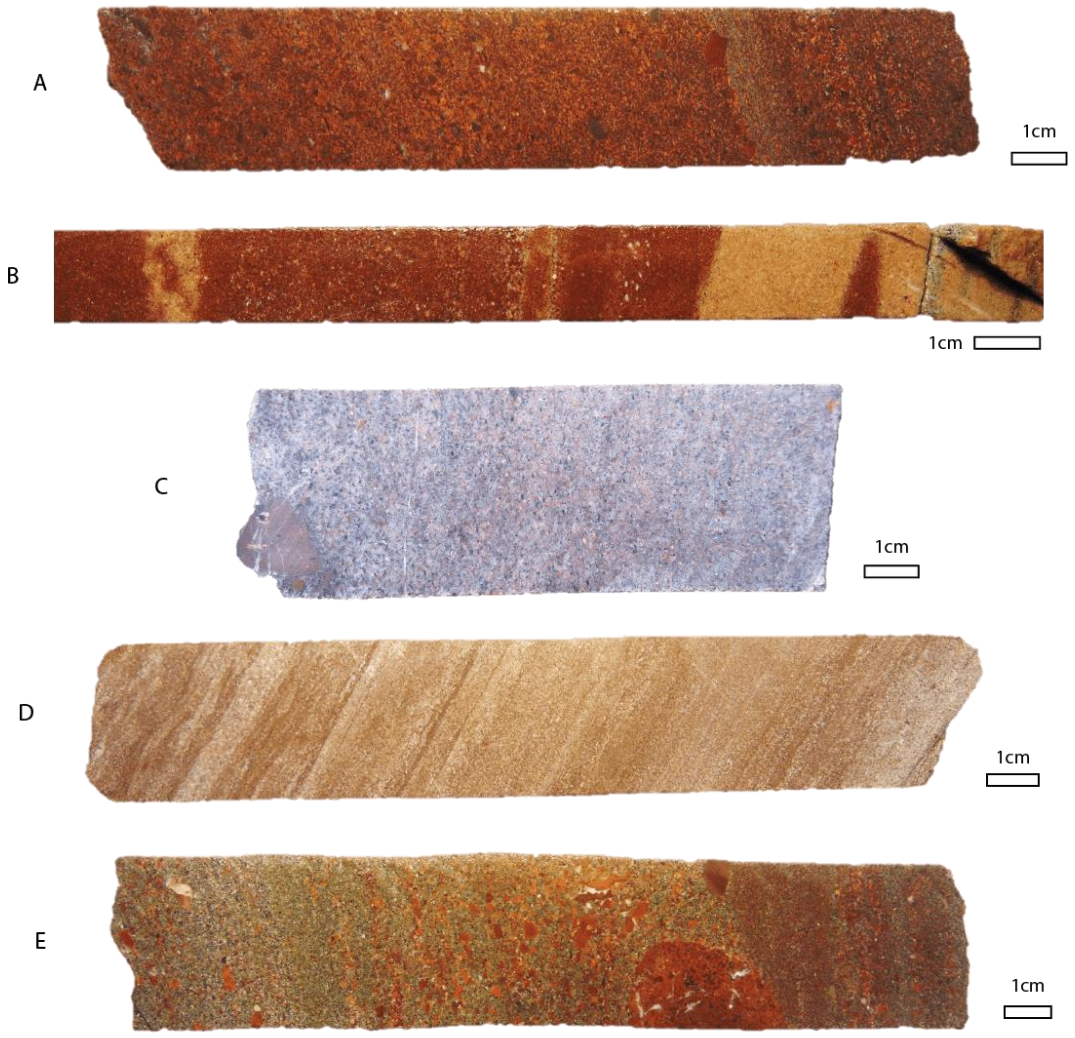

Fig. 3.8. Alteration textures in Copper Harbor Formation sandstone units. **(A)** hematised illite-rich lithic arenite. WP029 31.90m. **(B)** Selective beige hematite destruction in sandstone. WP059 126.30m. **(C)** Bleached grey lithic arenite. WP460 571.40m. **(D)** Faint hematite leaching in lithic arenite. WP038 118.65m. **(E)** Chlorite-altered lithic arenite. WP291 1156.90m.

Chlorite. Chlorite (clinochlore-1MIIb as determined by XRD) is present as blades on rims of detrital grains in uppermost Copper Harbor Formation sandstones and in siltstones and sandstones in the Nonesuch Formation; these rocks display the characteristic grey-green colour of chlorite. Blades are oriented perpendicular to grain surfaces (Figs. 3.8E, 3.9D,F) with thicknesses of ~20 µm in Copper Harbor Formation

rocks and <5 µm in Nonesuch Formation rocks. The absence of chlorite rims at grain line-line contacts suggests formation after a greater degree of compaction than that for illite, hence likely during mesodiagenesis. Chlorite rims nucleate on grains of varied composition, particularly mafic volcanic rock fragments. Quartz-rich sandstones are commonly devoid of chlorite.

Chlorite and hematite rims are mutually exclusive at the White Pine deposit and the former occurs mostly in rocks devoid of illite. Average Fe contents of chloritic and hematitic sandstones are 5.3% (n = 42) and 5.4% (n = 50) respectively, suggesting the former represents the chemical reduction of Fe in the latter. The inverse relationship between chlorite and illite suggests some chlorite may form via the replacement of precursor illite and, in rare instances, chlorite overgrowing illite can be observed.

The top of the Copper Harbor Formation is marked by a chlorite alteration zone 1-6 m thick that transitions downward over c. 0.5 m into hematite-bearing sandstones (Figs. 3.4 and 3.5). The zone is thinnest (< 1 m) on the northeast edge of White Pine deposit, thickens to ~4 m on the north side of the White Pine fault (see below) and becomes 6 m thick southwest of that fault. Other occurrences of chlorite zones are associated with syn-sedimentary faults and fractures and are best developed in well-sorted coarse-grained units exhibiting high primary porosity whereas units with mud drapes and laminae rarely contain isopachous chlorite rims. At the deposit-scale, chlorite alteration in Copper Harbor Formation units displays a spatial association with faults and fractures, but no such relationship is evident at drill-core scale.

Pyrobitumen. In places, pyrobitumen (formerly liquid petroleum) fills interstitial pores of upper Copper Harbor Formation sandstone, either in direct contact with detrital grains or as coatings on earlier formed illite and chlorite rims that mantle detrital grains (Figs. 3.10G and 3.11A). The highest concentrations of pyrobitumen are associated with the latter occurrence and it is absent in rocks that have hematite rims (likely due to reduction and dissolution of Fe). In rocks with high primary porosity, pyrobitumen may constitute up to 15% by volume. Interstitial pyrobitumen is also present in well-sorted quartz arenite units that maintained primary porosity during eodiagenesis as well as along zones of fracturing and on fault planes. Although liquid petroleum has been reported by earlier workers (Mauk & Hieshima, 1992), none was

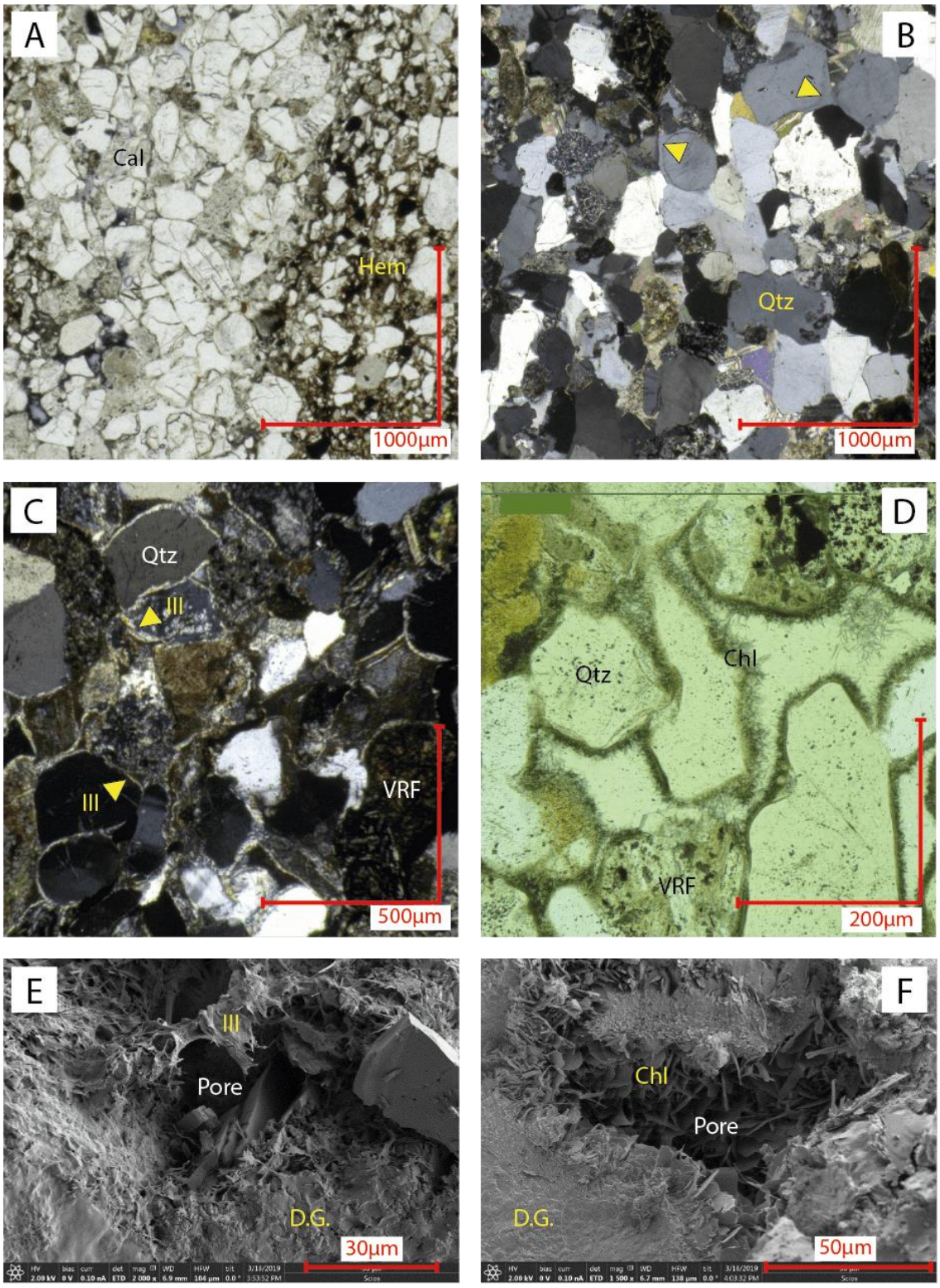

Fig. 3.9. Diagenetic and alteration textures in the Copper Harbor Formation. Cal – calcite, Hem – hematite, Qtz – quartz, Ill – illite, VRF – volcanic rock fragment, D.G. – detrital grain. **(A)** Plane polarized photomicrograph of selective beige hematite destruction and calcite cement along coarse sst laminae. CW-09-30 142.80m. **(B)** Cross polarized photomicrograph of bleached grey sandstone with quartz overgrowths (arrows). WP387 247.55m. **(C)** Cross polarized photomicrograph of hematised red sandstone with tangential illite rims. WP029 31.90m. **(D)** Plane polarized photomicrograph of isopachous chlorite rims in Upper Sandstone (Nonesuch Formation). **(E)** SEM image of illite rims in hematised sandstone. WP029 31.90m. **(F)** SEM image of chlorite-lined pore in sandstone. WP038 109.60m.

observed during this study. The concentration and thickness of the pyrobitumen zone increases towards the White Pine fault (see below). On the northeast side it is generally <2 m thick and restricted to uppermost Copper Harbor sandstones. On the southwest side, it is commonly >6 m thick and multiple strata-bound pyrobitumen zones occur to at least 31 m beneath the top of the Copper Harbor Formation. Nonesuch Formation contains localised accumulations of pyrobitumen in the Upper Sandstone near the White Pine fault and in the Tiebel Sandstone on the western edge of the deposit.

3.4.2. Mineralisation stage

Early-stage mineralisation: disseminated Cu-Ag ores. Cu-Ag minerals in the White Pine deposit forms a semi-continuous vertical zone that straddles upper Copper Harbor and lower Nonesuch rocks. The stratigraphically lowest Cu minerals are interstitial (pore-filling) native Cu in pyrobitumen-bearing upper Copper Harbor Formation sandstones devoid of hematite rims (Figs. 3.10G, 3.11A); it post-dates illite and chlorite rims and mantels pore-filling pyrobitumen. The base of the native-Cu zone often coincides with the first occurrence of pyrobitumen in Copper Harbor sandstones (these are typically well-sorted medium-grained quartz- and lithic-arenites with authigenic chlorite rims on grains but also having high primary porosity), which likely reflects a palaeo-oil-water contact. This generally occurs within a few meters of the base of the Nonesuch Formation but can be as much as 20.6 m below the Nonesuch-Copper Harbor contact. The top of the native Cu zone typically coincides with the Lower Transition Zone Bed but can be present in the Upper Sandstone Bed where it contains interstitial pyrobitumen; these locations are where the stratigraphic height of the Cu-mineralised zone ("fringe zone") within the Nonesuch Formation is greatest (see below).

In the Nonesuch Formation, ore comprises native Cu and Cu(-Fe) sulphides in organic-rich shale, siltstone and fine sandstone (Figs. 3.10A – F, 3.11B – H). Native Cu grains are typically 20 to 250 µm in size and display a rounded morphology indicating formation via replacement of precursor detrital grains or infilling of open pore space (Fig. 3.11C). Cu sulphides rarely exceed 100 µm and are commonly <20 µm, although aggregations of grains can form blebs up to ~3 mm in diameter. The majority of Cu sulphides show nucleation on detrital and authigenic chlorite (Figs. 3.11C, 3.11D, 3.11E) and mafic volcanic rock fragments commonly show partial or complete

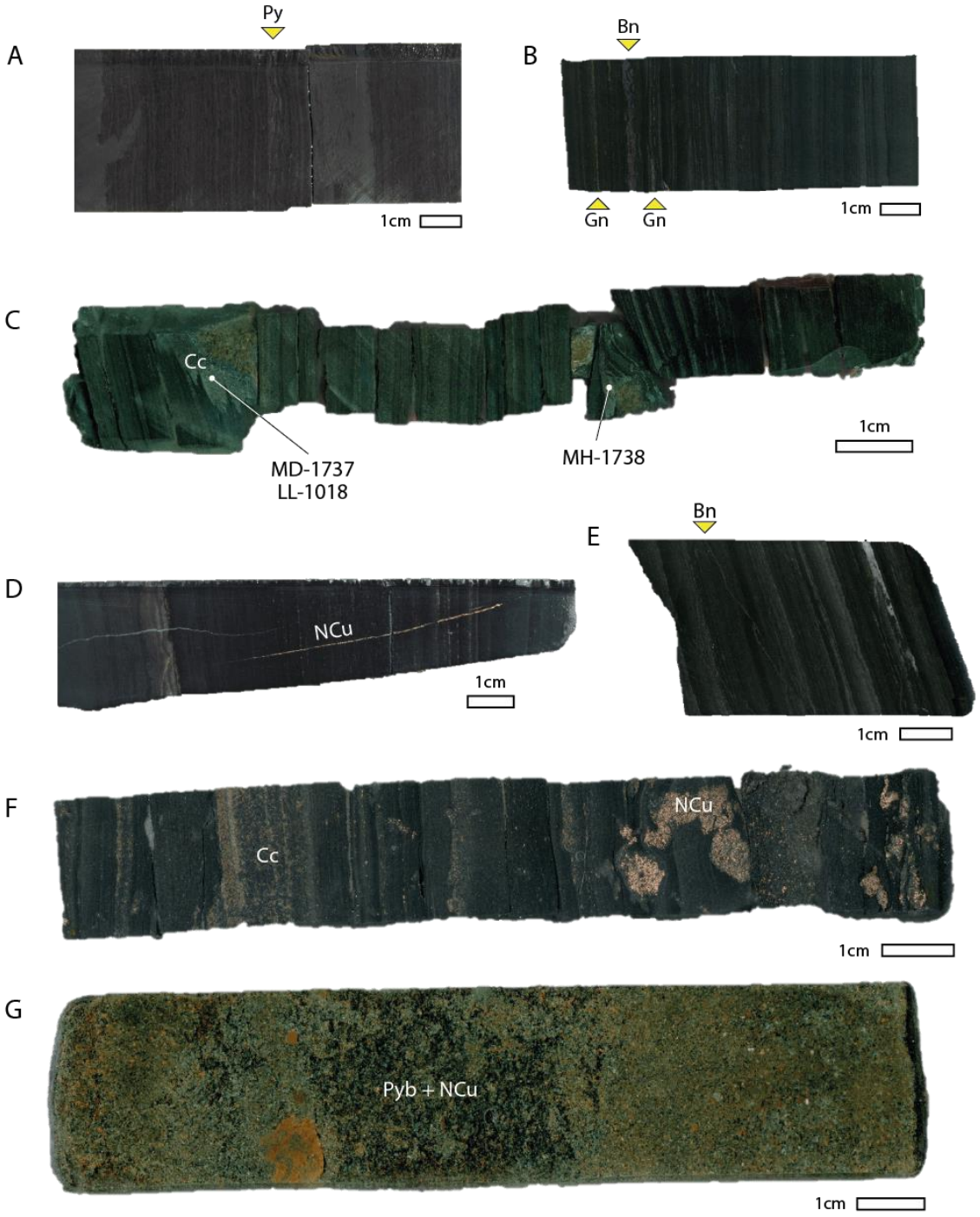

Fig. 3.10. Ore textures. Py – pyrite, Bn – bornite, Gn – greenockite, Cc – chalcocite, NCu – native copper, Pyb - pyrobitumen. **(A)** Pyrite along laminations, Widely Bed, Nonesuch Formation. WP299 250.66m. **(B)** Fringe zone with greenockite, and bornite partially replaced by chalcocite, Upper Transition Zone Bed, Nonesuch Formation. WP506 852.05m. **(C)** Replacive and sheet chalcocite, Upper Transition Zone Bed, Nonesuch Formation. Re-Os sample locations annotated. WP198 858.45m. **(D)** High angle native copper vein and disseminated native copper cutting Domino Bed, Nonesuch Formation.WP126 644.30m. **(E)** Purple bornite veinlets showing reverse kinematics, Widely Bed, Nonesuch Formation.WP506 852.10m. **(F)** native copper and chalcocite, Domino Bed and Lower Transition Zone Bed, Nonesuch Formation. Note native copper replacement of evaporite feature and shearing at base of unit with transposed folds. WP436 259.30m. **(G)** Interstitial pyrobitumen, chlorite and native copper in Copper Harbor Formation sandstone. WP121 630.75m.

replacement by Cu sulphides. Chalcocite forms ~10 µm rims around earlier native Cu grains in the Domino and Dark Grey Massive Beds (Figs. 3.11F, 3.11G). Inclusions of chalcocite within native Cu are uncommon.

Cu-mineralised Nonesuch Formation exhibits an upward and distal increase in the S:Cu ratio from native copper (Cu) to chalcocite (Cu_2S) and then, in a 20-60 cm thick interval at the upper limit of chalcocite referred to as the "fringe zone", bornite (Cu_5FeS_4) and chalcopyrite ($CuFeS_2$). The top of the fringe zone is marked by greenockite (CdS) (Fig. 3.10B) and trace amounts of galena (PbS) sphalerite ((Zn,Fe)S) and wurtzite (ZnS)). Cu grades within the Nonesuch can exceed 2% in carbonaceous units, such as the Domino, Dark Grey Massive and Thinly beds and in sandstones containing shale partings such as the Lower Transition and Upper Transition beds. Grades are commonly less than 0.1% in beds with little organic matter, such as the Upper Sandstone and Tiger beds. Grades are highest near the top of the ore zone, suggestive of continuous upward remobilisation of copper and, likely, sulphur (also, see below). Above the fringe zone, organic-rich rocks contain abundant but patchily distributed pyrite as fine grained (~10 µm) disseminated pyrite (Fig. 3.10A), clusters or framboids (average 50 µm in size but can exceed 200 µm) and less commonly, euhedral pyrite (average size of ~50 µm). Pyrite nucleates on detrital and authigenic chlorite grains similar to Cu(-Fe) sulphides, but pyrite replacement of mafic volcanic rock fragments is uncommon.

Native silver is the only Ag-bearing mineral observed at the White Pine deposit. It occurs in highest concentrations northeast of the mine area in organic-rich shales with the highest grades present towards the top of the ore zone. Notable is that native Ag flakes are visible at the Lower Transition Zone – Domino contact.

Several aspects of the fringe zone are worth highlighting separately. Zonation of copper minerals within the zone expand and contract in conjunction with the stratigraphic character of that zone: where it is restricted to within or just above the Thinly Bed, native Cu and chalcocite occur together whereas in locations where the fringe zone extends to above the Thinly Bed, native Cu occurs at the base of the Formation and chalcocite occurs separately above. SEM analyses of Cu minerals in the lower part of the fringe zone where it is thickest reveal Fe-oxide rims around chalcocite (Fig. 3.11H) and Cu- oxide rims around native Cu grains; these rims have ~10 µm widths. High-tenor copper sulphides replace lower-tenor copper sulphides and

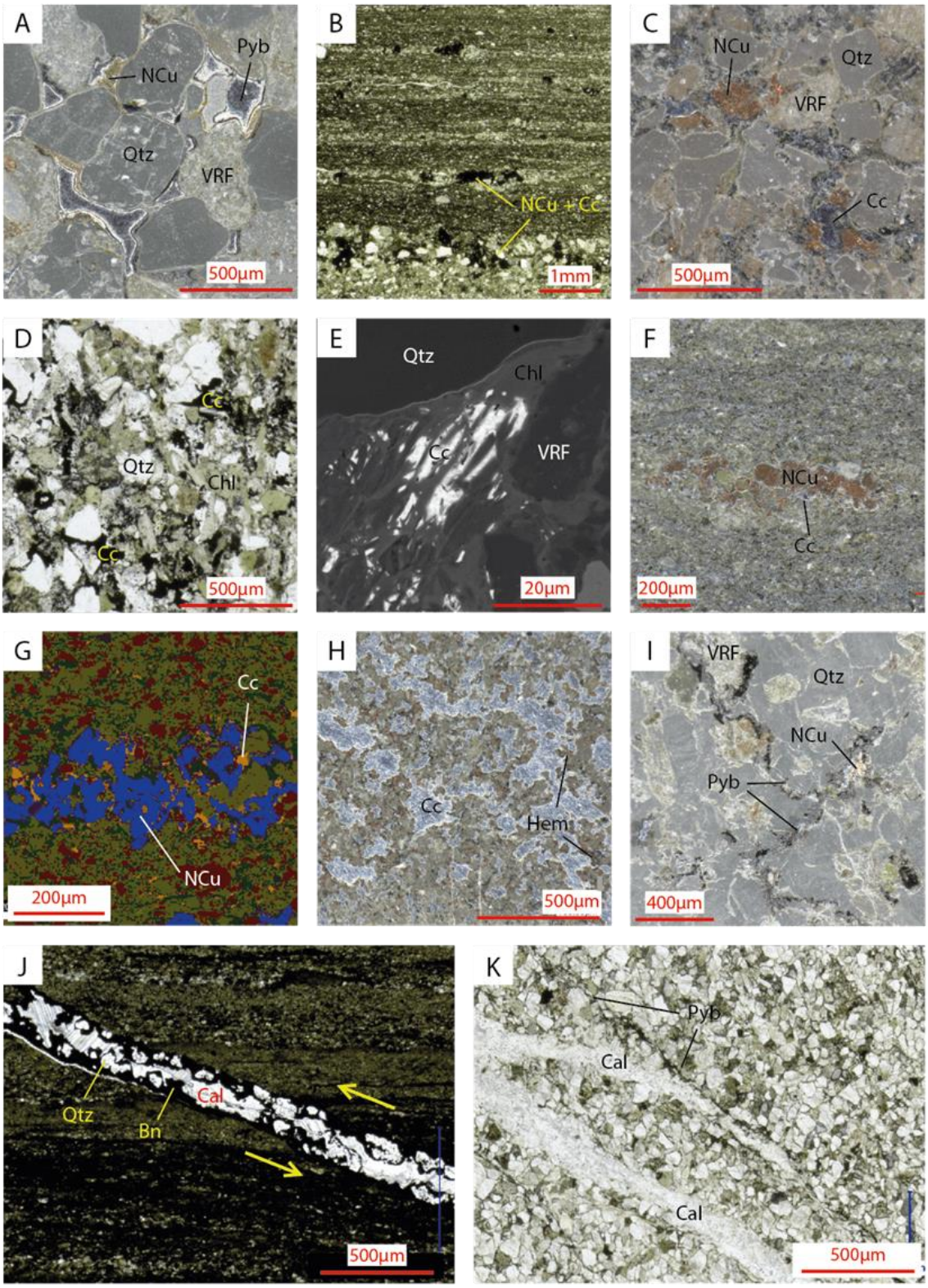

Fig. 3.11. Ore textures. NCu – native copper, Qtz – quartz, Pyb – pyrobitumen, VRF – volcanic rock fragment, Cc – chalcocite, Hem – hematite, Bn – bornite, Cal - calcite. **(A)** Reflected light photomicrograph of interstitial native copper and pyrobitumen in sandstone, Copper Harbor Formation. WP163 441.45m. **(B)** Plane polarized photomicrograph of native copper and chalcocite along sand laminae within siltstone unit, Thinly Bed, Nonesuch Formation, WP157 981.38m. **(C)** Reflected light photomicrograph of chalcocite replacing detrital and authigenic chlorite grains, Thinly Bed, Nonesuch Formation, WP157 981.38m. **(D)** Plane polarized light

photomicrograph of chalcocite replacing detrital and authigenic chlorite, Lower Transition Bed, Nonesuch Formation. WP398 728.00m. **(E)** SEM image of chalcocite replacing detrital chlorite grain, Lower Transition Bed, Nonesuch Formation. WP398 728.00m. **(F)** Reflected light photomicrograph of chalcocite surrounding native copper, Lower Transition Bed, Nonesuch Formation.WP157 981.38m. **(G)** False color SEM image of chalcocite surrounding native copper, Lower Transition Bed, Nonesuch Formation. WP157 981.38m. **(H)** Reflected light photomicrograph of hematite surrounding chalcocite, Dark Grey Massive Bed, Nonesuch Formation, WP038 108.20m. **(I)** Reflected light photomicrograph of native copper on late pyrobitumen vein, Copper harbor Formation. WP460 573.50m. **(J)** Plane polarized photomicrograph of veinlet displaying minor reverse kinematics, filled with early bornite on the margins and late calcite in the center, Upper Transition Zone Bed, Nonesuch Formation. WP506 852.35m. **(K)** Plane polarized photomicrograph of calcite veins re-utilising earlier pyrobitumen vein, Copper Harbor Formation. WP466 419.40m.

together with the oxidized rims indicate a migrating redox front through the fringe zone. In places, Cu sulphide minerals pseudomorph framboidal and euhedral pyrite grains.

Early-stage mineralisation syn-sedimentary faulting. The stratigraphic height of the fringe zone is variable and inverse to the thickness of the Parting Shale: it is stratigraphically lowest where the Parting Shale is thickest, which occurs in the hanging-wall of the White Pine fault, and stratigraphically highest where the Parting Shale is thin or absent (Fig. 3.16). We attribute the absence of Parting Shale in the White Pine area (Figs. 3.15B, 3.16) as due to erosional removal beneath the Upper Sandstone. Importantly, as shown on the cross section of Figure 3.16, restored to the Stripey Bed the height of the fringe zone is unaffected by the White Pine fault. This suggests that during mineralisation the fault was inactive and did not act as a conduit for fluids higher into the Nonesuch Formation; this inactivity is confirmed by the fact that there is little or no offset of the Tiebel Sandstone Bed (Fig. 3.16). Similar relationships are observed across syn-sedimentary faults reactivated as reverse faults that offset stratigraphy, Cu-mineral zonation patterns, alteration zones and pyrobitumen zones. The height of the fringe zone averages 0 to 50 cm above the Thinly Bed across most of the mine but rises abruptly near the intersection of the White Pine and Porcupine faults to ~11 m above the Thinly Bed. This suggests a hydrological effect of fluids being focused into the Nonesuch Formation due to a combination of fault-related pathways and attenuation of the Copper Harbor Formation aquifer above the Porcupine volcanic dome.

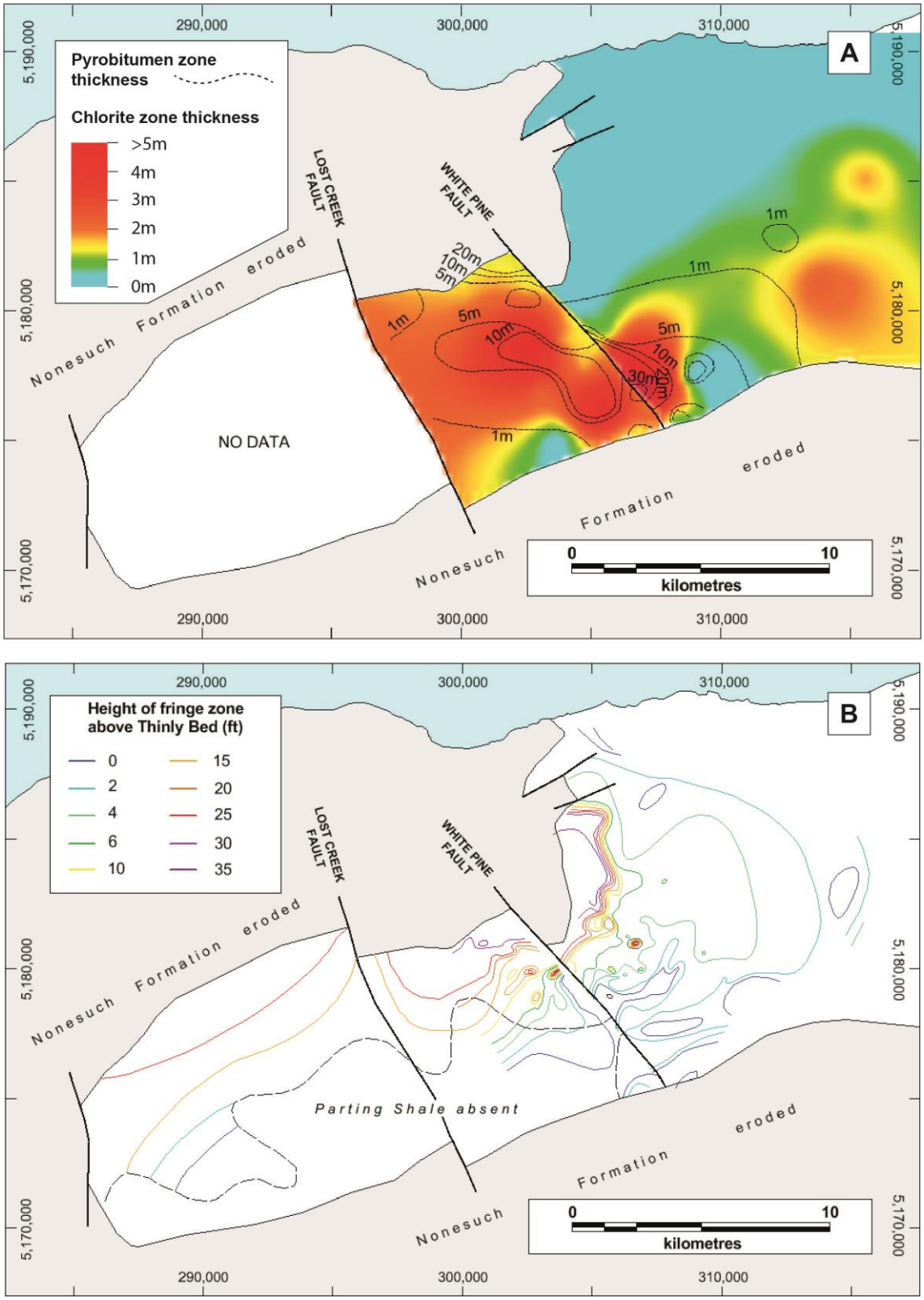

Fig. 3.12. (A) Thickness of chlorite (shaded) and pyrobitumen (isopachs) zones in the upper Copper Harbor Formation. **(B)** Stratigraphic height of the fringe zone in the lower Nonesuch Formation (modified after Brown, 1971; White and Wright, 1966).

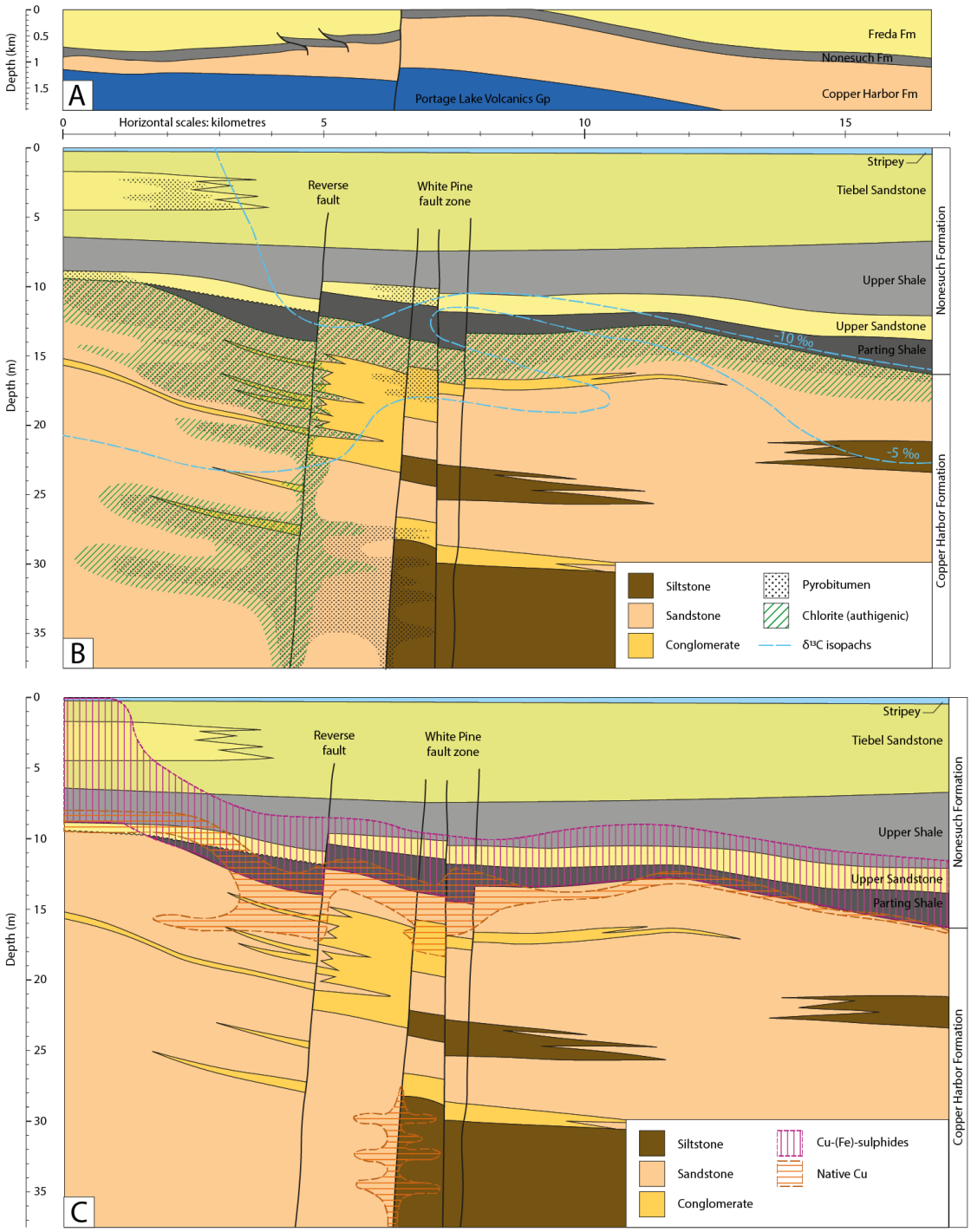

Fig. 3.13. Geological cross sections through White Pine. See Figure 3.6 for location. **(A)** Present-day geometry with no vertical exaggeration. **(B)** 250x vertically exaggerated section with alteration and pyrobitumen distribution. **(C)** 250x vertically exaggerated section with Cu mineral zones. Sections B and C are restored to the top of the Stripey Bed.

Late-stage mineralisation: structure-hosted Cu-Ag ores. A wide variety of styles of Cu-Ag mineralised veins and structures exist at White Pine. Their principal constituents, in order of decreasing abundance, are calcite, pyrobitumen, ore minerals (native Cu and Cu(-Fe) sulphides) and quartz (Figs. 3.10D, E). No native silver was observed in veins during this study. Mineralised veins are linear and display uniform thicknesses and

average 0.4 mm in width but 3 mm widths are common. Vein walls are commonly lined by an early phase of drusy quartz, 0.1-0.5 mm wide, with a later sulphide or native Cu fill in their centres (Fig. 3.11J). Copper sulphide and native Cu in veins are homogenous under SEM, indicative of a single phase of precipitation. Late calcite veins post-date the ore minerals, typically lining the centre of veins or intersecting and bifurcating early copper veins. No alteration halos are observed around veins.

Cu-Ag veins in Copper Harbor Formation sandstones are rare but can be observed near the White Pine fault zone where they occur as ~0.1 mm diameter native Cu grains nucleated on irregular and anastomosing late-stage pyrobitumen veins (Fig. 3.11I). These veins cut earlier chlorite rims and quartz cements but pre-date later faults and calcite veins and represent the paragenetically latest phase of mineralisation at White Pine.

In the Nonesuch Formation, mineralised veins and faults occur in shale and siltstone beneath the fringe zone and are most common near the White Pine fault zone and in the southwest portion of the mine where the density of brittle structures is highest. Northwest of the fault zone, mineralised veins display steep orientations (>60˚) whereas southwest of the fault zone they dip at shallow angles (<30˚) and display reverse offsets of up to 5 mm. Cu minerals in the veins correspond to those in the surrounding host rock, e.g. chalcocite veins occur only in shales containing disseminated chalcocite.

3.4.3. Post-mineralisation stage

Quartz cement. Quartz cement forms syntaxial overgrowths on detrital grains and infills pores (Fig. 3.9B). Quartz overgrowths or rims form adjacent to line-line contacts between quartz grains, indicative of pressure solution. Rims are common in upper Copper Harbor Formation sandstone and the Upper Sandstone of the lower Nonesuch Formation. Pore-filling quartz cements are restricted to the most quartz-rich (quartz arenite) rocks such as the lowermost Copper Harbor Formation at White Pine. Quartz cements post-date bleaching and emplacement of Cu-Ag minerals and overgrow hematite rims where preserved. Quartz cement is absent where illite and chlorite rims are present.

Calcite cement. Pore-filling and replacive calcite cement is present throughout the Oronto Group. The former post-dates all other phases of diagenesis, alteration and mineralisation, including most pyrobitumen emplacement, nucleating on all earlier mineral phases. Calcite cements are particularly well-developed in coarse sandstone and conglomerate, in places displaying poikilotopic textures. Calcite is commonly observed partially replacing and pseudomorphing detrital grains and earlier authigenic textures, particularly in volcanic rock fragments, and implies significant dissolution of some detrital grains occurred prior to calcite precipitation. Late-stage calcite cements are widespread both within and outside of White Pine deposit and display no apparent spatial association with ore.

Calcite veins. Calcite veins are predominantly linear (can be curvilinear adjacent to faults) with sharp margins and widths of between 1 to 10 mm (Figs. 3.14A–D). They form along fault planes, in damage zones around faults and in many cases terminate against faults. Offsets across reverse faults with associated calcite veining are typically in the order of centimetres to decimetres – greater than offsets across Cu-mineralised reverse faults. Calcite veins consistently cross-cut pyrobitumen veins and petrographic inspection reveals early pyrobitumen veins re-utilised by later calcite veins (Fig. 3.11K). In very rare instances (<<1% of Cu minerals), copper-mineral veins show re-utilisation by later calcite veins (Fig. 3.11J). The vast majority of calcite veins do not cut across faults and, where present adjacent to larger faults, many veins show evidence of rotation and transposition suggesting that the bulk of fault movement – and the generation of meter-scale stratigraphic offsets – occurred after calcite vein formation. There are rare instances of mutually cross-cutting relationships between small reverse faults and sub-vertical calcite veins thus a minor portion of these features formed coevally.

Pyrobitumen veins. Irregular, anastomosing pyrobitumen veins 0.005 to 0.2 mm wide cross-cut earlier chlorite, quartz and calcite cements in grey, hematite-depleted Copper Harbor Formation sandstone near the White Pine fault (Fig. 3.14A). These veins are typically steep and show a spatial relationship with faulting in core and thin section where they are observed to wrap into and terminate against faults, occur along fault surfaces as well as a binding matrix in cataclasites.

Anhydrite. Trace amounts of pore-filling anhydrite are observed in Copper Harbor sandstones at White Pine. It post-dates calcite cement and represents a late, sulphate-bearing oxidizing fluid.

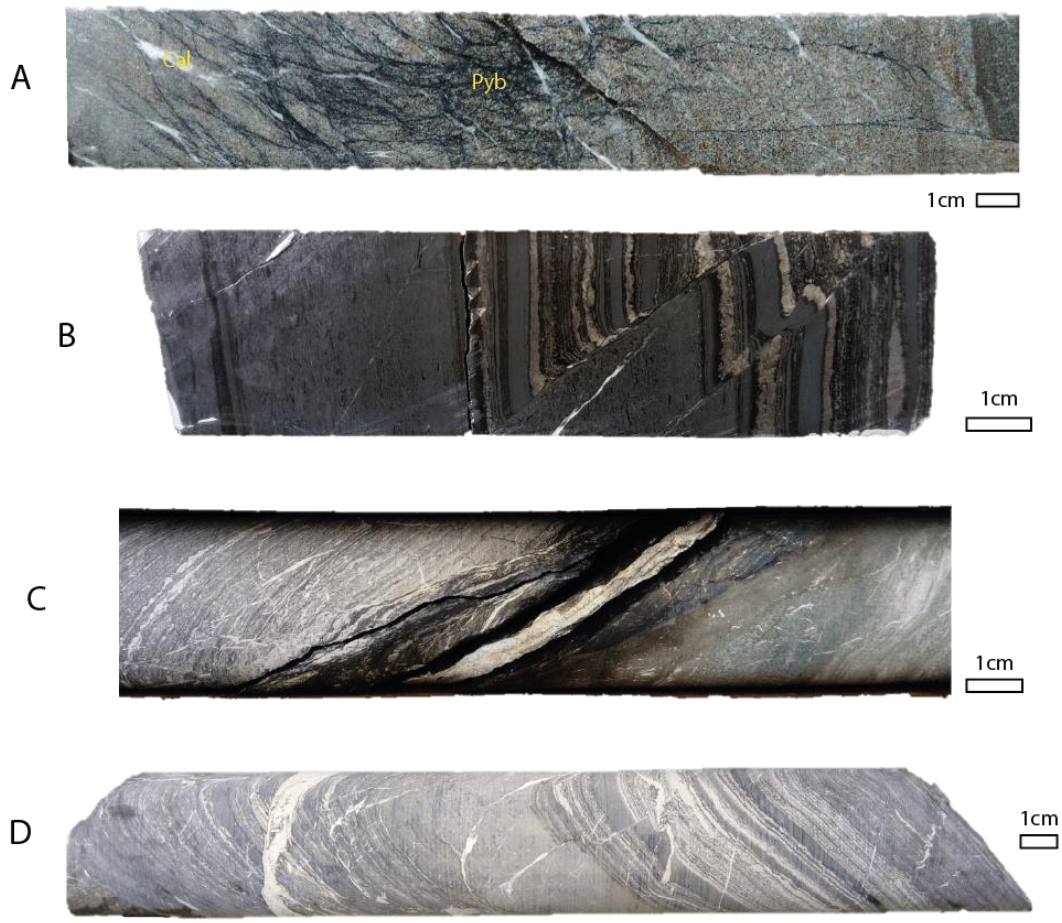

Fig. 3.14. Late structures – post-mineralisation veins and faults. Cal - calcite, Pyb - pyrobitumen. **(A)** Late calcite veins cross-cutting and re-utilising earlier pyrobitumen veins in the White Pine fault zone, Copper Harbor Formation. WP466 419.20m. **(B)** Steep reverse faults with associated calcite veining, Stripey Bed, Nonesuch Formation. WP501 767.50m. **(C)** Steep reverse fault with recent movement post-dating associated calcite and pyrobitumen veining, Marker Bed, Nonesuch Formation. WP501 785.95m. **(D)** Reverse faults with centimetre-scale offsets and associated calcite veining, Stripey Bed, Nonesuch Formation. WP501 794.46m.

3.4.4. Late faults

As noted previously, some faults in the White Pine area were syn-sedimentary for part of their history and many faults trend parallel to the strike of the outcrop belt (such as those in the southwest portion of the mine) hence were susceptible to later reactivation and inversion during Grenville orogenesis (those faults oriented less favourably for inversion often experienced reactivation as wrench faults). In the

underground workings of the White Pine mine and southwest of the White Pine fault, many east-west striking faults show late reverse movement (e.g. Mauk et al., 1992) and can offset stratigraphy by 10s of meters. In contrast, northeast of the White Pine Fault, north-south striking normal faults with 1s of meters of displacement dominate and these wrap into the southern tip of the White Pine fault. The majority of both normal and reverse faults dip steeply at between 60˚ and 90˚. Also worthy of note is that many fault surfaces in the Copper Harbor Formation are covered by pyrobitumen and contain milled rock fragments in a pyrobitumen and calcite-cemented matrix, this confirms that at least two episodes of hydrocarbon migration occurred, one prior to the early mineralisation event and another coeval with late-stage faulting.

The sub-vertical NW-SE trending White Pine fault zone is down-thrown on its southwest side with a maximum down-throw in the centre of the deposit of c. 220 m. On the north side of the deposit, the fault also has 2 km of horizontal stratigraphic separation. There, beds dip at ~55˚ in the hanging-wall (southwest side of the fault) and ~10˚ in the footwall (northwest side of the fault). The northern tip of the fault intersects the eastern edge of the Porcupine Mountain volcanic complex and coincides with a significant thickening of the Copper Harbor Formation. Thus, the White Pine fault shows evidence of syn-sedimentary movement spanning upper Copper Harbor to Tiebel Sandstone time and then reactivation post-Oronto Group deposition. Supporting this conclusion is the fact that fault plane surfaces commonly show normal dip-slip slickenlines overprinted by younger dextral strike-slip slickenlines. Further, the offset of Cu mineral and alteration zones (e.g. native copper, pyrobitumen and chlorite zones) across the fault suggests post-sedimentation movement also occurred post-mineralisation, as does the observation that Domino Bed shales locally display bedding-parallel shearing that post-dates emplacement of chalcocite and native copper minerals (right hand side of Fig. 3.10F). Hook folds and S-C fabrics attest to high degrees of strain, but the amount of offset is unclear.

3.5. Geochemical data

To gain a better understanding of the fluid compositions during the mineralisation events, we collected 430 samples from outcrop and c. 60 drill cores in the White Pine deposit and surrounding area. Optical imaging, X-Ray Diffraction (XRD) and illite crystallinity analyses was done at the University of St Andrews, UK. The

former was done using petrographic microscopes and a FEI Scios Dualbeam transmission electron microscope (TEM). XRD analyses were conducted on 69 sandstone samples chosen to avoid silt or mud laminations on the basis that detrital clays would dominate the diffraction spectra. Samples were crushed to < 0.5 cm size, mixed with sodium polymetaphosphate and distilled water in centrifuge tubes, and placed in an ultrasonic bath for 10 minutes to liberate clay particles into solution. A < 2 µm size fraction was separated by centrifuging for 20 minutes at 4000 rpm. Samples were air dried at 40˚C and powdered to make randomly oriented mounts. Analysis was via a Philips PW1830 generator, PW1710 diffractometer control and PW 1050/80 goniometer using a cobalt tube producing 30kV and 30mA with output measured in 0.02° steps for 1.0 second per step. Illite crystallinity values were calculated based on the full width to half maxima (FWHM) ratio of the first illite diffraction peak at c. 10˚ (2θ), following the method of Kübler and Jaboyedoff (2000).

Sulphur, carbon and oxygen isotope analyses were undertaken at the Scottish Universities Environmental Research Centre (SUERC), East Kilbride, UK. For S isotopes, a total of 33 sulphide mineral powders were extracted by micro-drilling chalcocite, bornite, pyrite and chalcocite, the latter intermixed with native copper. These were combusted to produce SO_2 gas which was analysed by a ThermoFisher Scientific MAT 253 dual inlet mass spectrometer. The measured ratio of ^{34}S to ^{32}S in the gas was converted to a raw $\delta^{34}S$ value based on an SO_2 gas standard of known $\delta^{34}S$. Raw $\delta^{34}S$ values were then reported in ‰ relative to the Vienna Canyon Diablo Troilite (VCDT). Multiple runs of powdered standards (chalcopyrite CP-1, -4.56 ‰; sphalerite NBS-123, +17.1 ‰; barite NBS-127, +20.30 ‰; and silver sulphide IAEA230 S-3, -32.2 ‰) were analysed using the conventional sulphur gas extraction line as unknowns prior to sample analysis to test calibration accuracy. Standard analyses were repeated to establish precision. A total of 144 calcite powder samples were collected by micro-drilling for C and O isotope and analyses were performed on an automated continuous flow VG Prism Series II Isotope Ratio Mass Spectrometer using international standard IAEA-CO-8 (calcite) and internal standard MAB2C. XRD analyses confirmed samples are calcite. Reproducibility of standards is ±0.2‰ and ±0.3‰ for carbon and oxygen respectively at 1σ; calibration was via NBS 19. C- and O-isotope ratios were calibrated to Vienna Pee Dee Belemnite (VPDB) and Vienna Standard Mean Ocean Water (VSMOW), respectively.

Re-Os dating was carried-out using NTIMS (negative thermal ionization mass spectrometry) on a Triton machine at the AIRIE Program, Colorado State University, Fort Collins, CO, USA. A ~95% pure chalcocite separate was obtained by micro-drilling to avoid oxidised portions and other copper minerals. A weighed amount of chalcocite powder was equilibrated with a mixed-double Os spike using a carius tube dissolution in inverse aqua regia. The double Os spike technique established for molybdenite (Markey et al., 2003) is routinely employed for sulphide minerals with high $^{187}Re/^{188}Os$ and high radiogenic-to-common Os ratios, permitting mass fractionation correction for Os and a precise correction for common Os. Results are blank corrected and reported at 2σ uncertainties, which include propagation of all analytical errors and the uncertainty in the ^{187}Re decay constant.

3.6. Analytical results

3.6.1. Illite crystallinity

Illite crystallinity was calculated for 34 samples of diagenetic illite-bearing Copper Harbor Formation collected from the uppermost 120 m of the Formation but concentrated in the top 10 m. Calculated peak temperature values range from 125 to 178˚C with a mean value of 148˚C and no clear spatial or stratigraphic trends, implying uniform temperature distribution across White Pine deposit. Assuming no significant thermal perturbations by convective fluid flow or local intrusive activity and a linear geothermal gradient of 35˚C km^{-1} (Hegarty et al., 2007), this equates to a depth of c. 3.8 km and would correspond to burial beneath middle to upper Freda Formation.

3.6.2. Carbon and oxygen isotopes

Data are differentiated on the basis of paragenetic age: sedimentary carbonate (Junior Member), early and late concretions, early and late diagenetic nodules, interstitial cement and veins. Values of $\delta^{13}C_{VPDB}$ and $\delta^{18}O_{VSMOW}$ vary from -15.06 to -1.29 ‰ and 10.41 to 41.32 ‰ respectively (Table A3.1; Fig. 3.15). $\delta^{18}O$ values range from 13 to 23 ‰ define a general trend of decreasing values linked to paragenetic features, with one exception: Junior Member 20.70 ‰, early concretions 19.50 ‰, early diagenetic features 20.62 ‰, late concretions 18.02 ‰, cement 18.95 ‰ and veins 16.00 ‰; the exception are late diagenetic features at 21.81 ‰. The few samples with $\delta^{18}O$ values >25‰ are likely due to incorporation of heavy, residual ^{18}O from

pyrobitumen during preparation. The stratigraphic trend for $\delta^{13}C$ in calcite cements decreases with stratigraphic position: from -4.16 ‰ in upper Copper Harbor Formation to -9.07 ‰ in Upper Sandstone Bed of the Nonesuch Formation.

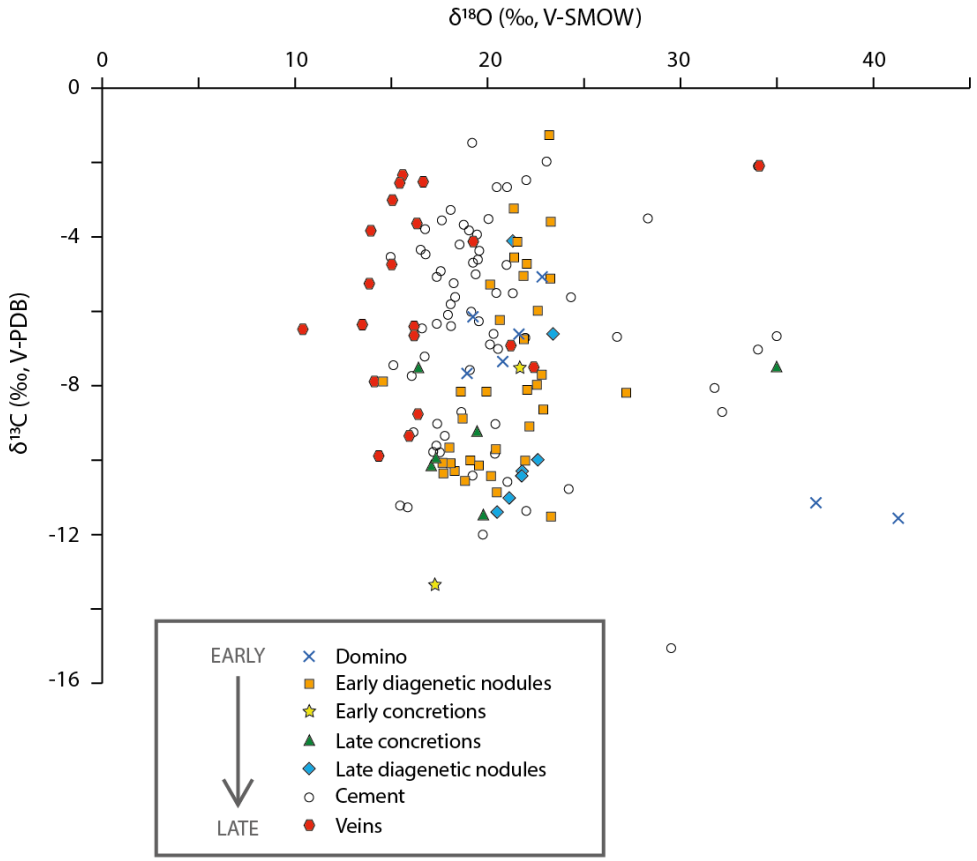

Fig. 3.15. Plot of carbon and oxygen isotope data by paragenetic feature (age).

3.6.3. Sulphur isotopes

$\delta^{34}S$ data are listed in Table A3.2 and plotted on histograms in Figure 3.16. Values range from -14.0 to 29.9 ‰ with a majority between 0 and 20 ‰ and a mean of 7.5 ‰. No mineralogical trends are discernible although the chalcocite-native copper association tends to display slightly lighter values of <8.1 ‰ and sulphide minerals in sandstone-dominated units (Copper Harbor Formation, Lower Transition Zone, Top Zone, Upper Sandstone, Upper Transition and Tiebel Sandstone) tend to have heavier $\delta^{34}S$ values relative to those that occur in sand-size laminae in siltstone units.

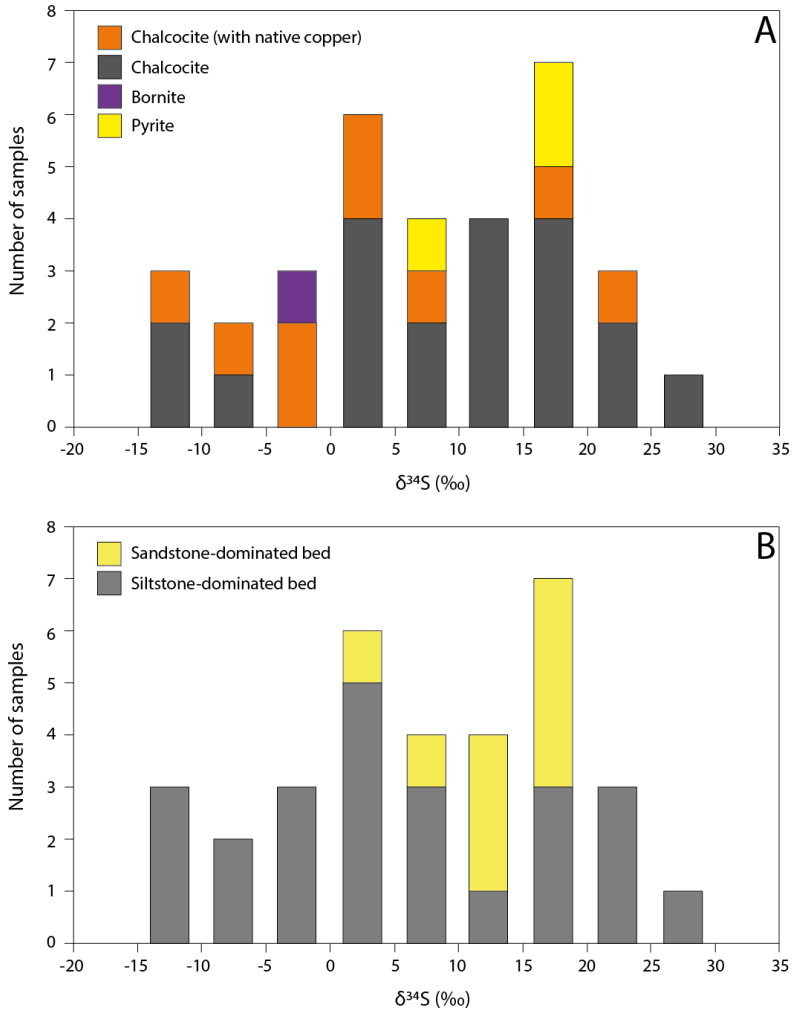

Fig. 3.16. Histogram of sulphur isotope analyses by **(A)** mineralogy and **(B)** host lithology.

3.6.4. Re-Os geochronology

Three samples of chalcocite from the Thinly Bed in drill hole WP198 (NW part of White Pine deposit) were dated using the Re-Os technique. An initial analysis of chalcocite (sample LL-1018, Fig. 3.10C, Table A3.3) was equilibrated with a single Re and Os spike and yielded a model age range of 1020 ± 13 to 986 ± 12 Ma. This sample had Re, radiogenic Os and common Os contents of 159 ppb, 1.72 ppb and 0.09 ppb, respectively. Despite the high ratio of radiogenic to common Os (~5%) the amount of common Os was sufficient to warrant a double spike method, which permits precise assessment of and corrections for common Os as well as a mass fractionation correction for Os; this method was used for samples MD-1737 and MD-1738 (Fig. 3.10C, Table A3.3). The lack of common Os in MD-1738 suggests contamination of the Re-Os system by host material (i.e. shale) was insignificant. However, the Re-Os age range of 1098 ± 4 to 1088 ± 4 Ma is incompatible with a U-Pb zircon age of 1085.57 ±

0.25 Ma in the underlying Copper Harbor Formation (Fairchild et al., 2017). The calculated Re-Os model age for sample MD-1737 varies with assumptions of the initial Os ratio ($^{187}Os/^{188}Os$, Os_i). The Os_i of surface waters during Nonesuch Formation deposition is poorly constrained because of uncertainties around the paleo-environmental setting of the Midcontinent Rift System, and specifically the relative contributions of seawater and continental-derived meteoric water. Cumming et al. (2013) outlined potential sources of Os which include Archean and early-Proterozoic cratons (Os_i ≈ 1.01), unradiogenic rift-related flood basalts (Os_i ≈ 0.13) and contemporary seawater Osi ≈ 0.3). An Osi in the range of 0.1 to 1 could therefore be expected. However, variations in the Os_i cause only a small change in Re-Os model ages. Os_i assumptions of 0.15 and 5 yield model ages of 1039 ± 4 Ma and 1035 ± 4 Ma respectively, and thus have minimal impact on the inferred age of mineralisation at White Pine.

3.7. Discussion

3.7.1. Pre-mineralisation basin architecture and faulting

The local basin architecture at White Pine played a principal role in focusing hydrothermal fluids during the mineralisation event and subsequent formation of the deposit. Three main architectural elements were identified: (i) palaeotopography associated with the Porcupine Mountain caldera; (ii) development of early syn-sedimentary growth faults during Copper Harbor Formation deposition; and (iii) creation of a reduced seal and cessation of faulting during early Nonesuch deposition.

The contact between the Copper Harbor Formation rocks the Porcupine Mountain and Portage Lake Volcanics in the White Pine area is marked by a well-developed paleosol. This contact defines an abrupt contrast between the high permeability Copper Harbor rocks and the much lower permeability volcanic units. That, combined with the fact that the Porcupine Mountain Volcanics was a palaeo-high, helped to focus mineralising fluid flow laterally along the flank of the high towards White Pine, resulting in precipitation of Cu-Ag minerals in the organic-rich shales of the Nonesuch Formation.

Although syn-sedimentary faults had minor displacement, that was enough to result in deposition of thicker packages of coarser-grained sediment with higher primary permeability in hanging-wall units. These sediments enabled higher fluid

fluxes accounting for the greater amounts of chlorite, pyrobitumen and native copper at multiple stratigraphic levels in the hanging-walls of those faults (Fig. 3.16B, C). The thickness and composition changes across the faults and gouge material on the fault planes may have resulted in compartmentalization of fluid flow during mineralisation.

Movement on syn-sedimentary faults ceased by the time the Tiebel Sandstone was deposited. This is evident by the stratigraphic height of the fringe zone which occupies a consistent position in the basal Tiebel Sandstone Bed across the White Pine fault suggesting that unit formed a coherent, un-faulted horizon during mineralisation. The transition to the organic-rich and marine-influenced sediments in the lowermost Nonesuch Formation represents a time of transgression during which the basin was hydrologically connected to marine waters. This transgression formed a reduced impermeable seal above the highly permeable and oxidized Copper Harbor rocks. Moreover, the thinning of the pyrobitumen zone towards the peripheries of the White Pine deposit implies that the seal was robust, given that it was capable of trapping liquid petroleum. Together, palaeotopography and syn-sedimentary faults compartmentalized fluid flow, focused it into the Nonesuch sediments, and triggered Cu-Ag mineralisation in the White Pine deposit.

3.7.2. Timing of mineralisation

Late calcite veins and reverse faults post-date and offset chlorite alteration, interstitial pyrobitumen and Cu-mineralised zones. Reverse faults represent inversion of what were originally syn-sedimentary normal faults as evident by their high angles (typically steeper than 60˚) combined with thickening and coarsening of sedimentary units in hanging-walls. East-west orientated syn-sedimentary faults, as in the southwest portion of White Pine, were particularly susceptible to inversion during northward-directed basin closure. Previous authors (Kelly and Nishioka, 1985; Mauk et al., 1992, Mauk and Hieshima, 1996) attributed the spatial association of higher copper grades with reverse faults to a second phase of mineralisation related to reverse faulting. However this interpretation has several shortcoming: (i) thrust faults are almost entirely devoid of copper minerals, (ii) the vast majority of copper minerals pre-date quartz cement, calcite cement and calcite veining, all of which pre-date reverse faulting, (iii) thrust faults are demonstrably reactivated syn-sedimentary normal faults – higher porosities in their hanging-walls explain the coincidence between faults and

concentrations of Cu, chlorite and pyrobitumen, (iv) thrust faults offset, and therefore post-date, earlier chlorite, pyrobitumen and Cu mineral zones, (v) vein-hosted Cu minerals observe the same zonation pattern as earlier disseminated Cu minerals suggesting no change in the geochemical or redox architecture between these two styles of mineralisation, and (vi) there is no discernible difference in $\delta^{34}S$ of disseminated and vein-hosted Cu minerals. In total, these are evidence that only one mineralisation event occurred at White Pine.

3.7.3. Diagenetic evolution

Copper Harbor Formation sandstones and conglomerates were deposited in a distal braided fluvial setting with local developed sabkhas including caliche horizons and evaporite textures (Jones et al., 2020), these settings would have certainly been a source of saline to brackish fluids. These denser, oxidised, seawater-derived residual brines would have acted as infiltrating wedges displacing meteoric water introduced by fluvial systems. Such a scenario is supported by the presence of sedimentary gypsum beds with $\delta^{34}S$ values of c. 25.9 ‰ in upper Copper Harbor Formation (E Stüeken 2019, personal communication, 7th November 2018). These early seawater-derived brines resulted in pervasive oxidiation of the Copper Harbor Formation early in the basin history, as evidenced by widespread hematite and illite.

Subsequent to this, liquid petroleum and reduced water were released from deeper portions of the Nonesuch Formation in response to increased burial. These reduced fluids migrated into the upper Copper Harbor Formation at White Pine, emplacing liquid petroleum and reducting hematite to chlorite, and overturning the local redox chemistry. Figs. 3.12A and 3.13B demonstrate that the principal control on the movement of these reduced fluids in the Copper Harbor Formation was syn-sedimentary faults (e.g. the White Pine fault) and lateral facies variations related to those faults.

After petroleum migration, the fluid chemistry in the upper Copper Harbor Formation at White Pine reverted to being oxidised, saline and sulphate-bearing. Analysis of primary fluid inclusions in veins associated with native copper lodes northeast of White Pine also led to the conclusion for the presence of saline brines with salinities varying between 2.8 to 19.8 % (Livnat, 1983). It was these brines that enabled the transport of Cu and Ag via complexation with Cl^- ions (Rose, 1976) to the

White Pine deposit where they were precipitated due to redox reactions. The migration parthways of mineralising fluids are archived in the distribution of copper minerals in the upper Copper Harbor and Nonesuch formations (figs. 3.12B and 3.13C). These reveal that like earlier reduced fluids, mineralising fluids in the upper Copper Harbor Formation utilised syn-sedimentary faults and enhanced primary permeability in the hangingwalls. In contrast, the flow of mineralising fluids into the overlying Nonesuch Formation was largely independent of these syn-sedimentary faults. Instead, the ingress of mineralising fluids into the Nonesuch Formation was controlled by a more cryptic architecture that included the thickness of reduced beds (Parting and Upper Shales), the Porcupine fault (Fig. 3.6) and the effect of the thinned Copper Harbor Formation aquifer over the Porcupine paleo-high.

Maximum temperatures at White Pine are constrained at ~150˚C by illite crystallinity in this study and are in broad agreement with previous estimates of 160˚C from illite/smectite thermometry (Price and McDowell, 1993), 140 to 150˚C from heat flow modelling beneath an estimated 4 km of sediments (Mauk and Hieshima, 1992) and 125 to 155˚C from clumped carbon isotopes (Gallagher et al., 2017). However, Ho and Mauk (1996) inferred maximum temperatures of less than 100˚C based on upper stabilities of pink bornite (75˚C) and djurleite (93˚C). The disparity between temperature estimates based on sulphide mineral stabilities and those derived from other geothermometers may be due to the reversibility of the reactions (Morimoto, 1962) and variation of stability field with stoichiometric composition (Roseboom, 1966).

3.7.4. Mineralisation stage

The mineralisation event at White Pine was triggered when oxidized brines interacted with a redox front that spanned the Copper Harbor and Nonesuch formations. This created native Cu in the most oxidized lower portions of the orebody, chalcocite in the main portion, and a condensed bornite-chalcopyrite-greenockite zone (the fringe zone) in the upper most reduced portion of the orebody. The fringe zone marks the the maximum extent of Cu-Ag mineralisation. Native copper precipitated in open pore spaces, and Cu-(Fe)-sulphides nucleated on detrital and authigenic chlorite as a source of Fe for precursor pyrite grains. The paucity of low-tenor Cu-Fe-sulphides

(bornite and chalcopyrite) and the abundance of low-sulphur copper minerals (native copper and chalcocite) suggest ore fluids were sulphate-poor.

3.7.5. Stable isotopes constraints on mineralising processes

The paucity of pyrite in barren portions of the lower Nonesuch Formation suggests a significant amount of sulphur was introduced into the system as part of the mineralisation process. The upper limit of the range of measured $\delta^{34}S$ values in Cu-(Fe)-sulphides corresponds to that of inferred late-Mesoproterozoic seawater (c. +26 ‰, Strauss, 1993; Johnston et al., 2005), the likely sulphur source. The broad spread of $\delta^{34}S$ values below this reflects thermochemical sulphate reduction (TSR), where at ~100˚C kinetic reactions produce a negative fractionation of up to 20 ‰ from the source reservoir (Machel et al., 1995 and references therein). This is exemplified in permeable sandstone beds where $\delta^{34}S$ values of Cu-(Fe)-sulphide minerals vary from 0.9 to 17.8 ‰. Sulphide minerals in shale-dominated beds display a broader range of $\delta^{34}S$ values, including some which are higher than that of the source reservoir, and several below what would be expected from TSR (i.e. < +5 ‰). We attribute this to a combination of (i) Rayleigh fractionation due to inefficient replenishment of the sulphate-bearing fluid at sulphide growth sites in lower permeability siltstone-dominated beds and (ii) partial or complete replacement of precursor diagenetic pyrite formed by bacterial sulphate reduction (BSR). Mauk (1993) identified a discrete population of pyrite with $\delta^{34}S$ values of c. -25 ‰, which are likely the product of BSR (Ohmoto and Rye, 1979). However, this population is not well represented in $\delta^{34}S$ values of Cu-(Fe)-sulphides minerals, which suggests replacement of precursor BSR-derived pyrite by Cu-(Fe)-sulphides was not the dominant mechanism of ore formation as suggested by earlier workers (Burnie et al., 1972; Mauk, 1993). We therefore favour TSR because of: (i) the concentration of sulphide minerals within porous sand laminae, (ii) the rarity of Cu-minerals pseudomorphing framboidal or euhedral pyrite grains, (iii) the wide spread of (predominantly positive) $\delta^{34}S$ values compatible with a seawater sulphate origin, (iv) the paucity of diagenetic pyrite in equivalent barren strata away from the deposit, and (v) a temperature range at formation in excess of 100˚C that was permissive for TSR but not BSR (Machel, 1995).

Successive generations of calcite at White Pine record a temporal change in $\delta^{18}O$ from 20.7 to 16.0 ‰ (Fig. 3.15). This trend towards isotopically light ^{16}O in calcite

coincides with increasing temperatures that are associated with progressively greater burial depths. The isotopic composition of calcite ($\delta^{18}O_{Calcite}$) precipitating from a fluid reflects an equilibrium reaction that is dependent on two variables: the temperature and the isotopic composition of the fluid ($\delta^{18}O_{Fluid}$) (e.g. Taylor, 1974). The temperature of the system controls the partition coefficient between fluid and mineral. In other words, in order to understand temporal changes in the $\delta^{18}O_{Fluid}$ of formation waters at White Pine it is first necessary to adjust for variations in temperature. As discussed above, constraints on the temperature trajectory at White Pine are poor, and complicate this task. Our best estimate for the temperature of formation of each generation of calcite features is as follows: the 'Junior' at c. 25˚C (surface), early concretions and nodules at c. 60˚C (~1km depth), late concretions and nodules at c. 80˚C (~2km depth), cement at c. 125˚C (~3.5km depth) and veins at c. 140˚C (~4.5km depth). We used partition coefficients for water to calcite from Zheng (1999) which show a strong negative shift from $\delta^{18}O_{Calcite}$ to $\delta^{18}O_{Fluid}$ over the entire range of temperatures expected at White Pine, from -31.2 ‰ at 25˚C to -13.9 at 140˚C. Thus, calculated $\delta^{18}O_{Fluid}$ values for each group of features are: 'Junior' -10.5 ‰, early concretions -4.4 ‰, early diagenetic nodules -3.28 ‰, late concretions -2.68 ‰, late diagenetic nodules 1.11 ‰, cement 3.15 ‰ and veins 2.1 ‰. These values reveal a steady rise in the $\delta^{18}O_{Fluid}$ of formation water at White Pine over time. The earliest calcite features record negative $\delta^{18}O_{Fluid}$ values. Negative $\delta^{18}O$ values typically suggest a meteoric (freshwater) produced by evaporation of seawater; a process which produces a vapour, and ultimately rainfall, that is enriched in light ^{16}O. That the lightest values are greater than -10 ‰ suggests limited degrees of evaporation, low paleo-latitudes, a coastal location or dilution of meteoric water by a larger component of seawater (Sheppard, 1986). The later calcite features record a fluid with slightly positive $\delta^{18}O$ values. Values of around 0 ‰ $\delta^{18}O$ typically indicate a dominantly seawater-derived fluid. However, given that these features formed relatively late in the diagenetic evolution of the basin, after the fluid had spent a protracted period of time in the Copper Harbor Formation aquifer, it is possible that the fluid was eventually buffered by heavy ^{18}O derived from silicate minerals. Calcite $\delta^{18}O$ data therefore suggest that prior to Cu-Ag mineralisation, formation water was seawater-dominated with a minor component of meteoric water. This is sympathetic to the interpretation of the Midcontinent Rift System as an estuarine embayment (Jones et

al., 2020). After mineralisation, formation water evolved by either the continued ingress of seawater, purging the component of meteoric water, or by rock-buffering with the Copper Harbor Formation aquifer.

In summary, the majority of Cu-Ag minerals at White Pine formed during a single continuous diagenetic evolution. Oxidized and saline brines containing copper chloride complexes (i) mixed in fluid-fluid reactions with liquid petroleum precipitating native Cu in sandstones under relatively oxidised conditions, (ii) fluid-rock reactions with in situ organic matter reduced sulphur by thermochemical sulphate reduction and precipitated native Cu and Cu-(Fe)-sulphide minerals under relatively reduced conditions. Late quartz and calcite cements reduced the porosity and permeability of the Copper Harbor Formation which resulted in hydrostatic pressure exceeding lithostatic pressure and the generation of late calcite veins.

3.7.6. Genetic model

The mineralisation process at White Pine is consistent with existing models for the formation of sediment-hosted stratiform copper deposits (e.g. Kirkham, 1989; Hitzman et al., 2005, Brown, 2014). Ore formation occurred during diagenesis at the interface between oxidised Copper Harbor Formation red beds, which acted as an aquifer, and interstitial petroleum in Copper Harbor Formation sandstone or reducing Nonesuch Formation shales. Red beds contain coarse, immature (predominantly intrabasinal) basaltic detritus that provided an abundant source of metals. Evaporites and marine facies assemblages in the upper Copper Harbor and Nonesuch Formations indicate sulphate was provided by seawater-derived brines. The restricted marine embayment paleo-environment (Jones et al., 2020) at low latitudes (e.g. 10 – 20˚, Fairchild et al., 2017 and references therein) is consistent with models of formation within hydrologically restricted marine-influenced basins (Kirkham, 1989; Brown, 1992; Hitzman et al., 2005).

Warm, ascending oxidised Cu-bearing brines migrated through Copper Harbor Formation red beds driven principally by burial compaction. At White Pine these fluids initially encountered interstitial liquid petroleum and precipitated native copper in a relatively oxidised, sulphur-poor environment. Continued ascent of fluids into more reduced Nonesuch Formation shales resulted in the sequential precipitation of a sulphur-poor assemblage of Cu minerals. The redox front migrated higher into the

Nonesuch Formation with time resulting in high-tenor copper minerals overprinting earlier lower tenor Cu, Zn- and Pb iron-sulphide minerals. Continued replenishment of strongly oxidizing brines resulted in copper-oxide and hematite rims forming around chalcocite and native copper grains at the base of the ore zone. Gross sulphide zonation at White Pine resembles that of many other shale-hosted SHC systems such as the Kupferschiefer, Poland (Oszczepalski, 1999) and Nkana, Zambia (Brems et al., 2009). The abundance of native copper and the predominance of the chalcocite zone over sulphur-rich minerals such as bornite and chalcopyrite indicates a sulphur-deficient system and, or, relatively oxidized conditions.

Burial compaction as the main driver of basinal fluids is consistent with fluid flow modelling by Swenson et al., (2004). We discount latent heat from the Porcupine volcanic caldera as a possible fluid driver (Brown, 2014; Brown, 2018) owing to the ~54 M.y. time gap between volcanism and mineralisation, and illite crystallinities suggestive of normal geothermal gradients (i.e. no evidence of elevated temperatures due to igneous activity). Meteoric recharge (Brown, 2006) is incompatible with sulphur isotope data presented in this study, and hydrogen and oxygen isotopes (Park and Ripley, 1999), both of which indicate a seawater-derived sulphate source. In addition, the Nonesuch Formation appears to have acted as an aquitard and prevented mixing of meteoric water with seawater-derived fluids in the Copper Harbor Formation aquifer.

White Pine is located on the flank of the Porcupine volcanic caldera which formed a paleo-topographic high near the basin edge. Exemplars of SHC deposits located on basin margins include Kamoa, Democratic Republic of Congo (Schmandt et al., 2013) and Dzhezkazgan, Kazakhstan (Box et al., 2012). Paleo-topographic highs with SHC deposits on their margins include Kafue anticline, Zambian Copperbelt (Selley et al., 2005), fore-Sudetic block, Kupferschiefer (Blundell et al., 2003) and the Wichita Mountains beneath the Permian copper shales of Oklahoma (Johnson, 1974). At White Pine the combination of an attenuated aquifer and a paleo-topographic high formed an efficient funnel for fluids flowing out of the basin, first with buoyant petroleum and later with oxidized brines containing sulphate and metals. At the deposit-scale fluids intersected syn-sedimentary faults providing pathways through stratigraphy. Coarse-grained and well-sorted sediments in the hanging walls of these faults promoted fluid flow and display similar behaviour to syn-sedimentary faults in other SHC deposits

such as Fishtie (Hendrickson et al., 2015) and Chambishi Southeast (Selley et al., 2005) in the Zambian portion of the Central African Copperbelt.

The 1039 ± 4 Ma Re-Os age of chalcocite is within error of native copper hosted in PLV Group basalt flows on the Keweenaw Peninsula, dated at 1060 to 1047 ± 20 Ma (Rb-Sr on calcite, epidote and microcline, Bornhorst et al., 1988), and post-mineralisation calcite veins at White Pine dated at 1047 ± 35 Ma (Rb-Sr, Ruiz et al., 1984). Ore formation is therefore interpreted to have occurred during the latter stages of mesodiagenesis, probably coeval with deposition of upper Freda Formation, at a depth of approximately 4 kilometres. Note that we did not observe evidence for, nor do our geochemical data indicate, a discrete second stage of mineralisation at White Pine that was associated with thrusting, as suggested by some workers (Mauk et al., 1992).

3.8. Conclusions

White Pine is located on the flank of a palaeo-high (Porcupine Mountain Volcanics) that, along with syn-sedimentary faults which influenced sedimentation such that coarser, better-sorted and more permeable sediments were deposited in hanging walls, focused fluid flow into the Nonesuch Formation. The ore-forming fluids at White Pine were seawater-derived brines that infiltrated fluvial sandstones and conglomerates of the underlying Copper Harbor Formation, which acted as both an aquifer and a source of metals. Metals were liberated during eodiagenesis via breakdown of basaltic volcanic detritus coeval with the growth of illite and hematite.

Ore fluids were approximately 125˚C and contained seawater-derived sulphate with a $\delta^{34}S$ of c. +25.9 ‰. They were reduced via the interaction with liquid petroleum in the Copper Harbor Formation and *in situ* organic matter in the Nonesuch Formation. The paucity of sulphur in Mesoproterozoic seawater and the inefficiency of thermochemical sulphate reduction at these relatively low temperatures produced a vertically zoned suite of sulphur-poor Cu minerals dominated by native copper and chalcocite. Ore formation likely occurred at 1039 ± 4 Ma, approximately 40 M.y. after deposition of the host Nonesuch Formation, at depths of ~4 km and contemporaneously with deposition of the Freda Formation. The timing and temperature of ore formation as well as the paragenetic history and fluid pathways suggest burial compaction was the principal fluid driving mechanism. A minor amount

of copper minerals were deposited in late structures that likely reflect a combination of basin inversion, fluid overpressure and occlusion of primary porosity. The metal association at White Pine – Cu and Ag with no significant concentrations of accessory elements – is similar to other low-temperature SHC systems.

3.9. References

Anjos, S.M.C., De Ros, L.F. and Silva, C.M.A., 1999. Chlorite authigenesis and porosity preservation in the Upper Cretaceous marine sandstones of the Santos Basin, offshore eastern Brazil. Clay mineral cements in sandstones, pp.289-316.

Bahlis, A.B. and De Ros, L.F., 2013. Origin and impact of authigenic chlorite in the Upper Cretaceous sandstone reservoirs of the Santos Basin, eastern Brazil. Petroleum Geoscience, 19(2), pp.185-199.

Baumann, S.D., Dylka, S.K. and Malone, D.H., 2018. Lithostratigraphic subdivisions of the Mesoproterozoic Copper Harbor Formation (Oronto Group) in Michigan and Wisconsin, USA. STRATIGRAPHY, 15(2), pp.135-152.

Bechtel, A. and Püttmann, W., 1991. The origin of the Kupferschiefer-type mineralization in the Richelsdorf Hills, Germany, as deduced from stable isotope and organic geochemical studies. Chemical Geology, 91(1), pp.1-18.

Berger, A., Gier, S. and Krois, P., 2009. Porosity-preserving chlorite cements in shallow-marine volcaniclastic sandstones: Evidence from Cretaceous sandstones of the Sawan gas field, Pakistan. AAPG bulletin, 93(5), pp.595-615.

Blundell, D.J., Karnkowski, P.H., Alderton, D.H.M., Oszczepalski, S. and Kucha, H., 2003. Copper mineralization of the Polish Kupferschiefer: a proposed basement fault-fracture system of fluid flow. Economic Geology, 98(7), pp.1487-1495.

Bornhorst, T.J. and Williams, W.C., 2013. The Mesoproterozoic Copperwood sedimentary rock-hosted stratiform copper deposit, Upper Peninsula, Michigan. Economic Geology, 108(6), pp.1325-1346.

Bornhorst, T.J., Paces, J.B., Grant, N.K., Obradovich, J.D. and Huber, N.K., 1988. Age of native copper mineralization, Keweenaw Peninsula, Michigan. Economic Geology, 83(3), pp.619-625.

Box, S.E., Syusyura, B., Seltmann, R., Creaser, R.A., Dolgopolova, A. and Zientek, M.L., 2012. Dzhezkazgan and associated sandstone copper deposits of the Chu-Sarysu basin, Central Kazakhstan. Society of Economic Geologists, pp.303-328.

Brady, J.M., 1960. Ore and sedimentation of the lower sandstone, at the White Pine mine, Michigan: Unpub (Doctoral dissertation, MS thesis, Michigan Technological University).

Brems, D., Muchez, P., Sikazwe, O. and Mukumba, W., 2009. Metallogenesis of the Nkana copper–cobalt South orebody, Zambia. Journal of African Earth Sciences, 55(3-4), pp.185-196.

Brown, A.C., 1971. Zoning in the White Pine copper deposit, Ontonagon County, Michigan. Economic Geology, 66(4), pp.543-573.

Brown, A.C., 1992. Sediment-hosted stratiform copper deposits. Geoscience Canada, 19(3).

Brown, A.C., 2006. Genesis of native copper lodes in the Keweenaw district, northern Michigan: a hybrid evolved meteoric and metamophogenic model. Economic Geology, 101(7), pp.1437-1444.

Brown, A.C., 2014. Latent thermal effects from Porcupine Volcanics calderas underlying the White Pine-Presque Isle stratiform copper mineralization, northern Michigan. Economic Geology, 109(7), pp.2035-2050.

Brown, A.C., 2018. Latent volcanic heat and further unique aspects of early diagenetic stratiform copper mineralization in the White Pine-Presque Isle District, northern Michigan. Mineralium Deposita, 53(5), pp.721-728.

Burnie, S.W., Schwarcz, H.P. and Crocket, J.H., 1972. A sulfur isotopic study of the White Pine Mine, Michigan. Economic Geology, 67(7), pp.895-914.

Cannon, W.F., 1994. Closing of the Midcontinent rift-A far—field effect of Grenvillian compression. Geology, 22(2), pp.155-158.

Cannon, W.F., Peterman, Z.E. and Sims, P.K., 1993. Crustal-scale thrusting and origin of the Montreal River monocline-A 35-km-thick cross section of the midcontinent rift in northern Michigan and Wisconsin. Tectonics, 12(3), pp.728-744.

Cannon, W.F., Nicholson, S.W., Woodruff, L.G., Hedgman, C.A., and Schulz, K.J., 1995, Geologic map of the Ontonagon and part of the Wakefiled 30’ x 60’ quadrangles, Michigan: U.S. Geological Survey Miscellaneous Investigations Series Map I-2499, scale 1:100,000.

Carpenter, R.H., 1963. Some vein-wall rock relationships in the White Pine mine, Ontonagon County, Michigan. Economic Geology, 58(5), pp.643-666.

Chen, G., Du, G., Zhang, G., Wang, Q., Lv, C. and Chen, J., 2011. Chlorite cement and its effect on the reservoir quality of sandstones from the Panyu low-uplift, Pearl River Mouth Basin. Petroleum Science, 8(2), pp.143-150.

Colbert, S.J., 2011. Fluid inclusion study of the Mesoproterozoic Nonesuch Formation--biogenic sources and thermal history of oil (Doctoral dissertation, Colorado State University. Libraries).

Cullers, R.L. and Berendsen, P., 1998. The provenance and chemical variation of sandstones associated with the Mid-continent Rift System, USA. European Journal of Mineralogy, pp.987-1002.

Cumming, V.M., Poulton, S.W., Rooney, A.D. and Selby, D., 2013. Anoxia in the terrestrial environment during the late Mesoproterozoic. Geology, 41(5), pp.583-586.

Daniels Jr, P.A., 1982. Upper Precambrian sedimentary rocks: Oronto Group, Michigan-Wisconsin. Geology and tectonics of the Lake Superior basin: Geological Society of America Memoir, 156, pp.107-133.

Davis, D.W. and Green, J.C., 1997. Geochronology of the North American Midcontinent rift in western Lake Superior and implications for its geodynamic evolution. Canadian Journal of Earth Sciences, 34(4), pp.476-488.

Dickas, A.B., 1986. Comparative Precambrian stratigraphy and structure along the mid-continent rift. AAPG Bulletin, 70(3), pp.225-238.

Dickas, A.B., Mudrey, M.G., Ojakangas, R.W. and Green, J.C., 1997. Segmented structure of the middle Proterozoic Midcontinent rift system, North America. SPECIAL PAPERS-GEOLOGICAL SOCIETY OF AMERICA, pp.37-46.

Dixon, S.A., Summers, D.M. and Surdam, R.C., 1989. Diagenesis and preservation of porosity in Norphlet Formation (Upper Jurassic), southern Alabama. AAPG Bulletin, 73(6), pp.707-728.

Eldridge, D.L., Guo, W. and Farquhar, J., 2016. Theoretical estimates of equilibrium sulfur isotope effects in aqueous sulfur systems: highlighting the role of isomers in the sulfite and sulfoxylate systems. Geochimica et Cosmochimica Acta, 195, pp.171-200.

Elmore, R.D., 1984. The Copper Harbor Conglomerate: A late Precambrian fining-upward alluvial fan sequence in northern Michigan. Geological Society of America Bulletin, 95(5), pp.610-617.

Elmore, R.D., Milavec, G.J., Imbus, S.W. and Engel, M.H., 1989. The Precambrian Nonesuch Formation of the North American mid-continent rift, sedimentology and organic geochemical aspects of lacustrine deposition. Precambrian Research, 43(3), pp.191-213.

Ensign, C.O., Jr., White, W.S., Wright, J.C., Patrick, J.L., Leone, R.J., Hathaway, D.J., Trammel, J.W., Fritts, J.J., and Wright, T.L., 1968, Copper depositsin the Nonesuch Shale, White Pine, Michigan, in Ridge, J.D., ed., Ore deposits of the United States, 1933–1967 (Graton-Sales Volume): American Institute of Mining, Metallurgy and Petroleum Engineers, p.460–488.

Fairchild, L.M., Swanson-Hysell, N.L., Ramezani, J., Sprain, C.J. and Bowring, S.A., 2017. The end of Midcontinent Rift magmatism and the paleogeography of Laurentia. Lithosphere, 9(1), pp.117-133.

Gallagher, T.M., Sheldon, N.D., Mauk, J.L., Petersen, S.V., Gueneli, N. and Brocks, J.J., 2017. Constraining the thermal history of the North American midcontinent rift system using carbonate clumped isotopes and organic thermal maturity indices. Precambrian Research, 294, pp.53-66.

Hamblin, W.K., 1958, The Cambrian Sandstones of Northern Michigan, 1958, Publication 51: Ann Arbor, University of Michigan/State of Michigan, Department of Conservation, Geological Survey Division, 146 p.

Hamilton, S.K., 1967. Copper mineralization in the upper part of the Copper Harbor Conglomerate at White Pine, Michigan. Economic Geology, 62(7), pp.885-904.

Hayes, T.S. and Einaudi, M.T., 1986. Genesis of the Spar Lake strata-bound copper-silver deposit, Montana; Part I, Controls inherited from sedimentation and preore diagenesis. Economic Geology, 81(8), pp.1899-1931.

Hendrickson, M.D., Hitzman, M.W., Wood, D., Humphrey, J.D. and Wendlandt, R.F., 2015. Geology of the Fishtie deposit, Central Province, Zambia: iron oxide and copper mineralization in Nguba Group metasedimentary rocks. Mineralium Deposita, 50(6), pp.717-737.

Hieshima, G.B. and Pratt, L.M., 1991. Sulfur/carbon ratios and extractable organic matter of the Middle Proterozoic Nonesuch Formation, North American Midcontinent rift. Precambrian research, 54(1), pp.65-79.

Hinze, W.J., Allen, D.J., Braile, L.W. and Mariano, J., 1997. The Midcontinent rift system: A major Proterozoic continental rift. Geological Society of America Special Papers, 312, pp.7-35.

Hitzman, M., Kirkham, R., Broughton, D., Thorson, J. and Selley, D., 2005. The sediment-hosted stratiform copper ore system. Economic geology, 100.

Hitzman, M.W., Broughton, D., Selley, D., Woodhead, J., Wood, D. and Bull, S., 2012. The Central African Copperbelt: diverse stratigraphic, structural, and temporal settings in the world's largest sedimentary copper district. Society of Economic Geologists Special Publication 16, (Paper 19), pp.487-514.

Ho, E.S. and Mauk, J.L., 1996. Relationship between organic matter and copper mineralization in the Proterozoic Nonesuch Formation, northern Michigan. Ore Geology Reviews, 11(1-3), pp.71-87.

Hubbard, H. A., 1975, Geology of Porcupine Mountains in Carp River and White Pine quadrangles, Michigan: U.S. Geological Survey Journal Research, v. 3, p. 519–528.

Huber, N.K., 1973. The Portage Lake Volcanics (Middle Keweenawan) on Isle Royale, Michigan (USGS publication No. 754-C).

Imbus, S.W., Engel, M.H. and Elmore, R.D., 1990. Organic Geochemistry and Sedimentology of Middle Proterozoic Nonesuch Formation--Hydrocarbon Source Rock Assessment of a Lacustrine Rift Deposit: Chapter 12.

Imbus, S.W., Macko, S.A., Elmore, R.D. and Engel, M.H., 1992. Stable isotope (C, S, N) and molecular studies on the Precambrian Nonesuch Shale (Wisconsin-Michigan, USA): Evidence for differential preservation rates, depositional environment and hydrothermal influence. Chemical Geology: Isotope Geoscience Section, 101(3-4), pp.255-281.

Johnson, K.S., 1974. Permian copper shales of southwestern United States. Annales de la Société géologique de Belgique.

Johnson, R. C., Andrews, R. A., Nelson, W. S., Suszek, T., and Sikkila, K., 1995, Geology and mineralization of the White Pine copper deposit: Unpublished report, Copper Range Company, 20 p.

Johnson, R.C., 2014, Technical report on the White Pine copper property, White Pine, Michigan, USA at website for Highland Copper Company Inc., https://docs.wixstatic.com/ugd/62921a_7cfa77e64c7e433bb9e5cb6c3314b5dc.pdf

Johnston, D.T., Wing, B., Farquhar, J., Kaufman, A.J., Strauss, H., Lyons, T.W., Kah, L.C., and Canfield, D.E., 2005, Active microbial sulfur disproportionation in the Mesoproterozoic: Science, v. 310, p. 1477-1479.

Jones, S.M., Prave, A.R., Raub, T.D., Cloutier, J., Stüeken, E.E., Rose, C.V., Linnekogel, S. and Nazarov, K., 2020. A marine origin for the late Mesoproterozoic Copper Harbor and Nonesuch Formations of the Midcontinent Rift of Laurentia. Precambrian Research, 336, p.105510.

Jowett, E.C., 1992. Role of organics and methane in sulfide ore formation, exemplified by Kupferschiefer Cu–Ag deposits, Poland. Chemical Geology, 99(1-3), pp.51-63.

Kelly, W.C. and Nishioka, G.K., 1985. Precambrian oil inclusions in late veins and the role of hydrocarbons in copper mineralization at White Pine, Michigan. Geology, 13(5), pp.334-337.

Kirkham, R.V., 1989. Distribution, settings, and genesis of sediment-hosted stratiform copper deposits. Geological Association of Canada Special Paper, 36, pp.3-38.

Li, G., Mauk, J.L. and Peacor, D.R., 1995. Preservation of clay minerals in the Precambrian (1.1 Ga) Nonesuch Formation in the vicinity of the White Pine copper mine, Michigan. Clays and Clay Minerals, 43(3), pp.361-376.

Livnat, A., Kelly, W.C., Essene, E.J., and Rye, R.O., 1983, P-T-X conditions of sub-greenschist burial metamorphism and copper mineralization, Keweenaw Peninsula, northern Michigan: Geological Society of America, Abstracts, v. 15, p. 629.

Machel, H.G., Krouse, H.R. and Sassen, R., 1995. Products and distinguishing criteria of bacterial and thermochemical sulfate reduction. Applied geochemistry, 10(4), pp.373-389.

Malone, D.H., Stein, C.A., Craddock, J.P., Kley, J., Stein, S. and Malone, J.E., 2016. Maximum depositional age of the Neoproterozoic Jacobsville Sandstone, Michigan:

Implications for the evolution of the Midcontinent Rift. Geosphere, 12(4), pp.1271-1282.

Markey, R., Hannah, J.L., Morgan, J.W. and Stein, H.J., 2003. A double spike for osmium analysis of highly radiogenic samples. Chemical Geology, 200(3-4), pp.395-406.

Mauk, J.L. and Hieshima, G.B., 1992. Organic matter and copper mineralization at White Pine, Michigan, USA. Chemical geology, 99(1-3), pp.189-211.

Mauk, J.L. and Hieshima, G.B., 1992. Organic matter and copper mineralization at White Pine, Michigan, USA. Chemical geology, 99(1-3), pp.189-211.

Mauk, J.L., 1993. Geologic and geochemical investigations of the White Pine sediment-hosted stratiform copper deposit. Ontonagon County, Michigan [Ph. D. dissert.]: Ann Arbor, University of Michigan.

Mauk, J.L., Kelly, W.C., Van Der Pluijm, B.A. and Seasor, R.W., 1992. Relations between deformation and sediment-hosted copper mineralization: Evidence from the White Pine part of the Midcontinent rift system. Geology, 20(5), pp.427-430.

Morimoto, N., 1962. Djurleite, a new copper sulphide mineral. Mineralogical Journal, 3(5-6), pp.338-344.

Nicholson, S.W., Schulz, K.J., Shirey, S.B. and Green, J.C., 1997. Rift-wide correlation of 1.1 Ga Midcontinent rift system basalts: implications for multiple mantle sources during rift development. Canadian Journal of Earth Sciences, 34(4), pp.504-520.

Nishioka, G. K., 1983, Origin of late veins in the White Pine copper deposit, northern Michigan: Master's thesis, University of Michigan, Ann Arbor, Michigan, 35 p.

Ohmoto, H., Rye, R.O. and Barnes, H.L., 1979. Geochemistry of hydrothermal ore deposits.

Ohr, M., 1993, Geochronology of diagenesis and low-grade metamorphism in pelites: Unpublished Ph.D. dissertation, The University of Michigan, Ann Arbor, Michigan,161 p.

Ojakangas, R.W. and Dickas, A.B., 2002. The 1.1-Ga Midcontinent Rift System, central North America: sedimentology of two deep boreholes, Lake Superior region. Sedimentary Geology, 147(1-2), pp.13-36.

Ojakangas, R.W., Morey, G.B. and Green, J.C., 2001. The Mesoproterozoic midcontinent rift system, Lake Superior region, USA. Sedimentary Geology, 141, pp.421-442.

Orvana, 2011, Copperwood Mine Orvana Resources US Corp Mine permit application: Published online by Michigan Department of Environmental Quality at website for Michigan.gov, http://www.michigan.gov/deq/0,4561,7-135-3311_4111_18442-262826--,00.html.

Oszczepalski, S., 1999. Origin of the Kupferschiefer polymetallic mineralization in Poland. Mineralium Deposita, 34(5-6), pp.599-613.

Park, Y.R. and Ripley, E.M., 1999. Hydrothermal flow systems in the Midcontinent Rift: oxygen and hydrogen isotopic studies of the North Shore Volcanic Group and related hypabyssal sills, Minnesota. Geochimica et cosmochimica acta, 63(11-12), pp.1787-1804.

Pratt, L.M., Summons, R.E. and Hieshima, G.B., 1991. Sterane and triterpane biomarkers in the Precambrian Nonesuch formation, North American midcontinent rift. Geochimica et Cosmochimica Acta, 55(3), pp.911-916.

Price, K.L. and McDowell, S.D., 1993. Illite/smectite geothermometry of the Proterozoic Oronto Group, midcontinent rift system. Clays and Clay Minerals, 41(2), pp.134-147.

Rose, A.W., 1976. The effect of cuprous chloride complexes in the origin of red-bed copper and related deposits. Economic Geology, 71(6), pp.1036-1048.

Roseboom, E.H., 1966. An investigation of the system Cu-S and some natural copper sulfides between 25 degrees and 700 degrees C. Economic Geology, 61(4), pp.641-672.

Ruiz, J., Jones, L.M. and Kelly, W.C., 1984. Rubidium-strontium dating of ore deposits hosted by Rb-rich rocks, using calcite and other common Sr-bearing minerals. Geology, 12(5), pp.259-262.

Schmandt, D., Broughton, D., Hitzman, M.W., Plink-Bjorklund, P., Edwards, D. and Humphrey, J., 2013. The Kamoa copper deposit, Democratic Republic of Congo: stratigraphy, diagenetic and hydrothermal alteration, and mineralization. Economic Geology, 108(6), pp.1301-1324.

Selley, D., Broughton, D., Scott, R.J., Hitzman, M., Bull, S.W., Large, R.R., McGoldrick, P.J., Croaker, M. and Pollington, N., 2005. A new look at the geology of the Zambian Copperbelt. Society of Economic Geologists, Inc., 100.

Sheppard, S.M.F, 1986. Characterization and isotope variations in natural waters. In Stable Isotopes in High Temperature Geological Processes J.W. Valley, H.P. Taylor Jr. and J.R. O'Neil (eds.). Rev. Mineral. 16, 165-184.

Soofi, M.A. and King, S.D., 2002. Post-rift deformation of the Midcontinent rift under Grenville tectonism. Tectonophysics, 359(3-4), pp.209-223.

Stein, C.A., Kley, J., Stein, S., Hindle, D. and Keller, G.R., 2015. North America's Midcontinent Rift: when rift met LIP. Geosphere, 11(5), pp.1607-1616.

Stein, C.A., Stein, S., Merino, M., Randy Keller, G., Flesch, L.M. and Jurdy, D.M., 2014. Was the Midcontinent Rift part of a successful seafloor-spreading episode?. Geophysical Research Letters, 41(5), pp.1465-1470.

Strauss, H., 1993. The sulfur isotopic record of Precambrian sulfates: new data and a critical evaluation of the existing record. Precambrian research, 63(3-4), pp.225-246.

Swanson-Hysell, N.L., Ramezani, J., Fairchild, L.M. and Rose, I.R., 2019. Failed rifting and fast drifting: Midcontinent rift development, Laurentia's rapid motion and the driver of Grenvillian orogenesis. Bulletin, 131(5-6), pp.913-940.

Swenson, J.B. and Person, M., 2000. The role of basin-scale transgression and sediment compaction in stratiform copper mineralization: Implications from White Pine, Michigan, USA. Journal of Geochemical Exploration, 69, pp.239-243.

Swenson, J.B., Person, M., Raffensperger, J.P., Cannon, W.F., Woodruff, L.G. and Berndt, M.E., 2004. A hydrogeologic model of stratiform copper mineralization in the Midcontinent rift system, northern Michigan, USA. Geofluids, 4(1), pp.1-22.

Symons, D.T.A., Kawasaki, K. and Diehl, J.F., 2013. Age and genesis of the White Pine stratiform copper mineralization, northern Michigan, USA, from paleomagnetism. Geofluids, 13(2), pp.112-126.

Symons, D.T.A., Kawasaki, K. and Diehl, J.F., 2013. Age and genesis of the White Pine stratiform copper mineralization, northern Michigan, USA, from paleomagnetism. Geofluids, 13(2), pp.112-126.

Taylor, H.P., 1974. The application of oxygen and hydrogen isotope studies to problems of hydrothermal alteration and ore deposition. Economic geology, 69(6), pp.843-883.

Vaughan, D.J., Sweeney, M.A., Friedrich, G., Diedel, R. and Haranczyk, C., 1989. The Kupferschiefer; an overview with an appraisal of the different types of mineralization. Economic Geology, 84(5), pp.1003-1027.

White, W.S. and Wright, J.C., 1954. The White Pine copper deposit, Ontonagon County, Michigan. Economic Geology, 49(7), pp.675-716.

White, W.S. and Wright, J.C., 1966. Sulfide-mineral zoning in the basal Nonesuch Shale, northern Michigan. Economic Geology, 61(7), pp.1171-1190.

White, W.S., 1971. A paleohydrologic model for mineralization of the White Pine copper deposit, northern Michigan. Economic Geology, 66(1), pp.1-13.

Wiese, R.G., 1973. Mineralogy and geochemistry of the parting shale, White Pine, Michigan. Economic Geology, 68(3), pp.317-331.

Woodruff, L.G., Cannon, W.F., Nicholson, S.W., Schulz, K.J. and Wild, R., 2013. Geology of the Keweenawan Supergroup, Porcupine Mountains, Ontonagon and Gogebic counties, Michigan. Institute on Lake Superior Geology, Proceedings, 59(2), pp.69-96.

Zartman, R.E., Nicholson, S.W., Cannon, W.F. and Morey, G., 1997. U–Th–Pb zircon ages of some Keweenawan Supergroup rocks from the south shore of Lake Superior. Canadian Journal of Earth Sciences, 34(4), pp.549-561.

Zheng, Y.F., 1999. Oxygen isotope fractionation in carbonate and sulfate minerals. Geochemical Journal, 33(2), pp.109-126.

Blank page

Chapter 4

Is the Midcontinent Rift actually a Midcontinent Sag?

Blank Page

Note to readers

It is important to highlight, and to clarify, an apparent discordance that exists between Chapter 3 (White Pine deposit) and Chapter 4 (this Chapter) concerning the existence and significance of syn-depositional faults. Chapter 3 describes smaller scale syn-sedimentary faults at White Pine which played an integral role in Cu-Ag mineralisation. These faults have lengths of up to several kilometres and record syn-depositional normal movement in the order of tens of meters. These faults are restricted to the upper Copper Harbor and lowermost Nonesuch formations. Syn-depositional movement on these faults caused subtle changes in sediment grainsize between the hanging- and foot-walls which was later exploited by fluids that included liquid petroleum and metalliferous brines. In contrast, this chapter addresses the nature of a much larger scale fault system which defines the present-day geometry of the Midcontinent Rift System. Here, individual faults are hundreds of kilometres in length with throws of several kilometres. Specifically, this chapter addresses the timing and kinematics of the larger scale fault system, and its significance in the geodynamic evolution of the Midcontinent Rift System. The two faults systems need not be mutually exclusive, and likely reflect spatial and temporal variations in the stress regime of the basin.

4.1. Introduction

The Geon 11-10 transition is a profound interval marked by assembly of the Rodinia supercontinent and one of the most intense episodes of global mafic igneous activity in Earth history (Hanson et al., 2004; Cawood and Pisarevsky, 2017). An archive of those events is preserved in the Midcontinent Rift System (MRS; Fig. 4.1), a >3000 km-long arcuate and segmented array of magnetic and gravity anomalies inferred to be a consequence of thick flood basalt flanked and overlain by a sedimentary cover sequence (King and Zietz, 1971; Van Schmus et al., 1985). The MRS formed in the concurrent Grenville hinterland and its voluminous volcanism is attributed to mantle plume activity, perhaps beneath a supercontinent-centroidal superplume (Hutchinson et al., 1990; Nicholson et al., 1997), although buoyant asthenosphere and melting beneath a thermally-isolated centroid of a supercontinent need not require mantle plumes (Anderson, 1994).

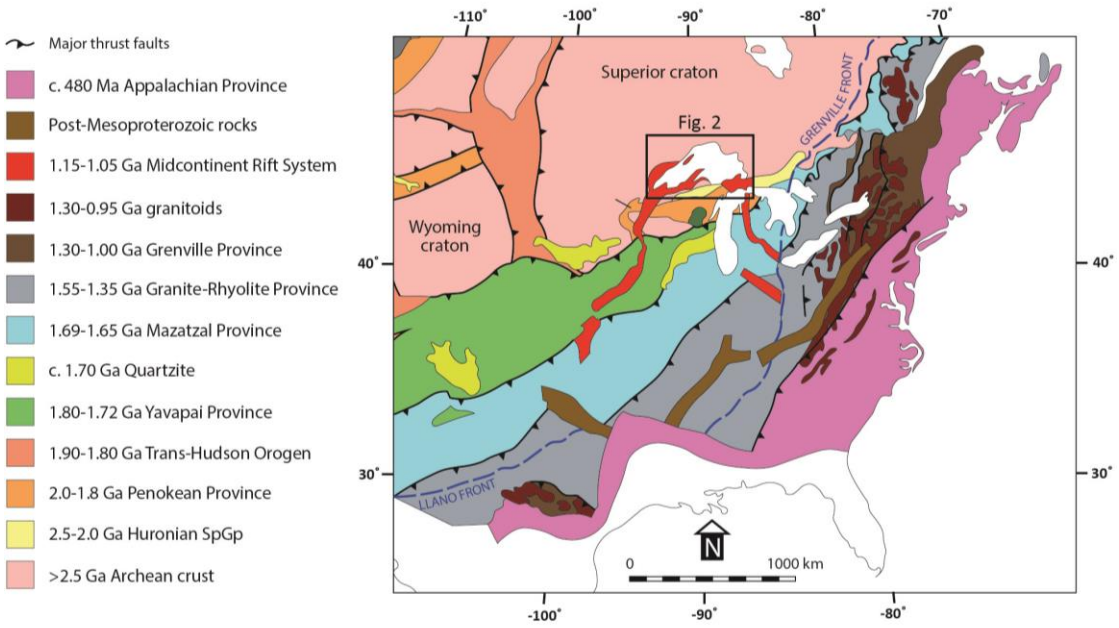

Fig. 4.1. Geological terrane map of eastern North America (modified after Whitmeyer and Karlstrom, 2007).

A commonly-invoked analogy is the East African Rift system (e.g. Ojakangas et al., 2001; Stein et al., 2014), however the EARS hosts a maximum of c. 3 km rift volcanics (King and Chapman, 1972; Prave et al., 2016) in ~50 km-wide rift grabens and half-grabens (Chorowicz, 2005) controlled by faults of maximum length c. 50-100 km

(Foster and Nimmo, 1996). Up to c. 100 km away from the central grabens, smaller and shorter half-grabens fill with thinner volcanics, and rift flanks continue another c. 100 km across-axis regionally, with further-diminished volcanic input. The EARS is anorogenic and substantial areas are entirely amagmatic (Chorowicz, 2005). Mantle tomography indicates small-scale subduction beneath the EARS, consistent with influence by crustal thickness discontinuities (King and Ritsema, 2000). Thus the inferred segmented and arcuate character of the MRS may be a purely topological analogue to Earth's best-understood, active rift system; with little robust, geodynamic or architectural similarity.

The cover sequence of the MRS hosts a giant stratiform copper province (Bornhorst and Barron, 2011), chronicles the palaeoecology and environmental chemistry at a critical time in the evolution of the eukaryotic biosphere (Fedorchuk et al., 2016; Strother and Wellman, 2016) and the volcanic rocks yield an exceptional paleomagnetic record that attests to fast, prolonged true polar wander and establishment of the geocentric axial dipole topology of Earth's magnetic field by at least late in the Mesoproterozoic Era (Swanson-Hysell et al., 2019).

The broad temporal coincidence between the age of the MRS and the Grenville orogeny naturally leads to considerations of a genetic link between the two. Here we report new information from the Michigan-Wisconsin portion of the northern MRS (Fig. 4.2) that includes U-Pb geochronology, data from outcrop sections, drill cores and borehole well logs and re-examination of reflection seismic profiles to improve understanding of the MRS's stratigraphic architecture and assess tectonic models invoked for its genesis. We also did 2-D backstripping to query concepts of accommodation space generation. The most circumspect interpretation of our collective findings is that the MRS, at least in the Lake Superior region, exhibits features more attributable to a sag-style, rather than rift-style, of basin formation.

4.2. Background

The MRS formed between 1109 and 1087 Ma, immediately prior to the Ottawan phase of the Grenville Orogeny (Rivers, 2015). It transects the Palaeoproterozoic Penokean, Yavapai and Mazatal terranes (accreted previously onto the composite Archaean Superior and Wyoming cratons; Holm et al., 2007) and cuts across crustal-scale shear zones including the Spirit Lake, Great Lakes and Niagara fault

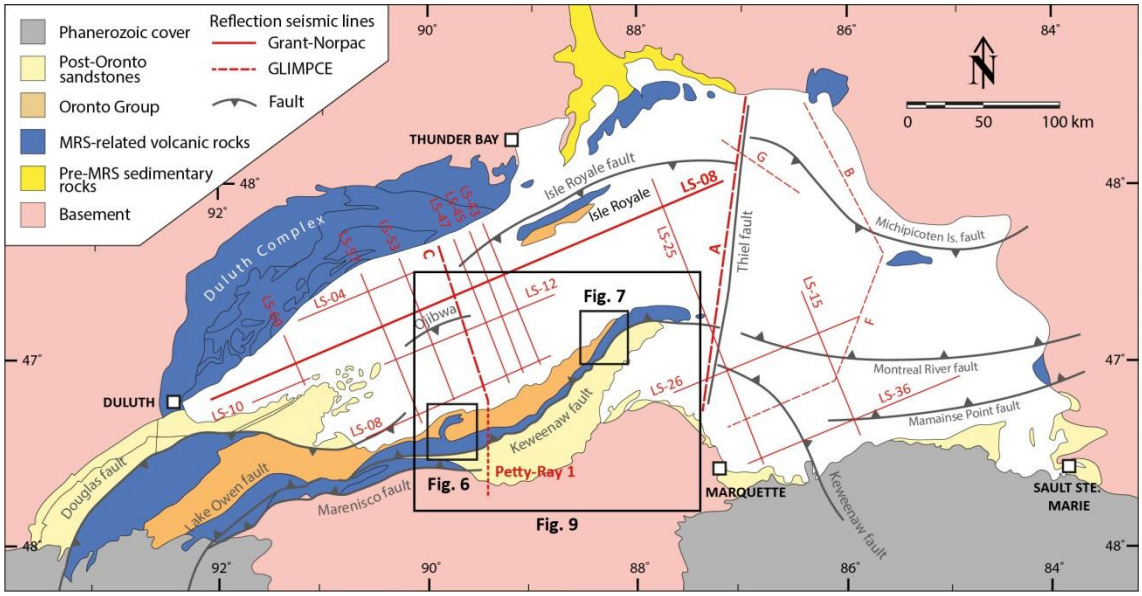

Fig. 4.2. Simplified geological map of the Lake Superior portion of the Midcontinent Rift System with reflection seismic lines (Cannon et al., 1999).

zones (Van Schmus et al., 1993). The MRS has two branches or arms (Fig. 4.1); each consists of numerous narrow segments, 100-200 km wide and several hundreds of km in length. The western one trends from northern Kansas to Lake Superior where it bends to an approximately east-west trend that coincides with significant broadening of the basin. The eastern branch extends southeast from Lake Superior, becoming narrower and losing character beneath the Michigan basin; recently the East Continent Gravity High, Fort Wayne Rift and an unnamed geophysical anomaly in Oklahoma and adjacent Texas were placed as components of the MRS (Stein et al., 2017).

The rock record of the MRS is known from sparse borehole data but mostly from outcrops along its northern portion; these define the Keweenawan Supergroup, a volcanic-sedimentary succession 10-30 km thick (Fig. 4.3). Early ideas about the basinal setting of that succession ranged from aulacogens to impactogens (e.g. Halls and Pesonen, 1982; Anderson and Burke, 1983; Gordon and Hempton, 1986; Hauser 1996), highlighting potential analogues such as the Eocene-Recent Baikal rift and Palaeocene upper Rhine graben. The most recent ideas about the origin of the MRS are championed by Stein et al., (2014, 2017) who suggest that the MRS is a consequence of motion of a microplate on the margin of Laurentia formed during separation of Amazonia from Laurentia; the analogue offered is the East Africa Rift System.

A mantle plume or hotspot is invoked in almost all models of the MRS to explain its enormous volume of volcanic rocks: c. 2 x 10^6 km^3 of basalt reaching thicknesses of 20 km and extruded over ~20 Myr (Hutchinson et al., 1990; Nicholson and Shirey, 1990; Cannon and Hinze, 1992; Klewin and Shirey, 1992; Nicholson et al., 1997; Davis and Green, 1997; Vervoort et al., 2007). However, the MRS differs from other plume-related flood basalt provinces in that those cover vast areas, rather than confined to narrow belts, and are an order-of-magnitude thinner (e.g. Deccan Traps 1.8 km thick, Patro and Sarma, 2007; Siberian Traps 3.7 km thick, Renne and Basu, 1991; Columbia River, >4.0 km thick, Reidel and Camp, 2013). The arcuate to sigmoidal shapes of the MRS also poses questions about stress field orientations and the origin of such an unusual geometry deep within a seemingly relatively stable craton. Such differences beg explanation.

4.3. Keweenawan Supergroup

The oldest unit of the Keweenawan Supergroup (Fig. 4.3) in the study area is the c. 100 m thick Bessemer Quartzite (Ojakangas and Morey, 1982). This unit and its lateral equivalents rest unconformably on underlying Archaean-Palaeoproterozoic rocks and, although not dated directly, is likely older than 1109 Ma (Ojakangas et al., 2001). Above these quartzites are the initial deposits of the MRS, the c. 5.8 km thick Powder Mill Group comprised of high-Al basalts, local pillow lava and lesser andesite. The Sheep Farm rhyolite at the top of the Group is 1098.24 ± 0.45 Ma in age (Swanson-Hysell et al., 2019) and the lower and middle parts of the Group are correlative to the Osler Group, lower North Shore Volcanic Group and Mamainse Point Formation that are known to be c. 1109 Ma in age (Nicholson et al., 1997; Davis and Green, 1997). The most extensively developed volcanic unit is the overlying Portage Lake Volcanic Group exposed along the length of the Keweenaw Peninsula and adjacent northern Wisconsin. It consists of subaerial tholeiitic basalt with local interbeds of conglomerate and totals 7.4 km in thickness (Ojakangas et al., 2001). Two flows are dated at 1093.37 ± 0.53 and 1091.59 ± 0.27 Ma (Swanson-Hysell et al., 2019) and the laterally equivalent Porcupine Mountain Volcanic structure has one age of 1093.6 ± 1.8 Ma (Zartman et al., 1997; but see New Geochronology section below). Correlative units include the Chengwatana Volcanic Group in Minnesota and Michipicoten Island Formation of eastern Lake Superior (Ojakangas et al., 2001).

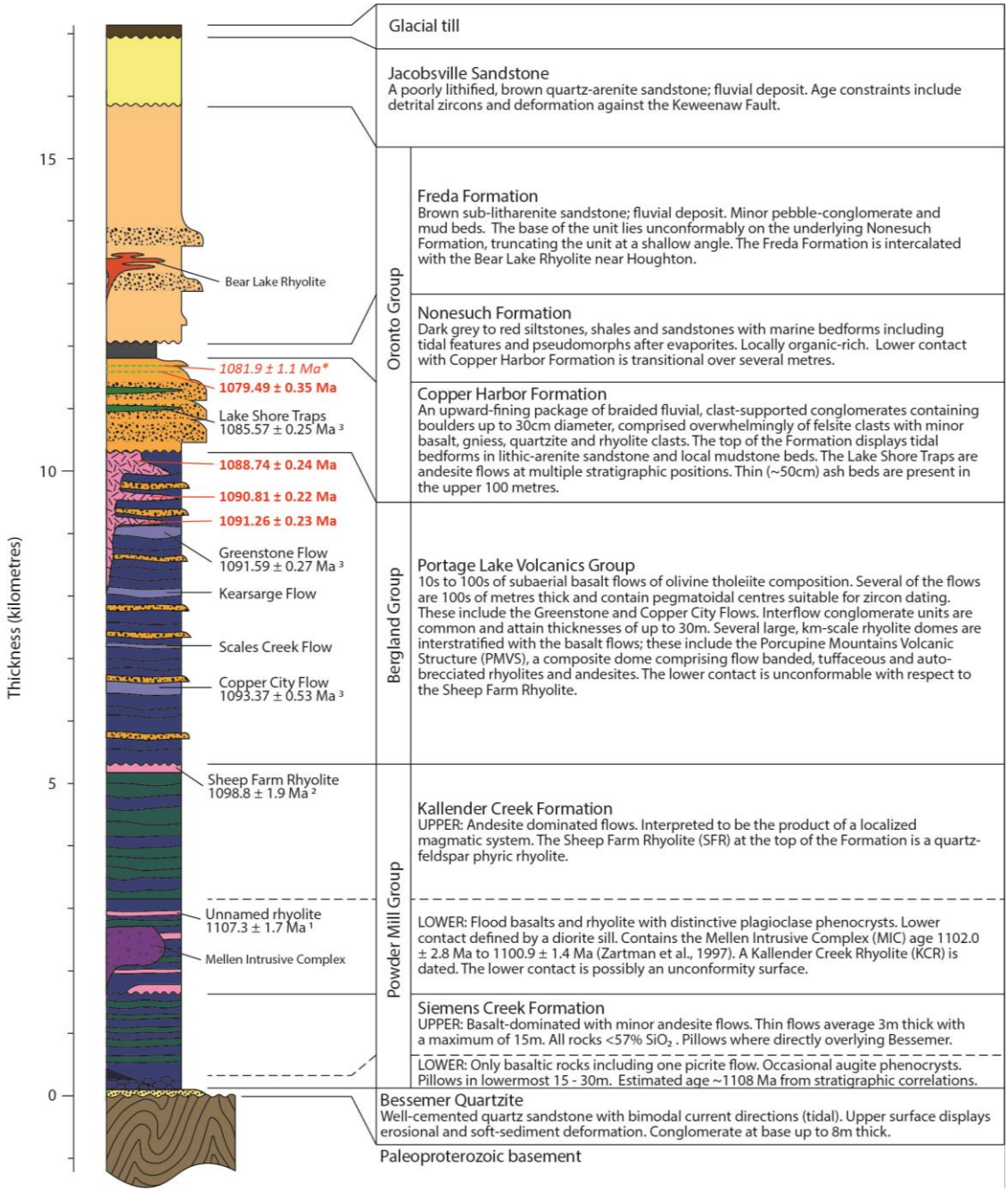

Fig. 4.3. Stratigraphic column of the Keweenaw Supergroup in the southwest Lake Superior area (modified after Nicholson et al., 1997; Ojakangas et al., 2001; Swanson-Hysell et al., 2019). Specific dates: 1. Davis and Green (1997); 2. Swanson-Hysell et al. (2019); 3. Fairchild et al. (2017); *inherited age (see main text).

The Oronto Group includes the Copper Harbor, Nonesuch and Freda formations (Fig 4.3). The Copper Harbor Formation is a 100 to 1800 m thick sequence of braided-fluvial pebble and boulder conglomerate, sandstone, minor mudstone (Daniels, 1982) and, in the middle part of the Formation, the Lake Shore Trap andesites dated at 1085.57 ± 0.25 Ma (Fairchild et al., 2017). The overlying Nonesuch Formation is 40 to 200 m thick and comprises variably organic-rich shale, siltstone and fine

sandstone and houses a world-class Cu deposit (Elmore et al., 1989); pyrite from the lower part of the Formation yielded a Re-Os isochron age of 1078 ± 24 Ma (Cumming et al., 2013). The Freda Formation is at least 3600 m thick and consists of fluvial sandstone with minor conglomerate and siltstone. The age of the Freda Formation is poorly constrained but paleomagnetic poles suggest a minimum age of1070 Ma for the lower part of the formation (Henry et al., 1977). The Solor Church Formation is the lateral equivalent of the Oronto Group in Minnesota.

The Jacobsville Sandstone unconformably overlies the Oronto Group rocks. Significantly different detrital zircon populations and sediment maturity between it and the underlying Oronto Group rocks imply that the intervening hiatus is considerable (Cannon et al., 1989; Ojakangas and Dickas, 2002; Malone et al., 2016). However, the age of the Jacobsville is contentious because maximum age constraints of 959 ± 19 Ma for detrital zircon (Malone et al., 2016) are younger than ages obtained for movement of the Keweenaw fault (see below) that cuts the Jacobsville. Lateral equivalents of the Jacobsville Sandstone include the texturally and compositionally similar Bayfield Group, Hinkley Sandstone and Fond du Lac Formation (Ojakangas et al., 2001).

Basin inversion affected the entire Keweenawan Supergroup and Jacobsville Sandstone as evident by deformation of those units along the Keweenaw fault (Bornhorst, 1992). The timing of inversion is constrained at 1060 ± 20 Ma by Rb-Sr closure ages of biotite from the Pelton Creek and Marenisco Faults, which are part of the Keweenaw fault system at the Michigan-Wisconsin border (Cannon et al., 1993), although Malone et al. (2016) interprets this age to record flexural uplift of rift shoulders. Regardless of the exact explanation of the biotite ages, their discrepancy with the younger detrital zircon ages derived from the Jacobsville Sandstone remains an unsolved temporal conundrum.

4.4. New geochronology

U-Pb dating of zircons from five samples was carried out at the National Environmental Isotope Facility, British Geological Survey, via chemical abrasion isotope dilution thermal ionisation mass spectrometry (CA-ID-TIMS). Resulting age plots are shown on Figure 4.4 and listed in Table 4.1.

Ages are calculated based on the weighted mean $^{206}Pb/^{238}U$ date of the youngest population that overlap within 2σ analytical uncertainty. In three samples, a single date is distinctly younger than the main population and this is interpreted to reflect residual Pb-loss. U-Pb dates have been determined relative to the gravimetrically calibrated EARTHTIME mixed U/Pb tracers (Condon et al., 2015; McLean et al., 2015) and ^{238}U and ^{235}U decay constants (Jaffey et al., 1971; Mattinson, 2010). Age uncertainties are reported at 95% confidence level in the ±X/Y/Z Ma format, where X is the analytical uncertainty in the absence of all external errors, Y includes X and the tracer calibration uncertainty, and Z includes Y and the ^{238}U decay constant uncertainty of Jaffey et al. (1971). In principle, when comparing and integrating with other U-Pb geochronology that utilise the same tracers (e.g. Fairchild et al., 2017; Swanson-Hysell et al., 2019) the X uncertainty can be used.

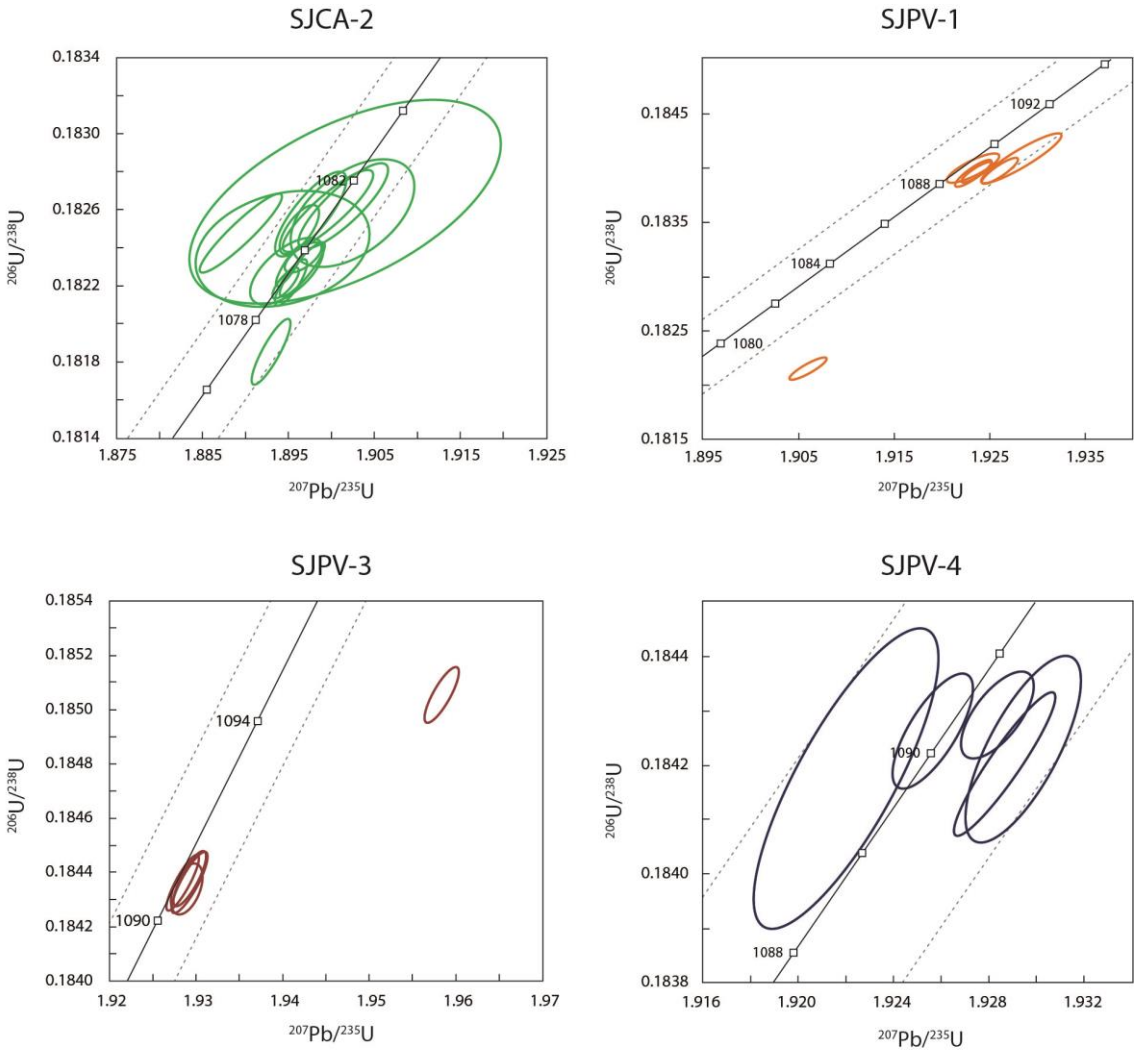

Fig. 4.4. U-Pb concordia plots. Data-point error ellipses are 2σ. Dashed lines are 95% confidence.

Sample ID	$^{206}Pb/^{238}U$ date	± X (abs, 2σ)	± Y (abs, 2σ)	± Z (abs, 2σ)	*n*	MSWD
SJCA-1	**1081.9**	**1.1**	1.28	1.68	3/6	0.013
SJCA-2	**1079.49**	**0.35**	0.74	1.32	6/15	2.1
SJPV-1	**1088.74**	**0.24**	0.70	1.30	5/6	0.51
SJPV-3	**1090.81**	**0.22**	0.70	1.30	4/5	0.14
SJPV-4	**1091.26**	**0.23**	0.70	1.30	5/5	0.72

Table 4.1. Summary of the U-Pb ages and their uncertainties for the five samples dated.

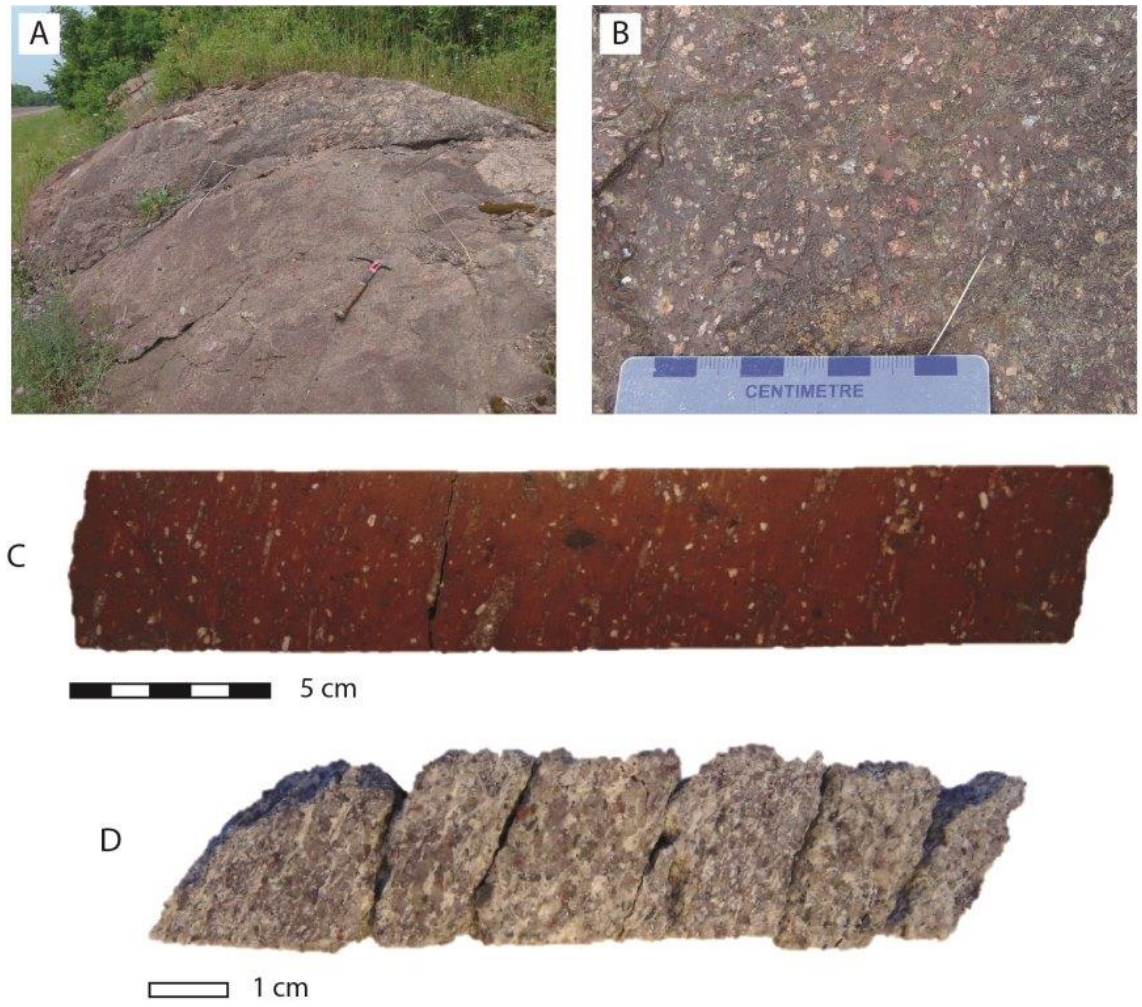

Fig. 4.5. Geochronology samples (for locations see Figs. 4.6 and 4.7). **A.** Porcupine rhyolite location SJPV-3, road cut on M-64 five km north of Bergland. **B.** Porcupine rhyolite texture SJPV-4, road cut on M-64 four km north of Bergland. **C.** Porcupine rhyolite sample SJPV-1 from drill hole WPB-1, 339.86 m depth. **D.** Copper Harbor Formation ash bed samples SJCA-2 from drill hole JBY-002, 185.88 m depth.

4.4.1. Porcupine Mountain Volcanics

The Porcupine Mountain volcanic structure (also referred to as Oak Bluff Formation) consists of rhyolite flows, breccias and sills intercalated with basalt of the middle and upper Portage Lake Volcanic Group. Three samples of felsic rocks were dated. SJPV-4 and SJPV-3 (Figs. 4.5A,B and 4.6) were collected from the base and top, respectively, of a plagioclase-porphyritic rhyolite sill near the base of the Porcupine Mountain structure correlative with the middle Portage Lake volcanic rocks. Zircon from SJPV-4 and SJPV-3 yielded weighted means $^{206}Pb/^{238}U$ dates of 1091.26 ± 0.23 Ma and 1090.81 ± 0.22 Ma, respectively. SJPV-1 is a pink-grey rhyolite with plagioclase phenocrysts and welded fiamme (Fig. 4.5C and 4.6) that was intersected in drill hole WPB-1 at a depth of 339.86 m, 50.3m below the base of the Copper Harbor Formation. Zircon yield a weighted mean $^{206}Pb/^{238}U$ date of 1088.74 ± 0.24 Ma, which provides a maximum age for deposition of the upper Copper Harbor Formation. Note that the 1093.6 Ma date from Zartman et al. (1997) for the Porcupine Mountain structure is a weighted mean $^{207}Pb/^{206}Pb$ date (using $^{238}U/^{235}U$ = 137.88) and is expected to be systematically older than closed system $^{206}Pb/^{238}U$ dates due to bias in $\lambda^{235}U$ and $^{238}U/^{235}U$ (Schoene et al., 2006; Hiess et al., 2012).

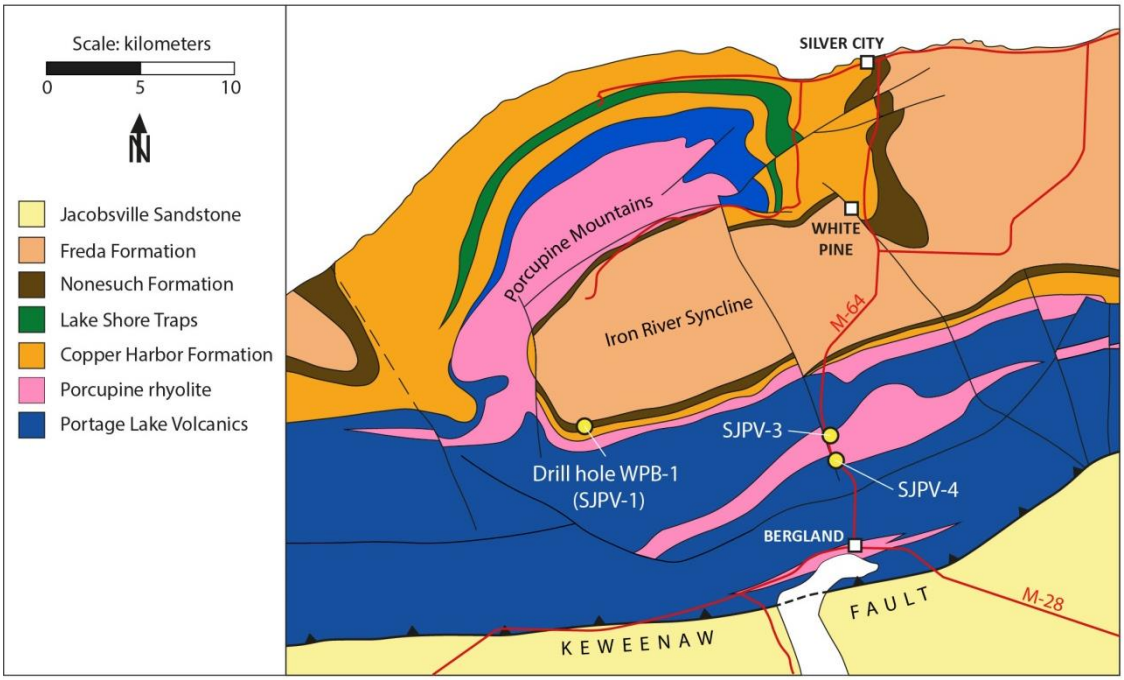

Fig. 4.6. Geological map of the Porcupine Mountains district with geochronology sample locations (Cannon et al., 1995).

4.4.2. Copper Harbor Formation

Two volcanic ash beds were identified in the upper Copper Harbor Formation recovered in drill core JBY-002 (see Fig. 4.7 for location). Each are 15-20 cm thick, light-grey and have quenched groundmass containing mm-scale subhedral quartz, euhedral biotite phenocrysts and minor feldspar phenocrysts (Fig. 4.5D). The bottom of the drill hole intersects the Seven Mile Point flow (depth of 228.90 m) of the uppermost Lake Shore Traps (Baumann et al., 2018) confirming that the ash beds are at or above the stratigraphic level of the Traps. Sample SJCA2 is 59.5 m below the base of the Nonesuch Formation (drill hole depth 185.88 m) and zircon yielded a range of $^{206}Pb/^{238}U$ dates, from 1077.2 to 1081.5 Ma, which we interpret as a mixture of zircons dating eruption and pre-eruptive materials. Excluding the youngest non-reproducible date yields a weighted mean $^{206}Pb/^{238}U$ date of 1079.49 ± 0.35 Ma. SJCA-1 is 11.6 m below the base of the Nonesuch Formation (drill hole depth 138.07 m) and zircon yielded a range of $^{206}Pb/^{238}U$ dates from 1081.3 to 1105 Ma. These are all older than the underlying age from SJCA-2 hence we interpret them as reflecting pre-eruptive materials.

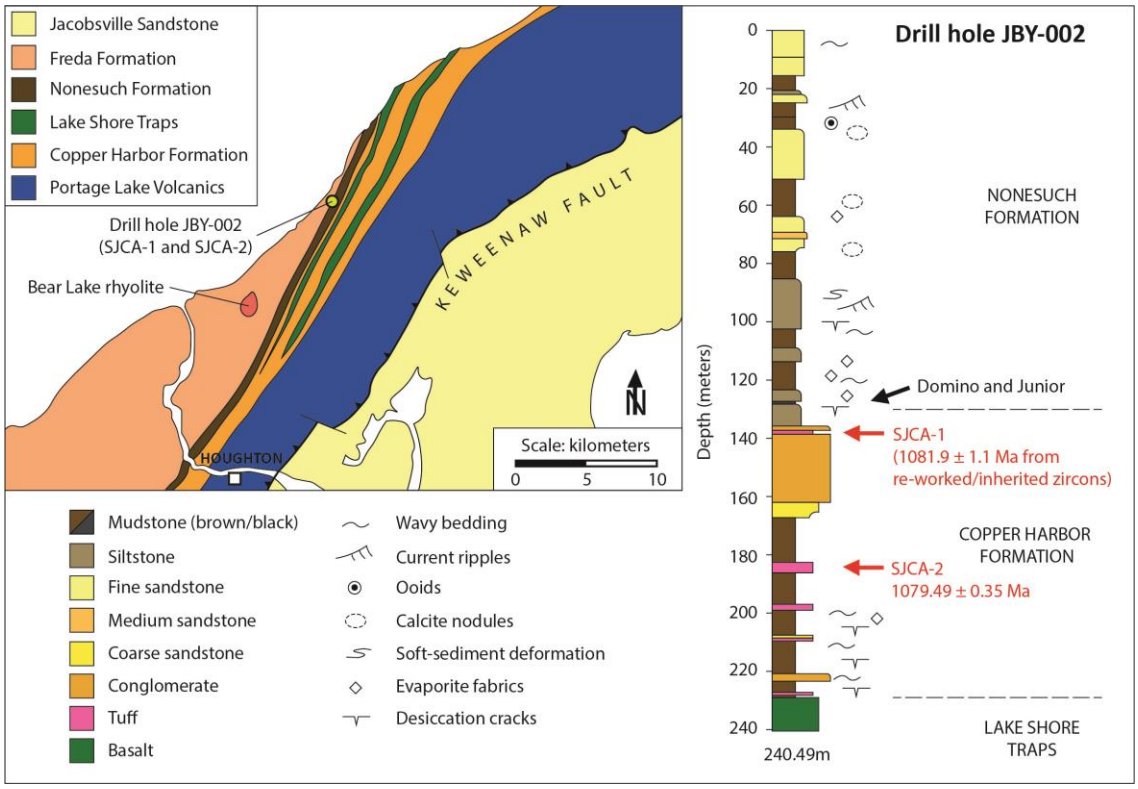

Fig. 4.7. Geological map (Cannon et al., 1999) and stratigraphic log of drill hole JBY-002 with geochronology sample locations.

4.5. Backstripping analysis

We undertook a standard 2-D backstripping analysis (Allen and Allen, 1990) to obtain a 1st-order approximation of the amount of 'accommodation' space (subsidence) that could be attributed to loading by flood basalt and its overlying sedimentary cover sequence. The calculations were completed using *Backstrip* software (http://www.ux.uis.no/~nestor/work/programs.html), assuming standard parameters for continental crust and bespoke input parameters for each lithology that included surface porosity (Φ_o), porosity depth coefficients (C) and grain density (ρ) (see Table 4.2 for parameters and table caption for references). Also, because nearly the entire Keweenawan succession is non-marine (excepting the thin, estuarine Nonesuch Formation; Jones et al., 2020), from the subaerial basalt flows of the Powder Mill and Portage Lake volcanics though the fluvial sediments of the Copper Harbor, Freda and Jacobsville formations, loading generated by water is not considered a major factor in the analysis. Unconformities were treated as a times of zero net subsidence. The burial history and subsidence curves are shown in Figures 4.8A and 4.8B.

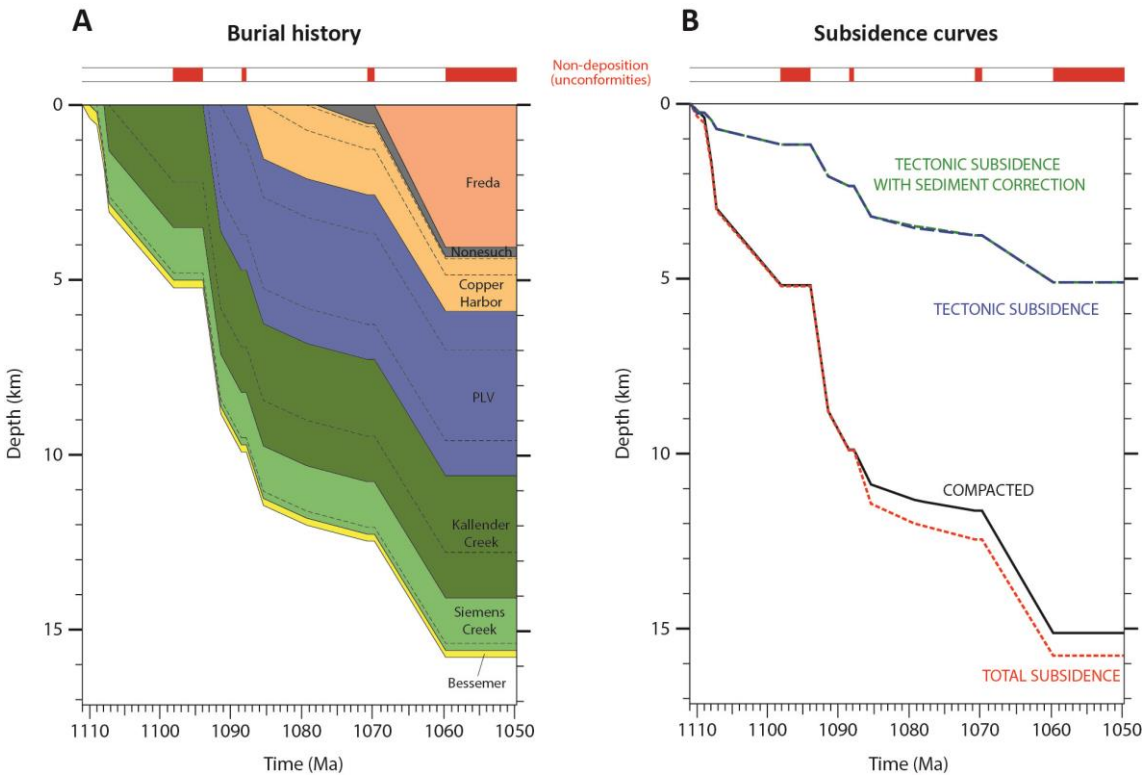

Fig. 4.8. A. Burial history of the Keweenawan Supergroup. **B.** Subsidence curves for the Midcontinent Rift System. See Table 4.2. for parameters.

Lithological unit	Thickness	Base			Top			ρ	*C*	Φ_o
		Base	Age	Water depth	Top	Age	Water depth			
	km	km	Ma	km	km	Ma	km	kg m^{-3}	km^{-1}	%
Bessemer Quartzite	0.20	17.15	1111.00	0.05	16.95	1110.00	0.05	2600	0.27	49%
Siemens Creek (lower)	0.20	16.95	1110.00	0.05	16.75	1109.00	0.00	2800	0.01	0%
Siemens Creek (upper)	1.30	16.75	1109.00	0.00	15.45	1108.00	0.00	2800	0.01	0%
Kallander Creek (lower)	1.30	15.45	1108.00	0.00	14.15	1107.30	0.00	2800	0.01	0%
Kallender Creek (upper)	2.20	14.15	1107.30	0.00	11.95	1098.24	0.00	2800	0.01	0%
Unconformity	0.00	11.95	1098.24	0.00	11.95	1094.10	0.00	0	0.00	0%
PLV (lower)	1.00	11.95	1094.10	0.00	10.95	1093.37	0.00	2800	0.01	5%
PLV (middle)	2.60	10.95	1093.37	0.00	8.35	1091.59	0.00	2800	0.01	5%
PLV (upper)	1.10	8.35	1091.59	0.00	7.25	1088.74	0.00	2800	0.01	5%
Unconformity	0.00	7.25	1088.74	0.00	7.25	1088.00	0.00	0	0.00	0%
Copper Harbor (lower)	1.00	7.25	1088.00	0.00	6.25	1085.57	0.00	2650	0.27	49%
Copper Harbor (middle)	0.44	6.25	1085.57	0.00	5.81	1079.49	0.05	2650	0.27	49%
Copper Harbor (upper)	0.06	5.81	1079.49	0.05	5.75	1078.10	0.05	2650	0.27	49%
Nonesuch	0.25	5.75	1078.10	0.05	5.50	1071.00	0.05	2650	0.27	63%
Unconformity	0.00	5.50	1071.00	0.05	5.50	1070.00	0.00	0	0.00	0%
Freda	3.50	5.50	1070.00	0.00	2.00	1060.00	0.00	2600	0.27	49%
Unconformity	0.00	2.00	1060.00	0.00	2.00	1050.00	0.00	0	0.00	0%
Jacobsville	2.00	2.00	1050.00	0.00	0.00	1040.00	0.00	2600	0.27	49%
	17.15									

Table 4.2. Parameters used in subsidence analysis and backstripping. Base, tops and thickness of units from seismic interpretation (this study), Nicholson et al. (1997) and Ojakangas et al. (2001). Ages of units: see stratigraphic column (Fig. 4.3). Water depths: from Ojakangas and Morey (1982) and Jones et al. (2020). ρ = substrate density (not bulk density), data from Sclater and Christie (1980) and Van Wijk et al. (2018). C = porosity depth coefficient, data from Sclater and Christie (1980), Van Wijk et al. (2018) and Witkosky and Wernicke (2018). Φ_o = initial porosity, data for sediments from Witkosky and Wernicke (2018), data for basalt from Van Wijk et al. (2018), interflow sediments accounted for using a weighted average.

Our model incorporates the thickness of the Keweenawan Supergroup as constrained by boreholes and onshore mapping: c. 17 km in total (Fig. 4.3). Using that and established age constraints, including our new dates, initial subsidence for the Bessemer Quartzite-Kallender Creek succession averaged c. 400 m/Myr (c. 5 km over c. 13 Myr). Subsidence slowed markedly during deposition of the upper Kallender Creek Formation before development of an unconformity surface representing a c. 4 Myr hiatus. Rapid subsidence marks the Portage Lake Volcanic Group, c. 900 m/Myr (c. 5 km over c. 5.2 Myr). Although age constraints on the overlying parts of the Oronto Group and Jacobsville Sandstone are poor, it is clear that these sedimentary units accumulated at a rate c. 3-6x less than that of the volcanic units: c. 150 m/Myr (c. 7 km over c. 48 Myr).

The results of the backstripping confirm that the rate of generation of accommodation space (subsidence) decreased sharply at c. 1088 Ma, coincident with the cessation of flood basalt effusion; only c. 2 km of the total c. 10 km of subsidence can be attributable to tectonic stretching prior to that time. Post 1088 Ma, during deposition of the mostly sedimentary succession, only c. 3 km of the total c. 7km of subsidence was due to tectonic subsidence. Consequently, subsidence that generated accommodation for the volcanic-sedimentary succession of the Keweenawan Supergroup can be attributed to mostly flood basalt and sedimentary loading.

4.6. Keweenawan stratigraphic cross-section

A stratigraphic cross-section from the upper Portage Lake Volcanics Group through to the lower Freda Formation was constructed using 13 stratigraphic logs compiled from boreholes and mapping along a 250 km-long transect from northern Wisconsin to the tip of the Keweenaw Peninsula in Michigan (see figure 4.9 for location and figure 4.10 for cross section). The base of the Nonesuch Formation was used as a datum for drawing the section.

The thickness of the Copper Harbor Formation along the transect varies from c. 100 m to as much as 1400 m. Everywhere the contact between the Portage Lake Volcanics and Copper Harbor Formation can be observed there is evidence for deep weathering in the immediately underlying basalt (Fig. 4.11), essentially a weathering crust that varies from many cm to several metres in thickness. Above this, in many places the lowermost beds of the Copper Harbor Formation form a 5-80 m thick unit of

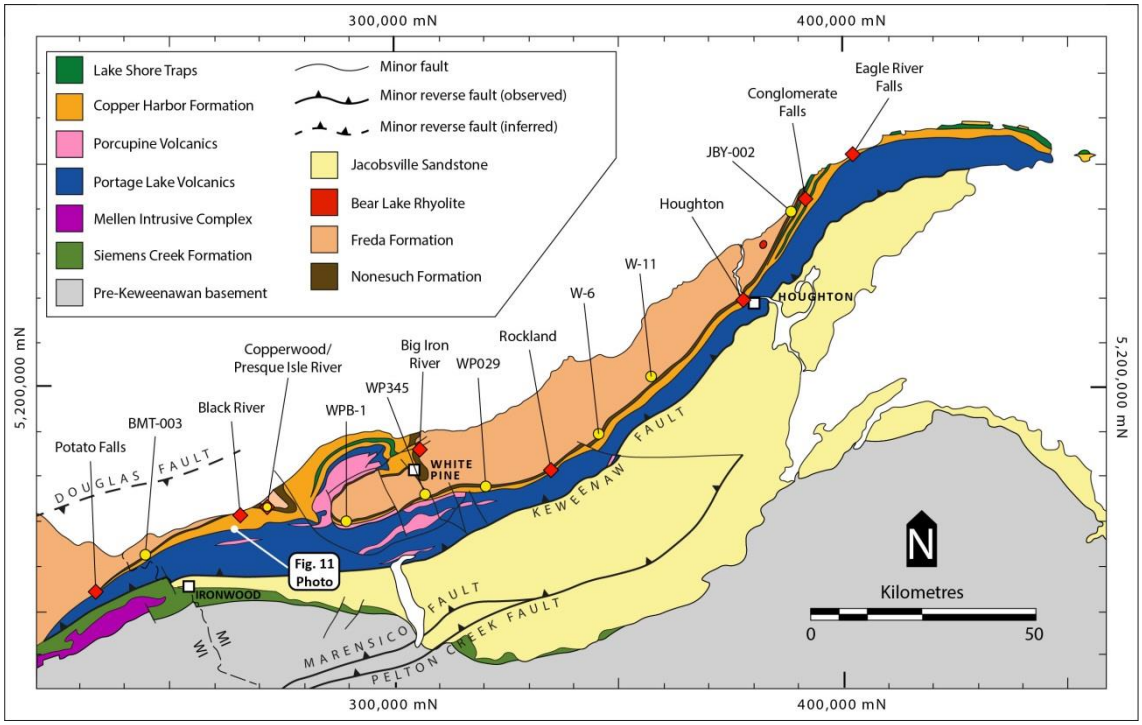

Fig. 4.9. Geological map of the Keweenaw Peninsula (Cannon et al., 1999) with location of drill holes (circles) and field transects (diamonds) used in cross section Figure 4.10.

planar to trough cross-bedded fine-grained quartzitic sandstone containing isolated cm-scale pebbles derived from the underlying basalt. This unit is overlain sharply by pebble to boulder conglomerate from 200-800 m thick in turn overlain by 100-500 m of interbedded conglomerate and coarse cross-bedded sandstone arranged in fining-upward cycles many metres thick. The top unit of the Formation is 50-500 m thick and consists dominantly of sandstone with lesser conglomerate and minor brown mudstone. This unit is thin to absent in western sections and over the Porcupine Mountain Volcanic but elsewhere contains caliche and calcrete features and, in western-most sections, evaporite fabrics and tide-influenced shallow-marine sedimentary features (e.g. Jones et al., 2020).

The transition from Copper Harbor Formation to Nonesuch Formation varies from having a gradational character over several to many metres to being sharp, with black shale sitting directly on conglomerate. Nevertheless, on the scale of the cross-section this contact defines a good datum in that the “Junior” (the term applied by mining company geologists to a several-cm-thick calcite bed in the basal Cu-bearing interval of the Nonesuch Formation) can be identified in every section along the 250-km long transect. The Nonesuch Formation varies from 80-200 m in thickness and was

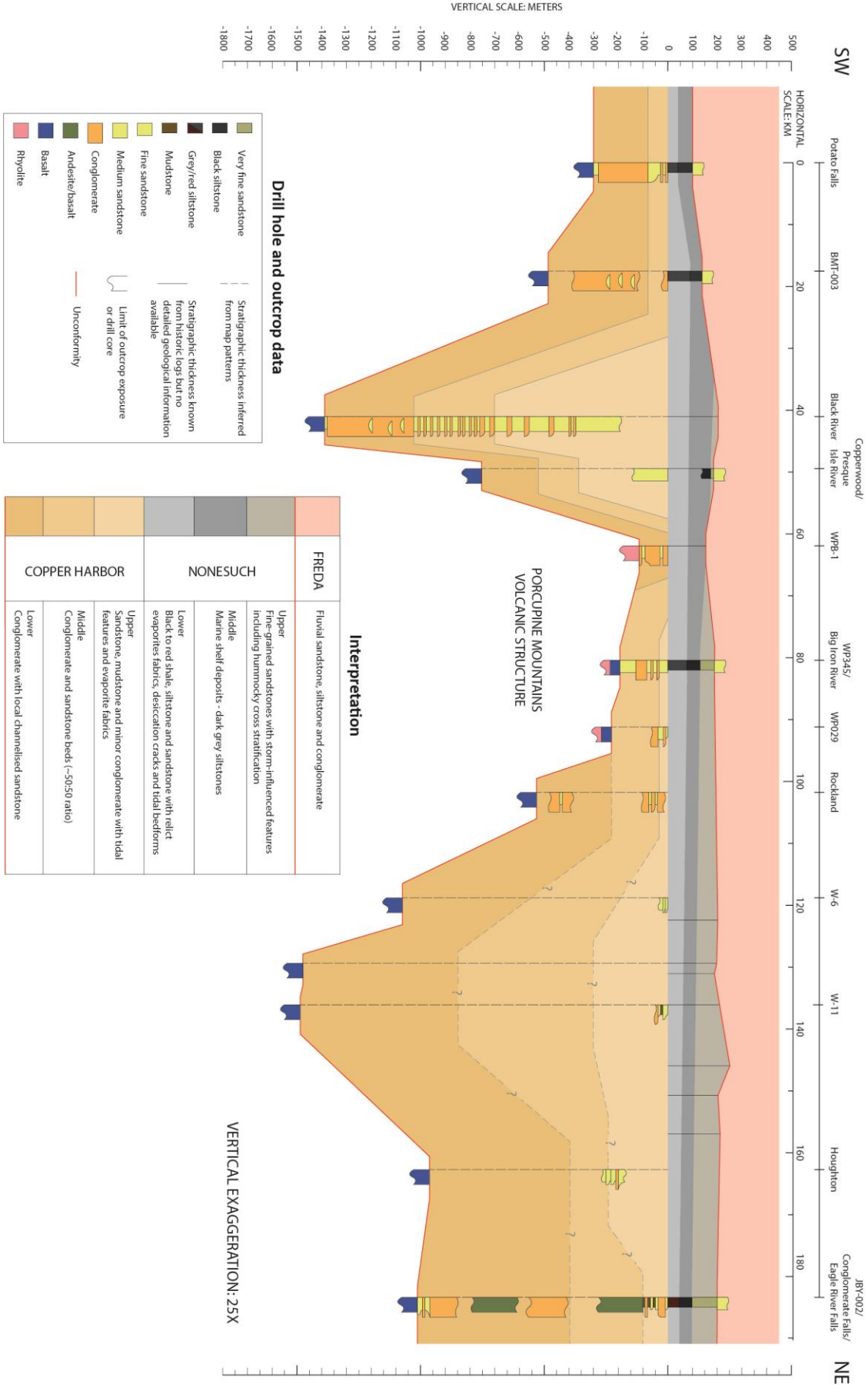
SW
NE
VERTICAL SCALE: METERS
HORIZONTAL SCALE: KM
Potato Falls
BMT-003
Copperwood/ Presque Isle River
Black River
WPB-1
WP345/ Big Iron River
WP029
Rockland
W-6
W-11
Houghton
JBY-002/ Conglomerate Falls/ Eagle River Falls
PORCUPINE MOUNTAINS VOLCANIC STRUCTURE
VERTICAL EXAGGERATION: 25X
Drill hole and outcrop data
Very fine sandstone
Black siltstone
Grey/red siltstone
Mudstone
Fine sandstone
Medium sandstone
Conglomerate
Andesite/basalt
Basalt
Rhyolite
Stratigraphic thickness inferred from map patterns
Stratigraphic thickness known from historic logs but no detailed geological information available
Limit of outcrop exposure or drill core
Unconformity
Interpretation
FREDA
Fluvial sandstone, siltstone and conglomerate
NONESUCH
Upper
Fine-grained sandstones with storm-influenced features including hummocky cross stratification
Middle
Marine shelf deposits - dark grey siltstones
Lower
Black to red shale, siltstone and sandstone with relict evaporites fabrics, desiccation cracks and tidal bedforms
COPPER HARBOR
Upper
Sandstone, mudstone and minor conglomerate with tidal features and evaporite fabrics
Middle
Conglomerate and sandstone beds (~50:50 ratio)
Lower
Conglomerate with local channelised sandstone

← Fig. 4.10. Geological cross section through the Oronto Group on the Keweenaw Peninsula; see Fig. 4.9 for locations of sections and wells.

recently reinterpreted as a tide- and storm-influenced estuary (Jones et al., 2020). The thickness variation is, in part, due to the base of the Freda Formation cutting down-section towards the southwest. The Freda Formation comprises red sandstone, lenses of pebbly sandstone and siltstone attributed to fluvial deposition and is as much as several thousands of metres thick (Daniels, 1982).

What our stratigraphic cross-section reveals is that the contact between the Portage Lake basalts and the conglomerates and sandstones of the Copper Harbor Formation shows considerable relief relative to the datum defined by the base of the Nonesuch Formation. Two explanations are plausible: the thickness differences reflect syn-depositional faulting (the interpretation proposed by many workers) or it outlines palaeotopography that became progressively onlapped and buried by the Copper Harbor sediments. To assess these contrasting interpretations, we re-examined the numerous reflection seismic lines that have been shot across the Lake Superior region (Fig. 4.2).

Fig. 4.11. Contact between the Portage Lake Volcanics and Copper Harbor Formation, Black River (see Fig. 4.9 for location).Basal bed of the Copper Harbor Formation contains ripples and below that is a palaeoweathering crust marked by variably altered and fragmented basalt. Reddish colour is due to oxidation during weathering.

4.7. Reflection seismic profiles

We have examined almost every reflection seismic profile available publicly that image the northern MRS (a total of 21 profiles covering 2630 km). Five lines belong to the 1986 Great Lakes International Multidisciplinary Program on Crustal Evolution (GLIMPCE), which emphasised the collection of deep-penetrating data to depths of c. 20 s TWT (two-way travel time). Fifteen lines were collected as part of a commercial oil and gas exploration survey in 1985 by Grant-Norpac/Argonne and penetrate to c. 8 s TWT. One line, the Geosource "Petty-Ray line 1" is a land-based extension of GLIMPCE line C and was part of a speculative commercial survey completed in 1984.

We use four of the longest and highest quality surveys as a basis for our reinterpretation of this part of the MRS basin: GLIMPCE A (Fig. 4.12), GLIMPCE C and the Petty Ray Line 1 extension (Fig. 4.13) and line LS-08 (Fig. 4.14). The first three provide across-strike cross-sections of the northern MRS basin whereas the line LS-08 was shot broadly strike-parallel to the basin. Two 1st-order observations have been highlighted by all workers (Figs. 4.12 and 4.13): (i) strike-normal cross-sections reveal reflector geometries that show overall tapering and thinning of the Keweenawan rocks away from their central occurrences where they are thickest; and (ii) the strike-parallel profile reveals a high relief basement topography across which the Keweenawan succession thins and thickens ('sub-basins'). Where we differ from those workers is on the geometries of the reflection traces and interpretation of those.

Five distinct units are objectively identifiable in the reflection seismic profiles (Figs. 4.12-4.14) and these are basement, pre-Portage Lake Volcanic units (Bessmer Quartzite, Siemens Creek and Kallander Creek formations), Portage Lake Volcanics, Oronto Group (Copper Harbor, Nonesuch and Freda formations) and Jacobsville Sandstone. This is a simplification of the Keweenawan Supergroup stratigraphy but nevertheless permits insight into the stratigraphic and structural architecture of the northern apex of the MRS.

Basement rocks define an interval from the base of the profiles upward into a heterogeneous pattern of stippled background and short sub-horizontal reflectors. More-continuous shallow to moderately dipping reflectors within this interval are likely a combination of processing artefacts, sills, dykes and genuine pre-Keweenawan features. The top of this interval is placed at a high-amplitude more-or-less continuous

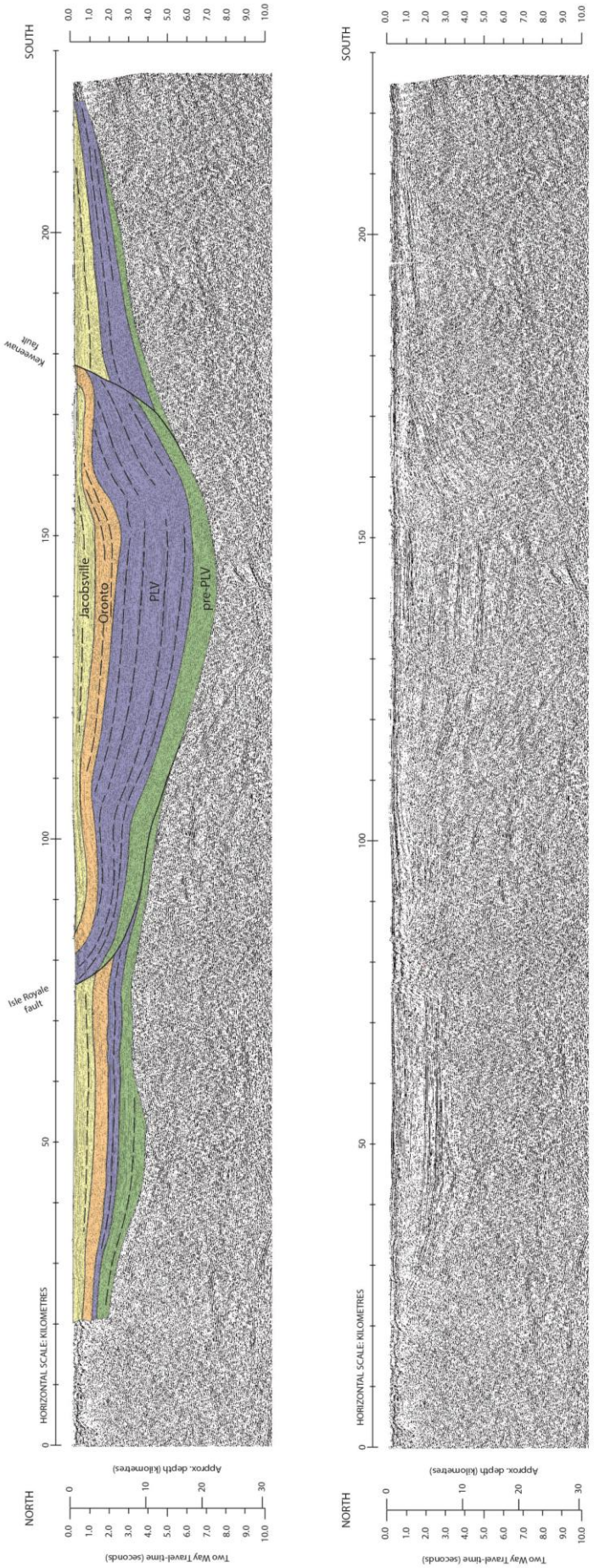

Fig. 4.12. GLIMPCE A seismic line. **TOP.** Interpretation. **BOTTOM**. Raw image.

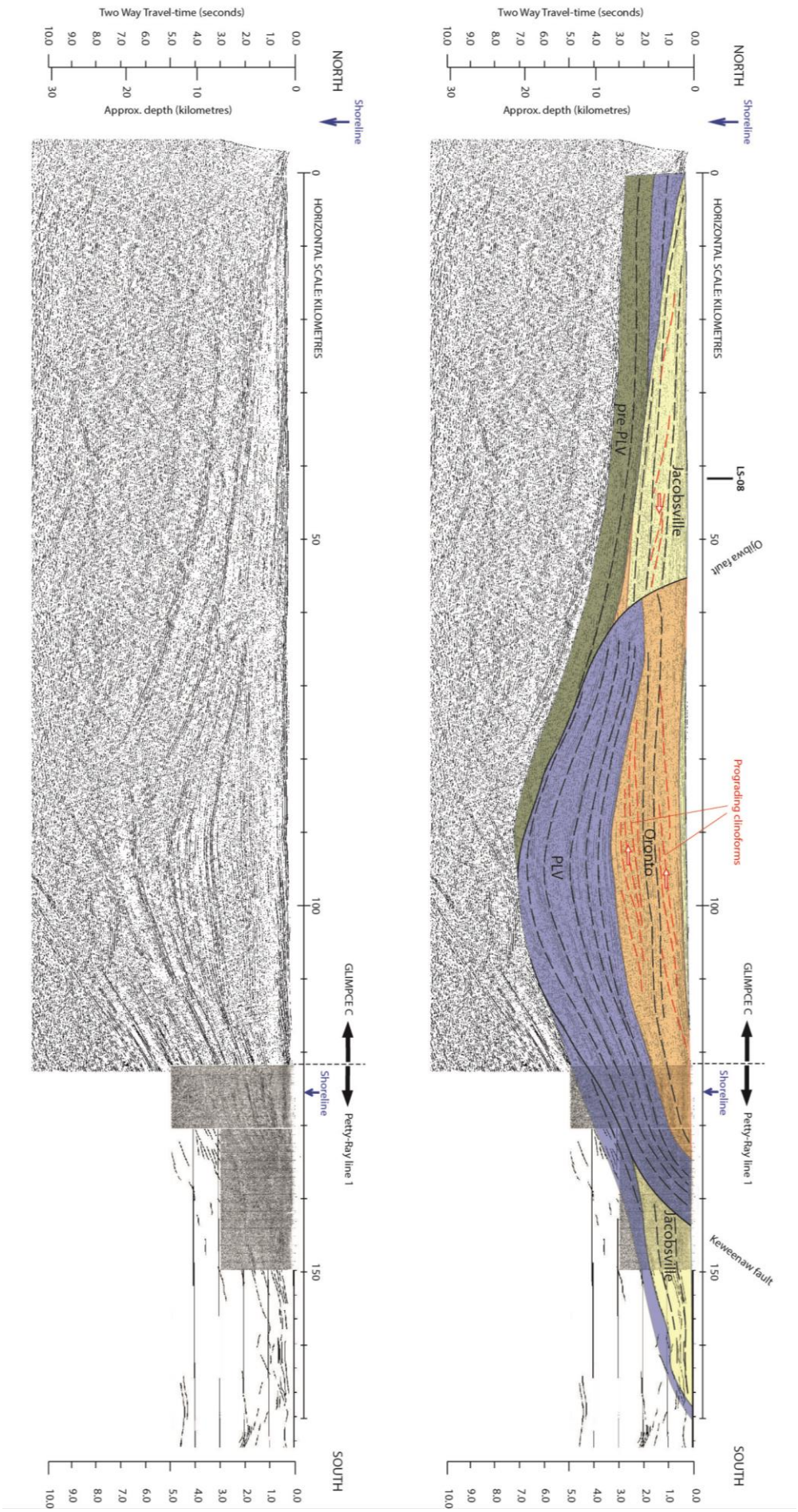

Fig. 4.13. GLIMPCE C and Petty-Ray 1 seismic lines. **TOP.** Interpretation. **BOTTOM.** Raw image.

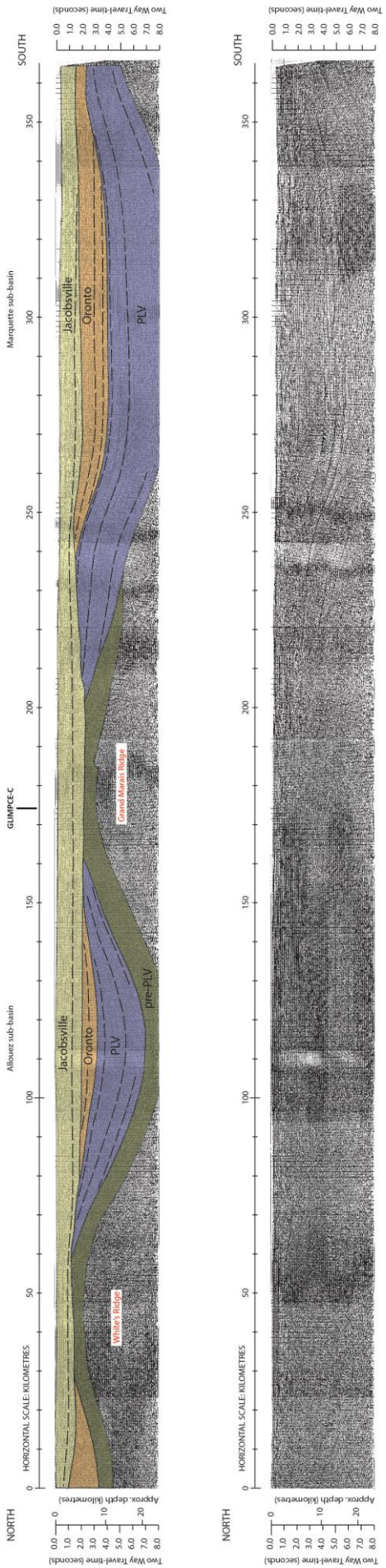

Fig. 4.14. LS-08 seismic line. **TOP.** Interpretation. **BOTTOM**. Raw image.

reflector, albeit not always clear across the length of the profiles, which we interpret as the contact between basement and the pre-Portage Lake volcanic unit (Figs. 4.12-4.14). What is striking is that nowhere along the profiles is this contact offset by obvious large-scale normal faulting and reflectors within the pre-Portage Lake Volcanics unit tend to largely parallel the contact rather than truncate against it, as would be the case in normal-fault-bounded basins. Above that reflector, the interval we assign to the pre-Portage Lake Volcanic unit is characterised by low internal resolution; those areas that do display moderately continuous reflectors likely represent individual basalt flows and show both truncation and onlap relationships internal to the unit, which can be readily interpreted as the margins of overlapping packages of basalt flows.

Although the contact with the overlying Portage Lake volcanics is ambiguous due to both the Kallender Creek and Portage Lake being basalt, hence displaying signal similarities, what we use to characterise the latter is the persistent presence of continuous high-amplitude reflectors, a probable consequence of high acoustic impedance contrasts between basalt flows and interflow sediments. Approximately 35 to 45 individual reflectors can be counted within the Portage Lake volcanic unit, with 4 to 6 of these being particularly pronounced. Isolated examples of low angle truncation and onlap relationships occur but in general individual reflectors can be traced for distances of several 10s to 100s of km. Reflectors also show clearly that they are more broadly spaced (i.e. corresponding to thicker units) in the basin's centre and taper (i.e. thin) away from there.

The contact between Portage Lake volcanics and overlying Oronto Group is sharp, owing to high acoustic impedance contrast between the basalts and the sedimentary cover sequence. Notable is that reflectors in the Portage Lake volcanics truncate against this surface at low to moderate angles, likely reflecting runout distance of basalt flows. The interval we define as the Oronto Group is typified by reflectors that are of moderate amplitude and laterally continuous. Two specific geometries worth noting are: (i) in the basin centre reflectors at depths of c. 2 s TWT are more continuous and of higher amplitudes compared to underlying and overlying units and we interpret this interval to be the Nonesuch Formation and (ii) in many places reflectors define what we interpret as prograding clinoforms in the inferred Copper Harbor Formation, Freda Formation and Jacobsville Sandstone (Figs. 4.13).

The interval we assign to the Jacobsville Sandstones is defined by moderate to high amplitude, laterally continuous, sub-horizontal reflectors at depths of up to 2.0 s TWT. However, at many locations these are obscured by high amplitude multiples of the Lake Superior lakebed. The base of the Jacobsville Sandstone unit is easily picked where it unconformably overlies more steeply dipping reflectors (bedding) in the underlying Oronto Group whereas where reflectors (bedding) in the Oronto Group and Jacobsville are sub-parallel the contact is difficult to identify (Figs. 4.12 and 4.14).

4.8. Discussion

What we find striking is the lateral continuity of seismic reflectors at the basin-scale. These reflectors must represent packages of both volcanic and sedimentary rocks that persist uniformly across the basin, and that changes in thickness are largely systematic for all units of the Keweenawan succession. At outcrop-map scale, the rocks have facies characteristics that likewise reflect lateral continuity and overall uniformity in lithological trends. Hence, these features are at odds with those that are hallmark to continental rift basins. Furthermore, subsidence rates in the northern MRS are directly linked to rock composition: mafic volcanites generated a load that drove rates between 400-900m/Myr and when volcanism ceased and sediment loading was initiated rates declined to c. 150m/Myr. Our new U-Pb ages corroborate and refine the timing of deposition of the Copper Harbor Formation to between 1089 and 1078 Ma, and that deposition of the overlying Nonesuch Formation began soon after. The latter age is the youngest yet evidence for volcanism continuing to near the Nonesuch-Copper Harbor contact and help pin down the timing of the decline in subsidence rates to 1079.49 ± 0.35 Ma. Thus, of the total 17 km thickness, loading of the lithosphere alone accounts for c. 12 km and, given that the backstripping analyses is a rather simple 1st-order approximation, it is reasonable to conclude that loading was the primary driver of subsidence.

We see no evidence in the seismic profiles or in our stratigraphic cross-section for the presence of major syn-depositional basin-defining normal faults (e.g. units with wedge-shaped terminations) during any time of deposition of the Keweenawan succession. The Isle Royale, Keweenaw and Ojibwa faults are coincident with abrupt steepening on Portage lake volcanic stratigraphy but not abrupt thickness changes that would suggest syn-depositional faulting; the internal stratigraphy of that Group can be

restored across faults. The only faults imaged are clearly reverse faults. Further, seismic reflectors and observations from outcrop, drill core and bore hole data indicate that thickness variations are not related to faults but instead appear to show the Copper Harbor sediments onlapping onto and burying a pre-existing paleotopography developed on the flood basalt which covers large portions of the basin including the crests of White's Ridge and the Grand Marais Ridge. This unconformity surface crops out at several localities on the cross section (Figs. 4.10, 4.11) where a weathering crust is developed. In deeper portions of the basin, including the Allouez and Marquette sub-basins, reflectors within the Portage Lake volcanics parallel those in the overlying Oronto Group unit and this may indicate a paraconformity or a conformable boundary. The key geometries and relationships observed in reflection seismic data are shown in the schematic diagram Figure 4.15.

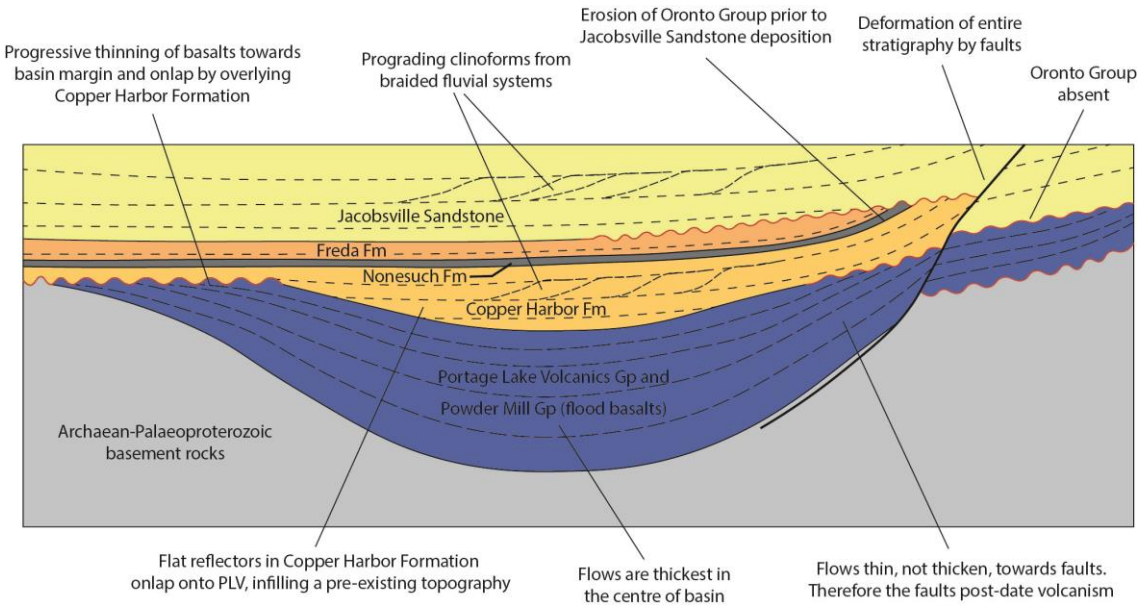

Fig. 4.15. Schematic diagram of key geometries and relationships observed in cross section and reflection seismic profiles.

Geochronology constraints limit the duration of the Copper Harbor Formation to c. 10 Myr. Although this appears to be a relatively short amount of time to create palaeotopography and then bury it, we note that Laurentia's low-latitude position at this time (Swanson-Hysell et al., 2019) would have placed the then fresh basalt into a

setting of high precipitation and temperatures thereby exposed to processes of rapid weathering and erosion on a non-vegetated land surface. The weathering crust at the top of the Portage Lake flood basalt attests to a period of intense weathering and erosion. Further, it is unknown how much of the inferred palaeorelief reflects the construction of broad volcanic mounds rather than a topography created purely from erosion. The apparent lack of a time-equivalent sedimentary record beyond the MRS hinders us from testing ideas of how much basalt was eroded but the clast composition of the Copper Harbor Formation, although locally variable, is c. 50% basalt, c. 45% felsites and andesites and c. 5% basement (e.g. Ojakangas et al., 2001; Baumann et al., 2018). This is *prima facie* evidence that the flood basalt was deeply eroded and in places had to have been breached. By the time of Nonesuch Formation deposition and encroachment of its estuarine seaway, this palaeotopography had been buried and no longer existed.

Combined with the facies features, it is difficult to relate these aspects of the Keweenawan succession to a rift-basin setting in which thermo-mechanical processes were the principal drivers of basin genesis. Instead, it appears that the MRS was more of a sag-style basin. Previous workers indeed invoked a sag-type setting for the Oronto Group rocks (e.g. Behrendt et al., 1988; Cannon et al., 1989; Cannon, 1992; Samson and West, 1994; Stein et al., 2015) but our analyses suggest that the flood basalts likewise formed in a sag-style basin driven by loading. Two lines of evidence supporting that inference are (i) the observation that seismic reflectors in the flood basalt taper (i.e. flow units thin) out of the basin axis, and (ii) the fact that older basalt flows dip more steeply than younger ones (Green, 1977). Further, an interesting observation is that the seismic profiles show temporal shifts in the deepest portions of the basin. The thickest Oronto Group stratigraphy is c. 20 km south of that in the Portage Lake Volcanic Group whereas the thickest Jacobsville Sandstone is c. 40 km north of that. We speculate that this may be a far-field response to the changing magnitude-of-tectonic-loading along the Grenville orogenic front, and shifting of the MRS's main depocenters in response to that orogenic loading.

In conjunction with existing and new geochronological constraints, the observations made in this study enable the reconstruction of the sequence of key events in the evolution of the MRS (Fig. 4.16). Basin formation commenced at c. 1111 Ma with deposition of the Bessemer Quartzite. Flood basalts of the Siemens Creek,

Kallender Creek and Portage Lake Volcanic Groups were deposited from c. 1110 to 1090 Ma in a basin which subsided uniformly and rapidly due to their mass. Volcanism ceased at c. 1089 Ma and basin flanks were eroded contemporaneously with sedimentation in the centres of the still subsiding basins. By Nonesuch Formation deposition at c. 1075 Ma the basin's palaeotopgraphy was largely subdued and marine transgression occurred. At c. 1060 Ma the Ottawan phase of Grenvillian orogenesis caused the first phase of basin deformation and inversion. The Freda Formation can thus be viewed as a far-field molasse that prograded across and locally eroded underlying units. As deformation progressed, strain was focused in the hanging walls of the Keweenaw, Isle Royale and Ojibwa faults (e.g. GLIMPCE A, Fig. 4.12) where steeply dipping Portage Lake Volcanic and Oronto Group units are overlain in angular unconformity by the Jacobsville Sandstone. We interpret this period of post-Oronto Group deformation to have offset Portage Lake Volcanics and Oronto Group units by several kms. Subsequently, erosion of these uplifted portions of the basin was followed by Jacobsville Sandstone deposition onto this unconformity surface at c. 980 Ma. We speculate that the Jacobsville Sandstone may also be a molasse deposit originating from the Rigolet phase of Grenville orogenesis, which also generated further fault movement , including cutting the Jacobsville Sandstone.

The process by which to obtain 20 km thicknesses of flood basalt (as inferred by geophysics; Cannon et al., 1989; Cannon, 1992; Sexton and Henson, 1994; Stein et al., 2015) in narrow basins remains problematic. However, Swanson-Hysell et al. (2019) have noted the temporal coincidence between the timing of onset of fast plate motion, as deduced by palaeomagnetic data archived in the Keweenawan succession, and the onset of development of the MRS. This leads us to speculate that the segmented branches of the MRS are, in effect, cratonal-scale tension gashes linked to the abrupt onset of rapid plate motion. These would have acted as moats for flood basalt and subsequent viscoelastic/sag-style lithospheric response as loading increased. Likewise, the temporal coincidence of the timing of the MRS with that of the Ottawan and Rigolet phases of the Grenville orogeny hints strongly at causality but this, too, remains to be resolved.

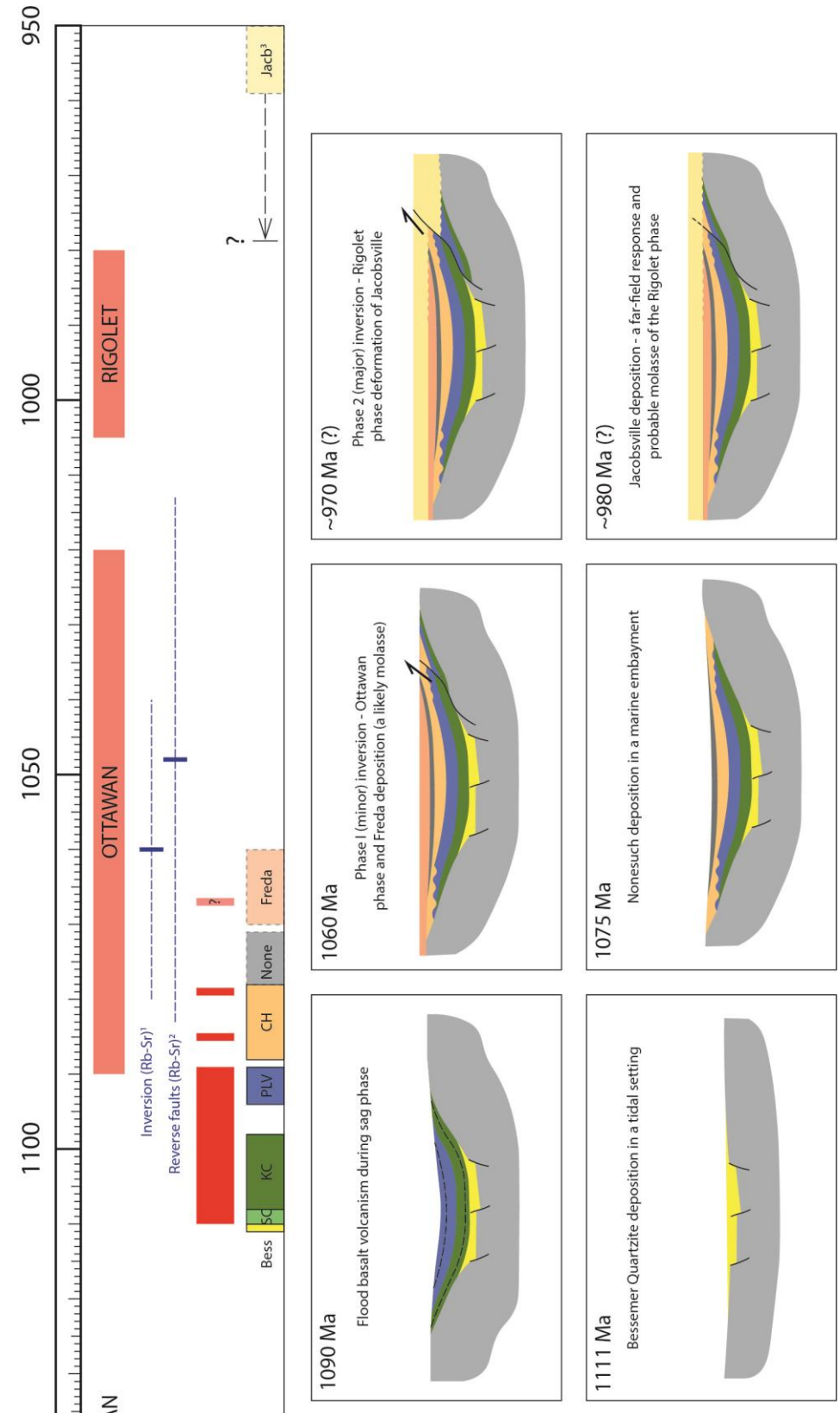

Fig. 4.16. Cartoon timeline of key events in the evolution of the Midcontinent Rift System.

4.9. Conclusions

Our findings call into question long-held views regarding the geodynamical evolution of the MRS. We highlight features archived in the exposed rock record of the MRS in its northernmost segment encompassing Lake Superior and the geometry of reflectors in seismic profiles across that region as evidence for our reinterpretation. Our key findings are highlighted below.

New geochronology data further constrain the evolution of the MRS and include the youngest recorded volcanism in the MRS at 1079.49 ± 0.35 Ma. Felsic volcanism in the Porcupine Mountains Volcanic Structure is constrained to a period of 2.5 Myr, between c. 1089 and 1078 Ma, immediately prior to the deposition of the Copper Harbor Formation. The latter age is a close approximation for the age of the basal Nonesuch Formation and a minimum age for the end of deposition of the Copper Harbor Formation.

Flood basalt volcanism spanned a period of 20 Myr from c. 1110 to 1090 Ma. After the cessation of volcanism, a period of subaerial exposure and erosion formed a palaeotopograph marked by 100s of m of relief that was infilled by the Copper Harbor Formation deposited between c. 1089 and 1078 Ma; well-rounded clasts of mafic and felsic compositions attest to erosion of the flood basalt and presence of basement-derived clasts show that the flood basalt had been breached. Palaeo-relief was largely buried by the time that the Nonesuch Formation was deposited during a marine transgression at c. 1078 Ma. The overlying fluvial Freda and Jacobsville sandstones likely represent two distinct molasse phases of sedimentation.

In seismic profiles, reflectors in flood basalt taper uniformly away from thickest areas along the basin axis indicating effusion into a sagging basin. Outcrop and drill core observations corroborate interpretations of reflection seismic data which show lateral continuity of units and sedimentary facies across the basin. The absence of growth faults in seismic data and the absence of their hallmark features in cores and outcrop are in contradiction with archetypal continental-crust rift basins.

Backstripping and subsidence modelling of the c. 17 km of the Keweenawan Supergroup shows the principal determinant of subsidence was the density of the basin-filling material. Subsidence occurred as rapidly as 900 m/Myr during deposition of volcanic units and slowed to c. 150 m/Myr at the onset of siliciclastic sedimentation. Lithospheric stretching was a minor contributor to basin subsidence.

Reverse faults offset, and hence post-date, the entire Keweenawan Supergroup. At depth these faults are shallowly dipping, exploiting bedding planes in the volcanic units. At surface the faults steepen and have snake-head anticlines at their tips. The earliest cut strata as young as the Freda Sandstone hence likely reflect the Ottawan phase of the Grenville Orogeny whereas later movement on reverse faults offset the Jacobsville Sandstone hence likely due to the Rigolet phase of the orogeny.

The geodynamic processes responsible for initiating and subsequently arresting effusion of the extraordinarily large volumes of flood basalt remain an enigma. Likewise, it is unclear why this volume of lava was confined to a narrow trough, resulting in a c. 20 km thick sequence of basalt in the apparent absence of a pre-existing structural framework. Volcanism and sedimentation spanned the beginning of the Ottawan phase of the Grenville Orogeny; a period of very rapid plate motion. We propose this rapid motion, east of the proto-Grenville Orogeny, caused what are, in effect, cratonal-scale tension gashes in the interior of the Laurentian continent and that these zones of weakness then became the focus of volcanism and subsidence. The loading of flood basalts in these basins created a positive feedback loop whereby subsidence promoted further ponding of lavas, which in turn drove further subsidence.

The Grenville Orogeny is manifested in the MRS as large reverse faults, warping and tilting of the crust which shifted basin depocentres over time, and shedding of molasses (Freda and Jacobsville formations). The early part of the MRS's evolution appears to be linked causally to the onset of rapid plate motion rather than some far-field effect solely due to the Orogeny. Its latter stages were likely induced by a return to a state of crustal isostatic equilibrium.

4.10. References

Allen, P.A. and Allen, J.R., 2013. Basin analysis: Principles and application to petroleum play assessment. John Wiley & Sons.Anderson and Burke, 1983

Anderson, D.L., 1994. The sublithospheric mantle as the source of continental flood basalts; the case against the continental lithosphere and plume head reservoirs. Earth and Planetary Science Letters, 123(1-3), pp.269-280.

Baumann, S.D., Dylka, S.K. and Malone, D.H., 2018. Lithostratigraphic subdivisions of the Mesoproterozoic Copper Harbor Formation (Oronto Group) in Michigan and Wisconsin, USA. STRATIGRAPHY, 15(2), pp.135-152.

Behrendt, J.C., Hutchinson, D.R., Lee, M., Thornber, C.R., Trehu, A., Cannon, W. and Green, A., 1990. GLIMPCE seismic reflection evidence of deep-crustal and upper-

mantle intrusions and magmatic underplating associated with the Midcontinent Rift system of North America. Tectonophysics, 173(1-4), pp.595-615.

Bornhorst, T.J. and Barron, R.J., 2011. Copper deposits of the western Upper Peninsula of Michigan. Geological Society of America Field Guide, 24, pp.83-99.

Bornhorst, T.J., 1992. An overview of the Keweenaw Peninsula native copper district. Michigan: Society of Economic Geologists Guidebook Series, 13, pp.33-62.

Cannon, W.F., 1992. The Midcontinent rift in the Lake Superior region with emphasis on its geodynamic evolution. Tectonophysics, 213(1-2), pp.41-48.

Cannon, W.F. and Hinze, W.J., 1992. Speculations on the origin of the North American Midcontinent rift. Tectonophysics, 213(1-2), pp.49-55.

Cannon, W.F., Green, A.G., Hutchinson, D.R., Lee, M., Milkereit, B., Behrendt, J.C., Halls, H.C., Green, J.C., Dickas, A.B., Morey, G.B. and Sutcliffe, R., 1989. The North American Midcontinent rift beneath Lake Superior from GLIMPCE seismic reflection profiling. Tectonics, 8(2), pp.305-332.

Cannon, W.F., Peterman, Z.E. and Sims, P.K., 1993. Crustal-scale thrusting and origin of the Montreal River monocline-A 35-km-thick cross section of the midcontinent rift in northern Michigan and Wisconsin. Tectonics, 12(3), pp.728-744.

Cannon, W.F., Nicholson, S.W., Woodruff, L.G., Hedgman, C.A., Schulz, K.J., 1995. Geologic map of the Ontonagon and part of the Wakefield 30’ x 60’ quadrangles, Michigan, 1:100,000 scale. U.S. Geological Survey Miscellaneous Investigation Series Map 1–2499.

Cannon, W.F., Kress, T.H., Sutphin, D.M., Morey, G.B., Meints, J., Barber-Delach, R., 1999. Online Files for Geologic Map and Mineral Deposits of Minnesota, Wisconsin, and Michigan: Version 3. USGS Open-File Report 97–455 (version 3, Nov. 1999).

Cawood, P.A. and Pisarevsky, S.A., 2017. Laurentia-Baltica-Amazonia relations during Rodinia assembly. Precambrian Research, 292, pp.386-397.

Chorowicz, J., 2005. The east African rift system. Journal of African Earth Sciences, 43(1-3), pp.379-410.

Condon, D.J., Schoene, B., McLean, N.M., Bowring, S.A. and Parrish, R.R., 2015. Metrology and traceability of U–Pb isotope dilution geochronology (EARTHTIME Tracer Calibration Part I). Geochimica et Cosmochimica Acta, 164, pp.464-480.

Cumming, V.M., Poulton, S.W., Rooney, A.D. and Selby, D., 2013. Anoxia in the terrestrial environment during the late Mesoproterozoic. Geology, 41(5), pp.583-586.

Daniels Jr, P.A., 1982. Proterozoic sedimentary rocks: Oronto Group, Michigan-Wisconsin. Geology and tectonics of the Lake Superior Basin: Geological Society of America Memoir, 156.

Davis, D.W. and Green, J.C., 1997. Geochronology of the North American Midcontinent rift in western Lake Superior and implications for its geodynamic evolution. Canadian Journal of Earth Sciences, 34(4), pp.476-488.

Elmore, R.D., Milavec, G.J., Imbus, S.W. and Engel, M.H., 1989. The Precambrian Nonesuch Formation of the North American mid-continent rift, sedimentology and organic geochemical aspects of lacustrine deposition. Precambrian Research, 43(3), pp.191-213.

Elmore, R.D., 1984. The Copper Harbor Conglomerate: A late Precambrian fining-upward alluvial fan sequence in northern Michigan. Geological Society of America Bulletin, 95(5), pp.610-617.

Fairchild, L.M., Swanson-Hysell, N.L., Ramezani, J., Sprain, C.J. and Bowring, S.A., 2017. The end of Midcontinent Rift magmatism and the paleogeography of Laurentia. Lithosphere, 9(1), pp.117-133.

Fedorchuk, N.D., Dornbos, S.Q., Corsetti, F.A., Isbell, J.L., Petryshyn, V.A., Bowles, J.A. and Wilmeth, D.T., 2016. Early non-marine life: evaluating the biogenicity of Mesoproterozoic fluvial-lacustrine stromatolites. Precambrian Research, 275, pp.105-118.

Foster, A. and Nimmo, F., 1996. Comparisons between the rift systems of East Africa, Earth and Beta Regio, Venus. Earth and Planetary Science Letters, 143(1-4), pp.183-195.

Hauser, E.C., van der Pluijm, B.A. and Catacosinos, P.A., 1996. Midcontinent rifting in a Grenville embrace. SPECIAL PAPERS-GEOLOGICAL SOCIETY OF AMERICA, pp.67-76.

Gordon, M.B. and Hempton, M.R., 1986. Collision-induced rifting: the Grenville Orogeny and the Keweenawan rift of North America. Tectonophysics, 127(1-2), pp.1-25.

Green. J.C., 1977. Keweenawan plateau volcanism in the Lake Superior region. In: W.R.A. Baragar. L.C. Coleman and J.M. Hall (Editors). Volcanic Regimes in Canada. Geol. Assoc. Canada, Spec. Pap. 16:407 -422.

Halls, H.C. and Pesonen, L.J., 1982. Paleomagnetism of Keweenawan rocks. Geol. Soc. Am. Mem, 156, pp.173-201.

Hanson, R.E., Crowley, J.L., Bowring, S.A., Ramezani, J., Gose, W.A., Dalziel, I.W., Pancake, J.A., Seidel, E.K., Blenkinsop, T.G. and Mukwakwami, J., 2004. Coeval large-scale magmatism in the Kalahari and Laurentian cratons during Rodinia assembly. Science, 304(5674), pp.1126-1129.

Hauser, E.C., van der Pluijm, B.A. and Catacosinos, P.A., 1996. Midcontinent rifting in a Grenville embrace. SPECIAL PAPERS-GEOLOGICAL SOCIETY OF AMERICA, pp.67-76.

Henry, S.G., Mauk, F.J. and der Voo, R.V., 1977. Paleomagnetism of the upper Keweenawan sediments: the Nonesuch Shale and Freda Sandstone. Canadian Journal of Earth Sciences, 14(5), pp.1128-1138.

Hiess, J., Condon, D.J., McLean, N. and Noble, S.R., 2012. 238U/235U systematics in terrestrial uranium-bearing minerals. Science, 335(6076), pp.1610-1614.

Holm, D.K., Anderson, R., Boerboom, T.J., Cannon, W.F., Chandler, V., Jirsa, M., Miller, J., Schneider, D.A., Schulz, K.J. and Van Schmus, W.R., 2007. Reinterpretation of Paleoproterozoic accretionary boundaries of the north-central United States based on a new aeromagnetic-geologic compilation. Precambrian Research, 157(1-4), pp.71-79.

Hutchinson, D.R., White, R.S., Cannon, W.F. and Schulz, K.J., 1990. Keweenaw hot spot: Geophysical evidence for a 1.1 Ga mantle plume beneath the Midcontinent Rift System. Journal of Geophysical Research: Solid Earth, 95(B7), pp.10869-10884.

Jaffey, A.H., Flynn, K.F., Glendenin, L.E., Bentley, W.T. and Essling, A.M., 1971. Precision measurement of half-lives and specific activities of U 235 and U 238. Physical review C, 4(5), p.1889.

Jones, S.M., Prave, A.R., Raub, T.D., Cloutier, J., Stüeken, E.E., Rose, C.V., Linnekogel, S. and Nazarov, K., 2020. A marine origin for the late Mesoproterozoic Copper Harbor and Nonesuch Formations of the Midcontinent Rift of Laurentia. Precambrian Research, 336, p.105510.

King, B.C. and Chapman, G.R., 1972. A Discussion on volcanism and the structure of the Earth-Volcanism of the Kenya rift valley. Philosophical Transactions of the Royal

Society of London. Series A, Mathematical and Physical Sciences, 271(1213), pp.185-208.

King, S.D. and Ritsema, J., 2000. African hot spot volcanism: small-scale convection in the upper mantle beneath cratons. Science, 290(5494), pp.1137-1140.

King, E.R. and Zietz, I., 1971. Aeromagnetic study of the midcontinent gravity high of central United States. Geological Society of America Bulletin, 82(8), pp.2187-2208.

Klewin, K.W. and Shirey, S.B., 1992. The igneous petrology and magmatic evolution of the Midcontinent rift system. Tectonophysics, 213(1-2), pp.33-40.

Malone, D.H., Stein, C.A., Craddock, J.P., Kley, J., Stein, S. and Malone, J.E., 2016. Maximum depositional age of the Neoproterozoic Jacobsville Sandstone, Michigan: Implications for the evolution of the Midcontinent Rift. Geosphere, 12(4), pp.1271-1282.

Mattinson, J.M., 2010. Analysis of the relative decay constants of 235U and 238U by multi-step CA-TIMS measurements of closed-system natural zircon samples. Chemical Geology, 275(3-4), pp.186-198.

McLean, N.M., Condon, D.J., Schoene, B. and Bowring, S.A., 2015. Evaluating uncertainties in the calibration of isotopic reference materials and multi-element isotopic tracers (EARTHTIME Tracer Calibration Part II). Geochimica et Cosmochimica Acta, 164, pp.481-501.

Nicholson, S.W. and Shirey, S.B., 1990. Midcontinent rift volcanism in the Lake Superior region: Sr, Nd, and Pb isotopic evidence for a mantle plume origin. Journal of Geophysical Research: Solid Earth, 95(B7), pp.10851-10868.

Nicholson, S.W., Schulz, K.J., Shirey, S.B. and Green, J.C., 1997. Rift-wide correlation of 1.1 Ga Midcontinent rift system basalts: implications for multiple mantle sources during rift development. Canadian Journal of Earth Sciences, 34(4), pp.504-520.

Ojakangas, R.W. and Dickas, A.B., 2002. The 1.1-Ga Midcontinent Rift System, central North America: sedimentology of two deep boreholes, Lake Superior region. Sedimentary Geology, 147(1-2), pp.13-36.

Ojakangas, R.W. and Morey, G.B., 1982. Keweenawan pre-volcanic quartz sandstones and related rocks of the Lake Superior region. World, RJ, and Hinze, EJ, eds. Geology and tectonics of the Lake Superior basin. Geol. Soc. Am. Mem, 156, pp.85-96.

Ojakangas, R.W., Morey, G.B. and Green, J.C., 2001. The Mesoproterozoic midcontinent rift system, Lake Superior region, USA. Sedimentary Geology, 141, pp.421-442.

Patro, B.P.K. and Sarma, S.V.S., 2007. Trap thickness and the subtrappean structures related to mode of eruption in the Deccan Plateau of India: results from magnetotellurics. Earth, planets and space, 59(2), pp.75-81.

Reidel, S.P., Camp, V.E., Tolan, T.L. and Martin, B.S., 2013. The Columbia River flood basalt province: Stratigraphy, areal extent, volume, and physical volcanology. The Columbia River flood basalt province: geological society of America special paper, 497, pp.1-43.

Renne, P.R. and Basu, A.R., 1991. Rapid eruption of the Siberian Traps flood basalts at the Permo-Triassic boundary. Science, 253(5016), pp.176-179.

Rivers, T., 2015. Tectonic setting and evolution of the Grenville Orogen: An assessment of progress over the last 40 years. Geoscience Canada, 42(1), pp.77-124.

Samson, C. and West, G.F., 1994. Detailed basin structure and tectonic evolution of the Midcontinent Rift System in eastern Lake Superior from reprocessing of GLIMPCE deep reflection seismic data. Canadian Journal of Earth Sciences, 31(4), pp.629-639.

Schoene, B., Crowley, J.L., Condon, D.J., Schmitz, M.D. and Bowring, S.A., 2006. Reassessing the uranium decay constants for geochronology using ID-TIMS U–Pb data. Geochimica et Cosmochimica Acta, 70(2), pp.426-445.

Sexton, J.L. and Henson Jr, H., 1994. Interpretation of seismic reflection and gravity profile data in western Lake Superior. Canadian Journal of Earth Sciences, 31(4), pp.652-660.

Stein, C.A., Stein, S., Merino, M., Randy Keller, G., Flesch, L.M. and Jurdy, D.M., 2014. Was the Midcontinent Rift part of a successful seafloor-spreading episode?. Geophysical Research Letters, 41(5), pp.1465-1470.

Stein, C.A., Kley, J., Stein, S., Hindle, D. and Keller, G.R., 2015. North America's Midcontinent Rift: when rift met LIP. Geosphere, 11(5), pp.1607-1616.

Stein, C.A., Stein, S., Merino, M., Randy Keller, G., Flesch, L.M. and Jurdy, D.M., 2014. Was the Midcontinent Rift part of a successful seafloor-spreading episode?. Geophysical Research Letters, 41(5), pp.1465-1470.

Strother, P.K. and Wellman, C.H., 2016. Palaeoecology of a billion-year-old non-marine cyanobacterium from the Torridon Group and Nonesuch Formation. Palaeontology, 59(1), pp.89-108.

Swanson-Hysell, N.L., Ramezani, J., Fairchild, L.M. and Rose, I.R., 2019. Failed rifting and fast drifting: Midcontinent rift development, Laurentia's rapid motion and the driver of Grenvillian orogenesis. Bulletin, 131(5-6), pp.913-940.

Van Schmus, W.R. and Hinze, W.J., 1985. The midcontinent rift system. Annual Review of Earth and Planetary Sciences, 13(1), pp.345-383.

Van Schmus, W.R., Bickford, M.E., Sims, P.K., Anderson, R.R., Shearer, C.K. and Treves, S.B., 1993. Proterozoic geology of the western midcontinent basement. Precambrian: Conterminous USA Geological Society of America, Boulder, Colo., Geology of North America, 2, pp.239-258.

Vervoort, J.D., Wirth, K., Kennedy, B., Sandland, T. and Harpp, K.S., 2007. The magmatic evolution of the Midcontinent rift: New geochronologic and geochemical evidence from felsic magmatism. Precambrian Research, 157(1-4), pp.235-268.

Zartman, R.E., Nicholson, S.W., Cannon, W.F. and Morey, G., 1997. U–Th–Pb zircon ages of some Keweenawan Supergroup rocks from the south shore of Lake Superior. Canadian Journal of Earth Sciences, 34(4), pp.549-561.

Blank page

Chapter 5

Conclusions

5.1. Overview

The late-Mesoproterozoic Midcontinent Rift System (MRS) is a curvilinear basin located in east-central North America. Effusion of flood basalts from 1109 to 1090 Ma was confined to the basin and resulted in a volcanic sequence several thousands of kilometres in length and locally 20 km thick. This is one of the most unique aspects of the MRS. The cessation of volcanism at c. 1090 was succeeded by sedimentation of the Oronto Group and Jacobsville Sandstone. The causes of basin formation, and its eventual demise and inversion, are the subject of debate. In broad terms the basin is the product of the amalgamation and breakup of the supercontinent Rodina.

The White Pine Cu-Ag deposit is a hybrid of two different styles of sediment-hosted stratiform copper mineralisation that formed contemporaneously: (i) native copper associated with pyrobitumen in Copper Harbor Formation red beds, and (ii) native copper and copper sulphide mineralisation in Nonesuch Formation shales.

The aim of this PhD was to understand the factors which influenced the fluid-flow regime responsible for the formation of the White Pine Cu-Ag deposit. This included the depositional environment of the succession, the properties of the rocks and fluids and how these may have changed over time, the fluid pathways and the causes of fluid migration. Our approach was to study the sedimentology of the Oronto Group (Chapter 2), the White Pine deposit (Chapter 3) and the structural and geodynamic aspects of the basin (Chapter 4).

5.2. Chapter 2 – Sedimentology

The upper Copper Harbor Formation and the entirety of the Nonesuch Formation contain an abundance of sedimentological features permissible to having formed in a marine setting. These features include desiccation and syneresis cracks indicative of repeated wetting and drying cycles, mud drapes, lenticular and flaser bedding, flat top ripples, herringbone ripples, evaporite nodules and hummocky cross stratification. In themselves, none is definitely of marine origin, but the weight of evidence leads us to conclude that the basin was connected to the ocean during deposition of these units. The repeated wetting and drying cycles, rarity of storm wave bedforms and the location of the basin within the interior of the Laurentian craton suggests a shallow and protected marine embayment. Bedforms in the lower and middle Copper Harbor Formation indicate deposition in a braided fluvial setting.

Question	Chapter	Key findings
What was the paleo-environment?	2	The Copper Harbor Formation was a distal braided fluvial system with sabkha environments. The Nonesuch Formation was deposited in a shallow marine embayment and also contains abundant evaporite fabrics.
What was the rate of sediment accumulation and what controlled it?	4	Volcanic rocks forming the lower Keweenawan Supergroup accumulated at a rate of 400-900m/Myr. Sedimentary rocks in the Oronto Group accumulated at ~150m/Myr. The principal driver of subsidence was the density of these volcanic and sedimentary rocks – not lithospheric stretching.
What was the timing, nature and extent of faults?	3,4	Basin-scale faults (e.g. Keweenaw fault) are post-depositional. Their reverse movement post-dates all but the Jacobsville Sandstone. Km-scale syn-sedimentary faults at White Pine were active during Copper Harbor deposition and played a key role in conditioning sedimentation and later channeling hydrothermal fluid flow.
What were the principal fluid flow pathways and how did they evolve over time?	3	The main focus of fluid flow was along the top of the Copper Harbor Formation aquifer. Syn-sedimentary faults also played a key role at the deposit-scale. Early authigenic chlorite was fundamental in preserving primary porosity pathways. Late-diagenetic quartz and calcite cements eventually occluded porosity.
What was the timing of fluid flow?	3, 4	Initial oxidised and saline pore fluids were displaced by reduced fluids and liquid petroleum during mesodiagenesis, at a depth of ~2km. Cu-Ag mineralisation occurred at ~4km depth at 1039 Ma, ~40 Myr after host rock deposition. Fluid movement was driven by burial compaction caused by deposition of the Freda Formation and the distal effects of the Ottawan phase of

		Grenville orogenesis.
What was the original composition of the mineralising fluid?	2,3	Mineralising fluids were inherited from prevailing seawater during deposition of the Copper Harbor and Nonesuch formations. The fluids were inherently oxidised and saline and may have derived additional salinity from the subsurface dissolution of evaporites. Metals were sourced from basaltic lithic fragments in the Copper Harbor Formation.
Why is there an abundance of chalcocite and native copper?	3	Late Mesoproterozoic seawater was characterised by a low dissolved sulphate content. This, coupled with an abundant source of Cu metal from volcanic rocks, produced high-tenor (low sulphur) minerals. In addition, native copper was the stable phase under the relatively oxidised conditions of pyrobitumen-bearing Copper Harbor Formation sandstones.
What was the temperature of ore formation?	3	Illite crystallinity reveals the maximum temperature in the upper Copper Harbor Formation at White Pine was approximately 150˚C. Mineralisation occurred shortly before these peak temperatures, at ~125˚C.
Can alteration be distinguished from diagrenesis?	3	Yes. Widespread diagenetic events include early illite and hematite rims, and late quartz overgrowths and calcite cement. Alteration related to the White Pine deposit exhibits the hallmarks of the reduced fluid phases which both bleached hematite and converted it to authigenic chlorite rims.

Table 5.1. Summary of key research questions and findings.

Caliche and calcrete horizons within the Copper Harbor indicate sabkha environments flanking the shores of the embayment under an arid climate. Recognition of calcite pseudomorphs after anhydrite or gypsum nodules confirms the presence of saline

surface water and defines the likely starting-point for the ore-forming brines evolved. The braided fluvial conglomerates and sandstones would have initially displayed excellent aquifer properties due to their homogeneity and lateral continuity. The units also lacked sedimentological or diagenetic aquitards and therefore permitted vertical as well as lateral fluid migration. The Copper Harbor Formation transitions gradationally into the overlying Nonesuch Formation over several meters. The Junior Member of the basal Nonesuch Formation can be correlated across the basin, suggesting the contact is isochronous. The contact therefore represents a flooding surface and contains the most carbonaceous part of the Nonesuch Formation.

5.3. Chapter 3 – The White Pine deposit

The White Pine deposit is located on the eastern flank of the Porcupine Mountains Volcanic Structure (PMVS), a caldera that formed a prominent paleo-topographic high during Copper Harbor deposition. The caldera is located on the southern margin of the deepest part of the basin. White Pine constitutes a natural focal point for fluids escaping during burial, with fluids sourced from a very large, and deep, catchment area or "kitchen". The distribution of alteration, bleaching and hydrocarbon staining suggests fluids migrated through the upper Copper Harbor Formation, beneath Nonesuch Formation shales. Small syn-sedimentary faults including the White Pine fault acted as cross-stratal fluid short-cuts.

Initial pore fluids in the redbed aquifer were seawater-derived brines. Detrital grains in the Copper Harbor Formation are rimmed by early diagenetic illite and hematite formed during eodiagenesis. These early-diagenetic phases are ubiquitous in the Copper Harbor Formation and record the breakdown of lithic fragments and labile minerals that released metals and cations into the ore fluids. Fluids were particularly rich in Mg and Fe owing to the abundance of mafic lithic fragments. Reduced pore fluids, possibly as a precursor to oil migration, resulted in the reduction of Fe and Mg and the formation of authigenic chlorite rims during mesodiagenesis. Chlorite rims formed in coarse-grained well-sorted sandstones in the upper Copper Harbor Formation and in the hanging walls of syn-sedimentary faults, and played an important role in maintaining these primary porosity pathways during continued burial compaction. Oil sourced from the down-dip extents of the Nonesuch Formation migrated into the White Pine anticline, utilising these same permeability pathways.

Mineralisation occurred at c. 1039 Ma, c. 40 M.y after deposition of the host rocks and during deposition of the Freda Formation at approximately 125˚C and a depth of 4 km. Mineralising fluids re-utilised earlier permeability pathways preserved by authigenic chlorite rims. In Copper Harbor Formation sandstones, ore fluids were reduced by liquid petroleum, producing native copper under relatively oxidised conditions. Reduction of ore fluids by *in situ* organic matter in Nonesuch Formation shales produced vertically and laterally zoned native copper and Cu-(Fe-)sulphide mineralisation. Copper sulphides nucleated on detrital and authigenic chlorite as a source of Fe, and thermochemical sulphate reduction was the dominant mechanism of sulphide precipitation. The bulk of mineralisation filled interstitial pores but later mineralisation occupied small-scale veinlets and fractures as fluids became over-pressured in response to porosity occlusion, basin inversion and, or, continued burial. Late quartz, calcite and minor anhydrite cements post-dated copper mineralisation.

5.4. Chapter 4 – Basin dynamics

Development of the Midcontinent Rift System (MRS) was initiated during a period of relative tectonic quiescence approximately 20 Myr prior to the Ottawan phase of the Grenvillian Orogeny (Stein et al., 2014). The earliest stratigraphic record of the MRS comprises clastic sedimentary units, such as the Bessemer Quartzite, that contain tidal bedforms indicating a marine influence on the interior of Laurentia during this time (Ojakangas and Morey, 1982). Clastic sedimentation was soon superseded by mafic volcanism, notable for the volume of flood basalts and their extraordinary thicknesses (Stein et al., 2015).

Crucially, the mode of accumulation of sedimentary and volcanic rocks in any given basin records much about its mechanisms of formation. Contrary to previous interpretations of the MRS (e.g. Behrendt et al., 1988; Cannon et al., 1989; Stein et al., 2015) this study did not identify major basin-bounding syn-volcanic normal faults in reflection seismic data. Laterally continuous reflectors representing individual flows within the Portage Lake Volcanics Group and Powder Mill Group thicken gradually towards the axial portion of the basin. No abrupt thickness changes, significant offsets nor wedge-shaped terminations were observed that might indicate syn-volcanic/depositional faulting. Younger flows are more shallowly dipping than the older flows they overlie, suggesting accommodation space was generated primarily by

syn-volcanic subsidence. With the exception of minor flows, tuffs and intrusions, volcanism in the MRS ended abruptly at c. 1090 Ma (Swanson-Hysell et al., 2019); coincident with the onset of the Ottawan phase of the Grenvillian Orogeny (Rivers et al., 2012).

Post-volcanic sedimentary units (the Oronto Group and Jacobsville Sandstone) also display laterally extensive, sag-like geometries. The oldest of these, the Copper Harbor Formation, infills a pre-existing topography above the Portage Lake Volcanics Group and is conformably overlain by the Nonesuch Formation. The Copper Harbor and Nonesuch formations record the second and final period of marine-influenced sedimentation in the MRS. The Freda Formation lies unconformably above the Nonesuch Formation. Its depositional age is estimated to be c. 1060 Ma and its relatively mature composition and evidence of deformation prior to deposition of the Jacobsville Sandstone, suggest it may be a molasse from the Ottawan phase of the Grenvillian Orogeny. The maximum age of the Jacobsville Sandstone (959 ± 19 Ma, Malone et al., 2016) is, within error of detrital zircon ages, coincident with the Rigolet phase of Grenville orogenesis and likely also represents a molasse. Migration of the axial portion of the basin over time suggests Grenville orogenesis caused significant warping and tilting of the crust.

New high precision U-Pb zircon ages provide important new constraints on the genesis of the upper Keweenawan Supergroup. Ages of the upper and lower parts of the Porcupine Mountains Volcanic Complex show volcanism lasted for 2.5 Myr, from 1091.26 ± 0.23 Ma to 1088.74 ± 0.24 Ma. The age of the uppermost rhyolite provides a maximum age of the Copper Harbor Formation which unconformably overlies it. An ash bed near the top of the Copper Harbor Formation, dated at 1079.49 ± 0.35 Ma, is the youngest magmatic zircon age in the MRS to date and constrains the age of the basal Nonesuch Formation to c. 1078.1 Ma.

Subsidence analysis of the 17 km-thick Keweenaw Supergroup incorporated these new high-precision U-Pb ages. The lower part of the stratigraphy, dominated by volcanic rocks, accumulated at a rate of between 400 and 900 m/Myr. Subsidence slowed rapidly during deposition of the Oronto Group and Jacobsville Sandstones to c. 150 m/Myr. Backstripping of units confirmed the majority of subsidence was driven by the loading of volcanic and sedimentary material on the crust, and not stretching.

The MRS lacks many of the diagnostic features of rift basins such as syn-sedimentary faults, alluvial fans, debris flows, proximally-sourced immature material and bimodal transverse and axial drainage patterns (c.f. White and Wright, 1960; Hambin and Horner, 1961; Daniels, 1982; Merk and Jirsa, 1982). Subsidence analysis and the geometries of volcanic and sedimentary units suggest basin formation was due primarily to loading, not stretching. The MRS formed in a relatively tectonically quiescent period prior to the main phase of the Grenvillian Orogeny, and an impactogen model (Gordon and Hempton, 1986) can therefore be discounted. Determining the causal geodynamical processes that initiated the basin was beyond the scope of this study. Subsequent to the deposition of the Nonesuch Formation, sediment accumulation in the basin records molasse shedding from the evolving Grenvillean orogenic belt to the east: initially the Freda Formation during the Ottawan phase and later the Jacobsville Sandstone during the Rigolet phase.

5.5. Future research

Phanerozoic sediments cover the MRS outside of the Lake Superior area, its extent in the subsurface is reliant on geophysical surveys and sparse drill cores but the true extent of the basin is unknown. Further study of cores from key areas would help provide constraints to better guestimate the true limits of the basin and insights into variations in the stratigraphy, structure and economic potential of the rest of the basin. In particular, mapping facies variations along the rift may provide a clearer picture of the paleogeography of Laurentia and the Grenville Mountains during the late Mesoproterozoic. An important question is assessing which parts of the basin may have been subject to marine incursions and what parts archive a complete record of terrestrial sedimentation during this key period of Earth's history.

The application of additional geochronology methods to date mineralisation or components of the mineral system is warranted. This would provide greater confidence in the mode of ore genesis (i.e. compaction drive) and provide insights into the age of authigenic minerals. Ar-Ar dating of illite may reveal discrete fluid flow events or dating of authigenic minerals such as xenotime or monazite using the U-Pb technique may reduce uncertainties. Ar-Ar dating of the Bear Lake rhyolite, coeval with deposition of the Freda Formation, would provide a significant constraint of the age of the upper Keweenaw Supergroup.

Analyses of fluid inclusions would elucidate the composition of fluids in the basin during their entrapment. Determining the salinity, temperature, halogen composition and δD–$\delta^{18}O$ of inclusions from quartz and calcite cement and calcite veins would enhance the understanding of basin's fluid flow regime.

5.6. References

Behrendt, J.C., Green, A.G., Cannon, W.F., Hutchinson, D.R., Lee, M.W., Milkereit, B., Agena, W.F. and Spencer, C., 1988. Results from GLIMPCE deep seismic reflection profiles over the mid-continent rift system. Geology, 16, pp.81-85.

Cannon, W.F., Green, A.G., Hutchinson, D.R., Lee, M., Milkereit, B., Behrendt, J.C., Halls, H.C., Green, J.C., Dickas, A.B., Morey, G.B. and Sutcliffe, R., 1989. The North American Midcontinent rift beneath Lake Superior from GLIMPCE seismic reflection profiling. Tectonics, 8(2), pp.305-332.

Daniels Jr, P.A., 1982. Upper Precambrian sedimentary rocks: Oronto Group, Michigan-Wisconsin. Geology and tectonics of the Lake Superior basin: Geological Society of America Memoir, 156, pp.107-133.

Gordon, M.B. and Hempton, M.R., 1986. Collision-induced rifting: the Grenville Orogeny and the Keweenawan rift of North America. Tectonophysics, 127(1-2), pp.1-25.

Hamblin, W.K. and Horner, W.J., 1961. Sources of the Keweenawan conglomerates of northern Michigan. The Journal of Geology, 69(2), pp.204-211.

Malone, D.H., Stein, C.A., Craddock, J.P., Kley, J., Stein, S. and Malone, J.E., 2016. Maximum depositional age of the Neoproterozoic Jacobsville Sandstone, Michigan: Implications for the evolution of the Midcontinent Rift. Geosphere, 12(4), pp.1271-1282.

Merk, G.P. and Jirsa, M.A., 1982. Provenance and tectonic significance of the Keweenawan interflow sedimentary rocks. In Geology and tectonics of the Lake Superior basin (Vol. 156, pp. 97-106). Geological Society of America.

Ojakangas, R.W. and Morey, G.B., 1982. Keweenawan pre-volcanic quartz sandstones and related rocks of the Lake Superior region. World, RJ, and Hinze, EJ, eds. Geology and tectonics of the Lake Superior basin. Geol. Soc. Am. Mem, 156, pp.85-96.

Rivers, T., 2015. Tectonic setting and evolution of the Grenville Orogen: An assessment of progress over the last 40 years. Geoscience Canada, 42(1), pp.77-124.

Stein, C.A., Stein, S., Merino, M., Randy Keller, G., Flesch, L.M. and Jurdy, D.M., 2014. Was the Midcontinent Rift part of a successful seafloor-spreading episode?. Geophysical Research Letters, 41(5), pp.1465-1470.

Stein, C.A., Kley, J., Stein, S., Hindle, D. and Keller, G.R., 2015. North America's Midcontinent Rift: when rift met LIP. Geosphere, 11(5), pp.1607-1616.

Swanson-Hysell, N.L., Ramezani, J., Fairchild, L.M. and Rose, I.R., 2019. Failed rifting and fast drifting: Midcontinent rift development, Laurentia's rapid motion and the driver of Grenvillian orogenesis. Bulletin, 131(5-6), pp.913-940.

White, W.S. and Wright, J.C., 1960. Lithofacies of the Copper Harbor Conglomerate, northern Michigan. US Geol. Surv. Prof. Pap.

Blank page

Chapter 6

Lessons applicable to the sediment-hosted stratiform Cu deposit model

6.1. Introduction

Numerous studies of sediment-hosted Cu (SHC) deposits and their environs have contributed to a broad body of knowledge on this style of ore deposit, and a good understanding of their formation mechanisms. Important similarities between deposits have highlighted common processes, locations and periods of Earth's history that are either critical for, or conducive to, the formation of large sediment-hosted stratiform Cu deposits (see Chapter 1). Differences between deposits may also highlight subtle sensitives of the underlying formation processes.

The aims of this chapter are twofold. Firstly, to integrate the findings of this study with the existing understanding of sediment-hosted stratiform Cu deposits in order to refine and enhance the genetic model. Secondly, to highlight and explicate the unique aspects of the White Pine and Midcontinent Rift System (MRS).

Direct detection of deposits, via geological, geochemical and geophysical techniques, and conceptual or predictive targeting through genetic models, are the two fundamental approaches to mineral exploration. Accurate and detailed genetic or conceptual models are a prerequisite for conducting successful and cost-effect predictive mineral exploration programs. In addition, the generative, or basin-selection stage of exploration, relies almost entirely on these conceptual models to identify basins which are likely to have produced sediment-hosted stratiform Cu systems.

The sections in this chapter link specific aspects of this study with previous research on the deposit type. Section 6.2 (Paleo-environment) corresponds to the finding of Chapter 2 (Sedimentology); Section 6.3 (Basin architecture) to Chapter 4 (basin dynamics); and Sections 6.4 (Fluid flow) and 6.5 (Ore deposition) to Chapter 3 (White Pine genesis).

6.2. Paleo-environment

The paleo-environmental setting of the MRS resembles that of other large sediment-hosted copper systems which typically formed in intracratonic basins in the interiors of supercontinents, at low paleo-latitudes (Jowett, 1989; Brown, 1997; Hitzman et al., 2010). Deposition of the Copper Harbor and Nonesuch formations occurred when the basin was at paleo-latitudes of less than 25˚ (Swanson-Hysell et al., 2019), in the interior of the proto-Rodinia supercontinent (Cawood and Pisarevsky, 2017). See paleo-reconstruction Fig. 6.1.

The stratigraphy of the Copper Harbor and Nonesuch formations records a combination of braided fluvial, sabkha and shallow-marine embayment depositional settings. The continentality of the basin and its low paleo-latitude promoted high rates of evaporation. Several attributes of the Copper Harbor and lower Nonesuch formations imply a protected or partially restricted marine embayment. Shallow water depths, an absence of storm-generated bedforms (below the upper Nonesuch Formation), the asymmetry of ripples, the presence of evaporites and preserved carbonaceous matter all suggest an embayment that was partially restricted from an open ocean (Jones et al., 2020). Evaporation of limited or periodic influxes of ocean water produced evaporite minerals and a residual brine or brackish water, and the low-energy setting promoted stratification of the water column conducive to the preservation of organic matter. In these regards the basin resembles other major SHC systems such as the Zechstein and Katangan basins (Hitzman et al., 2010). Most large SHC systems display a temporal link with global glaciation events, which likely elevated the sulphate budget of the oceans (Hitzman et al., 2010). The absence of global glaciation events in the Mesoproterozoic and the generally low seawater sulphate levels in the late-Mesoproterozoic (Kah et al., 2004) distinguishes White Pine from other SHC systems. We attribute the predominance of low-sulphur ore minerals (native copper and chalcocite) in the MRS to the low sulphate concentrations in the prevailing seawater.

An emerging question concerning the development of the MRS is the extent to which its constituent parts or sub-basins were linked. In the context of the Neoproterozoic basins of Southern Africa, which formed later in the history of Rodina, the Katangan basin of Zambia and the Democratic Republic of Congo is considerably more well-endowed with Cu resources than the equivalent age units in the Damara Belt of Namibia (Cox et al., 2007). Hitzman et al. (2005, 2010) attribute this to the Katangan basin's intermittent hydrological connection with the open ocean that resulted in thick evaporite sequences that produced efficient metal-transporting brines, and contained these brines for a protracted period (>350 Myr). The scope of this study was limited to the mineralised portion of the MRS that mantles the shoreline of Lake Superior, but a true understanding of the paleo-geography and prospectivity of the MRS requires analysis of all its constituent parts to determine which were subject to marine incursions and when, which produced evaporites or residual brines and

which had the requisite geodynamic conditions to produce Cu deposits. The location of seaways connecting the Lake Superior portion of the MRS to the ocean are a key unknown but we speculate they did not breach the juvenile Grenville Mountains to the (paleo-) south of the MRS (Fig. 6.1).

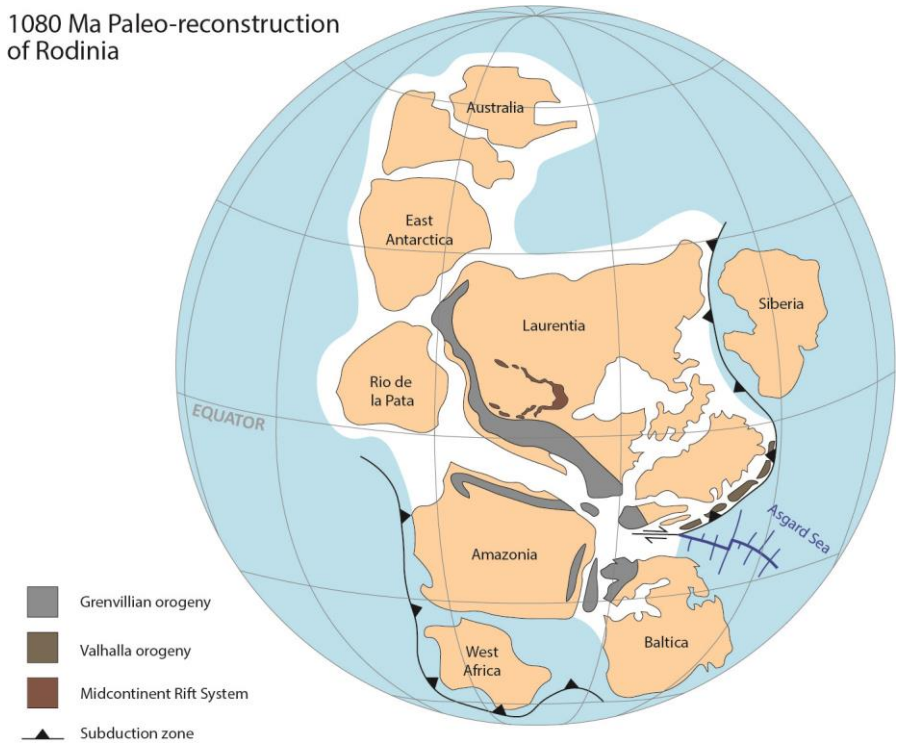

Fig. 6.1. Paleo-reconstruction of Rodinia at 1080 Ma (Nonesuch deposition). Modified after Cawood and Pisarevsky (2017) and Swanson-Hysell et al. (2019). Position of Midcontinent Rift from Stein et al. (2014).

6.3. Basin architecture

The geodynamic setting of the MRS displays both similarities and differences to other SHC basins. The MRS formed in an intracratonic setting during assembly of the supercontinent Rodinia (Li et al., 2008). The amalgamation and subsequent dispersal of Rodinia produced several other notable SHC systems including Redstone, Canada (Milton et al., 2017), and the Central African Copperbelt (Selley et al., 2005). However, whereas those SHC systems formed during continental dispersal in the Neoproterozoic, the MRS formed earlier in the amalgamation of Rodina, immediately prior to the Grenvillian Orogeny (Cawood et al., 2007). The driver of this localised extensional event is the subject of recent discussion and possible explanations include active rifting above a mantle plume (Hutchinson et al., 1990), seafloor spreading on

the eastern margin of Laurentia (Stein et al., 2014), and rapid plate motion in response to slab avalanche (Swanson-Hysell et al., 2019). However, the involvement of a mantle plume seems plausible regardless of the favoured mechanism of lithospheric extension, given the composition and large volume of mafic volcanic rocks in the MRS (Nicholson et al., 1997; Vervoort et al., 2007; Stein et al., 2015).

The MRS is unique amongst SHC systems for the large volume of basalts it contains. The only other system to contain noteworthy volumes of mafic rocks is the Zambian portion of the Central African Copperbelt (Kampunzu et al., 2000; Hitzman et al., 2012). The implications of the voluminous basalt in the MRS are likely twofold. First, the weathered basaltic detritus in the Copper Harbor Formation constituted a fertile source of Cu and other metals that were readily leachable by the comparatively feeble fluids in the MRS (i.e. low temperature and low salinity). Had these fluids not accessed such a fertile source of metals, White Pine would likely not have formed. In contrast, the relatively aggressive, higher temperature and higher salinity fluids of the Central African Copperbelt were able to form large deposits independently of such a rich source rock, by scavenging metals from a variety of benign sediments and basement rocks (Selley et al., 2005). Second, mafic volcanism in the MRS is the surface manifestation of a major thermal perturbation in the underlying asthenosphere. Irrespective of the cause of this anomaly, the elevated geothermal gradient in the crust likely overlapped with mineralisation at c. 1039 Ma. The heat may have contributed to the mineralising system by promoting circulation or convection of basinal fluids and by increasing their temperature and thus their capacity to transport metals. This resembles the coincidence of periods of mineralisation in the Central African Copperbelt with the Mwashya (c. 750 Ma) and Lufilian (c. 550 Ma) basalts; both of which are commonly interpreted as rifting events (Selley et al., 2005).

The amount of crustal extension in the MRS was very minor and appears not to have involved brittle faulting. Accommodation space was instead generated primarily by loading of volcanic and detrital material. The result was laterally continuous units with draped geometries evident in seismic profiles. This is compatible with the Copper Harbor Formation being a homogenous aquifer that promoted vertical and lateral fluid flow over 10s to 100s of kilometres, sealed beneath the laterally extensive Nonesuch Formation aquitard. The Freda Formation and Jacobsville Sandstone are syn-orogenic molasse deposits, formed in response to the Ottawan and Rigolet phases of Grenvillian

orogenesis respectively. Together they represent the distal effects of sedimentation in the foreland of the evolving Grenville Mountains and periods of simultaneous burial and crustal-shortening. In this regard the basin resembles the fore-arc setting of the Neuquén basin, Argentina (Pons et al., 2017).

6.4. Fluid flow

Initial pore water in the Copper Harbor Formation was the prevailing surface water: brackish to moderately saline estuarine water with a minor contribution of salinity from dissolution of anhydrite and gypsum. Although the precise composition and salinity of fluids were not determined in this study, they were likely similar to those in other low temperature SHC deposits (e.g. Paradox basin, Morrison and Parry, 1986; Kupferschiefer, Tonn et al., 1987).

The widespread nature of illite and hematite in the Copper Harbor Formation, including in the cores of grains and pebbles, suggests these fluids permeated widely. The volcanic-rich detritus of the Copper Harbor Formation provides a readily-leachable source of metals that is exceptional amongst SHC systems. The only significant alteration associated with the fluid flow regime that formed White Pine is authigenic chlorite, which preceded mineralisation and was the product of Fe and Mg leached from basaltic lithic fragments. Authigenic chlorite has not been described in other SHC systems but is reported in oil reservoir rocks that contain a high proportion of basaltic detrital grains and which are prone to generating fluids with an excess of Fe and Mg (e.g. Santos basin, Brazil, Anjos et al., 1999; Pearl River Mouth basin, China, Guojun et al., 2011). Rims of chlorite, and to a lesser extend illite, played a crucial role in maintaining primary porosity of sandstones by inhibiting both mechanical compaction and syntaxial quartz growth. The lack of sodic, magnesium or potassic alteration that characterises the Central African Copperbelt (Selley et al., 2018) is due to the relative low degrees of evaporation experienced in the MRS, which were insufficient to form minerals such as halite, carnallite or sylvanite.

Authigenic chlorite rims formed at the top of the aquifer (Copper Harbor Formation) and in the immediate vicinity of syn-sedimentary normal faults at White Pine, where Fe and Mg concentrations were high and conditions were relatively reduced. The distribution of pyrobitumen corresponds to that of authigenic chlorite and suggests migrating petroleum utilised primary permeability pathways that had

been preserved by earlier authigenic chlorite. The distribution of these phases suggests fluids were buoyant and flowed from high to low pressure areas in response to porosity reduction during burial.

6.5. Ore deposition

The age of disseminated chalcocite at White Pine was determined by Re-Os geochronology at 1039 Ma, approximately 40 Myr after deposition of the basal Nonesuch Formation. This is consistent with mineral paragenesis observations which suggest Cu-Ag mineralisation occurred relatively early in the basin history: post grain packing, spanning burial compaction but prior to occlusion of porosity by quartz and calcite cements. At the time of mineralisation the middle Freda Formation was being deposited and the basal Nonesuch Formation was buried at a depth of approximately 4 km and at a temperature of ~125˚C. The distal effects of the Ottawan phase of the Grenville Orogeny were appearing in the basin in the form of the unconformity surfaces at the base of the Freda Formation, the Freda molasse itself, and minor reverse faulting. The timing of mineralisation and alteration, and their distribution along a fluid escape route out of the basin, lead us to conclude that mineralising fluids were driven by burial compaction and the early effects of the Ottawan phase of Grenville orogenesis (Fig. 6.2).

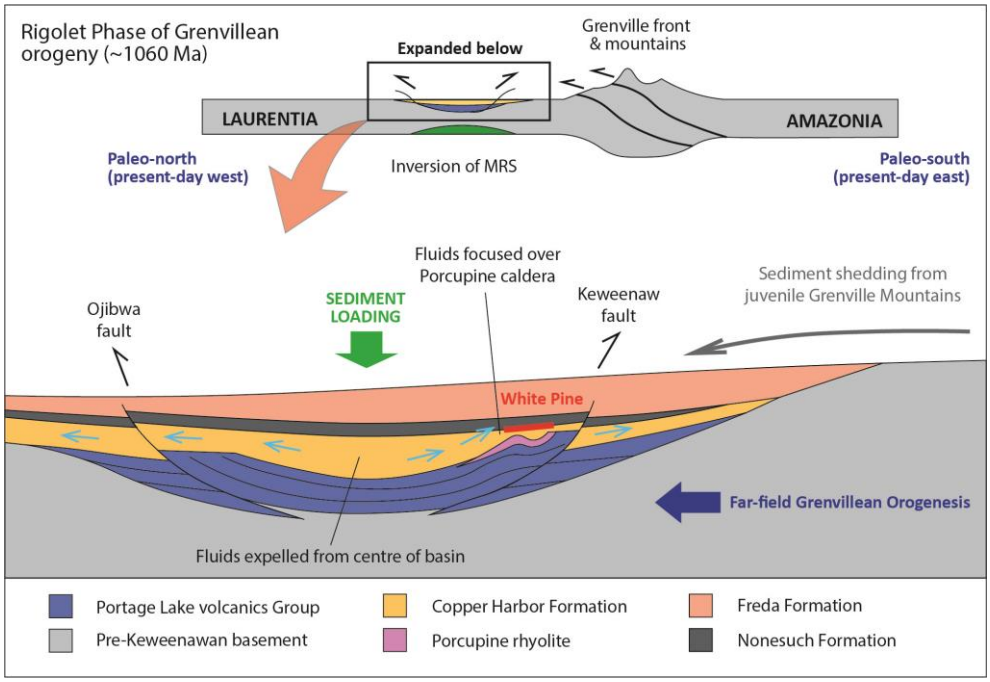

Fig. 6.2. Geodynamic setting of the Midcontinent Rift System at the time of mineralisation.

This study has enabled us to discount several genetic models that have previously been proposed for White Pine. Mauk et al., (1992) proposed a second stage of dominantly native Cu mineralisation at White Pine. Our research has demonstrated that mineralisation in reverse faults is volumetrically insignificant and temporally overlaps with main-stage mineralisation. Despite evidence of basin tilting due to Grenvillean Orogenesis, the symmetry of Cu occurrences either side of the rift axis, on Isle Royale and the Keweenaw Peninsula, and the sulphur isotope values of mineralisation are difficult to reconcile with the meteoric recharge model proposed by Brown (2006). New U-Pb age constraints on the Porcupine Mountains Volcanic Structure demonstrate that volcanism ceased c. 50 Myr prior to mineralisation and that latent heat from the caldera as proposed by Brown (2014) would have been insufficient to drive fluid flow.

The syn- to late-diagenetic timing of mineralisation resembles other SHC systems such as Spar Lake (c. 40-60 Myr after host rock deposition, Aleinikoff et al., 2012) and Dzhezkazgan (c. 10-20 Myr after host rock deposition, Box et al., 2012).

The White Pine paragenesis shows that liquid petroleum entered the Copper Harbor Formation sandstones before mineralisation. The same relative timing relationship between hydrocarbon accumulation and mineralisation is observed in many other SHC deposits including Mufulia (Zambia, Muchez et al., 2019), Dzhezkazgan (Kazakhstan, Box et al., 2012), Paradox basin (USA, Barton et al., 2018); and Spar Lake (Montana, Hayes et al., 2012). This suggests that in each basin, at the time of mineralisation, a portion of the stratigraphy had entered the oil window, and provides a rough approximation for the amount of time and the pressure-temperature conditions required to form a ‘fertile’ metal-bearing brine.

As fluids migrated towards the basin margin they encountered the attenuated Copper Harbor Formation aquifer above the Porcupine Mountains Volcanic Structure. This resulted in a portion of the fluid flow being routed through the basal Nonesuch Formation as shown in Fig. 6.3 and resembles basement highs in other SHC systems (e.g. Kafue anticline, Zambia, Selley et al., 2005; Fore Sudetic block, Kupferschiefer, Jowett, 1986). In contrast to many other interpretations of fluid flow regimes in SHC systems, we interpret fluid flow to have been sub-parallel to the mineral zones, out of the basin.

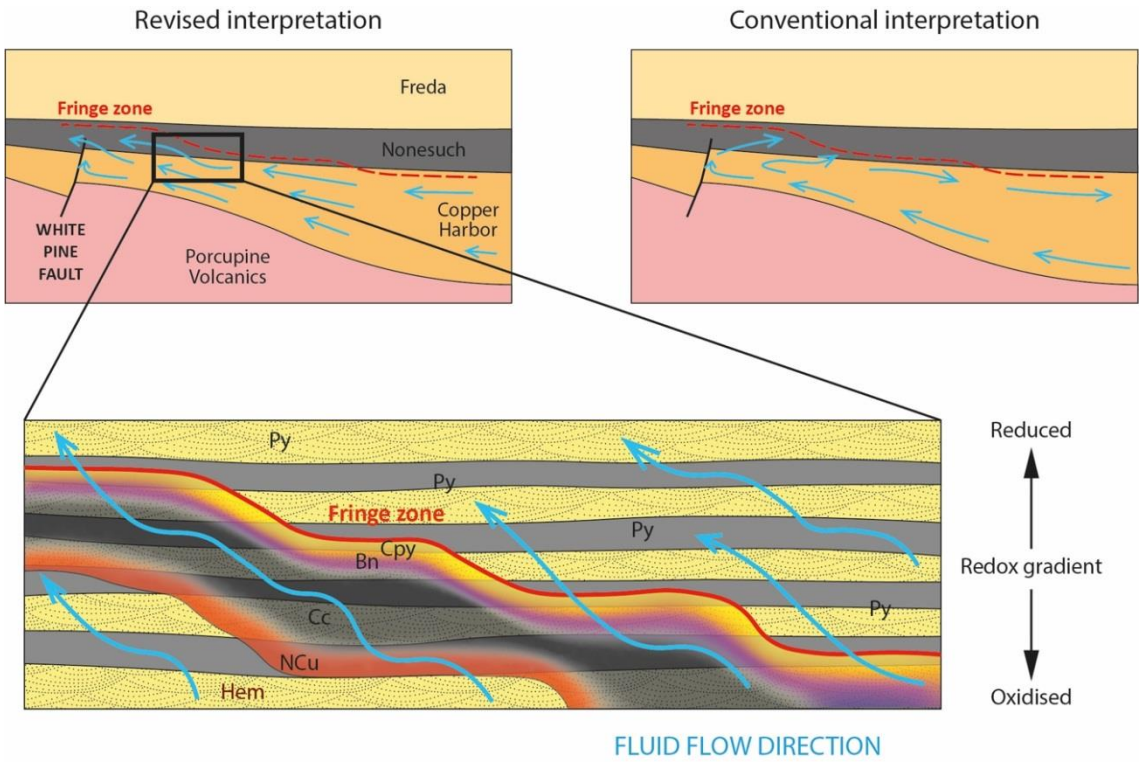

Fig. 6.3. Schematic representation of the paleo-fluid flow regime at White Pine.

Mineralisation in the Nonesuch Formation is peneconcordant displaying sulphide zoning similar to that seen in other shale-hosted SHC deposits (e.g. Kupferschiefer, Oszczepalski, 1999; Juramento, Durieux and Brown, 2007). Mineralisation rises higher in the stratigraphy adjacent to the Porcupine Mountains. Unique to White Pine is the presence of native copper at the base of the ore zone, the thickness of the chalcocite zone and the presence of greenockite (CdS) at the top of the ore zone. Sulphur isotopes indicate formation via thermochemical sulphate reduction. The precipitation of copper sulphides on chlorite grains as a source of Fe required for early stage minerals (pyrite, chalcopyrite and bornite) has not previously been described in other SHC systems. The presence of native copper with pyrobitumen in the upper Copper Harbor Formation is likely due to the relatively oxidised conditions which were insufficiently reduced to form Cu-sulphides.

6.6. References

Aleinikoff, J.N., Hayes, T.S., Evans, K.V., Mazdab, F.K., Pillers, R.M. and Fanning, C.M., 2012. SHRIMP U-Pb ages of xenotime and monazite from the Spar Lake red bed-associated Cu-Ag deposit, western Montana: Implications for ore genesis. Economic Geology, 107(6), pp.1251-1274.

Anjos, S.M.C., De Ros, L.F. and Silva, C.M.A., 1999. Chlorite authigenesis and porosity preservation in the Upper Cretaceous marine sandstones of the Santos Basin, offshore eastern Brazil. Clay mineral cements in sandstones, pp.289-316.

Barton, M.D., Barton, I. and Thorson, J., 2018. Paleofluid Flow in the Paradox Basin: Introduction. Guidebook series, 59.

Box, S.E., Syusyura, B., Seltmann, R., Creaser, R.A., Dolgopolova, A. and Zientek, M.L., 2012. Dzhezkazgan and associated sandstone copper deposits of the Chu-Sarysu basin, Central Kazakhstan. Econ. Geol. Sp. Publ, 16, pp.303-328.

Brown, A.C., 1997. World-class sediment-hosted stratiform copper deposits: Characteristics, genetic concepts and metallotects. Australian Journal of Earth Sciences, 44(3), pp.317-328.

Brown, A.C., 2006. Genesis of native copper lodes in the Keweenaw district, northern Michigan: a hybrid evolved meteoric and metamophogenic model. Economic Geology, 101(7), pp.1437-1444.

Brown, A.C., 2014. Latent thermal effects from Porcupine Volcanics calderas underlying the White Pine-Presque Isle stratiform copper mineralization, northern Michigan. Economic Geology, 109(7), pp.2035-2050.

Cawood, P.A., Nemchin, A.A., Strachan, R., Prave, T. and Krabbendam, M., 2007. Sedimentary basin and detrital zircon record along East Laurentia and Baltica during assembly and breakup of Rodinia. Journal of the Geological Society, 164(2), pp.257-275.

Cawood, P.A. and Pisarevsky, S.A., 2017. Laurentia-Baltica-Amazonia relations during Rodinia assembly. Precambrian Research, 292, pp.386-397.

Cox, D.P., Lindsey, D.A., Singer, D.A. and Diggles, M.F., 2003. Sediment-hosted copper deposits of the world: Deposit models and database. US Geological Survey Open-File Report, 3(107), p.50.

Durieux, C.G. and Brown, A.C., 2007. Geological context, mineralization, and timing of the Juramento sediment-hosted stratiform copper–silver deposit, Salta district, northwestern Argentina. Mineralium Deposita, 42(8), pp.879-899.

Guojun, C., Guichao, D., Gongcheng, Z., Qi, W., Chengfu, L. and Ji, C., 2011. Chlorite cement and its effect on the reservoir quality of sandstones from the Panyu low-uplift, Pearl River Mouth Basin.

Hayes, T.S., Landis, G.P., Whelan, J.F., Rye, R.O. and Moscati, R.J., 2012. The Spar Lake strata-bound Cu-Ag deposit formed across a mixing zone between trapped natural gas and metals-bearing brine. Economic Geology, 107(6), pp.1223-1249.

Hitzman, M., Kirkham, R., Broughton, D., Thorson, J. and Selley, D., 2005. The sediment-hosted stratiform copper ore system. Economic geology, 100.

Hitzman, M.W., Selley, D. and Bull, S., 2010. Formation of sedimentary rock-hosted stratiform copper deposits through Earth history. Economic Geology, 105(3), pp.627-639.

Hitzman, M.W., Broughton, D., Selley, D., Woodhead, J., Wood, D. and Bull, S., 2012. The Central African Copperbelt: diverse stratigraphic, structural, and temporal settings in the world's largest sedimentary copper district. Society of Economic Geologists Special Publication 16, (Paper 19), pp.487-514.

Hutchinson, D.R., White, R.S., Cannon, W.F. and Schulz, K.J., 1990. Keweenaw hot spot: Geophysical evidence for a 1.1 Ga mantle plume beneath the Midcontinent Rift System. Journal of Geophysical Research: Solid Earth, 95(B7), pp.10869-10884.

Jones, S.M., Prave, A.R., Raub, T.D., Cloutier, J., Stüeken, E.E., Rose, C.V., Linnekogel, S. and Nazarov, K., 2020. A marine origin for the late Mesoproterozoic Copper Harbor

and Nonesuch Formations of the Midcontinent Rift of Laurentia. Precambrian Research, 336, p.105510.

Jowett, E.C., 1986. Genesis of Kupferschiefer Cu-Ag deposits by convective flow of Rotliegendes brines during Triassic rifting. Economic Geology, 81(8), pp.1823-1837.

Jowett, E.C., 1989. Effects of continental rifting on the location and genesis of stratiform copper-silver deposits. In Geological Association of Canada (pp. 53-66).

Kah, L.C., Lyons, T.W. and Frank, T.D., 2004. Low marine sulphate and protracted oxygenation of the Proterozoic biosphere. Nature, 431(7010), p.834.

Kampunzu, A.B., Tembo, F., Matheis, G., Kapenda, D. and Huntsman-Mapila, P., 2000. Geochemistry and tectonic setting of mafic igneous units in the Neoproterozoic Katangan Basin, Central Africa: implications for Rodinia break-up. Gondwana Research, 3(2), pp.125-153.

Li, Z.X., Bogdanova, S.V., Collins, A.S., Davidson, A., De Waele, B., Ernst, R.E., Fitzsimons, I.C.W., Fuck, R.A., Gladkochub, D.P., Jacobs, J. and Karlstrom, K.E., 2008. Assembly, configuration, and break-up history of Rodinia: a synthesis. Precambrian research, 160(1-2), pp.179-210.

Mauk, J.L., Kelly, W.C., Van Der Pluijm, B.A. and Seasor, R.W., 1992. Relations between deformation and sediment-hosted copper mineralization: Evidence from the White Pine part of the Midcontinent rift system. Geology, 20(5), pp.427-430.

Milton, J.E., Hickey, K.A., Gleeson, S.A., Falck, H. and Allaz, J., 2017. In situ monazite dating of sediment-hosted stratiform copper mineralization in the Redstone Copper belt, Northwest Territories, Canada: Cupriferous fluid flow late in the evolution of a Neoproterozoic sedimentary basin. Economic Geology, 112(7), pp.1773-1806.

Morrison, S.J. and Parry, W.T., 1986. Formation of carbonate-sulfate veins associated with copper ore deposits from saline basin brines, Lisbon Valley, Utah; fluid inclusion and isotopic evidence. Economic Geology, 81(8), pp.1853-1866.

Muchez, P., Minnen, M., Dewaele, S. and Hulsbosch, N., 2019. The Geology of the Mufulira Deposit: Implications for the Metallogenesis of Arenite-Hosted Ore Deposits in the Central African Copperbelt. Ore Deposits: Origin, Exploration, and Exploitation, pp.57-74.

Oszczepalski, S., 1999. Origin of the Kupferschiefer polymetallic mineralization in Poland. Mineralium Deposita, 34(5-6), pp.599-613.

Pons, M.J., Franchini, M., Giusiano, A., Patrier, P., Beaufort, D., Impiccini, A., Rainoldi, A.L. and Meinert, L., 2017. Alteration halos in the Tordillos sediment-hosted copper deposit of the Neuquén Basin, Argentina. Ore Geology Reviews, 80, pp.691-715.

Selley, D., Broughton, D., Scott, R.J., Hitzman, M., Bull, S.W., Large, R.R., McGoldrick, P.J., Croaker, M. and Pollington, N., 2005. A new look at the geology of the Zambian Copperbelt. Society of Economic Geologists, Inc., 100.

Selley, D., Scott, R., Emsbo, P., Koziy, L., Hitzman, M.W., Bull, S.W., Duffett, M., Sabagenzi, S., Halpin, J. and Broughton, D.W., 2018. Structural configuration of the Central African Copperbelt: roles of evaporites in structural evolution, basin hydrology, and ore location. Economic Geology and The Bulletin of The Society of Economic Geologists, 21, pp.115-156.

Stein, C.A., Kley, J., Stein, S., Hindle, D. and Keller, G.R., 2015. North America's Midcontinent Rift: when rift met LIP. Geosphere, 11(5), pp.1607-1616.

Stein, C.A., Stein, S., Merino, M., Randy Keller, G., Flesch, L.M. and Jurdy, D.M., 2014. Was the Midcontinent Rift part of a successful seafloor-spreading episode?. Geophysical Research Letters, 41(5), pp.1465-1470.

Swanson-Hysell, N.L., Ramezani, J., Fairchild, L.M. and Rose, I.R., 2019. Failed rifting and fast drifting: Midcontinent rift development, Laurentia's rapid motion and the driver of Grenvillian orogenesis. Bulletin, 131(5-6), pp.913-940.

Tonn, H., Schmidt, F. P., Porada, H., and Horn, E. E., 1987, Untersuchungen von Flussigkeitseinschlussen im Zechstein als Beitrag zur Genese des Kupferschiefers [abs.]: Fortschr. Mineralogie, v. 65, p. 84.

Vervoort, J.D., Wirth, K., Kennedy, B., Sandland, T. and Harpp, K.S., 2007. The magmatic evolution of the Midcontinent rift: New geochronologic and geochemical evidence from felsic magmatism. Precambrian Research, 157(1-4), pp.235-268.

Appendices

A3. Supplementary data for White Pine

Table A3.1. Carbon and oxygen isotope data for White Pine.

Sample no.	Drill hole	Depth (m)	Group	Bed	$\delta^{13}C$ (‰, V-PDB)	$\delta^{18}O$ (‰, V-SMOW)
Early concretion						
310	WP387	292.88	Nonesuch	Top Zone	-7.55	21.69
294	WP184	219.20	Nonesuch	Dark Grey Massive	-13.38	17.30
Early diagenetic nodule						
308	WP184	202.65	Nonesuch	Marker	-4.73	22.02
328	WP163	420.76	Nonesuch	Marker	-4.57	21.36
307	WP184	205.50	Nonesuch	Marker	-1.29	23.17
325	WP163	425.44	Nonesuch	Massive Black Siltstone	-3.27	21.36
349	WP472	721.48	Nonesuch	Stripey	-7.98	22.55
324	WP163	425.86	Nonesuch	Stripey	-6.25	20.63
339	WP447	633.17	Nonesuch	Stripey	-4.16	21.55
348	WP472	722.18	Nonesuch	Stripey	-3.59	23.27
333	WP447	643.76	Nonesuch	Tiebel Sandstone	-11.52	23.27
317	WP387	281.43	Nonesuch	Tiebel Sandstone	-10.89	20.45
305	WP184	208.50	Nonesuch	Tiebel Sandstone	-10.56	18.83
301	WP184	211.38	Nonesuch	Tiebel Sandstone	-10.37	17.72
302	WP184	209.98	Nonesuch	Tiebel Sandstone	-10.29	18.30
303	WP184	209.39	Nonesuch	Tiebel Sandstone	-10.16	19.54
313-A	WP387	284.71	Nonesuch	Tiebel Sandstone	-10.10	18.07
300	WP184	211.57	Nonesuch	Tiebel Sandstone	-10.10	17.66
315	WP387	284.12	Nonesuch	Tiebel Sandstone	-10.03	19.12
304	WP184	209.03	Nonesuch	Tiebel Sandstone	-10.02	21.97
323	WP163	427.93	Nonesuch	Tiebel Sandstone	-9.71	20.40
336	WP447	639.48	Nonesuch	Tiebel Sandstone	-9.10	22.16
322	WP163	428.16	Nonesuch	Tiebel Sandstone	-8.90	18.71
306	WP184	208.17	Nonesuch	Tiebel Sandstone	-8.66	22.88
318	WP387	280.68	Nonesuch	Tiebel Sandstone	-8.16	19.93
337	WP447	638.63	Nonesuch	Tiebel Sandstone	-8.12	22.07
338	WP447	638.29	Nonesuch	Tiebel Sandstone	-6.00	22.61
311	WP387	288.36	Nonesuch	Red and Grey	-9.68	18.02
298-A	WP184	213.88	Nonesuch	Red and Grey	-7.90	14.61
332	WP447	647.39	Nonesuch	Brown Massive	-6.76	21.89
343	WP472	738.28	Nonesuch	Upper Transition	-10.43	20.18
295-A	WP184	217.54	Nonesuch	Upper Sandstone	-8.17	18.62
342	WP472	739.60	Nonesuch	Tiger	-7.73	22.82
331	WP447	649.26	Nonesuch	Dark Grey Massive	-8.19	27.21
309	WP387	293.25	Nonesuch	Dark Grey Massive	-5.13	23.23
319	WP163	438.71	Nonesuch	Red Massive	-5.30	20.15
64	WP029	21.50	CH	(grey)	-5.07	21.83

Late concretion						
312	WP387	286.35	Nonesuch	Tiebel Sandstone	-11.55	19.78
321	WP163	431.99	Nonesuch	Tiebel Sandstone	-10.23	17.10
316	WP387	282.48	Nonesuch	Tiebel Sandstone	-9.29	19.46
299	WP184	212.71	Nonesuch	Red and Grey	-10.04	17.36
296	WP184	216.75	Nonesuch	Brown Massive	-7.57	16.41
Late diagenetic nodule						
340	WP447	632.73	Nonesuch	Marker	-4.14	21.32
334	WP447	642.38	Nonesuch	Tiebel Sandstone	-11.42	20.51
344	WP472	732.61	Nonesuch	Tiebel Sandstone	-11.04	21.13
335	WP447	641.03	Nonesuch	Tiebel Sandstone	-10.43	21.80
345	WP472	730.91	Nonesuch	Tiebel Sandstone	-10.32	21.83
267	WP479	624.60	Nonesuch	Tiebel Sandstone	-10.02	22.63
320	WP163	434.58	Nonesuch	Upper Zone of Values	-6.62	23.43
Domino						
63	WP029	21.15	Nonesuch	Domino	-11.59	41.32
97	WP291	1153.00	Nonesuch	Domino	-11.17	37.09
133	WP436	259.30	Nonesuch	Domino	-7.70	18.95
341	WP472	741.16	Nonesuch	Domino	-7.36	20.79
73-A	WP042	557.75	Nonesuch	Domino	-6.65	21.67
127	WP429	395.50	Nonesuch	Domino	-6.19	19.23
329	WP447	650.15	Nonesuch	Domino	-5.11	22.87
Cement						
159	WP565	299.45	Freda	n/a	-7.57	19.19
138	WP552	374.10	Freda	n/a	-7.04	34.11
139	WP552	565.75	Freda	n/a	-6.90	20.17
158	WP565	110.20	Freda	n/a	-6.26	19.61
130	WP436	249.90	Nonesuch	Tiebel Sandstone	-15.06	29.61
108	WP345	177.10	Nonesuch	Tiebel Sandstone	-9.04	20.48
80	WP157	975.30	Nonesuch	Tiebel Sandstone	-6.45	16.67
125	WP429	388.05	Nonesuch	Tiebel Sandstone	-4.60	19.58
79	WP157	973.70	Nonesuch	Tiebel Sandstone	-3.82	19.12
85	WP198	852.30	Nonesuch	Massive Grey Siltstone	-11.22	15.57
253	WP157	980.60	Nonesuch	Upper Zone of Values	-6.68	22.04
61-A	WP029	16.80	Nonesuch	Brown Massive	-7.44	15.20
131	WP436	257.60	Nonesuch	Thinly	-9.83	20.48
91	WP242	891.58	Nonesuch	Thinly	-9.02	17.44
120	WP398	726.30	Nonesuch	Upper Sandstone	-12.02	19.86
96	WP291	1150.60	Nonesuch	Upper Sandstone	-11.26	15.93
126	WP429	390.60	Nonesuch	Upper Sandstone	-10.77	24.31
258	WP447	647.90	Nonesuch	Upper Sandstone	-10.58	21.10
87	WP198	858.95	Nonesuch	Upper Sandstone	-10.43	19.31
71	WP042	555.25	Nonesuch	Upper Sandstone	-9.76	17.30
92	WP242	893.30	Nonesuch	Upper Sandstone	-9.34	17.83
132	WP436	258.00	Nonesuch	Upper Sandstone	-8.69	18.73
62	WP029	18.10	Nonesuch	Upper Sandstone	-5.51	20.49
263	WP387	292.60	Nonesuch	Upper Sandstone	-4.75	21.01
111-A	WP345	187.40	Nonesuch	Dark Grey Massive	-7.02	20.61
330	WP447	649.74	Nonesuch	Red Massive	-11.37	22.10
88	WP198	863.70	CH	(grey)	-9.77	17.59

59-A	WP021	35.95	CH	(grey)	-9.61	17.39
82	WP157	982.10	CH	(grey)	-9.24	16.22
94	WP242	896.55	CH	(grey)	-8.70	32.25
128	WP429	395.85	CH	(grey)	-8.07	31.89
254	WP157	988.10	CH	(grey)	-7.74	16.15
83	WP157	990.00	CH	(grey)	-7.22	16.80
74	WP042	559.60	CH	(grey)	-6.70	26.76
122	WP398	728.85	CH	(grey)	-6.61	20.38
275-A	WP472	750.30	CH	(grey)	-6.45	16.65
134	WP436	259.80	CH	(grey)	-6.40	18.16
77	WP059	100.95	CH	(grey)	-6.33	17.46
259	WP447	657.60	CH	(grey)	-6.09	18.03
99	WP291	1156.90	CH	(grey)	-5.82	18.16
135	WP436	263.30	CH	(grey)	-5.61	18.38
274-A	WP472	744.00	CH	(grey)	-5.61	24.36
261	WP163	439.80	CH	(grey)	-5.52	21.38
270	WP387	295.25	CH	(grey)	-5.02	19.45
273	WP184	221.70	CH	(grey)	-4.67	19.30
282	WP163	461.50	CH	(grey)	-4.55	15.07
279	WP163	448.50	CH	(grey)	-3.94	19.52
281	WP163	460.60	CH	(grey)	-3.80	16.84
262	WP163	458.20	CH	(grey)	-3.28	18.17
283	WP447	651.85	CH	(grey)	-2.09	34.09
75	WP042	572.75	CH	(red)	-6.64	35.03
266	WP184	224.75	CH	(red)	-6.02	19.29
89-B	WP198	868.30	CH	(red)	-5.22	18.34
112-A	WP345	191.60	CH	(red)	-5.09	17.43
65	WP029	31.90	CH	(red)	-4.91	17.66
60	WP021	49.80	CH	(red)	-4.45	16.86
269	WP479	638.60	CH	(red)	-4.35	19.65
66	WP029	35.35	CH	(red)	-4.35	16.56
124	WP398	748.45	CH	(red)	-4.19	18.60
90	WP198	875.70	CH	(red)	-3.65	18.82
100	WP291	1164.10	CH	(red)	-3.54	17.66
123	WP398	737.70	CH	(red)	-3.51	20.11
116	WP345	351.45	CH	(red)	-3.50	28.42
76	WP042	585.00	CH	(red)	-2.67	21.10
115	WP345	305.40	CH	(red)	-2.66	20.56
117	WP345	392.30	CH	(red)	-2.47	22.08
114	WP345	271.80	CH	(red)	-1.98	23.15
118	WP345	398.10	PLV	n/a	-1.45	19.27
Veins						
286	WP501	778.46	Nonesuch	Marker	-4.77	15.00
326	WP163	423.46	Nonesuch	Marker	-3.83	13.94
287	WP501	763.22	Nonesuch	Marker	-3.04	15.04
277	WP472	724.40	Nonesuch	Marker	-2.55	15.44
327	WP163	421.91	Nonesuch	Marker	-2.35	15.59
346	WP472	726.44	Nonesuch	Massive Black Siltstone	-3.66	16.32
347	WP472	724.74	Nonesuch	Stripey	-2.54	16.64
314	WP387	284.44	Nonesuch	Tiebel Sandstone	-9.91	14.33
298-B	WP184	213.88	Nonesuch	Red and Grey	-6.47	10.41
297	WP184	216.46	Nonesuch	Brown Massive	-7.91	14.12

360	Outcrop	0.00	Nonesuch	Upper Sandstone	-7.52	22.40
295-B	WP184	217.54	Nonesuch	Upper Sandstone	-2.09	34.09
111-B	WP345	187.40	Nonesuch	Dark Grey Massive	-6.96	21.20
59-B	WP021	35.95	CH	(grey)	-9.35	15.93
274-B	WP472	744.00	CH	(grey)	-8.77	16.39
276	WP472	758.90	CH	(grey)	-6.66	16.15
275-B	WP472	750.30	CH	(grey)	-6.43	16.21
272	WP387	313.60	CH	(grey)	-4.12	19.25
89-A	WP198	868.30	CH	(red)	-6.37	13.48
112-B	WP345	191.60	CH	(red)	-5.27	13.88

Abbreviations: PLV, Portage Lake volcanics Group; CH, Copper Harbor Formation; Nonesuch, Nonesuch Formation; Freda, Freda Formation.

Table A3.2. Sulphur isotope date for White Pine.

Sample no.	Drill hole	Depth (m)	Formation	Bed	Mineral	Description	$\delta^{34}S$ (‰, V-CDT)
91	WP242	891.58	Nonesuch	Thinly	Cc (+ Ncu)	~1mm Cc grains along fine sand laminae in black siltstone	-14.0
86	WP198	856.37	Nonesuch	Thinly	Cc	1-3mm size replacive Cc grains along sand laminae in shale and around desiccation cracks (Re-Os geochronology sample)	-13.7
255	WP472	738.20	Nonesuch	Thinly	Cc	<1mm grains of disseminated Cc along fine sand laminae in black siltstone	-11.4
294	WP184	219.20	Nonesuch	Dark Grey Massive	Cc	1mm Cc grains in early calcite concretion	-9.5
81	WP157	981.38	Nonesuch	Thinly	Cc (+ Ncu)	>1mm sheets of Cc and NCu along sand laminae in siltstone	-7.9
67	WP038	108.20	Nonesuch	Dark Grey Massive	Cc (+ Ncu)	<1mm grains of evenly disseminated Cc and NCu in massive black siltstone	-3.1
360-A	(outcrop)	(n/a)	Nonesuch	Dark Grey Massive	Bn	2-3mm grains in 4mm wide linear vertical calcite vein	-1.4
72-A	WP042	557.00	Nonesuch	Dark Grey Massive	Cc (+ Ncu)	<1mm grains of evenly disseminated Cc and NCu in massive black siltstone	-0.2
97	WP291	1153.00	Nonesuch	Domino	Cc	Single 1mm thick sheet of Cc in massive grey siltstone	0.4
269	WP479	638.60	Nonesuch	Lower Transition Zone	Cc (+ Ncu)	<1mm evenly disseminated Cc and NCu in massive black siltstone	0.9
309	WP387	293.25	Nonesuch	Dark Grey Massive	Cc	<1mm disseminated Cc in massive black siltstone	0.9
127-A	WP429	395.50	Nonesuch	Domino	Cc	<1mm Cc sheets along sand laminae in black siltstone	2.1
93	WP242	895.95	Nonesuch	Domino	Cc (+ Ncu)	>2mm grains of replacive Cc and NCu in 1-3 mm sandstone laminae within black siltstone	3.6

Table A3.2. (Continued)

Sample no.	Drill hole	Depth (m)	Formation	Bed	Mineral	Description	$\delta^{34}S$ (‰, V-CDT)
341	WP472	741.16	Nonesuch	Domino	Cc	>1mm grains of Cc in Junior Member (2 cm thick calcite bed)	4.3
265	WP184	206.00	Nonesuch	Massive Black Siltstone	Py	<1mm disseminated euhedral pyrite grains in massive black siltstone	5.9
296	WP184	216.75	Nonesuch	Brown Massive	Cc	>1mm grains and irregular vein of Cc cutting late calcite concretion, massive brown-red siltstone	7.0
72-B	WP042	557.00	Nonesuch	Dark Grey Massive	Cc (+ NCu)	<1mm linear Cc-only vein cutting massive black siltstone	8.1
109-A	WP345	186.10	Nonesuch	Upper Sandstone	Cc	<1mm linear Cc-only vein cutting medium-grained chloritic sandstone	10.0
98	WP291	1154.00	Nonesuch	Lower Transition Zone	Cc	>1mm Cc grains in fine-grained chloritic sandstone with minor shale laminae	10.5
109-B	WP345	186.10	Nonesuch	Upper Sandstone	Cc	>1mm Cc grains in fine-grained chloritic sandstone	10.9
59	WP021	35.95	Nonesuch	Lower Transition Zone	Cc	>1mm Cc grains in fine-grained chloritic sandstone	12.6
127-B	WP429	395.50	Nonesuch	Domino	Cc	<1 and >1mm Cc grains in sand laminae within black siltstone	13.8
310	WP387	292.88	Nonesuch	Top Zone	Cc	1mm Cc grains in early calcite concretion	15.3
61	WP029	16.80	Nonesuch	Brown Massive	Py	1mm euhedral Py grains in calcite pseudomorph of evaporite nodule	16.3
134-A	WP436	259.80	Nonesuch	Lower Transition Zone	Cc (+ NCu)	Coarse (2mm) Cc cement in sandstone laminae	16.4
85	WP198	852.30	Nonesuch	Tiebel Sandstone	Py	Fine (<1mm) Py grains in fine-grained chloritic sandstone	17.3
87	WP198	858.95	Nonesuch	Upper Sandstone	Cc	Fine (<1mm) Cc blebs in chloritic cross bedded fine sandstone	17.8
121	WP398	728.00	Nonesuch	Domino	Cc	1mm Cc blebs along sandy laminae within grey siltstone	18.4

Table A3.2. (Continued)

Sample no.	Drill hole	Depth (m)	Formation	Bed	Mineral	Description	$\delta^{34}S$ (‰, V-CDT)
121	WP398	728.00	Nonesuch	Domino	Cc	1mm Cc blebs along sandy laminae within grey siltstone	18.4
119	WP398	724.85	Nonesuch	Thinly	Cc	1-2mm sheets of replacive Cc along sand laminae in black siltstone	18.9
110	WP345	186.65	Nonesuch	Domino	Cc (+ NCu)	1-2mm Cc and minor NCu grains in sand laminae within green-grey siltstone	21.6
331	WP447	649.26	Nonesuch	Dark Grey Massive	Cc	<1mm disseminated Cc in massive black siltstone	21.6
63	WP029	21.15	Nonesuch	Domino	Cc	1mm Cc sheets in black siltstone	24.1
131	WP436	257.60	Nonesuch	Thinly	Cc	1-2mm replacive Cc sheets along sand laminae within black siltstone	29.9

Abbreviations: Cc, chalcocite; NCu, native copper, Py, pyrite; Bn, bornite, Cpy, chalcopyrite.

Table A3.3. Re-Os geochronology data for White Pine.

AIRIE run no.	Drill hole	Depth (m)	Re (ppm)	^{187}Os (ppb)	Common Os (ppb)	Age (Ma)
MD-1737	WP198	856.37	0.3228	3.543	0.0232	1039.1
MD-1738	WP198	856.32	0.1918	2.227	0.0355	1098.5